Host Factor Determinants of Influenza A Virus Infection and Severity in Pigs

Glud, Helena Aagaard

Publication date:
2023

Document Version
Publisher's PDF, also known as Version of record

DTU Bioengineering
Department of Biotechnology and Biomedicine

Host Factor Determinants of Influenza A Virus Infection and Severity in Pigs

Helena Aagaard Glud

PhD Thesis, July 2023

Host Factor Determinants of Influenza A Virus Infection and Severity in Pigs

PhD Thesis
Helena Aagaard Glud
July, 2023

DTU Bioengineering
Department of Biotechnology and Biomedicine

Supervisors:
Senior researcher Kerstin Skovgaard
Department of Biotechnology and Biomedicine, Technical University of Denmark

Professor Lars Erik Larsen
Department of Veterinary and Animal Sciences, University of Copenhagen

Research Professor Gregers Jungersen
Department of Infectious Disease Immunology, Statens Serum Institut

Assessment committee:
Professor Niels Lorenzen (Chairman)
Section for Fish and Shellfish diseases, Technical University of Denmark

Professor François J. M. A. Meurens
Faculty of Veterinary Medicine, University of Montréal

Associate Professor Susanna Cirera
Department of Veterinary and Animal Sciences, University of Copenhagen

Host Factor Determinants of Influenza A Virus Infection and Severity in Pigs

Cover picture: Photo by Helena Aagaard Glud, 2020 (pigs from one of the experimental studies performed in the PhD project)

Contents

Preface and acknowledgements

The PhD thesis presents work carried out at the Department of Biotechnology and Biomedicine, Technical University of Denmark, from May 2020 to July 2023. This PhD project is funded by Novo Nordisk Foundation (grant NNF19OC0056326) as part of the research project FluZooMark. I have had the privilege to be a part of the journey from the beginning, which have given me the opportunity to visit the farms and sample the pigs before including them in our studies. Furthermore, I took part in designing the animal experiments from scratch, collecting samples during the experiments and during necropsy. The PhD project has been a great experience for me as it has been a mixture of project planning, execution of large animal studies, laboratory work, and research. Moreover, I have had the great opportunity to share my work at several conferences in Denmark, but also at OPTIONS for the Control of Influenza XI in Belfast, UK.

During my PhD project, I have worked together with so many great people, and I would not have succeeded without them. First of all my greatest shout-out and thank you goes to my supervisor Kerstin Skovgaard. I started working with Kerstin in 2019 where I did a special course during my Master's degree, and from there I knew I wanted to know more about innate immunology and influenza virus. Thankfully, she let me do my Master thesis with her, which continued into this PhD project. She is very talented and engaged in her work and together with her optimism, trustful and considerate nature she creates the perfect environment and foundation for personal development and a successful outcome of a PhD project. My co-supervisor Lars Erik Larsen has likewise been a great support. He is a great inspiration as he is very knowledgeable and has an impressive way to make collaborations between several people at numerous institutions very successful in his role as project coordinator on FluZooMark. In addition, he is very down to earth, easy to talk to, and always a great company at conferences and FluZooMark gatherings. Also a big thanks to everybody working in Lars' group at University of Copenhagen for great collaborations, discussions, and good times during my PhD. I also want to thank my co-supervisor Gregers Jungersen, who has been a great inspiration for me, especially in the early days of the project to for-

mulate the study and project plan. I wish to continue the work in the future and open up the immunology toolbox even more.

A very special thanks should also go to Karin Tarp and Betina Lyngfeldt Henriksen for their indispensable technical assistance during my project, I would not have made it without you. Not forgetting the rest of Kerstin's girls; Louise Brogaard, Sofie M. R. Starbæk, and Chrysillis Hellemann Polhaus. Thank you for the support, great discussions, and contributions to my work. I had the pleasure of sharing my second research stay with Chrysillis, which made my time at St. Jude Children's Research Hospital even more rewarding than my first stay. A special thanks to Richard Webby and Paul G. Thomas for letting me join the labs. A huge thanks to all the people at St. Jude Children's Research Hospital, especially Jennifer DeBeauchamp, Jeri-Carol Crumpton (JC), and Emma Sliger (Kaity) for making my stays at St. Jude a fantastic experience. Thanks to you, St. Jude and Memphis feels like my second home. Finally, my rock at home cheering me on, taking care of our home, making sure I have clean clothes, a full stomach, and a tiptop bike. Patrick, thank you for always believing in me. I could not have done it without you.

Thank you.

Helena Aagaard Glud

DTU Bioengineering, July 2023

List of abbreviations

ALI	air-liquid interface.
cDNA	complementary DNA.
Cq	quantification cycle.
cRNA	complementary RNA.
cRNP	complementary RNP.
DNB	DNA Nanoball.
dNTP	deoxynucleotide triphosphate.
dpi	day post infection.
dsDNA	double-stranded DNA.
dsRNA	double-stranded RNA.
dUTP	deoxyuridine phosphate.
FADD	FAS associated protein with death domain.
HA	hemagglutinin.
IAV	influenza A virus.
IFC	integrated fluidic circuit.
IFNs	interferons.
IRF	interferon regulatory factor.
ISGs	interferon stimulated genes.
JAK1	janus kinase 1.
LGP2	laboratory of genetics and physiology 2.
M	matrix.
M1	matrix protein 1.
M2	matrix protein 2.
MAVS	mitochondrial antiviral signaling protein.
MDA5	melanoma differentiation–associated gene 5.
MLKL	mixed lineage kinase domain like pseudokinase.
MOI	multiplicity of infection.
mRNA	messenger RNA.
MyD88	myeloid differentiation primary response protein 88.
NA	neuraminidase.
NEP	nuclear export protein.
NEs	nasal mucosal explants.
NF-κB	nuclear factor kappa-light-chain-enhancer of activated B cells.
NP	nucleoprotein.
NS	non-structural.
NS1	non-structural protein 1.
OAS	2’-5’-oligoadenylate synthetase.
PA	polymerase acidic protein.
PABII	poly(A)-binding protein II.
PAMPs	pathogen-associated molecular patterns.
PAP	poly(A) polymerase.
PB1	polymerase basic protein 1.

PB2	polymerase basic protein 2.
PKR	protein kinase R.
PRRs	pattern recognition receptors.
RdRp	RNA-dependent RNA polymerase.
RIG-I	retinoic acid-inducible gene I.
RIPK	receptor-interacting serine/threonine-protein kinase.
RLRs	retinoic acid-inducible gene I-like receptors.
RNA-seq	RNA sequencing.
RT-qPCR	reverse transcription quantitative real-time PCR.
SA	sialic acid.
siNEC	immortalized swine nasal epithelial cells.
ssRNA	single-stranded RNA.
STAT	signal transducer and activator of transcription.
TAB	TGF-beta-activated kinase 1 and MAP3K7-binding protein 1.
TAK1	TGFβ-activated kinase 1.
TBK1	TANK-binding kinase 1.
TLRs	Toll-like receptors.
TRAF	TNF receptor-associated factor.
TRIF	TIR-domain-containing adapter-inducing interferon-β.
TYK2	tyrosine kinase 2.
UNG	uracil-N-glycosylase.
vRNA	viral RNA.
vRNP	viral ribonucleoprotein.
ZBP1	Z-DNA Binding Protein 1.

Summary

Influenza A virus (IAV) causes respiratory infection and many cases of disease associated with IAV occur annually during seasonal epidemics. During the past 100 years, zoonotic events followed by IAV pandemics have led to deaths of hundreds of millions of people. IAV has a broad host range and can infect a variety of avian and mammalian species in which novel strains of IAVs can emerge. Transmission of novel IAV to a susceptible human population with no or limited pre-existing immunity may lead to a new pandemic with fatal outcomes. The most recent IAV pandemic in 2009 was caused by a virus originating from swine, but to date there is still a lack of knowledge in molecular determinants involved in the ability of IAV to break the species barrier. When IAV infect respiratory epithelial cells of a host, it is recognized by innate immune sensors, which initiate induction of several antiviral immune factors, including pro- and anti-inflammatory cytokines and interferons. The interferon response induces the production of several antiviral molecules both in the infected cell and in neighbouring cells. However, IAV can alter and evade the host immune response through several mechanisms, making host-pathogen interactions highly complex and relevant to study.

Paper 1 is a review, which emphasizes the threat of zoonotic and reverse zoonotic transmission of viruses between humans and animals. Especially spillover events between pigs and humans are likely to occur as pigs and humans share a great number of viruses and are in close contact during pig farming worldwide. **Paper 2** is a thorough exposition of the experimental infection study of pigs with different IAV (H1N1) strains that underlies the data generated in **Paper 3** and **Paper 4**. Pigs were inoculated with IAV strains with different adaptation levels to the host, which revealed significant differences in viral dynamics and pathological manifestations. Infection with IAV well-adapted to the host (swine-adapted) resulted in high viral load, but reduced pathogenicity and clinical impact compared to a human-adapted IAV and a less host-adapted ”pre-pandemic” IAV. The observed differences in viral dynamics and pathological changes could be connected to the immune dynamics, which is described in **Paper 3** and **Paper 4**. In **Paper 3**, the kinetics and dynamics of the an-

tiviral innate immune response were shown to differ depending on the infecting type of IAV strain in nasopharyngeal swabs after IAV challenge. IAV well-adapted to the host induced a fast and strong expression of innate factors compared to a more dampened response when infected with an IAV adapted to another host (in this case humans). Furthermore, infection with a less host-adapted ”pre-pandemic” strain resulted in a prolonged immune response. Importantly, the well-adapted IAV was able to bypass an important first line of defence by downregulation of both secreted and transmembrane mucins. In **Paper 4** it was further revealed that the well-adapted IAV regulated the host metabolism to improve viral replication in tracheal tissue. In **Paper 5**, the use of respiratory explant cultures to study antiviral host immune responses was described. The immune responses observed after IAV infection of explants were comparable to responses after *in vivo* infection of pigs. In addition, the use of air-liquid interface (ALI) cultures has likewise been investigated as a tool to study immune responses after IAV infection. Both models are promising 3R compliant tools to study host-pathogen interactions under very controlled conditions.

The work described in this thesis has contributed to our knowledge of kinetics and dynamics of the antiviral innate immune response after infection with IAV with different host adaptation levels. Host adaptation and the ability to evade the host immune response impacted the outcome of the antiviral response. Furthermore, it was shown that the innate immune response could be linked to viral load and severity of infection.

Resumé (Danish summery)

Influenza A virus (IAV) medfører respiratorisk infektion og mange tilfælde af sygdom associeret med IAV. Gennem de sidste 100 år har zoonotiske hændelser, efterfulgt af IAV pandemier, medført flere hundrede millioner af dødsfald blandt befolkningen. IAV har et bredt udvalg af værter og kan inficere mange forskellige fugle- og pattedyrsarter, hvor nye IAV stammer kan opstå. Overførsel af en ny IAV til en modtagelig human befolkning med ingen eller begrænset eksisterende immunitet, kan medføre en ny pandemi med et fatalt udfald. Den seneste IAV pandemi i 2009 var forårsaget af en virus, der stammede fra svin, men til dags dato er der stadig en mangel på viden i from af afgørende molekylære faktorer involveret i IAV's evne til at bryde barrieren mellem arter. Når IAV inficerer værtens respiratoriske epitel celler, bliver den genkendt af medfødte immunsensorer, som indleder frembringelsen af adskillige antivirale immunfaktorer, heriblandt pro- og anti-inflammatoriske cytokiner og interferoner. Interferon responset igangsætter produktionen af adskillige antivirale molekyler både i den inficerede celler og i nabocellerne. IAV kan dog ændre og undgå værtens immunrespons gennem mange mekanismer, hvilket gør vært-patogen interaktioner meget komplekse og relevante at studere.

Manuskript 1 er en gennemgang af litteratur, der understreger truslen af zoonotisk og revers zoonotisk overførsel af virus mellem mennesker og dyr. Specielt overførslen af virus mellem grise og mennesker er meget sandsynlig, da grise og mennesker deler et stort antal af virus og er i nær kontakt gennem den verdensomspændende produktion af grise. **Manuskript 2** er en grundig gennemgang af det eksperimentelle infektionsstudie af grise med forskellige IAV (H1N1) stammer, som ligger til grund for den data, der er genereret i **Manuskript 3** og **Manuskript 4**. Grisene blev inokuleret med IAV stammer med forskellige adaptions niveauer til værten, hvilket afslørede signifikante forskelle i virus dynamik og patologiske forandringer. Infektion med IAV veltilpasset til værten (grise-adapteret) resulterede i høj virus mængde men reduceret patogenitet og kliniske implikationer sammenlignet med en menneske-adapteret IAV og en mindre veltilpasset "pre-pandemisk" IAV. De observerede forskelle i virus dynamik og patologiske ændringer kunne relateres til immun-

dynamik, hvilket er beskrevet i **Manuskript 3** og **Manuskript 4**. I **Manuskript 3** blev det vist hvordan det antivirale immunrespons' kinetik og dynamik var forskellig i næsesvabere efter IAV infektion afhængig af den type IAV stamme, der blev inficeret med. IAV veltilpasset til værten forårsagede en hurtig og kraftig ekspression af innate faktorer i forhold til et mere dæmpet respons, når der blev inficeret med en IAV stamme adapteret til en anden vært (i dette tilfælde mennesker). Ydermere resulterede infektion med en mindre værts-adapteret "pre-pandemisk" stamme i et længerevarende immunrespons. Nok så vigtigt blev det vist, at den veltilpassede IAV kunne omgå en vigtig første forsvarslinje ved at nedregulere både udskilte og transmembrane muciner. I **Manuskript 4** blev det yderligere afsløret, at den veltilpassede IAV kunne regulere værtsmetabolismen for at fremme virus replikation i tracheal væv. I **Manuskript 5** blev brugen af respiratoriske eksplanter til at studere værtens immunrespons beskrevet. Immunresponset efter IAV infektion af eksplanterne var sammenligneligt med responset efter *in vivo* infektion af grise. Derudover blev brugen af luft-væske-grænsefladekulturer, som redskab til at undersøge værtens antivirale immunrespons efter IAV infektion beskrevet. Begge modeller er lovende modeller i overensstemmelse med de 3R'er til at studere værts-patogen interaktioner under meget kontrollerede forhold.

Arbejdet beskrevet i denne afhandling har bidraget til vores viden i forhold til kinetik og dynamik af det antivirale innate immunrespons efter infektion med IAV stammer med forskellig værtsadaptions niveauer. Værtsadaption og evnen til at omgå vært immunresponset påvirker udfaldet af det antivirale respons. Yderligere blev det afsløret, at det innate immunrespons kunne sammenholdes med viral mængde og omfanget af infektionen.

1 Introduction

Influenza is a viral respiratory disease, and World Health Organization reports 290,000 to 650,000 respiratory deaths annually worldwide [1]. In Europe alone, European Centre for Disease Prevention and Control estimates up to 50 million cases associated with seasonal influenza each year [2]. The burden of controlling influenza is not made lighter by its substantial zoonotic threat as influenza A virus (IAV) can infect a variety of avian and mammalian species [3–6] and can change its genome by mutations and reassortment [7]. IAV pandemics have led to deaths of hundreds of millions of people in the past 100 years [8–11], but even though the most recent IAV pandemic in 2009 was caused by virus originating in swine [12], there is a lack of knowledge of molecular determinants of both virulence and transmissibility of swine IAV. Why do some swine-adapted IAV strains have the ability to cross the species barrier and infect humans, and why do some novel viruses lead to human pandemics? Pigs are susceptible to IAV with both avian, swine, and human origin [13], but since host receptor distribution and binding preference of human and swine IAV are similar [14], other viral and/or host factors must affect the mechanism behind host tropism and the zoonotic potential. Indeed, different host factors, including age, sex/gender, obesity, and defective immune responses [15–20], have been demonstrated to influence susceptibility and severity of IAV infections. In Denmark, more than 30 million pigs are produced yearly, and farmers and animal caretakers are in close contact with these pigs. More than 50% of Danish swine are positive for IAV [21], therefore Denmark could be a potential hotspot for the development of novel IAV strains, but it also makes Denmark the perfect place to study IAV host tropism and zoonotic potential.

This PhD project is an integral part of the FluZooMark project, which aims to identify viral and host factors that determine the potential of swine influenza viruses to cross the species barrier and infect humans. The overall aim of this thesis was to emphasise and identify early host factors associated with IAV infection and severity. It aimed to contextualise these host factors with viral RNA load and histopathological evaluations. To fulfil these aims, several experimental infection trials in pigs were conducted using IAV strains adapted to either hu-

mans or pigs. This project sought to increase the knowledge of molecular orchestration of an efficient antiviral innate immune response and compare this response with viral dynamics. The hypotheses studied in this PhD project can be summarised as follows:

1. Different innate pathways are involved in controlling infection with human- and swine-adapted IAV after experimental infection of pigs
2. Kinetics and magnitude of genes involved in innate pathways are affected by IAV host adaptation
3. Immune dynamics can be connected to viral RNA load and pathological manifestations
4. IAV can alter/evade the host innate immune responses to its advantage
5. *In vitro* culture of swine respiratory epithelial cells grown at air-liquid interface can be used as a 3R compliant tool for hypothesis testing and study of host-pathogen interactions under low technical variations.

The thesis is divided into five main parts. This first part is included to give a brief introduction to the PhD project and to introduce the overall aims of the project. The second part outlines relevant background knowledge on IAV, the host innate immune response to IAV infection, and the essential methods used. Part 3 describes the experimental strategy used in the project, including animal trials and the ongoing establishment of *in vitro* models. Part 4 includes five manuscripts generated during the PhD project, and the last part provides an overall discussion of the project's outcome, including conclusions and perspectives for future work.

2 Background

2.1 Influenza A virus

2.1.1 Taxonomy and structure

The genus *influenzavirus A* belongs to the *Orthomyxoviridae* family, which also includes *influenzavirus B, C,* and *D*, as well as *Isavirus*, *Thogotovirus*, and *Quaranjavirus* [7, 22, 23]. Influenza A virus (IAV) is an enveloped virus with a segmented, single-stranded, negative-sense RNA genome. The viral envelope consists of a host cell-derived lipid bilayer containing three viral transmembrane proteins: hemagglutinin (HA), neuraminidase (NA), and the ion channel matrix protein 2 (M2). Underneath the viral envelope is a layer of the matrix protein 1 (M1) enclosing the eight viral ribonucleoprotein (vRNP) complexes, which encode at least 12 viral proteins. Each vRNP complex is composed of viral RNA (vRNA) associated with the RNA-dependent RNA polymerase (RdRp) complex, and multiple copies of nucleoprotein (NP) [7, 24] (Figure 2.1).

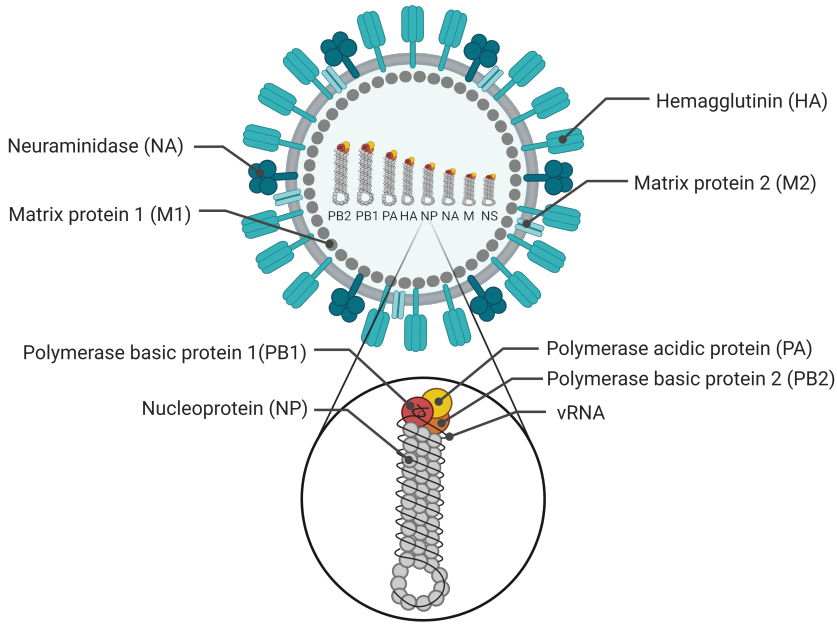

Figure 2.1: Schematic representation of influenza A virus (IAV) and viral ribonucleoprotein (vRNP). Hemagglutinin (HA), neuraminidase (NA), and the ion channel matrix protein 2 (M2) are transmembrane proteins situated within a host cell-derived lipid bilayer. Matrix protein 1 (M1) lines the inner surface of the lipid layer and encloses the eight vRNPs (PB2, PB1, PA, HA, NP, NA, M, and NS). The vRNP complexes consists of viral RNA (vRNA) associated with the RNA-dependent RNA polymerase (RdRp) complex (PB2, PB1, PA) and multiple copies of nucleoprotein (NP). Created with BioRender.com.

The three largest vRNP segments encode the RdRp proteins, polymerase basic protein 2 (PB2) in segment 1, polymerase basic protein 1 (PB1) in segment 2, and polymerase acidic protein (PA) in segment 3. Both segment 2 and 3 encode more than one viral protein each via an alternative reading frame (PB1 encodes PB1-F2) [25, 26] and ribosomal frameshifting (PA encodes PA-X) [27, 28], respectively. The fourth, fifth, and sixth largest segments encode HA, NP, and NA, respectively. The last two segments (matrix (M) and non-structural (NS)) also encode more than one viral protein each via splicing. The unspliced M segment encodes M1, and the spliced segment encodes M2. The unspliced NS segment encodes non-structural protein 1 (NS1), while the spliced segment encodes nuclear export protein (NEP), also known as NS2 [29, 30].

2.1.2 Life cycle

HA binds to terminal sialic acid (SA) residues of glycoproteins and glycolipids found on the host cell membrane, triggering viral uptake into the host cell by receptor-mediated endocytosis. IAV is internalised in an endosome, where the low pH activates the M2 ion channel, leading to further acidification of the endosome. The acidic environment results in a large conformational change in HA after host cell protease cleavage, exposing the fusion peptide. The fusion peptide is inserted into the endosomal membrane, opening the endosome, followed by the release of vRNPs into the host cell's cytosol. Unlike most negative-sense RNA viruses, IAV transcription and replication occur in the nucleus. Thus, the vRNPs are translocated into the nucleus using host importin α/β (Figure 2.2). Inside the nucleus, the RdRp transcribes and replicates the viral genome [24, 31, 32].

Transcription of vRNA into messenger RNA (mRNA) requires capped oligomers, which are snatched from host pre-mRNA by the RdRp complex. The PB2 subunit binds the capped end of host pre-mRNA, and the cap is cleaved off due to the endonuclease activity of the PA subunit. PB1 binds the viral RNA (vRNA), and transcription is initiated by the addition of the capped primer to the vRNA [24, 33]. The transcription elongation proceeds until the polymerase reaches a sequence of several uridine residues. Due to steric hindrance, uridine is reiteratively copied, adding a poly(A) tail to the transcript, which is required for nuclear export [34, 35]. The viral mRNAs are transported to the cytoplasm most likely

via the cellular NXF1/TAP pathway [36, 37] and translated into viral proteins by the host translational machinery. Newly synthesised proteins (RdRp proteins, NP, M1, and NEP) are imported back into the nucleus to take part in vRNA replication [24, 38] (Figure 2.2).

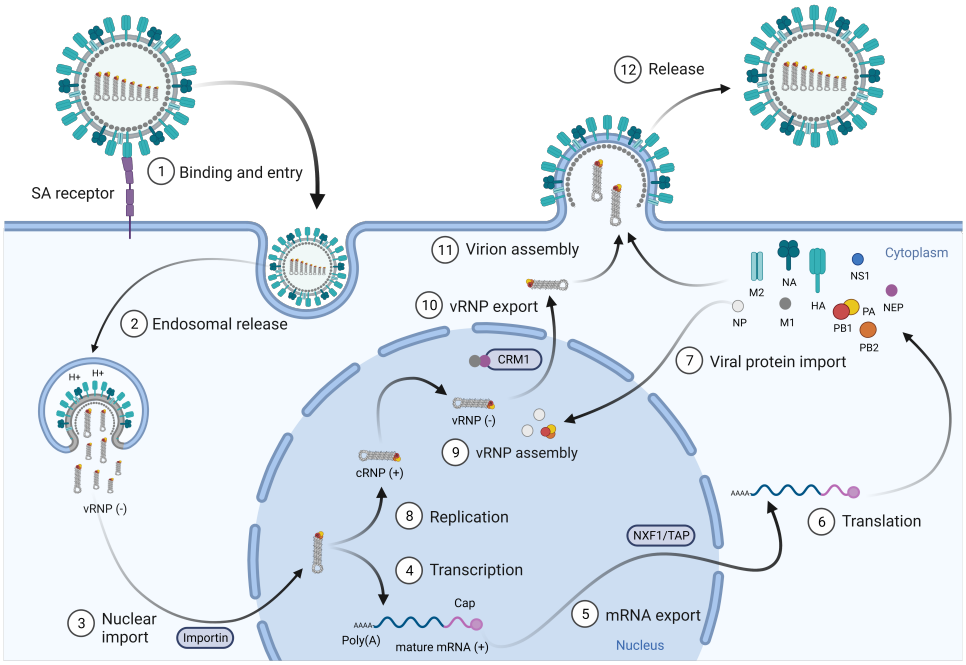

Figure 2.2: Schematic representation of influenza A virus (IAV) life cycle. 1) IAV binds sialic acid (SA) coated receptors on the host cell surface via hemagglutinin (HA) and is taken up by receptor-mediated endocytosis. 2) Increasing acidification within the endosome by the matrix protein 2 (M2) ion channel leads to the fusion of the endosome and viral membrane, releasing viral genomes in the form of viral ribonucleoprotein (vRNP) into the cytoplasm. 3) The vRNPs are imported into the nucleus by host importins. 4) The RNA-dependent RNA polymerase (RdRp) complex transcribes viral RNA (vRNA) into mRNA. 5) Newly synthesised mRNA is exported to the cytoplasm via the cellular NXF1/TAP pathway. 6) Host translational machinery translates viral mRNA into proteins. 7) Newly synthesised viral proteins are transported back into the nucleus to take part in viral replication. 8) Full length vRNPs are replicated via a complementary RNP (cRNP) intermediate. 9) Newly synthesised vRNPs are assembled in the nucleus using the newly synthesised viral proteins. 10) The vRNPs are exported into the cytoplasm via matrix protein 1 (M1) and nuclear export protein (NEP) and host export protein CRM1. 11) vRNPs are assembled into virions containing the viral structural proteins incorporated in the host cell membrane. 12) The new virions are released by the sialidase activity of neuraminidase (NA). Created with BioRender.com.

During replication, the RdRp converts the negative-sense vRNA into positive-sense complementary RNA (cRNA), which is assembled into a complementary RNP (cRNP) complex by NP and RdRp binding. The cRNP serves as a template for the production of new full-length vRNA. New vRNA can be either packed into vRNPs or serve as mRNA templates for the translation of more viral proteins. Newly synthesised vRNPs are exported from the nucleus by M1 and NEP. M1 interacts directly with the vRNPs, while NEP binds M1 and host cellular export protein, CRM1, to mediate export [39]. The vRNP is transported across

the cytosol to the cell surface via the cytoskeleton [40]. The vRNPs are assembled into virions, where the structural proteins have been anchored to the host cell membrane, making the viral envelope contain host cell lipids. The new virions are formed by budding, where NA ensures complete release of the virion by its sialidase activity [24, 32, 38] (Figure 2.2).

2.1.3 Evolution

IAV evolves and changes through two major mechanisms; antigenic drift and antigenic shift [41]. Antigenic drift occurs as a result of an accumulation of point mutations in the viral genome. Mutations arise during viral replication, and since the RdRp of IAV lacks a proofreading mechanism, IAV has a high mutation rate compared to other organisms with longer generation times and proofreading polymerases. Mutations changing amino acids in antigenic sites, especially in the two surface proteins (HA and NA), may lead to new IAV variants, which can escape from previously acquired host immunity [41–43]. Due to the segmented genome of IAV, viral reassortment can occur when two or more different IAVs co-infect a host cell. This can result in progeny virus that contain a novel combination of gene segments. When the reassortment results in progeny viruses that contain a novel HA and/or NA, it is termed antigenic shift [41–43]. These genetic variations of IAV contribute to the emergence of human epidemics and pandemics as well as zoonotic transmissions. Indeed, reassortment was involved in the latest three IAV pandemics, an H2N2 IAV in 1957 termed ”the Asian Flu”, an H3N2 IAV in 1968 termed ”the Hong Kong flu”, and an H1N1 IAV in 2009 termed ”pandemic H1N1 2009”. The two later, ”the Asian Flu” and ”the Hong Kong flu”, arose from a reassortment event between avian and human IAV [44], while the latest in 2009 was reassortment between three major IAV lineages circulating in swine. Though, these swine lineages also contained segments of avian and human origin [45].

2.1.4 Host range

IAV can infect a variety of avian and mammalian species, such as humans, pigs, poultry, ferrets, and horses [3–6]. IAV is classified into subtypes based on the two surface proteins, HA and NA. Currently, 16 HA (H1-H16) and nine NA (N1-N9) have been isolated from aquatic birds, which are also described to be the natural reservoir of IAV [5, 46]. Two subtypes have recently been isolated from bats, H17N10 and H18N11 [47, 48]. Currently,

two subtypes are circulating in humans and swine, namely H1N1 and H3N2 [41], while a third subtype, H1N2, is only circulating in swine [43]. HA is a major determinant of host range as HA initiates binding and entry into host cells via SA-containing receptors. The distribution of SA receptors throughout the respiratory system varies depending on the host. Humans and pigs have predominantly SA receptors linked to galactose by α-2,6 (SA-α-2,6) linkage in the entire respiratory tract with a minor presence of SA-α-2,3 receptors in the lower respiratory tract [4, 49, 50]. On the other hand, avian species express SA-α-2,6 and SA-α-2,3 in both the respiratory tract and intestinal tract, though the expression level varies between species [51]. IAV isolated from human and swine prefers SA-α-2,6 receptors, while avian IAV prefers SA-α-2,3 as receptor [52–54]. Thus, avian IAV must adapt to the human host environment by altering the receptor binding preference of HA (from SA-α-2,3 to SA-α-2,6), or by penetrating deep into the lungs to find the appropriate receptor (SA-α-2,3). Other factors, such as the balance between HA and NA content, optimum pH for HA stability, the viral polymerase complex, temperature of the host, and the host-specific immune responses are also important factors during inter-species transmission [46, 55].

2.2 Influenza A virus infection

IAV must evade the innate immune system to establish an infection and propagate successfully. However, the innate immune system possesses multiple mechanisms to prevent infection or restrict viral replication. The respiratory mucus layer act as a physical and chemical barrier by secreting soluble factors with antiviral effects, such as mucus and surfactants. If IAV passes through the physical and chemical barriers and infects the host cells, multiple innate pathways will be activated, resulting in the production of several antiviral innate factors and subsequent recruitment of immune cells.

2.2.1 Host innate immune response to IAV infection

First line of defence

In order to reach and infect the host cells, IAV must successfully penetrate the first line of defence, the airway mucus layer. The airway mucus of mammals exists in two layers: a more viscous gel-like layer situated on top of a periciliary liquid layer. The gel layer

contains secreted mucins, mainly MUC5AC and MUC5B, secreted from goblet cells and mucous cells of the submucosal glands, respectively [56–58]. The liquid layer contains the transmembrane mucins, such as MUC12 and MUC20 [59], presented on all epithelial cells of the respiratory tract. Mucins are heavily glycosylated with a terminal fucose or a sialic acid (SA), so the secreted mucins can act as decoy receptors binding and facilitating the removal of IAV by mucociliary clearance before IAV can reach and infect the underlying host cells. The transmembrane mucins attract water resulting in reduced viscosity, which facilitates ciliary beating essential for mucociliary clearance [56–58].

Antiviral innate immune response

If IAV does manage to reach and infect the host cells, the innate immune pathways are activated upon IAV recognition by pattern recognition receptors (PRRs), including Toll-like receptors (TLRs) and retinoic acid-inducible gene I-like receptors (RLRs) (Figure 2.3). IAV is recognized by its pathogen-associated molecular patterns (PAMPs), such as single-stranded RNA (ssRNA), double-stranded RNA (dsRNA), and triphsophorylated ssRNA [60, 61]. The RLRs, retinoic acid-inducible gene I (RIG-I) (*DDX58*), melanoma differentiation–associated gene 5 (MDA5) (*IFIH1*), and laboratory of genetics and physiology 2 (LGP2) (*DHX58*), are all present in the cytosol. RIG-I detects triphosphorylated ssRNA, while MDA5 and LGP2 recognize dsRNA [32, 62]. Uncapped triphosphorylated ssRNA (5'ppp ssRNA) is generated during viral replication and usually not found in host RNAs [63], while dsRNA is found in the vRNP complex as the genomic ends of the vRNA form a double-stranded structure that is bound to the RdRp complex (Figure 2.1) [38]. Three TLRs are involved in IAV recognition, TLR3, TLR7, and TLR8. They all recognise PAMPs contained within the endosome during degradation of the incoming IAV. TLR3 recognizes dsRNA [64], while TLR7 and TLR8 recognize ssRNA [65, 66]. Detection of IAV PAMPs by the PRRs leads to the activation of signal cascades to induce gene expression of immune genes through the activation of transcription factors, interferon regulatory factor (IRF) 3 and 7 (*IRF3* and *IRF7*) and nuclear factor kappa-light-chain-enhancer of activated B cells (NF-κB) (Figure 2.3) [60, 62].

TLR7 and TLR8 use the adaptor protein myeloid differentiation primary response protein 88

(MyD88) [67], while TLR3 requires TIR-domain-containing adapter-inducing interferon-β (TRIF) to activate downstream signaling [64, 68]. Upon TLR7/8 activation, MyD88 interact with IL-1R-associated kinases (IRAK1 and IRAK4) to activate TNF receptor-associated factor (TRAF) 6, which recruits and activates a complex by a ubiquitin scaffold, consisting of TGFβ-activated kinase 1 (TAK1) and TGF-beta-activated kinase 1 and MAP3K7-binding protein 1 (TAB) 1 and 2 (TAB1/2) [69] (Figure 2.3). TAK1 activates the IKK kinase complex (Ikkα, IKKβ, IKKγ/NEMO) by phosphorylation, which activate NF-κB [69]. In addition, MyD88 and TRAF6 interact with IRF7 positioning IRF7 in close proximity to IRAK1, which activates IRF7 by phosphorylation [67, 70, 71]. On the other hand, when TLR3 is activated, TRIF interacts directly with TRAF3, which recruits and activates the IKK complex by a ubiquitin scaffold [32]. The activated IKK complex interacts with TANK-binding kinase 1 (TBK1) and IKKϵ, which drives activation of IRF3 and IRF7 by phosphorylation (Figure 2.3) [72–74]. To activate NF-κB, TRIF recruits TRAF6, which activates NF-κB as described above [68, 75].

RIG-I undergoes conformational change upon binding of triphosphorylated ssRNA and is ubiquitinated by ubiquitin ligases TRIM25 and Riplet (*RNF135*). MDA5 does not require ubiquitination for activation. RIG-I/MDA5 interacts with and activates mitochondrial antiviral signaling protein (MAVS), which results in formation of a complex consisting of i.a. MAVS, TRAF3, and receptor-interacting serine/threonine-protein kinase (RIPK) 1. TRAF3 activates RIPK1 resulting in activation of the IKK kinase complex and NF-κB activation [32, 62]. In addition, the IKK kinase complex also activates TBK1/IKKϵ by phosphorylation, which results in activation of IRF3 and IRF7 [72–74]. LGP2 (not shown in Figure 2.3) does not have the ability to recruit MAVS but is thought to be involved in regulation of RIG-I and MDA5 [32, 62]. Thus, IAV can be detected by more than one PRR creating a high degree of redundancy at the detection level and subsequent activation of transcription factors.

Transcription factor activation (IRF3, IRF7, and NF-κB) results in the expression of interferons (IFNs), pro-inflammatory cytokines, and chemokines [60, 61]. Type I (mainly IFN-α and IFN-β) and III (IFN-λ) IFNs stimulate the expression of hundreds of ISGs in the infected cell as well as in neighbouring cells. Type I and type III IFNs bind their respective

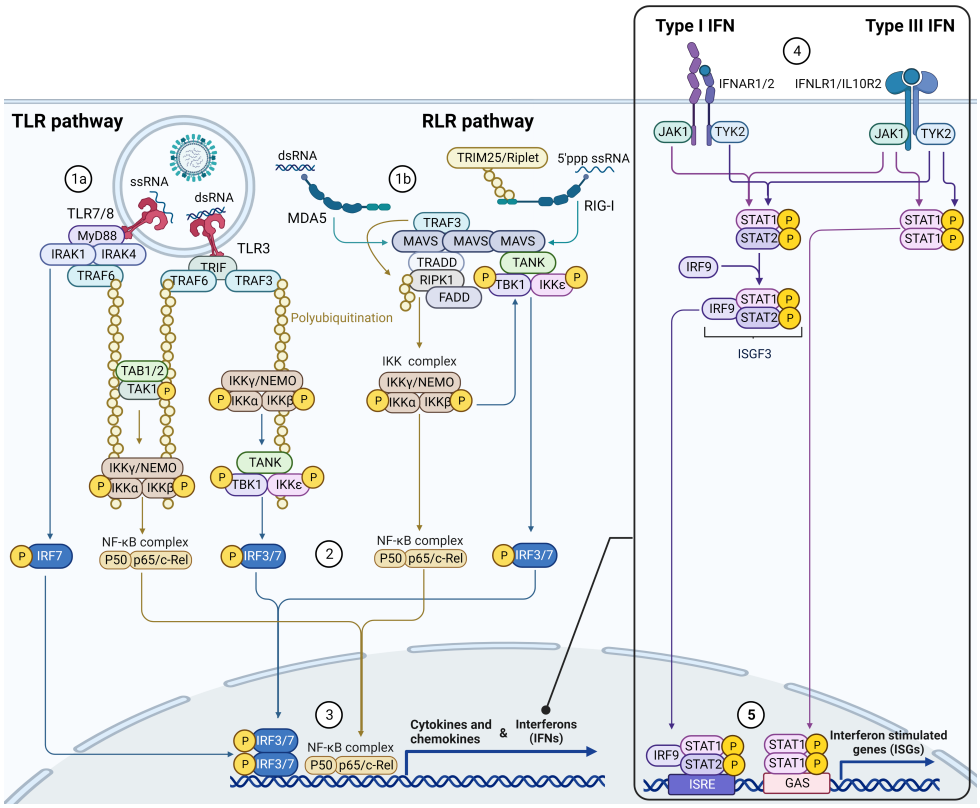

Figure 2.3: Antiviral innate immune response induced by influenza A virus (IAV). Toll-like receptors (TLRs) and retinoic acid-inducible gene I-like receptors (RLRs), are activated by different pathogen-associated molecular patterns (PAMPs). TLR3, TLR7, and TLR8 are expressed and activated in the endosome (1a), while retinoic acid-inducible gene I (RIG-I) and melanoma differentiation–associated gene 5 (MDA5) are activated in the cytosol (1b). The PRRs activate several signal cascades, all leading to the activation of transcription factors, IRF3, IRF7 and NF-κB (2). After translocation, the transcription factors initiate the expression of cytokines, chemokines, and interferons (IFNs) (3). The IFNs are secreted and activate the JAK/STAT pathway via their respective receptor on the cell surface (4), resulting in the expression of interferon stimulated genes (ISGs) (5). Created with BioRender.com.

receptor, IFNAR1/2 and IFNLR1/IL10R2, activating the JAK/STAT pathway. Janus kinase 1 (JAK1) and tyrosine kinase 2 (TYK2) is associated with the receptors and upon activation recruit signal transducer and activator of transcription (STAT) proteins (STAT1/2), which are phosphorylated by JAK1. Phosphorylation stimulates the assembly of the ISGF3 complex (STAT1, STAT2, and IRF9), which, together with dimers of STATs, act as a transcription factor of ISGs (Figure 2.3) [76]. The ISGs interfere with distinct steps in the viral life cycle, while cytokines and chemokines recruit and activate immune cells [61].

Previously, Z-DNA Binding Protein 1 (ZBP1) has been described as a cytoplasmic DNA sensor, but in 2016 it was reported to bind nuclei acid of IAV [77]. Upon activation, ZBP1

triggers apoptosis and necroptosis to kill the infected cell. Necroptosis is induced by RIPK3 via mixed lineage kinase domain like pseudokinase (MLKL) activation, while apoptosis requires a complex consisting of RIPK1, FAS associated protein with death domain (FADD), and Caspase-8 (not shown in Figure 2.3) [32, 77]. The ZBP1 complex is also involved in activating the NLRP3 inflammasome. Assembly of the NLRP3 inflammasome results in Caspase-1-mediated pyroptosis through the release of inflammatory cytokines and activation of gasdermin D (not shown in Figure 2.3) [32, 78].

2.2.2 Host-pathogen interactions

For each of the above antiviral pathways, IAV has developed several ways to evade their activation and/or their production of antiviral effector molecules.

One well-known host-pathogen interaction is the NS1 protein, which can interact with and attenuate the antiviral host response by many mechanisms. NS1 can limit host antiviral activation by at least three mechanisms: inhibition of the central PRR RIG-I, inhibition of host mRNA production and/or inhibition of ISGs. RIG-I inhibition can occur through several mechanisms: direct binding to RIG-I [63, 79], by sequestering its activating ligand [80, 81], or by binding to TRIM25 and/or Riplet to inhibit RIG-I ubiquitination [82, 83]. For processing of cellular pre-mRNAs (splicing and poly(A) addition) CPSF30 is required, but NS1 can interact with CPSF30 and inhibit the production of cellular mRNAs [84–86]. Likewise, poly(A) polymerase (PAP) catalyses synthesis of the poly(A) tail on host mRNA, but poly(A)-binding protein II (PABII), which binds to the growing tail, is needed to further stimulate long poly(A) tails. NS1 targets PABII and causes nuclear accumulation of cellular pre-mRNA with short poly(A) tails [87]. In addition, NS1 can interact with the IKK complex, affecting the activation of NF-κB. Together, all these mechanisms interfere with the production of inflammatory cytokines, IFNs and subsequent ISGs [88]. Furthermore, NS1 can also bind and inhibit the antiviral functions of ISGs, such as the 2'-5'-oligoadenylate synthetase (OAS) pathway and protein kinase R (PKR), which inhibit viral transcription and translation, respectively [89].

Other viral proteins have also been demonstrated to be important in host-pathogen inter-

actions. PA-X selectively targets and degrades host RNA polymerase II and its transcribed mRNAs [90, 91], while PB1-F2 interacts with MAVS and decreases the mitochondrial membrane potential. Since MAVS is located in the outer membrane of mitochondria and the mitochondrial membrane potential is essential for the formation of MAVS complexes, it results in the suppression of RIG-I/MDA5 signalling [92, 93].

Besides host shutoff, IAV can also interfere with host cell metabolism, such as the nucleotide metabolism described in **Paper 4**. Viruses rely on the host cell for all necessary components for viral propagation as they do not have their own metabolism [94, 95]. IAV has shown to alter host cell glucose uptake [96, 97] and lipid composition [98] most likely to ensure energy and components required for viral propagation. Another host mechanism IAV relies on is the transport through the cytosol via the host cytoskeleton as described above for vRNP [40]. In addition, HA, NP, and M1 of IAV also interact with cytoskeleton elements [99–102]. Thus, the cytoskeleton and its associated motor proteins are involved in trafficking of vRNPs and viral proteins. Furthermore, the cytoskeleton has been described to be involved in IAV virion assembly and release. However, specific cytoskeleton components play different positive or negative roles in the individual steps of the IAV assembly and release process [103]. Thus, IAV interacts with and takes advantage of the host cell metabolism and the cytoskeleton machinery during its life cycle, but the exact mechanisms remain to be resolved.

2.3 Methods for transcriptional analysis

The central dogma describes the flow of genetic information from DNA through RNA into proteins. Here, all the RNA molecules can be described as the transcriptome. The transcriptome reflects the state in a cell, a population of cells or an entire organism. Transcriptomic analyses provide a snapshot of the gene expression changes under various conditions. Thus, transcriptomic analyses are highly relevant in the study of host responses during viral infection.

2.3.1 Reverse transcription quantitative real-time PCR (RT-qPCR)

Reverse transcription quantitative real-time PCR (RT-qPCR) is used to detect and quantify gene expression of a specific set of genes of interest. Total RNA is transcribed into com-

plementary DNA (cDNA) to create a template for the real-time qPCR reaction. Reverse transcription is initiated using a mixture of oligo(dT)s and random primers, which anneal to the template RNA. The reverse transcriptase binds the RNA template in the presence of an annealed primer and synthesises cDNA by incorporating deoxynucleotide triphosphate (dNTP)s, which are included in the reaction mix. Prior to microfluidic qPCR, the cDNA is preamplified by PCR with gene-specific primers to ensure a sufficient amount of template for the qPCR, which is performed in reaction volumes of less than ten nanoliters (Figure 2.4) [104, 105].

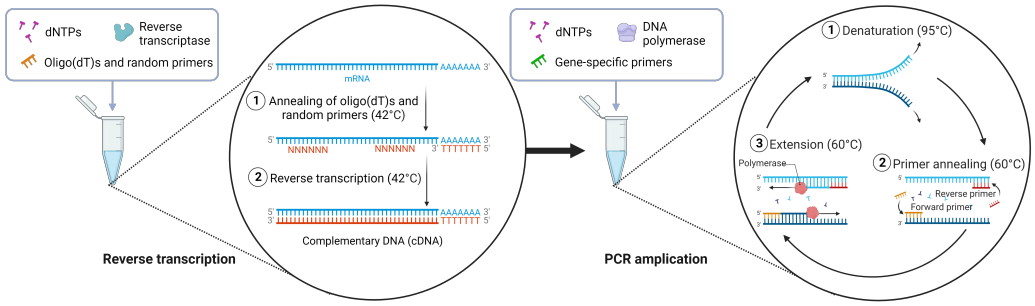

Figure 2.4: Schematic overview of reverse transcription and PCR amplification. Reverse transcription is initiated with the attachment of oligo(dT)s and random primers followed by synthesis of complementary DNA (cDNA) by reverse transcriptase. The cDNA is preamplified by denaturation, annealing, and elongation before quantification by microfluidic qPCR. Created with BioRender.com.

During a number of PCR amplification cycles, cDNA is denatured, followed by primer annealing and extension by the DNA polymerase (Figure 2.4). Time and temperature of each step can vary between protocols. The PCR becomes real-time by the use of a fluorescent DNA-binding dye, such as EvaGreen or SYBR Green I, or by fluorogenic probes. The dyes bind to the amplified double-stranded DNA (dsDNA) and emit a fluorescent signal, which is detected at the end of each cycle. The intensity of the fluorescent signal corresponds to the amount of dsDNA product, which doubles every cycle. When reagents are depleted in the reaction chamber, the amplification slows down and reaches a plateau of fluorescent signal. The amplification curve gets a sigmoidal shape with an initial lag phase, an exponential phase, and a plateau phase. Quantification is performed during the exponential phase of the reaction (Figure 2.5, left) [104, 105].

A threshold of detection is placed manually or applied by the software at the beginning of the

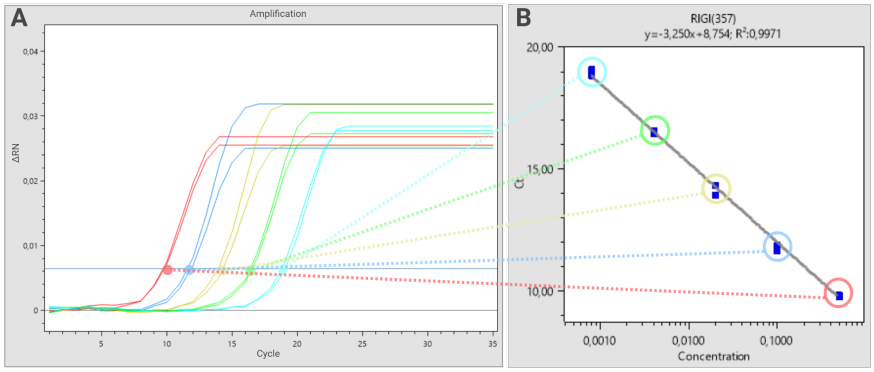

Figure 2.5: Amplification and calibration curve from a duplicate 5-fold dilution series of the gene *DDX58* (RIG-I). A) Amplification curve showing the fluorescent signal on the y-axis and the qPCR cycle number on the x-axis. The blue horizontal line indicates the threshold. B) Calibration curve showing the quantification cycle (Cq) values from the dilution series on the y-axis plotted against the $\log_{10}$ of the relative cDNA concentrations on the x-axis. Illustration obtained from Fluidigm Real-Time PCR Analysis software and modified with BioRender.com.

exponential phase. When the amplification curve reaches the specific threshold, the cycle number for this crossing point is measured as the quantification cycle (Cq). Thus, Cq values are inversely correlated with the initial dsDNA concentration, which means that a low Cq value equals high dsDNA concentration, while a high Cq value corresponds to a low ds-DNA concentration. A calibration curve is generated in each reaction to estimate both PCR efficiency and dynamic range for the specific primer assay. The dynamic range indicates the limits of quantifications for each primer assay. The PCR amplification efficiency for each assayed primer is determined from the slope of a calibration curve, which is produced from a dilution series plotting the Cq values against the $\log_{10}$ of the relative cDNA concentration (Figure 2.5, right). Theoretically, the dsDNA product should be doubled every cycle and reach a PCR efficiency of 100%. However, both higher and lower efficiencies can be obtained. Low efficiencies occur, e.g. when the primers are not optimally designed, or they form primer dimers. High efficiencies can occur due to the accumulation of unspecific amplification during the qPCR [104, 105].

To ensure that the amplified target product is a single specific product, a melting curve analysis is performed after the last qPCR cycle (Figure 2.6). The fluorescent dye is released upon denaturation of the dsDNA, providing melting temperatures for each amplified product. The melting temperature depends on the size and nucleotide composition of the DNA

product. GC-rich amplification products have a higher melting temperature compared to those containing more AT base pairs. Primer dimers are short and will melt at a lower temperature than the longer target DNA product, while carryover genomic DNA often contains introns resulting in a slightly higher melting temperature than the cDNA. Genomic DNA can be avoided by designing primers that span an exon/exon boundary. Primer design is described in Supplementary Text S3 from **Paper 3**. Besides melting curves, negative controls must be included in the RT-qPCR. A minus reverse transcriptase control, where reverse transcriptase is excluded, can identify any genomic DNA amplification and amplification of primer dimers. Furthermore, a non-template control, where no cDNA is added, will identify potential contamination of qPCR reaction components or primer dimers [104, 105].

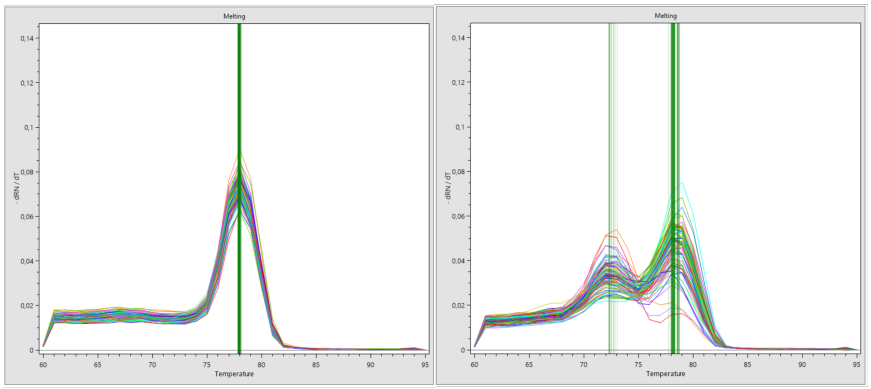

Figure 2.6: Melting curve analysis. The amplification of the gene *DDX58* (left) resulted in one specific product, while the amplification of the gene *MUC1* (right) yielded an unspecific product, most likely primer dimers. Illustration obtained from Fluidigm Real-Time PCR Analysis software.

Microfluidic high-throughput qPCR on the BioMark real-time platform

The real-time qPCR can be performed at high-throughput using the BioMark platform from Standard BioTools. The reactions are carried out using Dynamic Array integrated fluidic circuit (IFC) chips, which exist in different formats; 96 samples analysed in 96 assays (96.96), 48 samples analysed in 48 assays (48.48), and 192 samples analysed in 24 assays (192.24), facilitating 9,216, 2,304, and 4,608 reactions in a single run, respectively. Flex Six IFC is a reusable chip (six times) that combines 12 samples in 12 assays (6x 144 reactions).

The PCR protocol is slightly extended compared to the PCR preamplification described above. The thermal protocol for qPCR in a 96.96 Dynamic Array is initiated with a Ther-

mal Mix, ensuring that all reagents are sufficiently mixed before initiating a Hot Start. If uracil-N-glycosylase (UNG) is used to prevent PCR carryover contamination from previous PCR amplifications, this process occurs before the Hot Start. However, this step is not carried out in the qPCR described in **Paper 3** and **Paper 4** as the master mix used during reverse transcription does not contain deoxyuridine phosphate (dUTP). During Hot Start, DNA polymerase is activated to initiate the qPCR, which takes place as described above with a fluorescent dye and consists of 35 cycles. The protocol finishes with a Melting Phase to perform the melting curve analysis described above (Figure 2.7). qPCR data analysis is described in **Paper 3**.

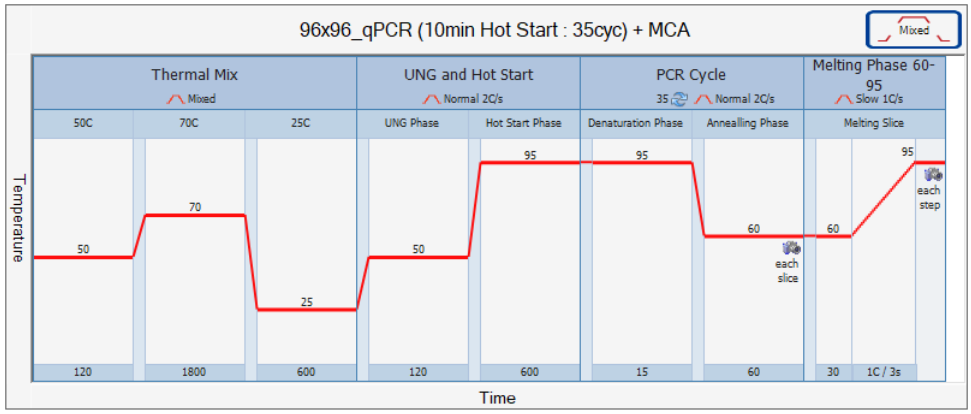

Figure 2.7: Thermal protocol for qPCR carried out using a 96.96. Dynamic Array integrated fluidic circuit (IFC) chip. The protocol contains four phases; Thermal Mix, UNG and Hot Start, qPCR cycles, and Melting Phase. The temperature in each step is shown on the y-axis, and the time in seconds each step is carried out is highlighted on the x-axis. Illustration obtained from Fluidigm Real-Time PCR Analysis software.

2.3.2 RNA sequencing

The development of high-throughput DNA sequencing methods has also led to new methods for transcriptomic analyses such as RNA sequencing (RNA-seq). The major strength of RNA-seq compared to RT-qPCR is the hypothesis-free approach, as no primers coding for specific genes of interest are necessary. This method can be used to identify the level of expression of each identified gene. DNBseq™ technology is a proprietary sequencing technology originally developed by Silicon Valley-based Complete Genomics [106], which is a part of BGI Genomics (Shenzhen, China) today. This technology provides high sequencing accuracy at a relatively low cost and is the method used to generate the RNA-seq data

included in **Paper 4**.

DNBseq technology

From total RNA extracted from a biological sample, polyA mRNA is purified using oligo(dT)-attached magnetic beads followed by mRNA fragmentation into smaller fragments. To generate cDNA, random primers are used for first- and second-strand synthesis of cDNA. End-repair and A-tailing of the double-stranded cDNA are performed to allow adaptor ligation and subsequent PCR amplification. The double-stranded PCR products are heat denatured into single-stranded cDNA. A splint oligonucleotide with complementary sequence to both the 5' and 3' terminal ends of the single-stranded cDNA is added to circularise the cDNA. Circular single-stranded cDNA undergoes a process called Rolling Circle Amplification using phi29 polymerase to generate a chain of copies of template DNA, which fold upon themselves to form DNA Nanoball (DNB)s [107, 108] (Figure 2.8).

The DNBs are loaded onto a flow cell consisting of multiple binding sites. Each binding site is only large enough to bind a single DNB, ensuring no interference of signals from neighbouring DNBs. Sequencing is performed using combinatorial Probe-Anchor Synthesis (cPAS) chemistry. A DNA anchor (complementary to the adaptor sequences) is annealed to the DNB adapter region. A fluorescently labelled dNTP is incorporated by the DNA polymerase and linked to the DNA anchor on the DNBs, followed by a wash of unbound dNTPs before high-resolution digital imaging. The fluorescent dye is cleaved to make the DNBs ready for the next cycle (Figure 2.8). The image data is converted into sequence data using base-calling. Data is typically supplied as large text files in FASTQ format [107, 108]. RNA-seq data analysis is described in **Paper 4**.

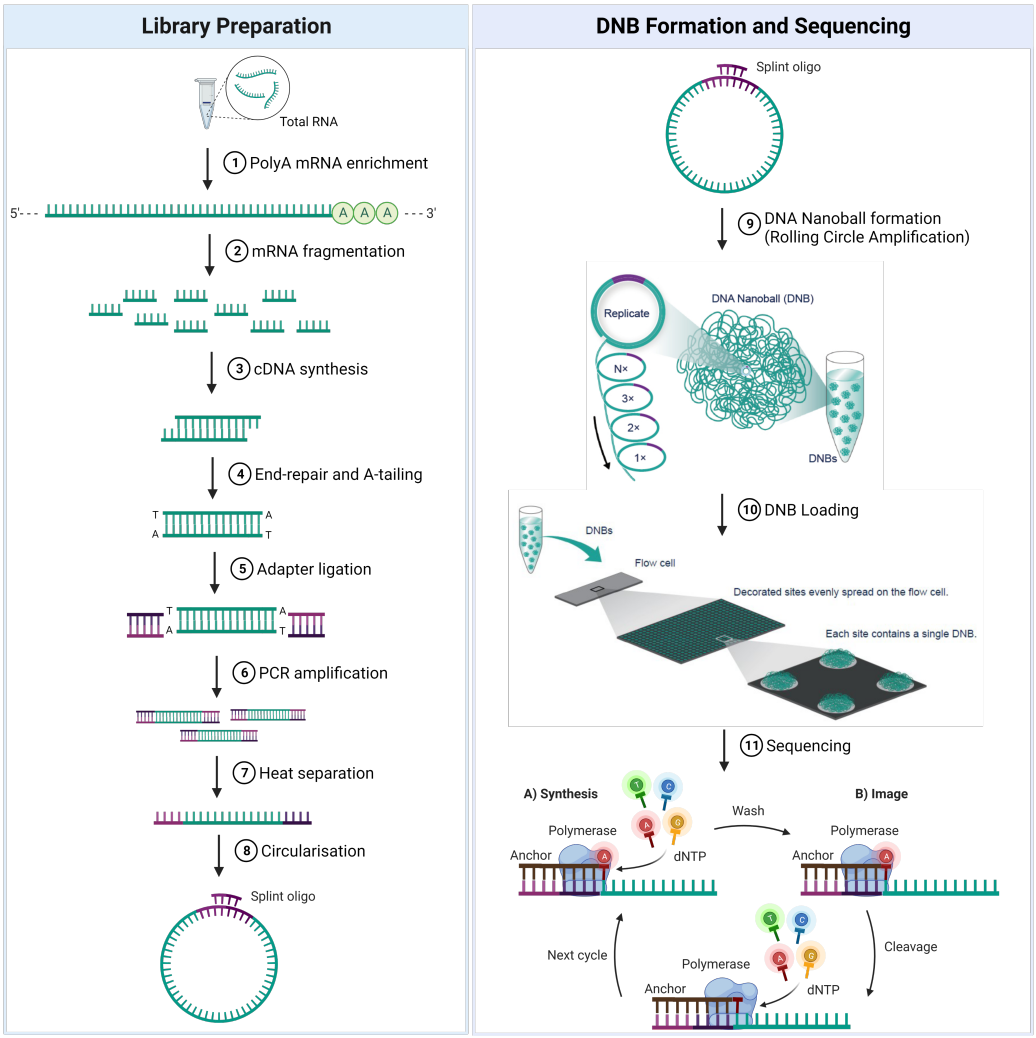

Figure 2.8: Experimental pipeline of DNBseq. 1) PolyA mRNA enrichment by oligo(dT) bead selection. 2) RNA fragmentation. 3) cDNA synthesis. 4) End repair and A-tailing 5) Adaptor ligation. 6) PCR amplification. 7) Double strand separation by heat. 8) Circularisation by a split oligonucleotide. 9) DNA Nanoball (DNB) formation. 10) Loading of DNBs on the flow cell. 11) Sequencing on the DNBseq platform: A) Fluorescently labelled dNTP is linked to the DNA anchor (complementary to the adaptor sequences), and excess dNTPs are washed away before high-resolution imaging (B). The fluorescent dye is cleaved, making the DNB ready for the next cycle. Created with BioRender.com, some illustrations are obtained from [108].

3 Experimental framework

During this PhD project, a number of animal experiments have been performed. One challenge study using H1N1 IAV strains (see description below), another using H3N2 IAV strains (A/SW/DK/102335-1/2013, A/DK/304/2020, and A/SW/S3974-2/2020), and one transmission study using the same H1N1 IAV strains. All data presented in **Paper 3** and **Paper 4** is from the same experimental challenge study in pigs using H1N1 IAV strains. The outline of the study is described in **Paper 2** and **Paper 3**. Therefore, section 3.1 will briefly summarise this study with additional relevant details. Furthermore, the use of *in vitro* models will be described in section 3.2, including results from a pilot study using respiratory air-liquid interface (ALI) cultures.

Animal models are needed to estimate disease severity and viral replication within the affected tissues of the respiratory tract, which is less available from humans due to the obvious ethical concerns associated with human experiments. Furthermore, studies using animal models can be conducted in controlled settings without the impact of other diseases or environmental factors. Pig models allow us to investigate IAV infection in an animal model, which is naturally susceptible to human IAV and closely mirrors humans with regards to clinical signs, respiratory physiology and anatomy, and antiviral immune responses [14]. In addition to the similar distribution and proportion of SA receptors (described in section 2.1.4), humans and swine also have a similar distribution of the mucus-secreting goblet cells [14], making pigs a great model for humans when studying the mucosal and innate immune response after IAV infection.

3.1 Animal experiment

The experimental study described in **Paper 2** and **Paper 3** was performed at the University of Copenhagen under biosafety level 2 conditions and under an animal study protocol approved by The Danish Animal Experimentation Council (protocol no. 2020-15-0201-00502). 42 Danish Landrace Crossbred pigs (7 weeks old) were included in the study. The pigs were divided into four groups, a control group (n=6) and three challenge groups (n=12). The chal-

lenge groups were inoculated with 3 ml of 10^7 $TCID_{50}$/ml of A/Swine/Denmark/2017_102-98/4_4p1/2017 (swH1N1pdm09), A/Denmark/238/2020 (huH1N1pdm09), and A/Swine/Mexico/AVX-39/2012 (mxH1N1pdm09), respectively. All included IAV strains are variants of the H1N1pdm09 IAV. The study is summarised in Figure 3.1, including sampling time and collected sample type. Multiple tissues were collected at euthanisation on days 3 and 14 after inoculation, together with swab and blood samples, which were collected at several time points throughout the study as indicated in Figure 3.1.

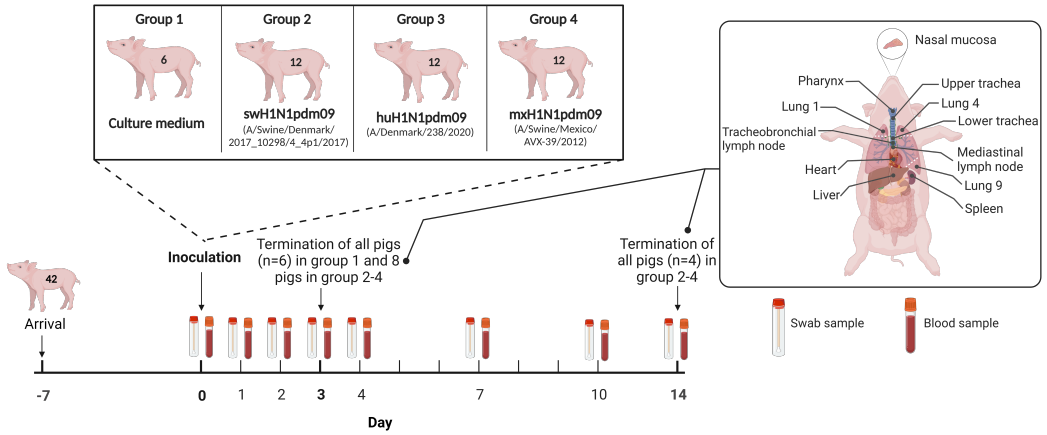

Figure 3.1: Outline of the *in vivo* animal experiment. Pigs were acclimatised for seven days. On day 0, swab and blood samples were collected before inoculation with culture medium (control) or influenza A virus (IAV). On day 3, all control pigs were euthanised together with eight pigs from the infected groups. On day 14, the remaining pigs were euthanised. Indicated tissues were collected at euthanisation. Throughout the study, swab and blood samples were collected (days 1-4, 7, 10, and 14 after inoculation).

3.2 Establishment of a solid *in vitro* model

In vivo experiments to study the host response to IAV and other pathogens in a well-suited animal model, such as pigs, are highly relevant and reliable. However, *in vivo* studies are very costly and time-consuming, and there can be a large animal-to-animal variation in larger animal models. An experimental infection study, as described above, is not the most 3R-compliant study either. The 3R's; replacement, reduction, and refinement, was first described in 1959 by Russell and Burch and proposed a set of guidelines for animal experiments [109]. Replacement is substituting conscious animals with insentient material, such as cell cultures. Reduction encourages reducing the number of animals within an experiment, while refinement asks to reduce the amount of distress to an absolute minimum

for the animals, which still has to be used [109]. In **Paper 5**, the use of *ex vivo* swine nasal mucosal explants (NEs) for transcriptional analysis of the innate immune response after IAV infection was described. This model complies with the 3R's as no pigs will be infected, and many NEs (up to 12 per pig, many more for a full-grown slaughter pig) can be obtained from each animal. However, *ex vivo* host transcriptional responses to IAV cannot always be translated to *in vivo* responses as the antiviral response can get masked by host responses to tissue damage introduced during excision [110] of the nasal mucosa or simply by culturing at ALI as described in **Paper 5**. NEs are isolated from different pigs, and the exact harvesting site can vary, which increases the variability between the different explants. In addition, contamination from bacteria or other respiratory viruses in the nasal cavity could potentially influence the results. NEs need to be cultured straight after isolation, making this model less flexible. This highlights the importance of establishing a flexible, abundantly available, and highly reproducible *in vitro* model.

A pilot study was conducted using immortalized swine nasal epithelial cells (siNEC) [111] (kindly provided by Victoria Meliopoulos, St. Jude Children's Research Hospital). The cells were expanded in flasks and plated onto 24-well transwell inserts (3.3×10^4 cells/per well) coated with rat-rail collagen (50μg/ml; Corning) in growth medium (DMEM/F12 supplemented with GlutaMax [200 mM; Gibco], insulin [10μg/ml; Sigma], transferrin [5μg/ml; Sigma], cholera toxin [100 ng/ml; Sigma], human epidermal growth factor [25 ng/ml; Thermo Fisher], bovine pituitary extract [30μg/ml; Corning], 5% fetal bovine serum [HyClone], retinoic acid [5×10^{-8} M; Sigma], penicillin-streptomycin [100μg/ml and 100 U/ml; Gibco], and amphotericin B [0.25 μg/ml; Gibco]). When the cells were 100% confluent, the apical medium was removed to grow the cells at ALI. Basal growth medium was replaced with ALI medium (DMEM/F12 supplemented with 200 mM GlutaMax [Gibco], 2% Nu-Serum [Corning], retinoic acid retinoic acid [5×10^{-8} M; Sigma], penicillin-streptomycin [100μg/ml and 100 U/ml; Gibco], and amphotericin B [0.25μg/ml, Gibco]). Cells were cultured at 37°C and 5% CO_2 with media changed every second day until they became differentiated. The apical surface was washed with PBS to remove mucus before inoculation with IAV (multiplicity of infection (MOI) of 0.1) diluted in culture medium (MEM supplemented with 200

mM GlutaMax [Gibco] and 0.075% bovine serum albumin [Gibco]). The cells were inoculated with the same IAV strains as used in **Paper 2** and **Paper 3** (see above) to compare *in vitro* results with *in vivo* results. Control cells were inoculated with infection media only. The cells were incubated at 37°C and 5% CO_2 for 1 hour. The inoculum was removed, and cells were washed with PBS. Control and infected cells were collected in RNA lysis buffer (Zymo Research, Irvine, California) immediately after inoculation (0 hours post infection), 1 day post infection (dpi), 2 dpi, and 3 dpi (Figure 3.2).

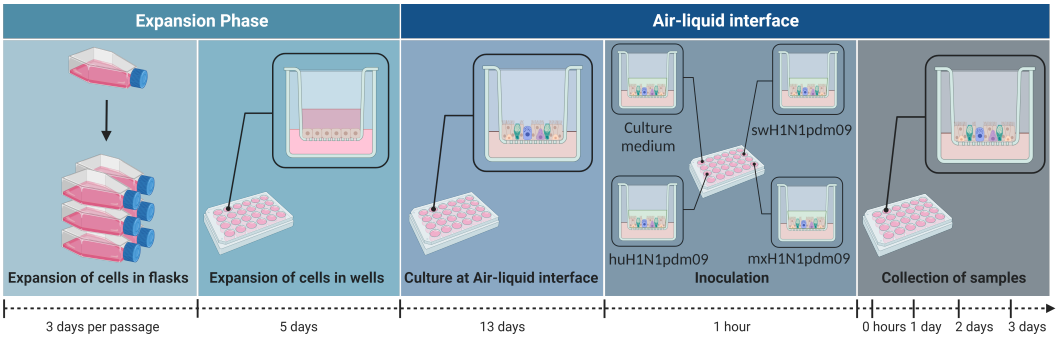

Figure 3.2: Outline of the *in vitro* experiment. siNECs were expanded in flasks before plating onto single transwell inserts. After five days, the cells were 100% confluent, and the apical medium was removed to culture the cells at air-liquid interface (ALI). The basal media was replaced with ALI media, and the cells were cultured for 13 days until they became differentiated. The cells were inoculated with culture medium (control) or influenza A virus (IAV) for 1 hour. Samples were collected immediately after inoculation (0 hours) and 1-3 days after inoculation.

RNA was extracted with the Quick-RNA Microprep Kit (Zymo Research, Irvine, California) as described in **Paper 3**. A panel of 81 genes (including six reference genes) involved in the antiviral innate immune response was investigated by microfluidic high-throughput qPCR. Expression levels at 3 dpi of selected genes relative to time-matched controls were compared to *in vivo* results described in **Paper 3** (Figure 3.3).

These preliminary results indicate that the *in vitro* results are comparable with *in vivo* results for selected key innate antiviral genes. PRRs, transcription factors, IFNs, and ISGs were induced after inoculation of pigs *in vivo* and ALI cultures *in vitro*. Both *in vitro* and *in vivo* results demonstrated lower expression levels of innate immune genes in the pigs/cells inoculated with the huH1N1pdm09 strain compared to the two other strains (swH1N1pdm09 and mxH1N1pdm09). In general, not many genes were differentially expressed *in vitro* after inoculation with the huH1N1pdm09 strain. The two other strains (swH1N1pdm09

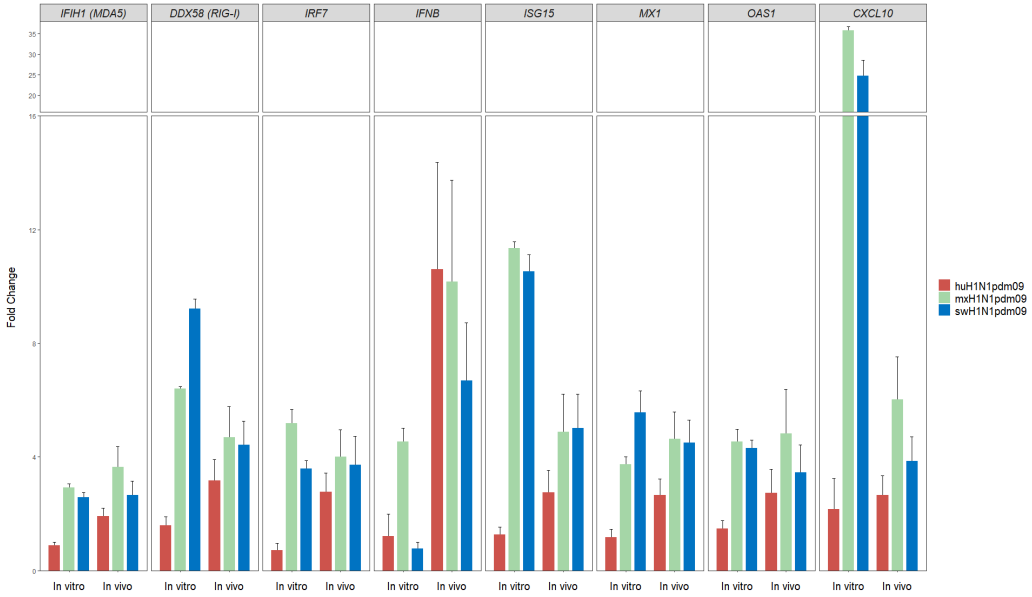

Figure 3.3: Antiviral innate immune responses are comparable *in vivo* and *in vitro*. Fold change levels described in Paper 3 (*in vivo*) and *in vitro* immortalized swine nasal epithelial cells (siNEC) cultured on air-liquid interface (ALI) 3 days after inoculation with swH1N1pdm09 (blue), huH1N1pdm09 (red), and mxH1N1pdm09 (green) compared to mock-inoculated pigs/cells.

and mxH1N1pdm09) induced a strong antiviral response. However, at 1 dpi significant differential expression of innate factors was only seen for three ISGs in the ALI cultures inoculated with the mxH1N1pdm09 (*BST2*, *ISG15*, and *IFIT1*) (data not shown). This is a huge contrast to the results obtained *in vivo* where many innate immune genes were already regulated at 1 dpi in all the infected groups. In contrast, most regulation was found at 3 dpi *in vitro*. Further, the magnitude of the response differed for some genes, especially *IFNB* and *CXCL10*, with *IFNB* being highly induced *in vivo* where *CXCL10* induction was stronger *in vitro*. Besides the obvious environmental differences, it should be noted that the pigs were inoculated with 3 ml of 10^7 $TCID_{50}$/ml of IAV, while the ALI cultures were inoculated with 100 µL IAV solution at a MOI of 0.1. MOI is the average number of virus particles infecting each cell, while $TCID_{50}$ is the dose which will infect 50% of challenged cells. Thus, some of the incongruences could be due to dosing differences.

4 Papers

4.1 Paper 1

Zoonotic and reverse zoonotic transmission of viruses between humans and pigs

Helena Aagaard Glud, Sophie George, Kerstin Skovgaard, and Lars Erik Larsen

Corresponding Author: Helena Aagaard Glud, haaglu@dtu.dk

Published in APMIS (2021) 129: 675–693.

doi:10.1111/apm.13178

It is not feasible to print supplementary material due to the file size;
it is freely available upon request
haaglu@dtu.dk

APMIS JOURNAL OF PATHOLOGY, MICROBIOLOGY AND IMMUNOLOGY

APMIS 129: 675–693

DOI 10.1111/apm.13178

REVIEW ARTICLE

Zoonotic and reverse zoonotic transmission of viruses between humans and pigs

HELENA AAGAARD GLUD,[1,*] SOPHIE GEORGE,[2,*] KERSTIN SKOVGAARD[1] and LARS ERIK LARSEN[2]

[1]Department of Biotechnology and Biomedicine, Technical University of Denmark, Kongens Lyngby, Denmark; [2]Department of Veterinary and Animal Sciences, University of Copenhagen, Copenhagen, Denmark

Glud HA, George S, Skovgaard K, Larsen LE. Zoonotic and reverse zoonotic transmission of viruses between humans and pigs. APMIS. 2021; 129: 675–693.

Humans and pigs share a close contact relationship, similar biological traits, and one of the highest estimated number of viruses compared to other mammalian species. The contribution and directionality of viral exchange between humans and pigs remain unclear for some of these viruses, but their transmission routes are important to characterize in order to prevent outbreaks of disease in both host species. This review collects and assesses the evidence to determine the likely transmission route of 27 viruses between humans and pigs.

Key words: Zoonosis; reverse zoonosis; viruses; pig; human.

Helena Aagaard Glud, Department of Biotechnology and Biomedicine, Technical University of Denmark, Søltofts Plads, Building 224, 2800 Kongens Lyngby, Denmark. e-mail: haaglu@dtu.dk

*These authors have contributed equally.

INTRODUCTION

Viruses circulating in wildlife reservoirs can spillover into susceptible human populations and contribute significantly to the global burden of human infectious diseases, which cause approximately 2.5 billion infections and 2.7 million deaths each year [1,2]. Before emerging as zoonotic human pathogens, wildlife-adapted viruses must first overcome a series of epidemiological barriers, such as behavioral barriers (level of human exposure to zoonotic viruses), interspecies barrier, and immunological barriers [3].

Livestock are able to facilitate viral spillover from wildlife to humans by acting as "epidemiological bridges" or intermediate hosts in the transmission chain [4,5]. Unsurprisingly, through thousands of years of close contact animal husbandry and intensive farming in recent decades, domesticated animals harbor eight times more zoonotic viruses than predicted in other non-domesticated mammalian species [6]. Opportunities for viral zoonosis accompany the expansion of human agricultural activities, which provoked over 50% of zoonotic emerging infectious disease (EID) events during the past 70 years [7]. Wildlife, however, is not the only threat to livestock; close contact humans can also be a source of viral zoonosis (hereafter referred to as reverse zoonosis and also known as zooanthroponosis and anthroponosis), which is somewhat understudied [8].

A recent study estimated that humans exchange the highest number of viruses with domesticated pigs (*Sus scrofa domesticus*) (n ≈ 31 viruses), cattle (n ≈ 31 viruses), horses (n ≈ 31 viruses), and dogs (n ≈ 27 viruses), surpassing both domestic cats (n ≈ 16 viruses) and goats (n ≈ 22 viruses) [6]. Pigs have served as intermediate, amplification, and "mixing" hosts in past human epidemics and pandemics (e.g., Japanese encephalitis [9], Nipah [10], and influenza A viruses [11]), and humans have spread viruses to pigs in return (e.g., influenza A virus [12]). Global demand for pork continues to rise and, although pig farming practices differ

Received 12 April 2021. Accepted 28 August 2021

worldwide, the movement of swine and multiple contact points with humans, i.e., at farms, breeding facilities, slaughterhouses, wet markets, and trade shows, intensifies the opportunities for viral transmission [13–15]. Furthermore, pigs are increasingly used for xenotransplantation and as animal models for human diseases and conditions due to their physiological, genetic, and immunological similarities to humans [16–19]. Therefore, understanding the viral exchange at the swine–human interface can help prevent zoonotic and reverse zoonotic viral outbreaks, leading to disease, deaths, culling of swine herds, and economic losses [20].

Predicting EIDs in humans and pigs is challenging. Viral zoonoses are considered rare in humans relative to the extensive viral diversity in the animal kingdom, and viral dynamics are strongly amenable to selection mechanisms resulting in rapid changes to viral landscapes [21–24]. Spillover events can occur incidentally into "dead-end" hosts, or viral outbreaks can ensue with sustained onward transmission within the novel host population, and can even become a persistent endemic threat [23,25]. Determining the natural reservoir species and intermediate hosts of EIDs after a spillover event is also demanding when routine surveillance is not in place [26]. Furthermore, the novel host of an EID can become a newfound viral reservoir and spillover into the next susceptible species, e.g., SARS-CoV-2 transmission chain from horseshoe bats-to-unknown mammalian intermediate-to-humans-to-mink-to-humans [26–28].

In this review, we collect genetic-, pathogenic-, and immunological-based evidence to determine the likely direction of viral transmission between humans and pigs with the purpose of identifying viral threats to human and pig health, and the roles humans and pigs play as direct viral reservoirs for each other.

MATERIALS AND METHODS

A framework of factors (Table S1) was designed and applied in scientific literature surveys to assess the infectivity and transmissibility of 27 viruses naturally found in humans and pigs within the past 70 years. The focus is largely on the detection of human or pig-associated viruses in the secondary host, genetic variation between viral strains isolated from the two hosts, viral entry into target host cells, detection of viral shedding that indicates viral replication in the host and transmission potential, viral dissemination in the host, and the ability for the host's immune system to suppress infection. This information is highlighted in Table S2 with distinctions drawn between humans and pigs where appropriate. The viruses were then determined to demonstrate zoonotic, reverse zoonotic, or bidirectional viral transmission according to the definitions in Box 1, and the results are summarized in Table 1.

The list of viruses shared by humans and pigs was taken from a recent study by Johnson et al., 2020 [6]. However, we were unable to find documentation of natural infection (either detection of viral genetic material or serological evidence of an antibody response against viral infection) in pigs for Ilheus, Ljungan, Monkeypox (experimental inoculation in pig skin only [29]), and Wesselsbron viruses (one study indicated serological evidence of infection in pigs but was inaccessible [30]). Tioman virus was included, despite undetected natural infection in pigs, due to evidence from an *in vivo* experimental infection study [31].

RESULTS AND DISCUSSION

Pigs as reservoirs for zoonotic viruses

The majority of the reviewed zoonotic viruses originate from wildlife reservoirs (Table 1). Pigs are significant intermediate and amplification hosts for the transmission of at least seven wildlife viruses to humans: Nipah (NiV), Japanese encephalitis (JEV), Eastern equine encephalitis (EEEV), Vesicular stomatitis (VSV), Reston ebola (RESTV), Menangle (MenPV), and potentially Tioman (TioV) (Table 1). Transmission routes of these zoonotic viruses from pigs to humans are illustrated in Fig. 1, which are generally linked to occupational exposure.

Global livestock abundance and destruction of wildlife habitats have been associated with increased zoonotic spillover risk [6]. Following a rapid increase in the past few decades, approximately 800 million to 1 billion pigs are produced globally each year in often dense and genetically homogenous populations [32,33], owing to 95% of genetic resources being exported from Europe and the USA to developing countries between 1990 and 2005 [34]. Although increased homogeneity in a

BOX 1. Definitions of viral transmission and reservoirs used in this review.

Zoonotic viruses amplify in pigs and shed sufficient amounts to infect close contact humans, but viruses infecting humans are unable to infect pigs, thereby, pigs are viral reservoirs for humans (pig-to-human transmission), or zoonotic viruses infect humans directly from another reservoir species without significant involvement of pigs.

Reverse zoonotic viruses amplify in humans and transmit to pigs, but pigs are unable to infect humans in return, in which case, humans are viral reservoirs for pigs (human-to-pig transmission).

Bi-directional zoonotic viruses are exchanged between humans and pigs, whereby, both hosts are reservoirs for the other (both zoonotic and reverse zoonotic).

Table 1. Summary of transmission routes and sources of the 27 reviewed viruses.

Virus and taxonomy	Transmission route (→ denotes direction)	Significant viral reservoir
Zoonotic viruses (1): Pigs as major sources of viruses		
Eastern equine encephalitis (EEEV); *Alphavirus; Togaviridae*.	Mosquito (*Aedes, Coquillettidia,* and *Uranotaenia* species) → human/pig [143]: vector-borne. Pig → mosquito: vector-borne [43]. Pig → pig/human: oronasal contact with infected oropharyngeal secretions or fecal-oral [43].	Birds are natural hosts (e.g., wading birds, passerine songbirds, and starlings) [143]. Pigs are potential amplification hosts [43].
Japanese encephalitis (JEV); *Flavivirus; Flaviviridae*.	Mosquito (*Culex* and *Aedes* species) → human/pig: vector-borne [143]. Pig → mosquito: viremia, vector-borne [44,45]. Pig → human: oronasal contact with infected oronasal secretions oronasal secretions [47]. Mosquito → mosquito: transovarial [9].	Aquatic birds are natural hosts. Pigs are amplification hosts [9].
Menangle (MenPV); *Rubulavirus; Paramyxoviridae*.	Fruit bat (*Pteropus* species) → pig: oronasal contact with environmental contamination [59,62]. Pig → pig: fecal-oral or urinary-oral or transplacental [144,145]. Pig → human: possibly infected bodily fluid in cuts [60].	Fruit bats (*Pteropus* species) are natural hosts [59,62]. Pigs are possible intermediate hosts [60,61].
Nipah (NiV); *Henipavirus; Paramyxoviridae*.	NiV-Malaysia: Fruit bat (*Pteropus* species) → pig: oronasal contact with environmental contamination [146]. Pig → pig: airborne or oronasal contact with infected oronasal secretions [147]. Pig → human: airborne or oronasal contact with infected oronasal secretions [148]. NiV-Bangladesh: Fruit bat (*Pteropus* species) → human: food-borne consumption of contaminated date palm sap [149]. Human → human: oronasal contact with infected human bodily fluids, limited transmission chain but caused ~50% of cases [149]. Pig → human: undocumented but possible [150].	Fruit bats (*Pteropus* species) [151,152]. Pigs are amplifications hosts for NiV-Malaysia and potentially for NiV-Bangladesh [10,150].
Reston ebola (RESTV); *Ebolavirus; Filoviridae*.	Fruit bat (likely *Miniopterus* species) → pig: oronasal contact with environmental contamination [153]. Pig → pig: oronasal contact with infected nasopharyngeal secretions [58]. Pig → human: oronasal contact with infected nasopharyngeal secretions [58,154].	Fruit bats (likely *Miniopterus* species) are natural hosts [153]. Pigs are intermediate hosts [154].
Tioman (TioV); *Rubulavirus; Paramyxoviridae*.	Fruit bat (*Pteropus* species) → pig/humans: oronasal contact with environmental contamination [64]. Pig → pig/human: possible airborne or oronasal contact with oronasal secretions [31].	Fruit bats (*Pteropus* species) are natural hosts [31,63]. Pigs are potentially intermediate hosts [64].

Table 1 *(continued)*

Virus and taxonomy	Transmission route (→ denotes direction)	Significant viral reservoir
Vesicular stomatitis (VSV); *Vesiculovirus; Rhabdoviridae*.	Vertebrate reservoir → biting insect: vector (biological and mechanical [50,155]). Biting insect → pig/human: vector. Pig → pig/human: possible vector [46,50], airborne, oronasal contact with infected oronasal secretions, or contact with infected vesicular lesions [48–50].	Unknown vertebrate reservoir host but likely multiple livestock (including pigs) and wildlife species [156].
Zoonotic viruses (2): Pigs as minor sources of viruses		
Banna (BAV); *Seadornavirus; Reoviridae*.	Mosquito (*Culex* and *Aedes* species) → human/pig: vector-borne [157,158].	Potentially mosquito as replication has been demonstrated in mosquito cell line (C6/36) and replication in mammalian cell lines is not possible (BHK-21 and Vero) [159]. Although replication in mice has been demonstrated (develop viremia), re-infection was not possible [160].
Cache Valley (CVV); *Orthobunyavirus; Bunyaviridae*.	Mosquito (*Aedes, Coquillettidia, Culex, Culiseta, Orthopodomyia, Psorophora,* and *Uranotaenia* species) → human/pig: vector-borne [161,162]. Mosquito → mosquito: transovarial demonstrated experimentally [163].	Deer [164,165].
Chandipura (CHPV); *Vesiculovirus; Rhabdoviridae*.	Sandfly (*Phlebotomine*) → human/pig: vector-borne (demonstrated in mice [166]). Sandfly → sandfly: transovarial and venereal [167].	Potentially sandfly (*Phlebotomine*) species as replication has been demonstrated in vector [166].
Encephalomyocarditis (EMCV); *Cardiovirus; Picornaviridae*.	Rodent → human/pig: fecal/urinal-oral [168]. Pig → pig: fecal-oral or oronasal contact with infected nasal secretions [169].	Rodents [169].
Foot-and-mouth disease (FMDV); *Aphthovirus; Picornaviridae*.	Pig → pig: airborne, oronasal contact with infected oronasal secretions, physical contact with secretions in cuts, environmental contamination (equipment, clothing, animal feed) [170]. Pig → human: potentially by direct contact with secretions through damaged skin [171,172].	African Cape buffalo (*Syncerus caffer*) (serotypes SAT-1, 2, and 3) [173].
Getah (GETV); *Alphavirus; Togaviridae*.	Mosquito (*Culex, Anopheles, Aedes, Armigeres,* and *Mansonia* species) → human/pig: vector-borne [174]. Pig → pig: vertically to fetus during early stage of pregnancy [175].	Potentially cattle (strong serological evidence) [174].
Louping ill (LIV); *Flavivirus; Flaviviridae*.	Tick (*Ixodes ricinus*) → human/pig: vector-borne [176,177]. Sheep → human: contact with infected sheep, sheep tissues, or raw milk [176–178].	Ticks (*Ixodes ricinus*), sheep, and red grouse [176,177].
Rabies (RABV); *Lyssavirus; Rhabdoviridae*.	Canine (*Carnivora*) or bat (*Chiroptera*) → pig/human: bite with infected saliva [71]. Pig → pig: uncommon unless infected with "furious" form and bite [73]. Pig → human: undocumented but possible [73]. Human → pig: unlikely due to behavioral factors. Human → human: only through organ/tissue transplant [72].	Canine (*Carnivora*) and bat (*Chiroptera*) species are natural hosts [71].

Table 1 *(continued)*

Virus and taxonomy	Transmission route (→ denotes direction)	Significant viral reservoir
Toscana (TOSV); *Phlebovirus; Bunyaviridae*.	Vertebrate → sandfly (*Phlebotomus*): vector-borne → pig/human [68,179,180].	Vector reservoir is sandfly (*Phlebotomus* species). Unknown vertebrate reservoir host but likely multiple livestock and wildlife species. Unclear contribution of pigs in epidemiology [179,180].
Venezuelan equine encephalitis (VEEV); *Alphavirus; Togaviridae*.	Horse or rodent → mosquito (*Ochlerotatus* or *Culex* species): vector-borne [70]. Mosquito → pig/human: vector-borne [69,70] Mosquito → human → mosquito: possible humans can develop sufficient viremia to infect mosquito [181]. Human → human: airborne or oronasal contact possible but unproven [182].	Horses are amplification host for epidemic subtypes, and rodents are reservoirs for endemic subtypes [70].
Reverse zoonotic viruses		
Norovirus (NoV); *Norovirus; Caliciviridae*.	Human → human: depending on strain fecal-oral, vomit-oral, food-/water-borne (dependent on strain) (reviewed in 86). Human → pig: possibly fecal-oral, but not directly detected [84,183,184]. Pig → pig: fecal-oral [83].	Unknown source of novel strains emerging in human populations but immunocompromised patients in nosomical settings are significant reservoirs [86].
Severe acute respiratory syndrome related-coronavirus (SARSr-CoV); *Betacoronavirus; Coronaviridae*.	Horseshoe bat (*Rhinolophus* species) → (unknown mammalian intermediary, possible recombination with pangolin-CoV) → human: oronasal contact with infected secretions or excretions [26,75,185,186]. Human → human: airborne [187]. Human → pig: foodborne via contaminated animal feed (restaurant leftovers) [76], possibly airborne/oronasal contact [78].	Horseshoe bat (*Rhinolophus* species) are natural hosts [185]. Humans are reservoir hosts [75].
Swine vesicular disease (SVDV); *Enterovirus; Picornaviridae*.	Human → pig: possibly fecal-oral or oronasal contact with infected oronasal secretions or contaminated environment containing recombinant coxsackievirus B (CV-B) and CV-A9 [79–81]. Pig → pig: oronasal contact with environmental contamination during transportation [188].	Humans are reservoir hosts for ancestral strain [80]. Virulence decreased through subsequent passages in pigs [81,189].
Bidirectionally transmitted viruses		
Hepatitis E (HEV); *Orthohepevirus*; *Hepeviridae*.	Pig → human: foodborne, consumption of raw or undercooked pig products, or direct contact [102,103]. Human → human: fecal-oral via consumption of feces-contaminated water (type 1 and 2 in developing countries), or blood transfusion [102,103]. Pig → pig: fecal-oral [103]. Human → pig: undetected but possible [104,105].	Pigs [102].

Table 1 *(continued)*

Virus and taxonomy	Transmission route (→ denotes direction)	Significant viral reservoir
Influenza A (IAV); *Alphainfluenzavirus*; *Orthomyxoviridae*.	Human ↔ pig: airborne or oronasal contact with infectious oronasal secretions [190]. Human → human: airborne or oronasal contact with infectious oronasal secretions [190]. Pig → pig: airborne or oronasal contact with infectious oronasal secretions [190].	Wild aquatic birds are natural hosts [191]. IAV subtypes circulate in human and pig populations [12].
Influenza C (ICV); *Gammainfluenzavirus; Orthomyxoviridae*.	Human ↔ pig: possible but unknown if ICV transmitted from pigs to humans or from humans to pigs [111,192]. Human → human: airborne or oronasal contact with infectious oronasal secretions [192]. Pig → pig: airborne or oronasal contact with infectious oronasal secretions, demonstrated in contact pigs experimentally infected with human and pig-derived ICV [113].	Humans [192].
Picobirnavirus (PBV); *Picobirnaviridae*.	Human ↔ pig: fecal-oral or oronasal contact with infected respiratory secretions [193,194].	Prokaryotes in host microbiome are likely hosts [98].
Ross River (RRV); *Alphavirus; Togaviridae*.	Marsupial or horse → mosquito (*Ades* and *Culex* species): vector-borne. Mosquito → human/pig: vector-borne [195]. Human → mosquito → human: vector-borne, occurs during urban epidemics [115,117]. Human/pig → mosquito → human/pig: possibly vector-borne [116,117,196].	Marsupials in Australia [197] or horses in South Pacific islands [196].
Rotavirus genogroup A (RVA); *Rotavirus; Reoviridae*.	Human ↔ pig: fecal-oral, respiratory, food/water-borne [108,198–200].	Diverse animal reservoirs including humans, porcine, bovine, ovine, pteropine, rodent, avian, and insectivore species [198,200].
Torque teno (TTV); *Alphatorquevirus* (huTTV), *Iotatorquevirus* (TTSuV1), *Kappatorquevirus* (TTSuVK2); *Anelloviridae*.	Human ↔ pig: contact with environmental contamination, e.g., contamination of TTSuV detected in veterinary vaccines, human drugs and pork products [92,93], and TTV found ubiquitously in the environment including water sources and hospitals [91,94].	Unknown sources of emergent strains.

swine herd is unlikely to increase their susceptibility to epidemics, the severity of epidemics is likely to be enhanced [35]. Furthermore, the frequency of animal turnover with immunologically naïve litters of piglets in swine herds can stunt the development of herd immunity against viral infections and enable viral persistence [36].

Deforestation and encroachment of pig farms into *Pteropus* fruit bat species habitats have been implicated in causing the zoonotic NiV epidemic in pigs and human pig farm workers in Malaysia and Singapore in 1999 [37]. The spillover of NiV-Malaysia (NiV-M) into pig herds was traced back to two introductions from fruit bats, with isolates from local bats, pigs, and humans sharing >99% nucleotide homology [10,38,39], indicating transmission between hosts required limited viral adaptation. However, humans developed more severe disease with 40% case fatality rate compared to 1-5% in pigs [40]. This difference in disease severity could be linked to higher expression of the receptor ephrin-B2 on human tracheal and bronchial airway

epithelial cells than in pigs, leading to more efficient infection [41]. NiV-M did not transmit between humans and viral RNA was isolated from 30% of infected throat swabs [42]; therefore, it seems unlikely that infected humans posed a risk to pigs.

Pigs contribute to the epidemiology of three zoonotic arthropod vector-transmitted viruses: EEEV, JEV, and VSV. In addition to causing viremia in pigs [43–45], EEEV can be recovered from oropharyngeal, rectal, and tonsil swabs, JEV can shed in oronasal secretions, and VSV can exude from ruptured vesicular fluids, providing further transmission routes to close contact humans (Fig. 1) [43,47–50]. However, VSV has infrequently infected farm and laboratory workers [51], likely due to the capability of human myxovirus resistance protein dynamin-like GTPase 1 (M×A) in reducing VSV replication by 90% compared to the porcine homolog Mx1, which inhibits only 25% of VSV replication [52–54].

Antibodies against RESTV were detected in 6.3% of exposed pig farm workers in the Philippines [55]. Unlike other ebolavirus species, which cause severe hemorrhagic fever in humans [56], RESTV is unable to suppress interferon (IFN) signaling immune response in humans [57]. However, pigs develop gross abnormalities in the lymphatic and respiratory systems after experimental infection and shed RESTV in nasopharyngeal secretions, which transmit RESTV to neighboring pigs [58].

An outbreak of MenPV occurred in an Australian piggery farm in 1997 with symptoms of reproductive disease in pigs, which included increased fetal death and abnormalities, and stillborn piglets [59]. Additionally, neutralizing antibodies were detected in adult pigs and two farm

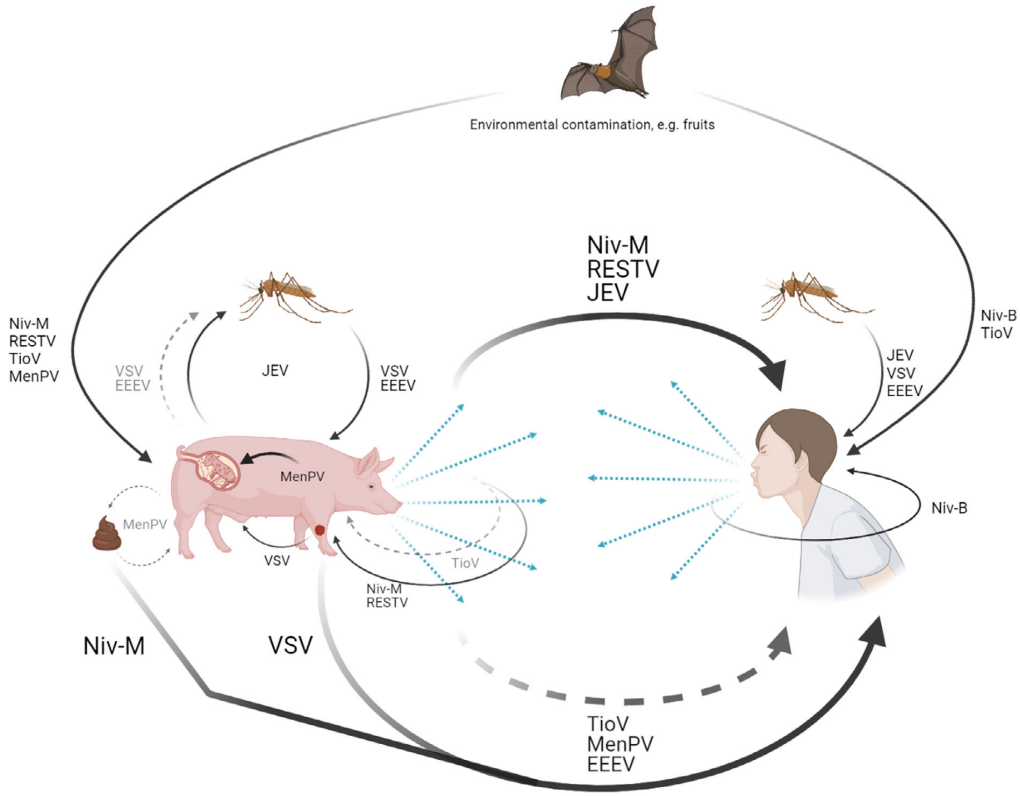

Fig. 1. Transmission routes for seven zoonotic viruses. Solid arrows indicate transmission route, while dashed arrows indicate potential transmission route. The figure was created with BioRender.com.

workers who developed an unexplained febrile illness [59,60]. MenPV isolated from a stillborn piglet replicated in secondary lymphoid organs and intestines in experimentally infected pigs and shed in oronasal secretions, feces, and urine for under a week [61]. The source of MenPV was assumed to be local *Pteropus* fruit bat species based on serological evidence and later confirmed following the isolation of MenPV from fruit bat urine samples, which shared 94% nucleotide homology to the pig isolates [59,62].

TioV was also discovered in *Pteropus* fruit bat species in Tioman Island, Malaysia [63]. Outbreaks of TioV have not been reported in either humans or pigs, but due to fruit bats harboring other zoonotic viruses, a serological survey of the Tioman Island population found 1.8% of islanders were seropositive for antibodies against TioV [64]. TioV is unable to inhibit IFN-α/β signaling in human kidney cells, but can interfere with proinflammatory cytokine interleukin 6 (IL-6) and IFN-β promoter induction to cause infection [65]. Following experimental infection in pigs, TioV was isolated from oral swabs and neutralizing antibodies developed without inducing clinical signs [31]. This implicates pigs as potential amplification hosts if TioV spills over from bats.

Other reservoir host species for zoonotic viruses

Pigs appear to be minor, incidental hosts in the transmission chain for eleven zoonotic viruses. Although, more research is required to substantiate the insignificant contribution from pigs in the maintenance of many of these viruses. The majority are vector-borne viruses: Toscana (TOSV), Venezuelan equine encephalitis (VEEV), Banna, Cache Valley, Chandipura, Getah, and Louping ill, and three are non-vector-borne viruses: rabies (RABV), encephalomyocarditis, and foot-and-mouth disease virus (Table 1).

Despite causing acute meningitis in humans [66,67], the reservoir host species maintaining TOSV remains unknown, but likely involves a cyclic combination of arthropod, wildlife, and domesticated animals, akin to most other arbovirus maintenance cycles (Table 1). One serological survey detected IgG antibodies against TOSV in 22% of tested pigs in Spain [68], but further research efforts in pigs are lacking. Serological surveys for VEEV infection in pigs have also received limited attention since the last survey conducted in 1971 [69]. However, horses and rodents have been identified as the main amplifying hosts for epidemic and endemic strains of VEEV [70].

Other zoonotic viruses present a threat to the wider human population, beyond immediate farm and laboratory workers. Each year, RABV causes 59,000 deaths in humans usually bitten by rabid canines or bats [71]. Although RABV has been isolated from human secretions, the risk of human-to-human transmission is almost exclusively through organ transplantations [72]. RABV incidence in pigs is rare, and the "furious" form causing aggression with biting has only been recorded once in China [73]. As a generalist virus capable of infecting a wide range of species, RABV genetic diversity correlates with geographical origin rather than specialization in different host species, as RABV isolated from a pig shared 99.7% nucleotide homology in the partial N gene to a circulating "street" strain from a rabid canine isolated in the previous year [73].

Humans as reservoirs for reverse zoonotic viruses

Humans have spread three viruses: severe acute respiratory syndrome-related coronaviruses (SARSr-CoV), swine vesicular disease (SVDV), and noroviruses (NoV), to pigs through varied transmission routes (Table 1) illustrated in Fig. 2 together with bidirectionally transmitted viruses (addressed in the next section).

Although SARSr-CoV originate from *Rhinolophus* horseshoe bat species and spilled over into humans through an intermediary species, humans rapidly became an effective transmitting host and viral reservoir for SARS-CoV in 2003 and SARS-CoV-2 in 2019 [74,75]. SARS-CoV was transmitted to pigs in China presumably via contaminated feed from restaurant leftovers [76], but there has been no evidence of natural infection in swine with SARS-CoV-2. However, both SARSr-CoV appear to replicate poorly in pigs [77,78], possibly due to less efficient viral attachment to the porcine angiotensin-converting enzyme 2 (ACE2) homolog receptor, which shares 81% nucleotide identity with the human ACE2 receptor [75,78].

During human meningitis epidemics between 1948 and 1964, SVDV emerged in pigs as a genetic sublineage of human-infecting coxsackievirus B (CV-B) [79–81]. Periodic outbreaks in pigs arose in Europe and Asia until 2007 with SVDV becoming progressively adapted to swine as later SVDV isolates (post-1990s) lost the ability to bind human decay-accelerating factor as a co-receptor and infect humans [82].

Highly genetically diverse NoV infect a broad range of species, but strains belonging to genogroup II (GII) exclusively infect humans and pigs [83]. Human-associated NoV (huNoV) have been

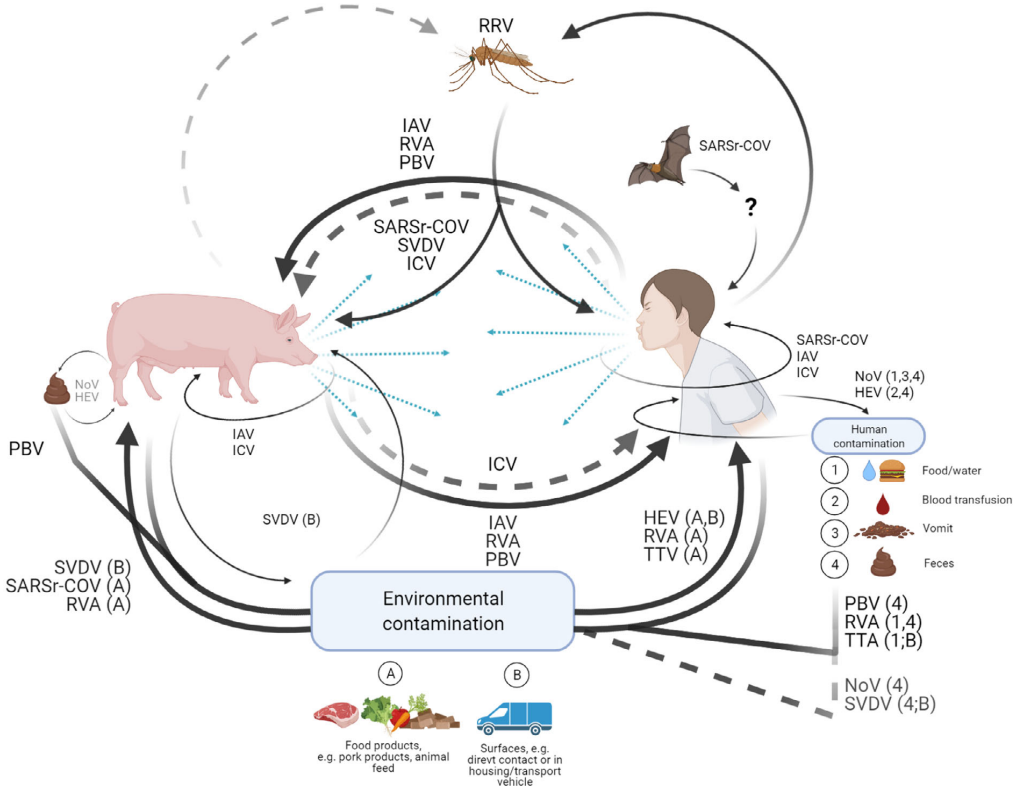

Fig. 2. Transmission routes for three reverse zoonotic and seven bidirectionally transmitted viruses. Solid arrows indicate transmission route, while dashed arrows indicate potential transmission route. The figure was created with BioRender.com.

detected in pigs, but porcine-associated NoV (porNoV) have never been detected in humans [84–86]. porNoV were unable to bind histo-blood group antigens (HBGA) as co-receptors on human cells, whereas huNoV-GII.P4 was able to bind to duodenal and buccal tissues from either A+ or H+ phenotype HBGA pigs [84,87].

Bidirectional viral transmission

Theoretically, a virus with the ability to infect and induce viral shedding in both humans and pigs can transmit between the two species. Non-enveloped viruses are typically stable in the environment, which increases potential routes for transmission [88–90]. Seven viruses demonstrate bidirectional transmission by this principal (Table 1 and Fig. 2), four of which are non-enveloped: Torque teno (TTV), picobirnavirus (PBV), hepatitis E (HEV), rotavirus A (RVA), and three are enveloped: influenza A (IAV), influenza C (ICV), and Ross River (RRV).

TTV and PBV are considered opportunistic pathogens due to their ubiquitous detection in both diseased and healthy human and pig populations and in various environments [91–96]. Although specific TTV species of varying genome sizes are associated with human or pig infection, human-associated *Alphatorquevirus* TTV species (huTTV) have been detected in 80% of pig sera samples and porcine-associated *Iotatorquevirus* and *Kappatorquevirus* TTV species (TTSuV1 and TTSuVK2) have been detected in 92.5% of human sera samples [97], indicating viral exchange between the hosts. Growing evidence indicates PBV infects prokaryotes in the microbiome of humans and pigs [98]. Nevertheless, a genetic association between PBV

isolated from humans and pigs has been suggested [99–101].

Humans are typically infected with HEV following the consumption of raw or undercooked pork products in developed countries and through the fecal-oral transmission route in developing countries via consumption of water contaminated with human feces [102,103]. Viremia peaks during the incubation period and the early symptomatic phase, with viral shedding in feces [102, 103]. While pigs are significant sources of HEV for humans, experimental infection in pigs with HEV isolated from humans has also been demonstrated [104,105].

Similar to NoV, RVA attaches to HBGAs as coreceptors to infect host cells, the phenotype of which depends on the VP8 domain of protease-cleaved protein (P) types rather than the host species [106]. Unlike NoV, however, reassortant viruses with segments of human RVA origin have been found in pigs and vice versa [107,108].

The exchange of IAV between humans and pigs is well known. Reassortant IAV generated with segments originating from human and swine IAV have been found in both host populations [12]. One high profile example was the novel genotype of H1N1 virus, which caused a human pandemic in 2009 after a quadruple reassortant IAV containing segments from avian IAV, human H3N2 subtype, Eurasian avian-like swine IAV, and classical swine H1N1 subtype jumped from pigs into humans and back into pigs [109,110].

Although humans were the only known natural host for ICV [111,112], ICV has also been isolated from naturally infected pigs [109]. ICV strains isolated from humans during 1988-1990 were highly related to the swine isolates obtained in China during 1981–1982 [111,113], strongly suggesting interspecies transmission between humans and pigs; although, it is unknown whether the virus had transmitted from pigs to humans or from humans to pigs [111]. There is increasing evidence that other influenza species (influenza B and influenza D) are able to infect both humans and pigs and transmit between the two hosts [114].

Unlike all other zoonotic arboviruses in Table 1, RRV can potentially transmit between humans and pigs via mosquitoes. Human-to-mosquito-to-human transmission has been demonstrated during urban epidemics and pigs can also develop viremia, albeit at lower viral titers than humans [115–117].

Viral emergence, molecular evolution, and generation of diversity

To spill over into human or pig populations, either viruses possess intrinsic ability to pass through epidemiological barriers when the permitting factors align (without significant alteration to the viral genome) or viruses must first undergo substantial genetic changes to infect new host cells and evade host immune responses. Genetic divergence is driven by mutation, recombination, and reassortment and the resulting variants, haplotypes, or reassortants either propagate or diminish by various selective processes as the virus adapts to the new host [118,119].

RNA viruses are exceedingly more likely to be zoonotic than DNA viruses [120], given their high nucleotide substitution rates of approximately 1×10^{-3} nucleotide substitutions per site per year (ns/s/y) on average and rapid ability to adapt [121]. This is reflected in our review as all except one virus encode an RNA genome (Table S2). Nucleotide substitutions in most viruses with RNA genomes occur during replication by error-prone, viral-encoded RNA polymerases, while viruses with DNA genomes employ the host cell DNA polymerase with exonuclease activity to correct errors and are additionally subjected to post-replication repair systems [119,122]. However, TTV has a DNA genome with a comparable mutation rate to RNA viruses ($0.53\text{-}0.55 \times 10^{-3}$ ns/s/y [123]) and is highly genetically diverse, which could be attributed to the persistent nature of TTV infections in the host [124].

Nucleotide substitution rates and the number of susceptible host species are uncorrelated across the reviewed viruses (Table S2). Vector-borne RNA viruses generally exhibit significantly lower mutation rates than non-vector-borne RNA viruses, with highly genetically similar strains infecting wide ranges of hosts (Table S2). For non-vector-borne RNA viruses, it is plausible that maintaining high mutation rates is necessary to adapt to a wide range of hosts. Encephalomyocarditis and foot-and-mouth disease viruses infect a broad range of hosts (30 and 72 documented hosts, respectively) and exhibit significantly higher mutation rates (1.61 and 1.45×10^{-3} ns/s/y, respectively) than vector-borne viruses [6,121,125]. However, the number of infected hosts is not a reliable proxy for mutation rate; Chandipura virus (CHPV) has a host range of 6 and the highest mutation rate at 6.577×10^{-3} ns/s/y, RABV has the widest host range (126 known hosts) but a lower mutational rate (0.09×10^{-3} ns/s/y), and SVDV rapidly adapted to swine after introduction from humans (3.84×10^{-3} ns/s/y) (Table S2). Instead, mutation rates are more likely influenced by the efficiency of virus–host cell interactions, host immune evasion, and viral reproductive strategies, among many other biotic and abiotic factors.

Major genetic changes in viruses can occur by recombination and reassortment events when host cells are co-infected with at least two viral strains (variants or distant relatives), which interact during replication to form progeny with genetic material from both strains [118,119]. In general, recombination is prevalent in single-stranded, positive-sense RNA viruses with the exception of Flaviviruses where recombination is rarely observed [118]. Novel SVDV emerged in pigs because of a probable recombination event between human-infecting coxsackievirus B (CV-B) and CV-A9; although, it is unknown whether the recombination event occurred in pigs or humans [80]. Polymerase (P) types of human- and pig-associated NoV frequently recombine with common breakpoints between open reading frame junctions [126–130], but such recombinants have only been detected in pigs [85]. Even though single-stranded, negative sense RNA viruses in general show lower rates of recombination, reassortment is frequently observed in Orthomyxoviridae, such as influenza A virus, which belong to the single-stranded, negative sense RNA viruses. Reassortment is restricted to segmented RNA viruses and can result in rapid genetic change by formation of reassortants with novel genome combinations [118]. Twenty-five percent of the assessed viruses in this review have a segmented genome, potentially making these viruses more disposed to fast adaptation to a new host/interspecies transmission.

Challenges in determining viral transmission

Our assessment of viral transmission is based on past strains of viruses. The viral landscape is under constant selective pressures, and the rapid and continuous generation of extensive genetic diversity is challenging to anticipate. Emergence of novel antigenic variants of viruses can undermine vaccination efforts, and vaccine availability against the majority of viruses is low (Table S2). Identifying the host factors a virus would need to adapt to is one modeling strategy to predict future variants, e.g., identifying viral–host protein interactions between the protein homologs in different hosts or the use of alternative host cell receptors.

RESTV is currently non-pathogenic to humans, but substitutions of three amino acids in RESTV VP24 protein might enable binding to human karyopherin alpha5, which block innate immunity pathways in the same manner as other related pathogenic ebolaviruses [57,131,132]. In addition, a truncation in RESTV VP30 in a fraction of the RESTV isolates from pigs is characteristic of the Zaire ebolavirus adaptation to human cells during several months of human-to-human transmission in the 2013-2016 ebolavirus disease outbreak [133].

Alternatively, wildlife viruses may attenuate as they passage through swine herds. NiV-M, which was transmitted from bats-to-pigs-to-humans, caused a 40% case fatality rate in humans, while NiV-Bangladesh genotype was transmitted directly from bats-to-humans via contaminated date palm sap causing over 70% case fatalities and has even transmitted onward to first contact humans [134]. The nucleotide difference between the two genotypes (8.2% [39]) is the most likely explanation for the difference in case fatality rates. Thus, viral attenuation through nucleotide changes in an intermediary host is a potential outcome.

Interactions between viruses and bacteria in the host microbiome may be another hidden factor facilitating viral transmission between humans and pigs. Certain bacteria express HBGAs to facilitate attachment of NoV to B cells, and *CagA*-positive *Helicobacter pylori* induces HBGA expression in the mucosa of individuals without a functional FUT2 gene and HGBA phenotype [135,136]. This can potentially increase the replication efficiency of particular NoV and RVA genotypes infecting humans and pigs.

Routine surveillance programs have been established for only some viruses in pigs (e.g., IAV [137]), and a few others are notifiable to international health bodies upon detection [138]. Many outbreaks lack real-time monitoring and sampling in swine herds and humans, which can make retrospective analyses difficult and viral records incomplete (e.g., SARS-CoV-2 [26]). The choice of screening assays may also exclude some viruses. However, recent technical developments of next-generation sequencing or probe-based techniques with high-throughput capabilities allow characterizing entire viromes of large populations a viable option. The overall aim of surveillance programs for emerging pathogens and zoonosis should be to act as early detection/warning systems because the success of limiting the spread of, e.g., a new zoonotic virus to a great extent relies on the possibility to contain it *before* it jumps to the first human. This in turn calls for more basic research into identification of reliable viral and host markers of species specificity for the different types of viruses combined with a *One Health*-oriented *design of the monitoring programs, i.e., by the inclusion of more targeted sampling of people in close contact with animals, e.g., swine*.

Experimental studies involving human volunteers are rare. Only IAV, ICV, NoV, and RVA have been administered in challenge studies, usually with

human-derived isolates, common circulating genotypes in the population, or attenuated viral strains [139–142]. Therefore, experiments with viruses to study human-related dynamics rely on cell culture, explants, or animal models, which have some restrictions for application in a human population. Nevertheless, these experiments provide valuable data, particularly concerning specific virus–cell interactions.

CONCLUDING REMARKS

The list of 27 viruses shared by humans and pigs are generally regarded as zoonotic [6]. Reverse zoonosis or humans' ability to transmit viruses to other animals is overlooked in some cases [8]. This review gathered evidence to assess the direction of viral transmission in the context of humans and pigs. Where direct detection was lacking, we theorized whether the virus could infect and transmit to the other host based on viral entry requirements, ability to establish infection, activation of immune responses, and shed in transmissible routes.

Transmission routes and viral sources are illustrated in Figs 1 and 2. Pigs are or have potential to be significant reservoirs, intermediaries, and amplifiers for at least seven zoonotic viruses; humans have been the source of three reverse zoonotic viruses in pigs; and humans and pigs possibly exchange seven viruses back and forth (Table 1).

The authors thank the FluZooMark group for contributing to discussions of the content of the review.

CONFLICT OF INTEREST

The authors have no conflicts of interest to declare.

FUNDING INFORMATION

The work presented in this review is part of the FluZooMark project supported by Novo Nordisk Foundation (grant NNF19OC0056326).

REFERENCES

1. Jones KE, Patel NG, Levy MA, Storeygard A, Balk D, Gittleman JL, *et al*. Global trends in emerging infectious diseases. Nature. 2008;451(7181):990–3. https://doi.org/10.1038/nature06536
2. Grace D, Mutua F, Ochungo P, Kruska R, Jones K, Brierley L, *et al*. Mapping of Poverty and Likely Zoonoses Hotspots. Zoonoses Project 4. Report to the UK Department for International Development. International Livestock Research Institute: Nairobi, Kenya. 2012.
3. Plowright RK, Parrish CR, McCallum H, Hudson PJ, Ko AI, Graham AL, *et al*. Pathways to zoonotic spillover. Nat. Rev. Microbiol. 2017;15(8):502–10. https://doi.org/10.1038/nrmicro.2017.45
4. Jones BA, Grace D, Kock R, Alonso S, Rushton J, Said MY, *et al*. Zoonosis emergence linked to agricultural intensification and environmental change. Proc. Natl Acad. Sci. 2013;110(21):8399–404. https://doi.org/10.1073/pnas.1208059110
5. Kock R. Drivers of disease emergence and spread: Is wildlife to blame? Onderstepoort J Vet Res. 2014;81(2):1–4.
6. Johnson CK, Hitchens PL, Pandit PS, Rushmore J, Evans TS, Young CCW, *et al*. Global shifts in mammalian population trends reveal key predictors of virus spillover risk. Proc Biol Sci. 2020;287(1924):20192736.
7. Rohr JR, Barrett CB, Civitello DJ, Craft ME, Delius B, DeLeo GA, *et al*. Emerging human infectious diseases and the links to global food production. Nature Sustainab. 2019;2(6):445–56.
8. Messenger AM, Barnes AN, Gray GC. Reverse zoonotic disease transmission (zooanthroponosis): a systematic review of seldom-documented human biological threats to animals. PLoS One. 2014;9(2):e89055.
9. Erlanger TE, Weiss S, Keiser J, Utzinger J, Wiedenmayer K. Past, present, and future of Japanese encephalitis. Emerg Infect Dis. 2009;15(1):1–7. https://doi.org/10.3201/eid1501.080311
10. Chua KB, Bellini WJ, Rota PA, Harcourt BH, Tamin A, Lam SK, *et al*. Nipah virus: a recently emergent deadly paramyxovirus. Science. 2000;288(5470):1432–5. https://doi.org/10.1126/science.288.5470.1432
11. Vijaykrishna D, Poon LL, Zhu HC, Ma SK, Li OT, Cheung CL, *et al*. Reassortment of pandemic H1N1/2009 influenza A virus in swine. Science. 2010;328(5985):1529. https://doi.org/10.1126/science.1189132
12. Anderson TK, Chang J, Arendsee ZW, Venkatesh D, Souza CK, Kimble JB, *et al*. Swine influenza a viruses and the tangled relationship with humans. Cold Spring Harb. Perspect Med. 2021;11(3):a038737–https://doi.org/10.1101/cshperspect.a038737
13. United States Department of Agriculture (USDA). Livestock and Poultry: World Markets and Trade. Foreign Agricultural Service. 2020 October 9. Retrieved from https://apps.fas.usda.gov/psdonline/circulars/livestock_poultry.pdf
14. Food and Agriculture Organisation of the United Nations (FAO). Pigs and Management & Housing. 2014 Nov 23. Retrieved from: http://www.fao.org/ag/againfo/themes/en/pigs/AP_management.html
15. Bowman AS, Walia RR, Nolting JM, Vincent AL, Killian ML, Zentkovich MM, *et al*. Influenza A (H3N2) virus in swine at agricultural fairs and transmission to humans, Michigan and Ohio, USA, 2016. Emerg Infect Dis. 2017;23(9):1551–5.
16. Meurens F, Summerfield A, Nauwynck H, Saif L, Gerdts V. The pig: a model for human infectious diseases. Trends Microbiol. 2012;20(1):50–7.
17. Dawson HD, Loveland JE, Pascal G, Gilbert JG, Uenishi H, Mann KM, *et al*. Structural and

functional annotation of the porcine immunome. BMC Genom. 2013;15(14):332. https://doi.org/10.1186/1471-2164-14-332
18. Mair KH, Sedlak C, Käser T, Pasternak A, Levast B, Gerner W, *et al*. The porcine innate immune system: An update. Dev. Comp. Immunol. 2014;45(2):321–43. https://doi.org/10.1016/j.dci.2014.03.022
19. Starbæk SMR, Brogaard L, Dawson HD, Smith AD, Heegaard PMH, Larsen LE, *et al*. Animal models for influenza a virus infection incorporating the involvement of innate host defenses: enhanced translational value of the porcine model. ILAR J. 2018;59(3):323–37.
20. Uddin Khan S, Atanasova KR, Krueger WS, Ramirez A, Gray GC. Epidemiology, geographical distribution, and economic consequences of swine zoonoses: a narrative review. Emerg Microbes Infect. 2013;2(12):e92.
21. Warren CJ, Sawyer SL. How host genetics dictates successful viral zoonosis. PLoS Biol. 2019;17(4):e3000217.
22. Carlson CJ, Zipfel CM, Garnier R, Bansal S. Global estimates of mammalian viral diversity accounting for host sharing. Nat Ecol Evol. 2019;3(7):1070–5. https://doi.org/10.1038/s41559-019-0910-6
23. Parrish CR, Holmes EC, Morens DM, Park EC, Burke DS, Calisher CH, *et al*. Cross-species virus transmission and the emergence of new epidemic diseases. Microbiol Mol Biol Rev. 2008;72(3):457–70.
24. Park M, Loverdo C, Schreiber SJ, Lloyd-Smith JO. Multiple scales of selection influence the evolutionary emergence of novel pathogens. Philos Trans R Soc Lond B Biol Sci. 2013;368(1614):20120333.
25. Centers for Disease Control and Prevention (CDC). Principles of Epidemiology in Public Health Practice. 2012 May. Retrieved from: https://www.cdc.gov/csels/dsepd/ss1978/SS1978.pdf
26. Friend T, Stebbing J. What is the intermediate host species of SARS-CoV-2? Future Virol. 2021;16(3):153–6.
27. Oude Munnink BB, Sikkema RS, Nieuwenhuijse DF, Molenaar RJ, Munger E, Molenkamp R, *et al*. Transmission of SARS-CoV-2 on mink farms between humans and mink and back to humans. Science. 2021;371(6525):172-7.
28. Larsen HD, Fonager J, Lomholt FK, Dalby T, Benedetti G, Kristensen B, *et al*. Preliminary report of an outbreak of SARS-CoV-2 in mink and mink farmers associated with community spread, Denmark, June to November 2020. Euro Surveill. 2021;26(5):2100009.
29. Soekawa M, Moriguchi R, Morita C, Kitamura T, Tanaka Y. Electron-microscopical observations on the development of vaccinia, cowpox and monkeypox viruses in pig skin. Zentralbl Bakteriol Orig A. 1977;237(4):425–43.
30. Baba SS, Fagbami AH, Ojeh CK, Olaleye OD, Omilabu SA. Wesselsbron virus antibody in domestic animals in Nigeria: retrospective and prospective studies. New Microbiol. 1995;18(2):151–62.
31. Yaiw KC, Bingham J, Crameri G, Mungall B, Hyatt A, Yu M, *et al*. Tioman virus, a paramyxovirus of bat origin, causes mild disease in pigs and has a predilection for lymphoid tissues. J. Virol. 2008;82(1):565–8.
32. Drew TW. The emergence and evolution of swine viral diseases: to what extent have husbandry systems and global trade contributed to their distribution and diversity? Rev Sci Tech. 2011;30(1):95–106.
33. Food and Agriculture Organisation of the United Nations (FAO). FAOSTAT Production of Pigs in. World 1980 - 2019. Accessed: 2020 Mar 5. Available from: http://www.fao.org/faostat/en/#data/QA/visualize
34. Gollin D, Van Dusen E, Blackburn H. Animal genetic resource trade flows: Economic assessment. Livestock Sci. 2009;120(3):248–55. https://doi.org/10.1016/j.livsci.2008.07.017
35. Springbett AJ, MacKenzie K, Woolliams JA, Bishop SC. The contribution of genetic diversity to the spread of infectious diseases in livestock populations. Genetics. 2003;165(3):1465–74.
36. Pitzer VE, Aguas R, Riley S, Loeffen WL, Wood JL, Grenfell BT. High turnover drives prolonged persistence of influenza in managed pig herds. J R Soc Interface. 2016;13(119):20160138.
37. Chua KB, Chua BH, Wang CW. Anthropogenic deforestation, El Niño and the emergence of Nipah virus in Malaysia. Malays J Pathol. 2002;24(1):15–21.
38. AbuBakar S, Chang LY, Ali AR, Sharifah SH, Yusoff K, Zamrod Z. Isolation and molecular identification of Nipah virus from pigs. Emerg Infect Dis. 2004;10(12):2228–30.
39. Harcourt BH, Lowe L, Tamin A, Liu X, Bankamp B, Bowden N, *et al*. Genetic characterization of Nipah virus, Bangladesh, 2004. Emerg Infect Dis. 2005;11(10):1594–7.
40. Looi LM, Chua KB. Lessons from the Nipah virus outbreak in Malaysia. Malays J Pathol. 2007;29(2):63–7.
41. Sauerhering L, Zickler M, Elvert M, Behner L, Matrosovich T, Erbar S, *et al*. Species-specific and individual differences in Nipah virus replication in porcine and human airway epithelial cells. J Gen Virol. 2016;97(7):1511–9. https://doi.org/10.1099/jgv.0.000483
42. Chua KB, Lam SK, Goh KJ, Hooi PS, Ksiazek TG, Kamarulzaman A, *et al*. The presence of Nipah virus in respiratory secretions and urine of patients during an outbreak of Nipah virus encephalitis in Malaysia. J Infect. 2001;42(1):40–3. https://doi.org/10.1053/jinf.2000.0782
43. Elvinger F, Baldwin CA, *et al*. Eastern equine encephalomyelitis virus. In: Straw BE, Zimmerman J, D'Allaire S, editors. Diseases of Swine, 9th edn. Blackwell Publishing Company; Ames, IA. 2006. p. 554–7.
44. Burke DS, Tingpalapong M, Ward GS, Andre R, Leake CJ. Intense transmission of Japanese encephalitis virus to pigs in a region free of epidemic encephalitis. Southeast Asian J Trop Med Public Health. 1985;16(2):199–206.
45. Ricklin ME, Garcìa-Nicolàs O, Brechbühl D, Python S, Zumkehr B, Posthaus H, *et al*. Japanese encephalitis virus tropism in experimentally infected pigs. Vet Res. 2016;24(47):34.
46. Velazquez-Salinas L, Pauszek SJ, Stenfeldt C, O'Hearn ES, Pacheco JM, Borca MV, *et al*. Increased virulence of an epidemic strain of vesicular stomatitis virus is associated with interference of the innate response in pigs. Front Microbiol. 2018;15(9):1891.

47. Ricklin ME, García-Nicolás O, Brechbühl D, Python S, Zumkehr B, Nougairede A, *et al*. Vector-free transmission and persistence of Japanese encephalitis virus in pigs. Nat Commun. 2016;23(7):10832.
48. Howerth EW, Stallknecht DE, Dorminy M, Pisell T, Clarke GR. Experimental vesicular stomatitis in swine: effects of route of inoculation and steroid treatment. J Vet Diagn Invest. 1997;9(2):136–42. https://doi.org/10.1177/104063879700900205
49. Stallknecht DE, Perzak DE, Bauer LD, Murphy MD, Howerth EW. Contact transmission of vesicular stomatitis virus New Jersey in pigs. Am J Vet Res. 2001;62(4):516–20. https://doi.org/10.2460/ajvr.2001.62.516
50. Mead DG, Gray EW, Noblet R, Murphy MD, Howerth EW, Stallknecht DE. Biological transmission of vesicular stomatitis virus (New Jersey serotype) by Simulium vittatum (Diptera: Simuliidae) to domestic swine (Sus scrofa). J Med Entomol. 2004;41(1):78–82. https://doi.org/10.1603/0022-2585-41.1.78
51. Letchworth GJ, Rodriguez LL. Vesicular stomatitis. Vet J. 1999;157(3):239–60. https://doi.org/10.1053/tvjl.1998.0303
52. Asano A, Ko JH, Morozumi T, Hamashima N, Watanabe T. Polymorphisms and the antiviral property of porcine Mx1 protein. J Vet Med Sci. 2002;64(12):1085–9. https://doi.org/10.1292/jvms.64.1085
53. Sasaki K, Tungtrakoolsub P, Morozumi T, Uenishi H, Kawahara M, Watanabe T. A single nucleotide polymorphism of porcine MX2 gene provides antiviral activity against vesicular stomatitis virus. Immunogenetics. 2014;66(1):25–32. https://doi.org/10.1007/s00251-013-0745-2
54. Schwemmle M, Weining KC, Richter MF, Schumacher B, Staeheli P. Vesicular stomatitis virus transcription inhibited by purified MxA protein. Virology. 1995;206(1):545–54. https://doi.org/10.1016/s0042-6822(95)80071-9
55. Miranda ME, Miranda NL. Reston ebolavirus in humans and animals in the Philippines: a review. J Infect Dis. 2011;204(Suppl 3):S757–60. https://doi.org/10.1093/infdis/jir296
56. Kobinger GP, Leung A, Neufeld J, Richardson JS, Falzarano D, Smith G, *et al*. Replication, pathogenicity, shedding, and transmission of Zaire ebolavirus in pigs. J Infect Dis. 2011;204(2):200–8. https://doi.org/10.1093/infdis/jir077
57. Guito JC, Albariño CG, Chakrabarti AK, Towner JS. Novel activities by ebolavirus and marburgvirus interferon antagonists revealed using a standardized in vitro reporter system. Virology. 2017;15(501):147–65. https://doi.org/10.1016/j.virol.2016.11.015
58. Marsh GA, Haining J, Robinson R, Foord A, Yamada M, Barr JA, *et al*. Ebola Reston virus infection of pigs: clinical significance and transmission potential. J Infect Dis. 2011;204(Suppl 3):S804–9. https://doi.org/10.1093/infdis/jir300
59. Philbey AW, Kirkland PD, Ross AD, Davis RJ, Gleeson AB, Love RJ, *et al*. An apparently new virus (family paramyxoviridae) infectious for pigs, humans, and fruit bats. Emerg. Infect. Dis. 1998;4(2):269–71. https://doi.org/10.3201/eid0402.980214
60. Chant K, Chan R, Smith M, Dwyer DE, Kirkland P. Probable human infection with a newly described virus in the family paramyxoviridae. Emerg. Infect. Dis. 1998;4(2):273–5. https://doi.org/10.3201/eid0402.980215
61. Bowden TR, Bingham J, Harper JA, Boyle DB. Menangle virus, a pteropid bat paramyxovirus infectious for pigs and humans, exhibits tropism for secondary lymphoid organs and intestinal epithelium in weaned pigs. J Gen Virol. 2012;93(Pt 5):1007–16. https://doi.org/10.1099/vir.0.038448-0
62. Barr JA, Smith C, Marsh GA, Field H, Wang LF. Evidence of bat origin for Menangle virus, a zoonotic paramyxovirus first isolated from diseased pigs. J Gen Virol. 2012;93(Pt 12):2590–4. https://doi.org/10.1099/vir.0.045385-0
63. Chua KB, Wang LF, Lam SK, Crameri G, Yu M, Wise T, *et al*. Tioman virus, a novel paramyxovirus isolated from fruit bats in Malaysia. Virology. 2001;283(2):215–29. https://doi.org/10.1006/viro.2000.0882
64. Yaiw KC, Crameri G, Wang L, Chong HT, Chua KB, Tan CT, *et al*. Serological evidence of possible human infection with Tioman virus, a newly described paramyxovirus of bat origin. J Infect Dis. 2007;196(6):884–6. https://doi.org/10.1086/520817
65. Caignard G, Lucas-Hourani M, Dhondt KP, Labernardière JL, Petit T, Jacob Y, *et al*. The V protein of tioman virus is incapable of blocking type I interferon signaling in human cells. PLoS One. 2013;8(1):e53881.
66. Charrel RN, Gallian P, Navarro-Mari JM, Nicoletti L, Papa A, Sánchez-Seco MP, *et al*. Emergence of Toscana virus in Europe. Emerg Infect Dis. 2005;11(11):1657–63.
67. Vilibic-Cavlek T, Zidovec-Lepej S, Ledina D, Knezevic S, Savic V, Tabain I, *et al*. Clinical, virological, and immunological findings in patients with toscana neuroinvasive disease in croatia: report of three cases. Trop Med Infect Dis. 2020;5(3):144.
68. Navarro-Marí JM, Palop-Borrás B, Pérez-Ruiz M, Sanbonmatsu-Gámez S. Serosurvey study of Toscana virus in domestic animals, Granada, Spain. Vector Borne Zoonotic Dis. 2011;11(5):583–7. https://doi.org/10.1089/vbz.2010.0065
69. Scherer WF, Dickerman RW, Campillo-Sainz C, Zarate ML, Gonzales E. Ecologic studies of Venezuelan encephalitis virus in southeastern México. V. Infection of domestic animals other than equines. Am J Trop Med Hyg. 1971;20(6):989–93. https://doi.org/10.4269/ajtmh.1971.20.989
70. Weaver SC, Ferro C, Barrera R, Boshell J, Navarro JC. Venezuelan equine encephalitis. Annu Rev Entomol. 2004;49:141–74. https://doi.org/10.1146/annurev.ento.49.061802.123422
71. World Health Organization (WHO). Rabies. 2020 Apr. Retrieved from: https://www.who.int/news-room/fact-sheets/detail/rabies
72. Manning SE, Rupprecht CE, Fishbein D, Hanlon CA, Lumlertdacha B, Guerra M, *et al*. Advisory Committee on Immunization Practices Centers for Disease Control and Prevention (CDC). Human rabies prevention--United States, 2008: recommendations of the Advisory Committee on Immunization Practices. MMWR Recomm Rep. 2008;57(RR-3):1-28.
73. Jiang Y, Yu X, Wang L, Lu Z, Liu H, Xuan H, *et al*. An outbreak of pig rabies in Hunan province,

China. Epidemiol. Infect. 2008;136(4):504–8. https://doi.org/10.1017/S0950268807008874
74. Zhong NS, Zheng BJ, Li YM, Poon XZH, Chan KH, *et al*. Epidemiology and cause of severe acute respiratory syndrome (SARS) in Guangdong, People's Republic of China, in February, 2003. The Lancet. 2003;362(9393):1353–8. https://doi.org/10.1016/S0140-6736(03)14630-2
75. Zhou P, Yang XL, Wang XG, Hu B, Zhang L, Zhang W, *et al*. A pneumonia outbreak associated with a new coronavirus of probable bat origin. Nature. 2020;579(7798):270-3.
76. Chen W, Yan M, Yang L, Ding B, He B, Wang Y, *et al*. SARS-associated coronavirus transmitted from human to pig. Emerg Infect Dis. 2005;11(3):446–8. https://doi.org/10.3201/eid1103.040824
77. Weingartl HM, Copps J, Drebot MA, Marszal P, Smith G, Gren J, *et al*. Susceptibility of pigs and chickens to SARS coronavirus. Emerg Infect Dis. 2004;10(2):179–84. https://doi.org/10.3201/eid1002.030677
78. Pickering BS, Smith G, Pinette MM, Embury-Hyatt C, Moffat E, Marszal P, *et al*. Susceptibility of domestic swine to experimental infection with severe acute respiratory syndrome coronavirus 2. Emerg Infect Dis. 2021;27(1):104–12. https://doi.org/10.3201/eid2701.203399
79. Zhang G, Haydon DT, Knowles NJ, McCauley JW. Molecular evolution of swine vesicular disease virus. J Gen Virol. 1999;80(Pt 3):639–51. https://doi.org/10.1099/0022-1317-80-3-639
80. Bruhn CA, Nielsen SC, Samaniego JA, Wadsworth J, Knowles NJ, Gilbert MT. Viral meningitis epidemics and a single, recent, recombinant and anthroponotic origin of swine vesicular disease virus. Evol Med Public Health. 2015;2015(1):289–303. https://doi.org/10.1093/emph/eov026
81. Lomakina NF, Yu Shustova E, Strizhakova OM, Felix Drexler J, Lukashev AN. Epizootic of vesicular disease in pigs caused by coxsackievirus B4 in the Soviet Union in 1975. J Gen Virol. 2016;97(1):49–52. https://doi.org/10.1099/jgv.0.000318
82. Jimenez-Clavero MA, Escribano-Romero E, Ley V, Spiller OB. More recent swine vesicular disease virus isolates retain binding to coxsackie-adenovirus receptor, but have lost the ability to bind human decay-accelerating factor (CD55). J Gen Virol. 2005;86(Pt 5):1369–77. https://doi.org/10.1099/vir.0.80669-0
83. Vinjé J. Advances in Laboratory Methods for Detection and Typing of Norovirus. J. Clin. Microbiol. 2015;53(2):373–81. https://doi.org/10.1128/JCM.01535-14
84. Farkas T, Nakajima S, Sugieda M, Deng X, Zhong W, Jiang X. Seroprevalence of noroviruses in swine. J Clin Microbiol. 2005;43(2):657–61. https://doi.org/10.1128/JCM.43.2.657-661.2005
85. Villabruna N, Koopmans MPG, de Graaf M. Animals as reservoir for human norovirus. Viruses. 2019;11(5):478. https://doi.org/10.3390/v11050478
86. de Graaf M, van Beek J, Koopmans MP. Human norovirus transmission and evolution in a changing world. Nat Rev Microbiol. 2016;14(7):421–33. https://doi.org/10.1038/nrmicro.2016.48
87. Cheetham S, Souza M, McGregor R, Meulia T, Wang Q, Saif LJ. Patterns of human norovirus-like particles to buccal and intestinal tissues of gnotobiotic pigs in relation to A/H histo-blood group antigen expression. J. Virol. 2007;81(7):3535–44.
88. Firquet S, Beaujard S, Lobert PE, Sané F, Caloone D, Izard D, *et al*. Survival of enveloped and non-enveloped viruses on inanimate surfaces. Microbes Environ. 2015;30(2):140–4. https://doi.org/10.1264/jsme2.ME14145
89. Geoghegan JL, Senior AM, Di Giallonardo F, Holmes EC. Virological factors that increase the transmissibility of emerging human viruses. Proc. Natl Acad. Sci. 2016;113(15):4170–5.
90. Bushman FD, McCormick K, Sherrill-Mix S. Virus structures constrain transmission modes. Nature Microbiol. 2019;4(11):1778–80.
91. Griffin JS, Plummer JD, Long SC. Torque teno virus: an improved indicator for viral pathogens in drinking waters. Virol J. 2008;3(5):112. https://doi.org/10.1186/1743-422X-5-112
92. Kekarainen T, Martínez-Guinó L, Segalés J. Swine torque teno virus detection in pig commercial vaccines, enzymes for laboratory use and human drugs containing components of porcine origin. J Gen Virol. 2009;90(Pt 3):648–53. https://doi.org/10.1099/vir.0.006841-0
93. Jiménez-Melsió A, Parés S, Segalés J, Kekarainen T. Detection of porcine anelloviruses in pork meat and human faeces. Virus Res. 2013;178(2):522–4. https://doi.org/10.1016/j.virusres.2013.09.035
94. D'Arcy N, Cloutman-Green E, Klein N, Spratt DA. Environmental viral contamination in a pediatric hospital outpatient waiting area: implications for infection control. Am J Infect Control. 2014;42(8):856–60. https://doi.org/10.1016/j.ajic.2014.04.014
95. Martínez LC, Masachessi G, Carruyo G, Ferreyra LJ, Barril PA, Isa MB, *et al*. Picobirnavirus causes persistent infection in pigs. Infect Genet Evol. 2010;10(7):984–8. https://doi.org/10.1016/j.meegid.2010.06.004
96. Yinda CK, Vanhulle E, Conceição-Neto N, Beller L, Deboutte W, Shi C, *et al*. Gut virome analysis of cameroonians reveals high diversity of enteric viruses. Including potential interspecies transmitted viruses. Msphere. 2019;4(1):e00585–18. https://doi.org/10.1128/mSphere.00585-18
97. Ssemadaali MA, Effertz K, Singh P, Kolyvushko O, Ramamoorthy S. Identification of heterologous Torque Teno Viruses in humans and swine. Sci Rep. 2016;25(6):26655. https://doi.org/10.1038/srep26655
98. Krishnamurthy SR, Wang D. Extensive conservation of prokaryotic ribosomal binding sites in known and novel picobirnaviruses. Virology. 2018;516:108–14. https://doi.org/10.1016/j.virol.2018.01.006
99. Bányai K, Martella V, Bogdán Á, Forgách P, Jakab F, Meleg E, *et al*. Genogroup I picobirnaviruses in pigs: evidence for genetic diversity and relatedness to human strains. J Gen Virol. 2008;89(Pt 2):534–9. https://doi.org/10.1099/vir.0.83134-0
100. Carruyo GM, Mateu G, Martínez LC, Pujol FH, Nates SV, Liprandi F, *et al*. Molecular characterization of porcine picobirnaviruses and development of a specific reverse transcription-PCR Assay. J. Clin. Microbiol. 2008;46(7):2402–5.
101. Chen M, Sun H, Hua X. Segment 2 sequences analysis of genogroup II picobirnavirus in pig stool in

China. Acta Virol. 2019;63(1):126–8. https://doi.org/10.4149/av_2019_108
102. Kamar N, Dalton HR, Abravanel F, Izopet J. Hepatitis E virus infection. Clin Microbiol Rev. 2014;27(1):116–38. https://doi.org/10.1128/CMR.00057-13
103. Park WJ, Park BJ, Ahn HS, Lee JB, Park SY, Song CS, *et al*. Hepatitis E virus as an emerging zoonotic pathogen. J. Vet. Sci. 2016;17(1):1–11. https://doi.org/10.4142/jvs.2016.17.1.1
104. Halbur PG, Kasorndorkbua C, Gilbert C, Guenette D, Potters MB, *et al*. Comparative pathogenesis of infection of pigs with hepatitis E viruses recovered from a pig and a human. J Clin Microbiol. 2001;39(3):918–23. https://doi.org/10.1128/JCM.39.3.918-923.2001
105. Meng XJ, Halbur PG, Shapiro MS, Govindarajan S, Bruna JD, Mushahwar IK, *et al*. Genetic and experimental evidence for cross-species infection by swine hepatitis E virus. J Virol. 1998;72(12):9714–21. https://doi.org/10.1128/JVI.72.12.9714-9721.1998
106. Guo Y, Candelero-Rueda RA, Saif LJ, Vlasova AN. Infection of porcine small intestinal enteroids with human and pig rotavirus A strains reveals contrasting roles for histo-blood group antigens and terminal sialic acids. PLoS Pathog. 2021;17(1):e1009237. https://doi.org/10.1371/journal.ppat.1009237
107. Wu FT, Bányai K, Jiang B, Liu LT, Marton S, Huang YC, *et al*. Novel G9 rotavirus strains cocirculate in children and pigs, Taiwan. Sci Rep. 2017;18(7):40731. https://doi.org/10.1038/srep40731
108. Abass G, Dubal ZB, Rajak KK, Kale BM, Raorane A, Dudhe N, *et al*. Molecular characterization of porcine rotavirus A from India revealing zooanthroponotic transmission. Animal Biotechnol. 2021;8:1–13. https://doi.org/10.1080/10495398.2020.1868486
109. Mostafa A, Abdelwhab EM, Mettenleiter TC, Pleschka S. Zoonotic Potential of influenza A viruses: a comprehensive overview. Viruses. 2018;10(9):497. https://doi.org/10.3390/v10090497
110. Taubenberger JK, Kash JC. Influenza virus evolution, host adaptation, and pandemic formation. Cell Host Microbe. 2010;7(6):440–51. https://doi.org/10.1016/j.chom.2010.05.009
111. Kimura H, Abiko C, Peng G, Muraki Y, Sugawara K, Hongo S, *et al*. Interspecies transmission of influenza C virus between humans and pigs. Virus Res. 1997;48(1):71–9. https://doi.org/10.1016/s0168-1702(96)01427-x
112. Matsuzaki Y, Mizuta K, Sugawara K, Tsuchiya E, Muraki Y, Hongo S, *et al*. Frequent reassortment among influenza C viruses. J Virol. 2003;77(2):871–81. https://doi.org/10.1128/jvi.77.2.871-881.2003
113. Guo YJ, Jin FG, Wang P, Wang M, Zhu JM. Isolation of influenza C virus from pigs and experimental infection of pigs with influenza C virus. J Gen Virol. 1983;64(Pt 1):177–82. https://doi.org/10.1099/0022-1317-64-1-177
114. Lee J, Wang L, Palinski R, Walsh T, He D, Li Y, *et al*. Comparison of pathogenicity and transmissibility of influenza B and D viruses in pigs. Viruses. 2019;11(10):905. https://doi.org/10.3390/v11100905
115. Koolhof IS, Carver S. Epidemic host community contribution to mosquito-borne disease transmission: Ross River virus. Epidemiol Infect. 2017;145(4):656–66. https://doi.org/10.1017/S0950268816002739
116. Spradbrow PB. Letter: Experimental infection of sheep and pigs with Ross River virus. Aust Vet J. 1973;49(8):403–4.
117. Rosen L, Gubler DJ, Bennett PH. Epidemic polyarthritis (Ross River) virus infection in the Cook Islands. Am J Trop Med Hyg. 1981;30(6):1294–302. https://doi.org/10.4269/ajtmh.1981.30.1294
118. Pérez-Losada M, Arenas M, Galán JC, Palero F, González-Candelas F. Recombination in viruses: Mechanisms, methods of study, and evolutionary consequences. Infect Genet Evolut. 2015;30:296–307.
119. Sanjuán R, Domingo-Calap P. Genetic diversity and evolution of viral populations. Encyclopedia of Virology 4th ed. Academic Press; 2021. 53-61 p.
120. Kreuder Johnson C, Hitchens PL, Smiley Evans T, Goldstein T, Thomas K, Clements A, *et al*. Spillover and pandemic properties of zoonotic viruses with high host plasticity. Sci Rep. 2015;7(5):14830. https://doi.org/10.1038/srep14830
121. Jenkins GM, Rambaut A, Pybus OG, Holmes EC. Rates of molecular evolution in RNA viruses: a quantitative phylogenetic analysis. J Mol Evol. 2002;54(2):156–65. https://doi.org/10.1007/s00239-001-0064-3
122. Smith EC. The not-so-infinite malleability of RNA viruses: Viral and cellular determinants of RNA virus mutation rates. PLoS Pathog. 2017;13(4):e1006254. https://doi.org/10.1371/journal.ppat.1006254
123. Cadar D, Kiss T, Ádám D, Cságola A, Novosel D, Tuboly T. Phylogeny, spatio-temporal phylodynamics and evolutionary scenario of Torque teno sus virus 1 (TTSuV1) and 2 (TTSuV2) in wild boars: fast dispersal and high genetic diversity. Vet Microbiol. 2013;166(1–2):200–13. https://doi.org/10.1016/j.vetmic.2013.06.010
124. Nieto D, Aramouni M, Grau-Roma L, Segalés J, Kekarainen T. Dynamics of Torque teno sus virus 1 (TTSuV1) and 2 (TTSuV2) DNA loads in serum of healthy and postweaning multisystemic wasting syndrome (PMWS) affected pigs. Vet Microbiol. 2011;152(3–4):284–90. https://doi.org/10.1016/j.vetmic.2011.05.020
125. Hicks AL, Duffy S. Cell tropism predicts long-term nucleotide substitution rates of mammalian RNA viruses. PLoS Pathog. 2014;10(1):e1003838.
126. Bull RA, Hansman GS, Clancy LE, Tanaka MM, Rawlinson WD, White PA. Norovirus recombination in ORF1/ORF2 overlap. Emerg Infect Dis. 2005;11(7):1079–85. https://doi.org/10.3201/eid1107.041273
127. Wang QH, Han MG, Cheetham S, Souza M, Funk JA, Saif LJ. Porcine noroviruses related to human noroviruses. Emerg Infect Dis. 2005;11(12):1874–81. https://doi.org/10.3201/eid1112.050485
128. Shen Q, Zhang W, Yang S, Yang Z, Chen Y, Cui L, *et al*. Recombinant porcine norovirus identified from piglet with diarrhea. BMC Vet Res. 2012;3(8):155. https://doi.org/10.1186/1746-6148-8-155
129. Chhabra P, de Graaf M, Parra GI, Chan MC, Green K, Martella V, *et al*. Updated classification of norovirus genogroups and genotypes. J Gen Virol. 2019;100(10):1393–406. https://doi.org/10.1099/jgv.0.001318

130. Cavicchio L, Tassoni L, Laconi A, Cunial G, Gagliazzo L, Milani A, *et al*. Unrevealed genetic diversity of GII Norovirus in the pig population of North East Italy. Sci Rep. 2020;10(1):9217.
131. Wauquier N, Becquart P, Padilla C, Baize S, Leroy EM. Human fatal zaire ebola virus infection is associated with an aberrant innate immunity and with massive lymphocyte apoptosis. PLoS Negl Trop Dis. 2010;4(10):e837. https://doi.org/10.1371/journal.pntd.0000837
132. Pappalardo M, Juliá M, Howard MJ, Rossman JS, Michaelis M, Wass MN. Conserved differences in protein sequence determine the human pathogenicity of Ebolaviruses. Sci Rep. 2016;24(6):23743. https://doi.org/10.1038/srep23743
133. Albariño CG, Wiggleton Guerrero L, Jenks HM, Chakrabarti AK, Ksiazek TG, *et al*. Insights into Reston virus spillovers and adaption from virus whole genome sequences. PLoS One. 2017;12(5):e0178224. https://doi.org/10.1371/journal.pone.0178224
134. Lo MK, Lowe L, Hummel KB, Sazzad HM, Gurley ES, Hossain MJ, *et al*. Characterization of Nipah virus from outbreaks in Bangladesh, 2008–2010. Emerg Infect Dis. 2012;18(2):248–55.
135. Jones MK, Watanabe M, Zhu S, Graves CL, Keyes LR, Grau KR, *et al*. Enteric bacteria promote human and mouse norovirus infection of B cells. Science. 2014;346(6210):755–9.
136. Ruvoën-Clouet N, Magalhaes A, Marcos-Silva L, Breiman A, Figueiredo C, David L, *et al*. Increase in Genogroup II.4 norovirus host spectrum by CagA-positive helicobacter pylori infection. J. Infect. Dis. 2014;210(2):183–91.
137. Simon G, Larsen LE, Dürrwald R, Foni E, Harder T, Van Reeth K, *et al*. European surveillance network for influenza in pigs: surveillance programs, diagnostic tools and Swine influenza virus subtypes identified in 14 European countries from 2010 to 2013. PLoS One. 2014;9(12):e115815. https://doi.org/10.1371/journal.pone.0115815
138. World Organisation for Animal Health (OIE). OIE-Listed diseases 2021. Retrieved from: https://www.oie.int/animal-health-in-the-world/oie-listed-diseases-2021/
139. Sherman AC, Mehta A, Dickert NW, Anderson EJ, Rouphael N. The Future of flu: a review of the human challenge model and systems biology for advancement of influenza vaccinology. Front Cell Infect Microbiol. 2019;17(9):107. https://doi.org/10.3389/fcimb.2019.00107
140. Lindesmith L, Moe C, Lependu J, Frelinger JA, Treanor J, Baric RS. Cellular and humoral immunity following Snow Mountain virus challenge. J Virol. 2005;79(5):2900–9. https://doi.org/10.1128/JVI.79.5.2900-2909.2005
141. Frenck R, Bernstein DI, Xia M, Huang P, Zhong W, Parker S, *et al*. Predicting Susceptibility to Norovirus GII.4 by use of a challenge model involving humans. J. Infect. Dis. 2012;206(9):1386–93. https://doi.org/10.1093/infdis/jis514
142. Ward RL, Bernstein DI, Shukla R, McNeal MM, Sherwood JR, Young EC, *et al*. Protection of adults rechallenged with a human rotavirus. J Infect Dis. 1990;161(3):440–5. https://doi.org/10.1093/infdis/161.3.440
143. Go YY, Balasuriya UB, Lee CK. Zoonotic encephalitides caused by arboviruses: transmission and epidemiology of alphaviruses and flaviviruses. Clin Experi Vaccine Res. 2014;3(1):58–77. https://doi.org/10.7774/cevr.2014.3.1.58
144. Kirkland PD, Love RJ, Philbey AW, Ross AD, Davis RJ, Hart KG. Epidemiology and control of Menangle virus in pigs. Aust Vet J. 2001;79(3):199–206. https://doi.org/10.1111/j.1751-0813.2001.tb14580.x
145. Love RJ, Philbey AW, Kirkland PD, Ross AD, Davis RJ, Morrissey C, *et al*. Reproductive disease and congenital malformations caused by Menangle virus in pigs. Aust Vet J. 2001;79(3):192–8. https://doi.org/10.1111/j.1751-0813.2001.tb14578.x
146. Halpin K, Hyatt AD, Fogarty R, Middleton D, Bingham J, Epstein JH, *et al*. Pteropid bats are confirmed as the reservoir hosts of henipaviruses: a comprehensive experimental study of virus transmission. Am J Trop Med Hyg. 2011;85(5):946–51. https://doi.org/10.4269/ajtmh.2011.10-0567
147. Middleton DJ, Westbury HA, Morrissy CJ, van der Heide BM, Russell GM, Braun MA, *et al*. Experimental Nipah virus infection in pigs and cats. J Comp Pathol. 2002;126(2-3):124–36. https://doi.org/10.1053/jcpa.2001.0532
148. Goh KJ, Tan CT, Chew NK, Tan PS, Kamarulzaman A, Sarji SA, *et al*. Clinical features of Nipah virus encephalitis among pig farmers in Malaysia. N Engl J Med. 2000;342(17):1229–35. https://doi.org/10.1056/NEJM200004273421701
149. Luby SP, Hossain MJ, Gurley ES, Ahmed BN, Banu S, Khan SU, *et al*. Recurrent zoonotic transmission of nipah virus into humans, Bangladesh, 2001–2007. Emerg. Infect. Dis. 2009;15(8):1229–35. https://doi.org/10.3201/eid1508.081237
150. Kasloff SB, Leung A, Pickering BS, Smith G, Moffat E, Collignon B, *et al*. Pathogenicity of Nipah henipavirus Bangladesh in a swine host. Sci Rep. 2019;9(1):5230. https://doi.org/10.1038/s41598-019-40476-y
151. Yob JM, Field H, Rashdi AM, Morrissy C, van der Heide B, Rota P, *et al*. Nipah virus infection in bats (Order Chiroptera) in Peninsular Malaysia. Emerg. Infect. Dis. 2001;7(3):439–41. https://doi.org/10.3201/eid0703.010312
152. Chua KB, Koh CL, Hooi PS, Wee KF, Khong JH, Chua BH, *et al*. Isolation of Nipah virus from Malaysian Island flying-foxes. Microbes Infect. 2002;4(2):145–51. https://doi.org/10.1016/s1286-4579(01)01522-2
153. Jayme SI, Field HE, de Jong C, Olival KJ, Marsh G, Tagtag AM, *et al*. Molecular evidence of Ebola Reston virus infection in Philippine bats. Virol J. 2015;17(12):107. https://doi.org/10.1186/s12985-015-0331-3
154. Barrette RW, Metwally SA, Rowland JM, Xu L, Zaki SR, Nichol ST, *et al*. Discovery of swine as a host for the Reston ebolavirus. Science. 2009;325(5937):204–6. https://doi.org/10.1126/science.1172705
155. Smith PF, Howerth EW, Carter D, Gray EW, Noblet R, Mead DG. Mechanical transmission of vesicular stomatitis New Jersey virus by Simulium vittatum (Diptera: Simuliidae) to domestic swine (Sus scrofa). J Med Entomol. 2009;46(6):1537–40. https://doi.org/10.1603/033.046.0643
156. Rozo-Lopez P, Drolet BS, Londoño-Renteria B. Vesicular stomatitis virus transmission: a comparison

of incriminated vectors. Insects. 2018;9(4):190. https://doi.org/10.3390/insects9040190
157. Attoui H, Mohd Jaafar F, de Micco P, de Lamballerie X. Coltiviruses and seadornaviruses in North America, Europe, and Asia. Emerg Infect Dis. 2005;11(11):1673–9. https://doi.org/10.3201/eid1111.050868
158. Jaafar FM, Attoui H, Mertens PPC, de Micco P, de Lamballerie X. Structural organization of an encephalitic human isolate of Banna virus (genus Seadornavirus, family Reoviridae). J Gen Virol. 2005;86(Pt 4):1147–57. https://doi.org/10.1099/vir.0.80578-0
159. Xia H, Liu H, Zhao L, Atoni E, Wang Y, Yuan Z. First Isolation and Characterization of a Group C Banna Virus (BAV) from Anopheles sinensis Mosquitoes in Hubei, China. Viruses. 2018;10(10):555. https://doi.org/10.3390/v10100555
160. Attoui H, Jaafar FM, Belhouchet M, Tao S, Chen B, Liang G, *et al.* Liao ning virus, a new Chinese seadornavirus that replicates in transformed and embryonic mammalian cells. J Gen Virol. 2006;87(Pt 1):199–208. https://doi.org/10.1099/vir.0.81294-0
161. Centers for Disease Control and Prevention (CDC). Cache Valley virus. 2019 Nov. Retrieved from: https://www.cdc.gov/cache-valley/index.html
162. Nguyen NL, Zhao G, Hull R, Shelly MA, Wong SJ, Wu G, *et al.* Cache valley virus in a patient diagnosed with aseptic meningitis. J. Clin. Microbiol. 2013;51(6):1966–9.
163. Hayles LB, Lversen JO. Cache Valley virus: experimental infection in Culiseta inornata. Can J Microbiol. 1980;26(3):287–90.
164. Armstrong PM, Andreadis TG, Anderson JF. Emergence of a new lineage of cache valley virus (Bunyaviridae: Orthobunyavirus) in the Northeastern United States. Am J Tropical Med Hygiene. 2015;93(1):11–7.
165. Andreadis TG, Armstrong PM, Anderson JF, Main AJ. Spatial-temporal analysis of Cache Valley virus (Bunyaviridae: Orthobunyavirus) infection in anopheline and culicine mosquitoes (Diptera: Culicidae) in the northeastern United States, 1997–2012. Vector Borne Zoonotic Dis. 2014;14(10):763–73. https://doi.org/10.1089/vbz.2014.1669
166. Mavale MS, Fulmali PV, Ghodke YS, Mishra AC, Kanojia P, Geevarghese G. Experimental transmission of Chandipura virus by Phlebotomus argentipes (diptera: psychodidae). Am J Trop Med Hyg. 2007;76(2):307–9.
167. Sudeep AB, Gurav YK, Bondre VP. Changing clinical scenario in Chandipura virus infection. Indian J Med Res. 2016;143(6):712–21. https://doi.org/10.4103/0971-5916.191929
168. Oberste MS, Gotuzzo E, Blair P, Nix WA, Ksiazek TG, Comer JA, *et al.* Human febrile illness caused by encephalomyocarditis virus infection, Peru. Emerg Infect Dis. 2009;15(4):640–6. https://doi.org/10.3201/eid1504.081428
169. Billinis C, Paschaleri-Papadopoulou E, Anastasiadis G, Psychas V, Vlemmas J, Leontides S, *et al.* A comparative study of the pathogenic properties and transmissibility of a Greek and a Belgian encephalomyocarditis virus (EMCV) for piglets. Vet Microbiol. 1999;70(3–4):179–92. https://doi.org/10.1016/s0378-1135(99)00145-5
170. Paton DJ, Gubbins S, King DP. Understanding the transmission of foot-and-mouth disease virus at different scales. Curr Opin Virol. 2018;28:85–91. https://doi.org/10.1016/j.coviro.2017.11.013
171. Armstrong R, Davie J, Hedger RS. Foot-and-mouth disease in man. Br Med J. 1967;4(5578):529–30. https://doi.org/10.1136/bmj.4.5578.529
172. Prempeh H, Smith R, Müller B. Foot and mouth disease: the human consequences. BMJ. 2001;322(7286):565–6.
173. Hall MD, Knowles NJ, Wadsworth J, Rambaut A, Woolhouse ME. Reconstructing geographical movements and host species transitions of foot-and-mouth disease virus serotype SAT 2. Mbio. 2013;4(5):e00591.
174. Liu H, Zhang X, Li LX, Shi N, Sun XT, Liu Q, *et al.* First isolation and characterization of Getah virus from cattle in northeastern China. BMC Vet Res. 2019;15(1):320. https://doi.org/10.1186/s12917-019-2061-z
175. Izumida A, Takuma H, Inagaki S, Kubota M, Hirahara T, Kodama K, *et al.* Experimental infection of Getah virus in swine. Nihon Juigaku Zasshi. 1988;50(3):679–84.
176. Jeffries CL, Mansfield KL, Phipps LP, Wakeley PR, Mearns R, Schock A, *et al.* Louping ill virus: an endemic tick-borne disease of Great Britain. J. Gen. Virol. 2014;95(5):1005–14.
177. Dobler G. Zoonotic tick-borne flaviviruses. Vet Microbiol. 2010;140(3–4):221–8. https://doi.org/10.1016/j.vetmic.2009.08.024
178. Davidson MM, Williams H, Macleod JA. Louping ill in man: a forgotten disease. J Infect. 1991;23(3):241–9. https://doi.org/10.1016/0163-4453(91)92756-u
179. Alkan C, Bichaud L, de Lamballerie X, Alten B, Gould EA, Charrel RN. Sandfly-borne phleboviruses of Eurasia and Africa: epidemiology, genetic diversity, geographic range, control measures. Antiviral Res. 2013;100(1):54–74. https://doi.org/10.1016/j.antiviral.2013.07.005
180. Moriconi M, Rugna G, Calzolari M, Bellini R, Albieri A, Angelini P, *et al.* Phlebotomine sand fly-borne pathogens in the Mediterranean Basin: Human leishmaniasis and phlebovirus infections. PLoS Negl Trop Dis. 2017;11(8):e0005660. https://doi.org/10.1371/journal.pntd.0005660
181. Wang E, Bowen RA, Medina G, Powers AM, Kang W, Chandler LM, *et al.* Virulence and viremia characteristics of 1992 epizootic subtype IC Venezuelan equine encephalitis viruses and closely related enzootic subtype ID strains. Am J Trop Med Hyg. 2001;65(1):64–9. https://doi.org/10.4269/ajtmh.2001.65.64
182. Beckham JD, Arbovirus TKL. Arbovirus Infections. Continuum: Life Learning Neurol. 2015;21:1599–611.
183. Cheetham S, Souza M, Meulia T, Grimes S, Han MG, Saif LJ. Pathogenesis of a genogroup II human norovirus in gnotobiotic pigs. J Virol. 2006;80(21):10372–81. https://doi.org/10.1128/JVI.00809-06
184. Souza M, Cheetham SM, Azevedo MS, Costantini V, Saif LJ. Cytokine and antibody responses in gnotobiotic pigs after infection with human norovirus genogroup II.4 (HS66 Strain). J. Virol. 2007;81(17):9183–92.
185. Fan Y, Zhao K, Shi ZL, Zhou P. Bat Coronaviruses in China. Viruses. 2019;11(3):210.

186. Corman VM, Muth D, Niemeyer D, Drosten C. Hosts and sources of endemic human coronaviruses. Adv Virus Res. 2018;100:163-88.
187. Hoffmann M, Kleine-Weber H, Schroeder S, Krüger N, Herrler T, Erichsen S, *et al*. SARS-CoV-2 cell entry depends on ACE2 and TMPRSS2 and is blocked by a clinically proven protease inhibitor. Cell. 2020;181(2):271–80.
188. Dekker A, Moonen P, de Boer-Luijtze EA, Terpstra C. Pathogenesis of swine vesicular disease after exposure of pigs to an infected environment. Vet Microbiol. 1995;45(2–3):243–50. https://doi.org/10.1016/0378-1135(95)00032-6
189. Bellini S, Alborali L, Zanardi G, Bonazza V, Brocchi E. Swine vesicular disease in northern Italy: diffusion through densely populated pig areas. Rev Sci Tech. 2010;29(3):639–48. https://doi.org/10.20506/rst.29.3.2006
190. Webster RG. Influenza virus: transmission between species and relevance to emergence of the next human pandemic. Arch Virol Suppl. 1997;13:105–13. https://doi.org/10.1007/978-3-7091-6534-8_11
191. Yoon SW, Webby RJ, Webster RG. Evolution and ecology of influenza A viruses. Curr Top Microbiol Immunol. 2014;385:359–75. https://doi.org/10.1007/82_2014_396
192. Sederdahl BK, Williams JV. Epidemiology and clinical characteristics of influenza C virus. Viruses. 2020;12(1):89. https://doi.org/10.3390/v12010089
193. Kylla H, Dutta TK, Roychoudhury P, Malik YS, Mandakini R, Subudhi PK. Prevalence and molecular characterization of porcine Picobirnavirus in piglets of North East Region of India. Trop. Anim. Health Prod. 2017;49(2):417–22.
194. Smits SL, Poon LL, van Leeuwen M, Lau PN, Perera HK, Peiris JS, *et al*. Genogroup I and II picobirnaviruses in respiratory tracts of pigs. Emerg Infect Dis. 2011;17(12):2328–30. https://doi.org/10.3201/eid1712.110934
195. Claflin SB, Webb CE. Ross river virus: many vectors and unusual hosts make for an unpredictable pathogen. PLoS Pathog. 2015;11(9):e1005070. https://doi.org/10.1371/journal.ppat.1005070
196. Togami E, Gyawali N, Ong O, Kama M, Cao-Lormeau VM, Aubry M, *et al*. First evidence of concurrent enzootic and endemic transmission of Ross River virus in the absence of marsupial reservoirs in Fiji. Int J Infect Dis. 2020;96:94–6. https://doi.org/10.1016/j.ijid.2020.02.048
197. Harley D, Sleigh A, Ritchie S. Ross river virus transmission, infection, and disease: a cross-disciplinary review. Clin. Microbiol. Rev. 2001;14(4):909–32.
198. De Grazia S, Martella V, Rotolo V, Bonura F, Matthijnssens J, Bányai K, *et al*. Molecular characterization of genotype G6 human rotavirus strains detected in Italy from 1986 to 2009. Infect Genet Evol. 2011;11(6):1449–55. https://doi.org/10.1016/j.meegid.2011.05.015
199. Fu ZF, Hampson DJ. Natural transmission of group A rotavirus within a pig population. Res Vet Sci. 1989;46(3):312–7.
200. Vlasova AN, Amimo JO, Saif LJ. Porcine rotaviruses: epidemiology, immune responses and control strategies. Viruses. 2017;9(3):48. https://doi.org/10.3390/v9030048

SUPPORTING INFORMATION

Additional supporting information may be found online in the Supporting Information section at the end of the article.

Table S1. Framework of viral factors with associated relevance and assumptions considered in the review.
Table S2. Highlights of collected data based on the framework of factors in Table S1, which is used to inform viral transmission direction in Table 1. Distinctions are drawn between humans and pigs where appropriate.

4.2 Paper 2

Experimental infection of pigs and ferrets with "pre-pandemic," human-adapted, and swine-adapted variants of the H1N1pdm09 Influenza A virus reveals significant differences in viral dynamics and pathological manifestations

Charlotte Kristensen, **Helena Aagaard Glud**, Jeri-Carol Crumpton, Karen Martiny, Ashley Webb, Pia Ryt-Hansen, Ramona Trebbien, Henrik Elvang Jensen, Jakob Nybo Nissen, Ignacia Mena, Charlotte Kristiane Hjulsager, Kerstin Skovgaard, Richard J. Webby, and Lars Erik Larsen

Corresponding Author: Charlotte Kristensen, chark@sund.ku.dk

Submitted for publication in PLOS Pathogens

It is not feasible to print supplementary material due to the file size;
it is freely available upon request
haaglu@dtu.dk

Experimental infection of pigs and ferrets with "pre-pandemic," human-adapted, and swine-adapted variants of the H1N1pdm09 Influenza A virus reveals significant differences in viral dynamics and pathological manifestations

Charlotte Kristensen[a*], Helena A. Glud[b], Jeri-Carol Crumpton[c], Karen Martiny[a], Ashley Webb[c], Pia Ryt-Hansen[a], Ramona Trebbien[d], Henrik E. Jensen[a], Jakob N. Nissen[d#], Kerstin Skovgaard[b], Richard J. Webby[c], Lars E. Larsen[a]

[a]Department of Veterinary and Animal Sciences, University of Copenhagen, Frederiksberg C, Denmark.

[b]Department of Biotechnology and Biomedicine, Technical University of Denmark, Kgs. Lyngby, Denmark.

[c]Department of Infectious Diseases, St. Jude Children's Research Hospital, Memphis, TN, United States of America.

[d]Department of Virus and Microbiological Special Diagnostics, Statens Serum Institut, Copenhagen S, Denmark.

[#]Current Address: Novo Nordisk Foundation Center for Protein Research, University of Copenhagen, Copenhagen N, Denmark

***** Corresponding author

Email: chark@sund.ku.dk (CK)

Abstract

Influenza A viruses are RNA viruses that cause epidemics in humans and are enzootic in the pig population globally. In 2009, pig-to-human transmission of a reassortant H1N1 virus (H1N1pdm09) caused the first influenza pandemic of the 21st century. This study investigated the infection dynamics, pathogenesis, and lesions in pigs and ferrets inoculated with swine-adapted, human-adapted, and "pre-pandemic" H1N1pdm09 viruses. Additionally, the direct-contact and aerosol transmission properties of the three H1N1pdm09 isolates were assessed in ferrets. In pigs, inoculated ferrets, and ferrets infected by direct contact with inoculated ferrets, the pre-pandemic H1N1pdm09 virus induced an intermediary viral load, caused the most severe lesions, and had the highest clinical impact. The swine-adapted H1N1pdm09 virus induced the highest viral load, caused intermediary lesions, and had the least clinical impact in pigs. The human-adapted H1N1pdm09 virus induced the highest viral load, caused the mildest lesions, and had the least clinical impact in ferrets infected by direct contact. The mismatch between viral load and clinical impact presumably reflects the importance of viral host adaptation. Interestingly, the swine-adapted H1N1pdm09 virus was transmitted by aerosols to two-thirds of the ferrets, suggesting there is a risk of human-to-human aerosol transmission of swine-adapted H1N1pdm09 viruses.

Author summary

Influenza A viruses (IAVs) have a high evolutionary rate and evolve through genetic drift and reassortment events, elevating their pandemic threat. The last pandemic caused by IAV was a consequence of a spillover of IAV from pigs to humans in 2009 (referred to as H1N1pdm09). The

viral and host markers important for host adaptation of IAVs are poorly defined, which makes it difficult to evaluate the pandemic potential of novel swine IAV strains. A method of predicting the risk of human-to-human transmission of IAVs is by using the ferret as an animal model. In this study, we assessed the degree of host adaptation to pigs and ferrets of three different H1N1pdm09 viruses by virological, clinical, and pathological measures. We found that a swine-adapted H1N1pdm09 had the highest viral fitness but the lowest virulence in pigs and that a human-adapted H1N1pdm09 had the highest viral fitness but the lowest virulence in ferrets. In both animal models, we found that an H1N1pdm09 virus resembling a pre-pandemic variant had an intermediary viral fitness but the highest virulence. Our findings indicate that host adaptation is important for the viral fitness and virulence and that an increased viral fitness is not always related with a higher virulence.

Keywords: influenza, H1N1pdm09, experimental infection, pigs, ferrets, viral load, pathogenesis, host response, host adaptation.

Introduction

Influenza A viruses (IAVs) cause respiratory disease in humans and other animals. IAVs are negative single-stranded RNA viruses with a genome consisting of eight segments. The genome encodes at least 10 essential proteins [1,2]. IAVs are classified into subtypes according to the two surface glycoproteins: hemagglutinin (HA) and neuraminidase (NA) [3]. Three subtypes of IAV (H1N1, H1N2, and H3N2) are enzootic in pigs worldwide [4,5], with H1N1 and H3N2 viruses causing annual epidemics in humans [6]. Sustained genetic differences within IAV subtypes are termed clades [7].

In April 2009, a novel lineage of H1N1 IAV caused the first influenza pandemic of the 21st century. The virus had an HA belonging to the swine influenza virus clade 1A.3.3.2 and was designated H1N1pdm09 [8]. H1N1pdm09 originated from a combination of three IAV lineages circulating in swine: classical swine influenza virus (Csw), Eurasian avian-like swine H1N1 lineage (Clade 1C or EAsw), and the swine triple-reassortant H3N2 lineage (TRsw) [9–12]. The results of retrospective studies strongly indicate that the virus emerged in Mexican swine after multiple reassortment events among the Csw, EAsw, and TRsw lineages [13].

Approximately one month after the first human case, the H1N1pdm09 virus was detected in a pig farm in Canada, a consequence of reverse zoonotic transmission [14] and additional spillover events from humans to swine followed [15]. Subsequently, the H1N1pdm09 viruses became established in swine populations globally [4] resulting in the circulation of "swine-adapted" viruses that differ antigenically from the viruses circulating in humans [4,16–18].

Swine-adapted H1N1pdm09 viruses have also contributed to a range of reassortment events involving human seasonal IAVs and other enzootic swine IAVs [16, 19–24], thereby increasing viral diversity and the perceived zoonotic and pandemic risk. Knowledge is lacking concerning the basic mechanisms that contribute to the zoonotic potential of swine IAVs, hindering accurate pandemic risk assessments. The zoonotic potential of swine IAV is most likely determined by a combination of viral genetic traits and host-specific factors. There is an urgent need to elucidate the tangled relationship between IAVs in swine and humans and to characterize viruses adapted to each host.

This study compared the pathogenesis, infection dynamics, and impact of swine-adapted, human-adapted, and "pre-pandemic" H1N1pdm09 viruses in experimentally infected pigs and ferrets.

Materials and Methods

Pig experiment

Preparation of virus inoculum. The viruses selected for inoculation were A/swine/Denmark/2017_10298/4_4p1/2017 (H1N1) (swH1N1pdm09), a swine-adapted virus; A/Denmark/238/2020 (H1N1) (huH1N1pdm09), a human-adapted virus; and A/Swine/Mexico/AVX-39/2012 (H1N1) (mxH1N1pdm09), a "pre-pandemic" H1N1pdm09 virus (13). The two Danish virus isolates, swH1N1pdm09 and huH1N1pdm09, were propagated and passaged three times in Madin–Darby canine kidney (MDCK) cells. The viruses were stored in aliquots at −80°C until used. The mxH1N1pdm09 virus was kindly provided by Nacho Mena and Adolfo Garcia-Sastre of Mount Sinai School of Medicine and was also passaged in MDCK cells. The titers of the three viruses were determined by tissue culture infectious dose 50% (TCID50) assay in MDCK cells. All virus isolates were diluted in Eagle's Minimum Essential Medium (MEM) (Gibco) to obtain a TCID50/mL of 10^7 before inoculation.

Study design. Forty-two 7-week-old Danish Landrace Crossbred pigs (body weight; 7400–12,300 g) that tested negative for swine IAV and antibodies to the virus were included. All pigs were fed with non-pelleted feed (NAG Svinefoder 5) during the study and had *ad libitum* access to water. The pigs were allocated to four groups by minimization (ARRIVE guidelines), with sex and size as nuisance variables, to ensure a balance between the groups (Fig 1). Each group (experimental unit) was housed in a separate isolation unit and had an acclimatization period of 1 week. Groups 2–4 included 12 pigs, whereas group 1 included six pigs. The pigs were enumerated as 1–6, 7–18, 19–30, and 31–42 in groups 1, 2, 3, and 4, respectively. Before inoculation, all pigs were sedated by intramuscular injection (Text S1). All pigs in groups 2–4 were inoculated intranasally (in the right nostril) with 3 mL of virus, with a titer of 10^7 TCID50/mL, by using MAD

Nasal™ intranasal mucosal atomization devices (Teleflex, Morrisville, NC, cat. no. MAD100). Group 1 pigs (the control group) were mock infected intranasally with cell culture medium only, again using the mucosal atomization devices. Pigs in groups 2, 3, and 4 were inoculated with swH1N1pdm09, huH1N1pdm09, and mxH1N1pdm09, respectively. Control pigs and eight pigs from each IAV-infected group were euthanized 3 days post inoculation (DPI), whereas the remaining pigs (pigs 15–18 from group 2, 27–30 from group 3, and 39–42 from group 4) were euthanized on day 14 post inoculation.

The animal experiment was performed under Biosafety level 2 conditions in accordance with an animal study protocol approved by the Danish Animal Experimentation Council (protocol no. 2020-15-0201-00502).

Observations and sampling. The pigs were weighed at 0, 3, and 14 DPI. Body temperature measurements, nasal swabs, and blood samples were collected at −3, 0, 1, 2, 3, 4, 7, 10, and 14 DPI. At 0, 3, and 14 DPI, the samples were collected after sedation but before inoculation and euthanasia, except for those collected from the four pigs in each IAV-infected group at 3 DPI, which lived until 14 DPI. More details of the observation and sampling can be found in Text S1.

On the day of inoculation (0 DPI), all pigs were tested by nasal swabbing for porcine circovirus type 2 (PCV2), porcine reproductive and respiratory syndrome virus (PRRSV) types 1 and 2, and *Mycoplasma hyopneumoniae* as described previously [25].

Necropsy and histopathology. Pigs were sedated before euthanasia, following the same protocol described in Text S1. They were exsanguinated by cutting the axillary artery. At necropsy, gross lesions were recorded, lung lesions compatible with IAV infection (red or dark red lobular atelectasis) were sketched, and the lungs were photographed. Lesion severity was graded as described previously (26), and the highest atelectasis score for all lung lobes was chosen to provide

one gross lesion score for each pig. Furthermore, the number of affected lung lobes was registered. Specimens of tissues mentioned in Table S1 were collected from each pig for IAV quantification by RT-qPCR, sequencing, and histopathological examination. All samples were collected aseptically. Tissue specimens for IAV quantification and sequencing were placed in 1.5-mL Eppendorf tubes and stored at −80°C until analyzed. Specimens for histopathology were fixed in 10% neutral-buffered formalin for a week, embedded in paraffin wax, sliced into 2–3 µm sections, and stained with hematoxylin and eosin (H&E). Histologically, all lung tissues (LU1, LU4, and LU9) from animals at 3 DPI were graded using a modified scoring scheme [27] (Table S2). The highest histopathological score for all lung tissues was chosen to provide one histopathological score for each pig. Based on the quality of the tissue preparation, histological evaluations were performed of the nasal mucosa and upper trachea of one pig from the control group at 3 DPI, of two pigs from each inoculated group at 3 DPI, and of two pigs from each inoculated group at 14 DPI. Immunohistochemical staining targeting cytokeratin (for epithelial cells) was performed on selected representative sections to confirm hyperplasia of type II pneumocytes [28].

Ferret study

Preparation of virus inoculum. The viruses used for inoculating ferrets were identical to those used in the swine experiment and were propagated as described above. All virus isolates were diluted in sterile PBS before inoculation. The swH1N1pdm09 virus was diluted to 10^5 TCID50/mL, the huH1N1pdm09 strain to 5×10^4 TCID50/mL, and the mxH1N1pdm09 strain to 5×10^5 TCID50/mL.

Study design. In total, the study used 36 male ferrets (aged 9–23 weeks; body weight: 0.97–1.48 kg) (Triple F Farms) that were negative for IAV antibodies by the HI test. Donor and

recipient ferrets were housed separately. After 1 week of acclimatization, three donor ferrets from each group were sedated with 4% isoflurane and inoculated intranasally with 0.5 mL of virus (250 µL of virus diluted in sterile PBS in each nostril), using a syringe. Ferrets from group 1 were inoculated with swH1N1pdm90, those from group 2 with huH1N1pdm09, and those from group 3 with mxH1N1pdm09. After inoculation, donor ferrets were housed in separate cages. Data from donor ferrets were not included in this study. Three additional ferrets (henceforth referred to as "inoculated ferrets") were inoculated with each virus and euthanized at 3 DPI. The group 1 inoculated ferrets were numbered 1–3, the group 2 ferrets were numbered 4–6, and the group 3 ferrets were numbered 7–9.

Twenty-four hours after inoculation, each donor ferret was co-housed with one naïve ferret (DC recipient). DC ferrets were assigned the numbers 10-12 in group 1, 13-15 in group 2, and 16-18 in group 3. Additionally, naïve ferrets were placed in a cage adjacent to donor and DC ferrets separated by double-layered perforated dividers to allow respiratory droplet transmission to assess aerosol transmission (AT recipient). AT ferrets were assigned the numbers 19-21 in group 1, 22-24 in group 2, and 25-27 in group 3. The ferret experiment was conducted in triplicates for each strain (one donor, one DC recipient, and one AT recipient). Donor, DC and AT ferrets were euthanized at 14 DPI (Fig 2).

The ferret experiment was performed at St. Jude Children's Research Hospital (Memphis, TN) in biosafety level 2 enhanced facilities and with the approval of the hospital Animal Care and Use Committee under protocol 428.

Observations and sampling. Body weight and temperature were measured at 0, 2, 5, 7, and 9 DPI. Nasal washes for quantification of IAV by real-time RT-PCR were performed at 2, 5,

7, and 9 DPI after the administration of 0.4 mL of ketamine I.M as described previously [29], and the samples were stored at −80°C until analyzed.

Necropsy and histopathology. Ferrets were euthanized by intracardiac administration of 1.0 mL of Euthasol after sedation with 0.4 mL of a ketamine/xylazine mixture. Specimens of organs mentioned in Table S1 were collected from inoculated ferrets at 3 DPI and from DC ferrets at 14 DPI for IAV quantification IAV by RT-qPCR, sequencing, and histopathological examination. Specimens collected for IAV quantification and sequencing were stored at −80°C until analyzed. Specimens for histopathological examination were processed as for the pig tissues. Lung sections from all inoculated and DC ferrets were examined together with one section of the nasal turbinates and trachea from each group of inoculated and DC ferrets. These sections were selected based on the quality of the histopathological preparation.

Serological tests

ELISAs for anti-IAV antibodies were performed using the IDEXX Influenza A ELISA Kit (IDEXX laboratories, Westbrook, ME) as described previously [30]. ELISA results were calculated as a signal-to-noise ratio (S/N), using the cut-off recommended by the vendor.

RNA extraction and quantification of IAV by real-time RT-PCR

Nasal swab samples were vortex mixed for 10 s and centrifuged for 3 min at 9651 × *g*. For each sample, 200 µL of the supernatant was mixed with 400 µL of RLT buffer (QIAGEN, Hilden, Germany) containing 2-mercaptoethanol (ME) (Merck, Darmstadt, Germany). Nasal mucosa,

tracheal tissues, and lung tissues (70 mg of each) were lysed by bead beating in a TissueLyser LT (QIAGEN) for 3 min at 30 Hz in 1400 µL of RLT buffer and centrifuged for 3 min at 9651 × *g*. After centrifugation, 600 µL of the supernatant was used for RNA extraction, which was performed as described previously [31]. Extracted RNA was eluted in 60 µL of RNase-free water and stored at −80°C.

The PCR assay used to detect IAV was an in-house modified version of a real-time RT-PCR assay targeting the matrix gene [32]. The primers RimF (5′-CTT CTA ACC GAG GTC GAA ACG-3′) and RimR (5′-AGG GCA TTT TGG ACA AAK CGT CTA-3′) and the dual-labeled probe MAprobeDL (5′-FAM CCC AGT GAG CGA GGA CTG CAG CGT BHQ-1-3′) were used. The master mix had a final volume of 25 µL, containing 3 µL of RNA solution, 13 µL of SensiFAST™ Probe No-ROX One-Step Mix (Meridian Bioscience, Boxtel, The Netherlands), 0.55 µL of RiboSafe RNase Inhibitor (Meridian Bioscience), 0.28 µL of reverse transcriptase (Meridian Bioscience), 7 µL of RNase-free water, and 2 µL of primer–probe mix (0.08 µL of each primer [0.4 µmol of each], 0.06 µL of probe [0.3 µmol], and 1.78 µL of RNase-free water). The RT-qPCR was performed on a Rotor-Gene Q platform (QIAGEN, Hilden, Germany) using the following program: 30 min at 50°C then 2 min at 95°C, followed by 40 cycles of 15 s at 95°C, 15 s at 55°C, and 20 s at 72°C. Positive and negative controls were included in all runs. Nucleic acid from IAVs was quantified in nasal swabs/washes, nasal mucosa, tracheal tissue, and lung tissue based on a 10-fold dilution series of the target sequence with known copy numbers.

Sequencing of virus and phylogeny

Full-genome sequencing was performed on the inoculum virus. RNA was extracted as described previously, and all segments were amplified in one tube by using a previously published protocol [31]. Next-generation sequencing and generation of consensus sequences and MUSCLE alignment was performed as described previously [31]. No genetics changes in the inoculum strains were observed after the passages in MDCK cells.

A maximum-likelihood tree of HA gene segments was generated with selected reference sequences and by using ModelFinder [33] and IqTree [34]. The best-fit model was the substitution model: K3Pu+F+I. Reference sequences originating from the human H1N1pdm09 subtype from 2009–2020 were obtained from annual reports of the European Centre for Disease Prevention and Control (ECDC). A pairwise comparison of the coding nucleotide HA sequences of the inoculum strains was performed using CLC Main Workbench version 22.0 (QIAGEN, Aarhus, Denmark) to measure the percentage identity.

Statistical analysis

A blinded inter-observer agreement study of the histopathological scoring was performed. Descriptive statistics for nasal shedding (measured with nasal swabs or washes) by pigs at 1–12 DPI (n = 4), inoculated ferrets (n = 3), DC ferrets (n = 3), and AT ferrets (n = 3) consisted of the median and the interquartile range (25%–75%). The total amount of virus shed over time (the total viral load) was calculated as the area under the curve (AUC) for nasal swab samples collected from pigs at 1–3 DPI (n = 12), nasal washes from DC ferrets at 2–9 DPI (n = 3), and nasal washes from AT ferrets at 2–9 DPI (n = 3).

No animals were excluded from the experiments, but the nasal wash for ferret no. 10 in the AT swH1N1pdm09 group at 9 DPI was missing. To test for a normal distribution of the data, a

Shapiro–Wilk test and an analysis of QQ plots in RStudio were performed. In pigs, the differences in body weight gain were examined by two-way ANOVA with a Tukey correction of the *P* values, and the results are reported as the mean ± SD with a 95% confidence interval (CI) for the differences. There was a lack of normal distributions for viral shedding at 1–3 DPI (n = 12), the total viral load at 1–3 DPI (n = 12), the severity of lung lobe lesions at 3 DPI (n = 8), and the number of affected lung lobes at 3 DPI (n = 8). These data points are, therefore, reported as medians with the interquartile ranges (25%–75%), and they were analyzed by Kruskal–Wallis tests and by a post hoc Dunn test with a pairwise comparison and Bonferroni correction of the *P* values with a 95% CI for the differences in mean ranks between the groups. Statistical analyses were performed in RStudio Team (http://www.rstudio.com), with *P* values of 0.05 or less being considered to indicate statistical significance. Data were illustrated using GraphPad Prism version 9.0.0 for Windows (GraphPad Software, San Diego, California USA, www.graphpad.com).

Results

Genetic characterization

A maximum-likelihood tree of the H1pdm09 study viruses and selected reference viruses is presented in Figure S1. Although the mxH1N1pdm09 virus was isolated in 2012, 3 years after being first detected in humans, phylogenetic analyses strongly support this strain being a “pre-pandemic” version of the virus [13]. The tree also illustrates the genetic differences between the huH1N1pdm09 and swH1N1pdm09 viruses. The swH1N1pdm09 virus clusters within the swine H1N1pdm09 clade (1.A.3.3.2) [16], whereas the huH1N1pdm09 virus clusters with the human clade 6B, alongside a few swine H1N1pdm09 isolates. The huH1N1pdm09 inoculum strain had

93.6% and 93.1% nucleotide identity of the HA gene when compared with the swH1N1pdm09 and mxH1N1pdm09 inoculum strains, respectively. The swH1N1pdm09 virus had 92.1% nucleotide identity of the HA gene when compared with the mxH1N1pdm09 strain.

Pig study

Clinical signs were more severe in pigs in the mxH1N1pdm09 group. Gains in body weight and rectal temperature measurements are summarized in Table 1, with the clinical signs being detailed in supplementary text S1. All pigs tested negative for PCV2, PRRSV types 1 and 2, and *Mycoplasma hyopneumoniae* by nasal swabbing at 0 DPI. Pigs in the mxH1N1pdm09 and huH1N1pdm09 groups had gained significantly less weight at 3 DPI when compared to control pigs ($P \leq 0.001$ and $P \leq 0.01$, respectively). Furthermore, weight gain was significantly higher in the swH1N1pdm09 group than in the mxH1N1pdm09 group ($P \leq 0.05$). Sneezing was observed in two pigs in the swH1N1pdm09 group and lethargy in three pigs in each of the IAV-inoculated groups. Detailed statistics for weight gain are presented in S1 Data.

Table 1. Summary of clinical observations from the pig experiment.*

Group	Rectal temperature[1]	Mean weight gain: 0 to 3 DPI (kg)[2]	Mean weight gain: 0 to 14 DPI (kg)[3]
Control	0/6	1.38 ± 0.28^{a}	-
swH1N1pdm09	1/12	1.02 ± 0.41^{ac}	4.27 ± 0.67
huH1N1pdm09	3/12	0.71 ± 0.24^{bc}	4.13 ± 0.87
mxH1N1pdm09	5/12	0.52 ± 0.43^{b}	3.58 ± 1.69

*****Means followed by a different superscript letter are significantly different by two-way ANOVA test ($P < 0.05$).
[1] Proportion of pigs with a rectal temperature above 40°C on at least 1 day during the study
[2] Mean weight gain of pigs from day 0 to 3 DPI ± SD, N = 42
[3] Mean weight gain of pigs from day 0 to 14 DPI ± SD, N = 12

Pigs in the swH1N1pdm09 group had significantly higher viral loads. No shedding of IAV was detected at 0 DPI in any study animal. The viral load was significantly higher in the mxH1N1pdm09 group than in the huH1N1pdm09 group at 1 DPI ($P < 0.05$) (Fig 3). The viral load was also significantly higher in the swH1N1pdm09 group than in the huH1N1pdm09 group at 2 and 3 DPI ($P < 0.001$ and $P < 0.05$, respectively). Furthermore, the viral load was significantly higher in the swH1N1pdm09 group than in the mxH1N1pdm09 group at 2 DPI ($P < 0.05$). The total viral load expressed as the median area under the curve (AUC) differed among the groups, being 1.95×10^9 ($1.46–2.51 \times 10^9$) copies/mL for the swH1N1pdm09 group, 3.34×10^8 ($3.23 \times 10^7–5.05 \times 10^8$) copies/mL for the huH1N1pdm09 group, and 1.19×10^9 ($2.47 \times 10^8–2.32 \times 10^9$) copies/mL for the mxH1N1pdm09 group (Fig S2). The total viral load was significantly higher in the swH1N1pdm09 group than in the huH1N1pdm09 group ($P < 0.05$) (S1 Data).

In all groups, the median viral shedding as detected by nasal swabbing was highest at 4 DPI: 1.96×10^9 ($0.33–3.83 \times 10^9$) copies/mL for the swH1N1pdm09 group, 5.84×10^8 ($1.96–12.30 \times 10^8$) copies/mL for the huH1N1pdm09 group, and 1.51×10^9 ($0.70–2.35 \times 10^9$) copies/mL for the mxH1N1pdm09 group (Fig S3).

Most pigs seroconverted. The NP ELISA for IAV at 14 DPI showed that all four pigs in the mxH1N1pdm09 group, three of four pigs in the huH1N1pdm09 group, and two of four pigs in the swH1N1pdm09 group had seroconverted (S1 Data).

The highest viral loads were in lungs of pigs inoculated with mxH1N1pdm09 or swH1N1pdm09 virus. Pigs in the mxH1N1pdm09 group had the highest lung viral load [2.48×10^9 (3.77×10^8–5.40×10^9) copies/mL], whereas pigs in the swH1N1pdm09 and huH1N1pdm09 groups had the highest viral loads in the upper trachea [2.03×10^9 (6.30×10^8–6.83×10^9) copies/mL and 2.76×10^8 (8.23×10^7–7.54×10^8) copies/mL, respectively] (Fig 4; S1 Data). A few pigs in each IAV-infected group were PCR positive for viral RNA in their lungs, nasal mucosa, and upper and lower trachea at 14 DPI (S1 Data).

Lesions were significantly more severe in mxH1N1pdm09-infected pigs. Pulmonary emphysema was observed in some pigs, including some controls; otherwise, no gross lesions were observed in the controls. Almost all pigs inoculated with IAV showed multifocal, lobular, atelectasis with a varying degree of redness (Fig S4). However, no gross lesions were observed at 3 DPI in one swH1N1pdm09-inoculated pig or in two pigs inoculated with huH1N1pdm09 virus. Four pigs developed pleuritis and pericarditis, and one pig in the swH1N1pdm09 group also had purulent rhinitis (Table S3). The severity of atelectasis and the number of affected lung lobes differed among the groups at 3 DPI (Table 2). Atelectasis was significantly more severe in the mxH1N1pdm09 group than in the huH1N1pdm09 group ($P < 0.05$). Furthermore, there were significantly fewer affected lung lobes in the swH1N1pdm09 group than in the mxH1N1pdm09 group ($P < 0.05$). At 14 DPI, one pig in the swH1N1pdm09 group and two pigs in the huH1N1pdm09 group showed mild atelectasis, whereas none of the pigs in the mxH1N1pdm09 group had lesions (Table S3). Detailed statistics for lesions are presented in S1 Data.

Table 2. Group median macroscopic scores (+ 25% and 75% quantiles) from inoculated pigs at 3 DPI (n = 8)*.

Group	Severity of affected lung lobes[1]	No. of affected lung lobes
swH1N1pdm09	2.00 [1.00; 3.00]^{ab}	1.00 [1.00; 2.00]^{a}
huH1N1pdm09	1.50 [0.25; 2.00]^{a}	2.00 [0.25; 2.75]^{ab}
mxH1N1pdm09	3.00 [2.25; 3.00]^{b}	3.50 [2.25; 4.00]^{b}

*Medians followed by a different superscript letter are significantly different by a Kruskal–Wallis test ($P < 0.05$).

[1] Median [25%;75% quantiles] of the highest atelectasis score obtained from affected lung lobes from each pig.

Histopathological changes were more severe in mxH1N1pdm09-infected and swH1N1pdm09-infected pigs. Some histopathological background lesions were found in control pigs and were, therefore, not taken into account in the histopathological grading (Text S1; Figs S5A & B). Pulmonary lesions were similar in all infected groups; however, their severity and the percentage of bronchi/bronchioles affected differed between and within groups (Fig 5; Figs 6A & B; Table S4). The total histopathological scoring was evaluated by a blinded inter-observer agreement study with weighted kappa coefficients (κW) of 0.67, which is considered to represent substantial agreement (S1 Data) [35]. The histopathological scoring for all pigs euthanized at 3 DPI is presented in S1 Data. The control pig showed no inflammation in the nasal mucosa and upper trachea at 3 DPI. All IAV-inoculated pigs showed acute, moderate, suppurative, necrotizing rhinitis (Fig S6), and all pigs, except one mxH1N1pdm09-infected pig, had acute, necrotizing tracheitis of varied severity at 3 DPI (Figs S7A and B).

Background lung lesions similar to those observed in the control pigs, together with a few additional changes, were found in some infected pigs from each group at 14 DPI (Figs S8A and B; Table S4). Moderate hyperplasia of type 2 pneumocytes was observed at 14 DPI in all IAV-infected groups (Fig 7). Only mild or no lesions of the nasal mucosa and trachea tissues were observed at 14

354 DPI (Fig S7C). A more detailed description of the nasal and tracheal lesions at 3 and 14 DPI is
355 presented in Table S4.

356

357 Ferret study

358 **Clinical impact varied among inoculated, DC, and AT ferrets.** No ferrets
359 developed clinical signs or fever (defined as a temperature above 40°C), but the inoculated and DC
360 ferrets had increased body temperatures at 2 DPI (Figs S9A and B; Text S1). In inoculated ferrets,
361 the median body temperature increase was similar across groups, but the highest body temperature
362 increase was observed in the huH1N1pdm09 group and the lowest in the mxH1N1pdm09 group
363 (Fig S9A; Table S5). In DC ferrets, the highest increase in body temperatures at 2 DPI was in the
364 swH1N1pdm09 and mxH1N1pdm09 groups, as compared with the huH1N1pdm09 group (Fig
365 S9B). The body temperatures of DC ferrets had decreased almost to or below baseline at 5, 7, and 9
366 DPI, whereas the body temperatures of the AT ferrets decreased or remained stable during the study
367 (Fig S9C).

368 The average weight loss in inoculated and DC ferrets was higher in the mxH1N1pdm09
369 group than in the huH1N1pdm09 and swH1N1pdm09 groups (Table S5; Figs S10A and B). In
370 contrast, the weight loss in AT ferrets was highest in the huH1N1pdm09 group and lowest in the
371 swH1N1pdm09 and mxH1N1pdm09 groups (Fig S10C).

372 **The huH1N1pdm09-infected ferrets had the highest viral load**. The viral load
373 was measured in all inoculated ferrets at 2 DPI. The viral load was higher in the inoculated ferrets
374 in the huH1N1pdm09 group than in those in the swH1N1pdm09 and mxH1N1pdm09 groups (Fig
375 8A; Table S5).

All ferrets in the huH1N1pdm09 DC group tested positive for IAV on all sampling days, whereas all swH1N1pdm09 DC ferrets were positive at 2, 5, and 9 DPI and all mxH1N1pdm09 DC ferrets were positive at 5 and 7 DPI (Fig 8B). On all sampling days, the highest viral load was detected in the huH1N1pdm09 DC group, peaking at 4.73×10^9 (1.43×10^9–1.60×10^{10}) copies/mL at 2 DPI. The viral load in the swH1N1pdm09 and mxH1N1pdm09 DC ferrets also peaked at 2 DPI, reaching 6.14×10^8 (1.14×10^8–1.92×10^9) copies/mL in the swH1N1pdm09 ferrets and 2.31×10^9 (6.69×10^8–3.95×10^9) copies/mL in the mxH1N1pdm09 ferrets. DC ferrets also exhibited higher viral shedding at 2 DPI when compared with inoculated ferrets.

All huH1N1pdm09 AT ferrets tested positive for IAV at 5 and 9 DPI, +- one ferret in the huH1N1pdm09 group tested negative for IAV at 7 DPI. Two ferrets in the swH1N1pdm09 group tested positive at different time points (7 DPI and 9 DPI), whereas one ferret remained negative for IAV throughout the study period. One mxH1N1pdm09 AT ferret tested positive for IAV at 2 and 5 DPI, and another tested positive for IAV at 5, 7, and 9 DPI; the last mxH1N1pdm09 AT ferret remained negative throughout the study (Fig 8C). The numbers of DC and AT ferrets that tested positive at least once during the study are summarized in Table S5.

The total viral load of DC and AT ferrets as determined from nasal washes is expressed as the median AUC (Figs S11A and B). The total viral load was highest in the huH1N1pdm09 groups, followed by the mxH1N1pdm09 groups and then the swH1N1pdm09 groups.

The highest viral lung load was found in mxH1N1pdm09 inoculated ferrets. The viral load in tissues collected at 3 DPI from inoculated ferrets is shown in Figure 9 and summarized in Table S5. The highest median viral load in inoculated ferrets was found in the nasal turbinates. In the lungs, the swH1N1pdm09 and mxH1N1pdm09 groups had the highest viral loads in the cranial lung lobes (LU1 and LU4), whereas the highest viral lung load was detected in

399 the caudal lung lobe (LU9) in the huH1N1pdm09 inoculated group. Overall, the highest median
400 viral lung load was found in the mxH1N1pdm09 group. One huH1N1pdm09 DC ferret (no. 13)
401 tested positive for IAV in the nasal turbinates at 14 DPI (1.05×10^5 copies/mL), whereas the
402 remaining DC ferrets tested negative for IAV in all tissue samples.

403 **The huH1N1pdm09-infected groups showed the mildest histopathological**
404 **changes.** Some histopathological changes, which were considered to be unrelated to IAV
405 infection, were found in all groups (Text S1) and were not taken into account in the
406 histopathological evaluation. Lesions were observed in one of three swH1N1pdm09 inoculated
407 ferrets, one of three huH1N1pdm09 inoculated ferrets, and two of three mxH1N1pdm09 inoculated
408 ferrets (Table S6). The lesions ranged from acute, mild, suppurative bronchiolitis with a focal or
409 multifocal distribution (Fig S12A) to acute, mild, necrotizing bronchointerstitial pneumonia (Fig
410 S12B). The lesions affected <10% of the bronchioles.

411 Only mild pulmonary lesions were found in DC ferrets at 14 DPI. These represented mild,
412 suppurative bronchiolitis with a focal or multifocal distribution, affecting <10% of the bronchioles
413 (Table S6).

414 In the nasal turbinates, acute, moderate, suppurative, necrotizing rhinitis was observed in all
415 inoculated groups at 3 DPI (Fig S13). Additionally, all inoculated ferrets presented acute, mild
416 tracheitis at 3 DPI, with mild infiltration of neutrophils in the lamina propria and some neutrophils
417 migrating through the tracheal epithelial cells. No lesions were observed in the nasal or tracheal
418 tissues from huH1N1pdm09-infected DC ferrets at 14 DPI, whereas there was mild infiltration of
419 neutrophils in the lamina propria of both tissues from mxH1N1pdm09-infected and
420 swH1N1pdm09-infected DC ferrets.

421

Discussion

The overall aim of this study was to compare the infection dynamics and pathogenesis of three strains of H1N1pdm09 in pigs and ferrets. The higher virus replication of the swH1N1pdm09 and mxH1N1pdm09 viruses in pigs indicates that these viruses are more adapted to pigs than the huH1N1pdm09 virus. Additionally, lung lesions were significantly more severe in the mxH1N1pdm09-infected group than in the huH1N1pdm09-infected group, and the clinical impact of the mxH1N1pdm09 strain in pigs was greater than that of the swH1N1pdm09 strain. These findings indicate that after at least 10 years of circulation in pigs, the swH1N1pdm virus has increased its ability to replicate in pigs but appears to have reduced pathogenicity, perhaps reflecting pathogen–host adaptation. These results support previous findings of host-adaptation of IAVs that have circulated in their hosts for at least 5 years, including human H1N1pdm09 viruses (investigated in pigs [36] and in human cells and mice [37]), an equine H3N8 influenza [38], and an avian H5N1 influenza [39]. In contrast to another study [36], the viral lung load was highest in pigs infected with the swine-origin (sw and mx) viruses and the clinical impact of the swine-adapted H1N1pdm09 in pigs was less than that of the human-adapted H1N1pdm09 virus. Overall, however, the viral dynamics, clinical signs, and lesions corresponded to those reported by others in pigs experimentally infected with different H1N1pdm09 strains [26,40,41].

Some of the pigs showed signs of emphysema that were probably due to excessive gasping at euthanasia, a phenomenon described previously [42]. All pigs in this study tested negative for PCV2, PRRSV types 1 and 2, and *Mycoplasma hyopneumoniae*. However, because they were from a commercial sow herd, they may have harbored opportunistic bacterial pathogens that could have contributed to some of the clinical and pathological changes seen. For example, four pigs developed polyserositis (pleuritis and pericarditis) and three of these became lethargic during the study. This

446 lethargy was probably not a response to the IAV infection but rather the result of a bacterial co-
447 infection [43,44].

448 In contrast to the findings in pigs, the huH1N1pdm09 strain replicated most efficiently and
449 induced the lowest weight loss in inoculated and DC ferrets, whereas infection with the
450 swH1N1pdm09 strain resulted in the lowest viral load and an intermediary weight loss. This finding
451 supports the relevance of the ferret model in human-adapted IAV transmission studies [45,46]. The
452 histopathological changes in inoculated and DC ferrets corresponded to those reported by others in
453 ferrets experimentally infected with PR8 and H1N1pdm09 IAV strains [47]. Furthermore, the viral
454 dynamics of inoculated and DC ferrets corresponded to those reported in ferrets experimentally
455 infected with an H1N1pdm09 strain, with viral shedding being highest at the beginning of the
456 infection and with the viral load being highest in the nasal turbinates or lungs [48,49]. In contrast to
457 the findings of Munster et al. [49] and Belser et al. [50], who experimentally infected ferrets with
458 A/California/07/2009 (H1N1)pdm09, we observed only a limited clinical impact in our ferret study.
459 This could be because the strains we used have acquired host adaptations important for decreasing
460 the pro-inflammatory responses [37,38].

461 In the ferret study, the highest clinical impact, the highest viral load in the lungs, the most
462 severe lung lesions, and an intermediary total viral load were found in the mxH1N1pdm09-infected
463 inoculated and DC ferrets, which is comparable to the results of the pig experiment. Additionally, in
464 both animal models, the two swine-origin viruses produced the highest viral load in the lungs and
465 more severe lung lesions when compared to the huH1N1pdm09 strain. This finding is consistent
466 with that of Pulit-Penalosa et al. [51], who found that swine-origin H1N1 and H1N2 viruses
467 generally produced higher viral loads in the lower respiratory tract of ferrets when compared with
468 human-origin H1N1pdm09 strains. The higher viral load in the lungs and the higher clinical impact
469 in ferrets inoculated with the swine-origin viruses may be explained by the fact that subsequent

back-titrations of the inoculum showed that ferrets in these groups received 1–1.5 log10 more virus than did those in the huH1N1pdm09 group. One study investigated the clinical signs and virus kinetics in ferrets inoculated with a low dose (10^2 TCID50), a medium dose (10^4 TCID50), and a high dose (10^6 TCID50) of A/California/04/2009. The researchers found that the viral shedding, viral clearance, and greatest weight loss were delayed in the lower-dose group and delayed to an intermediate extent in the medium-dose group, as compared with the high-dose group. Furthermore, the low-dose group had the highest total viral load (AUC) as a result of increased peak viral shedding and delayed viral clearance [52]. Therefore, the differences in the clinical impact and viral kinetics of the inoculated ferrets should be interpreted with caution.

The mxH1N1pdm09 virus was isolated from a pig in Mexico in 2012, but phylogenetically it is situated at a node before the first detected human virus in 2009. Hypothesizing that this strain represents an early precursor of the strain that jumped to humans, it is interesting that this virus appears to be less adapted than the swH1N1pdm09 virus to pigs but better adapted to ferrets. This in turn may indicate that the precursor H1N1pdm09 virus circulated in pigs for a limited time before jumping to humans.

In the AT ferrets, the huH1N1pdm09 virus induced the highest level of viral shedding, but, in contrast to the outcome in the inoculated and DC ferrets, infection also resulted in weight loss. Similar to the dynamic of the huH1N1pdm09 virus in pigs, shedding of the swH1N1pdm09 virus by ferrets was delayed and at a lower level than with the mxH1N1pdm09 virus. Consistent with our findings, another study found that IAV strains differ in their capacity for aerosol transmission between ferrets [53]. Infection with the swH1N1pdm09 strain resulted in positive nasal washes at 1 DPI from two of three AT ferrets. Therefore, we speculate that these viruses have the potential to adapt and be transmitted between humans, because the ferret respiratory droplet transmission model resembles transmission in humans [54]. Two sporadic cases of swine-to-human transmission of

swine-adapted H1N1pdm09 strains were documented in Denmark in 2021, further emphasizing that the clade 1A.3.3.2 viruses have indeed retained their ability to infect humans despite being long adapted to swine [55,56].

This study highlights the relevance of host adaptation; however, more studies are required to determine which mutations are important for host adaptation. Additionally, further work is needed to investigate the innate immune responses to elucidate whether the different clinical outcomes are due to different regulation of the immune system by the viruses.

Acknowledgements

The authors thank Keith A. Laycock, PhD, ELS, for scientific editing of the manuscript. The authors also thank Charlotte K. Hjulsager, senior scientist, for practical and scientific advices.

References

1. Dadonaite B, Gilbertson B, Knight ML, Trifkovic S, Rockman S, Laederach A, et al. The structure of the influenza A virus genome. Nat Microbiol. 2019 Nov;4: 1781-1789. doi: 10.1038/s41564-019-0513-7. Epub 2019 Jul 22. PMID: 31332385; PMCID: PMC7191640.

2. Dou D, Revol R, Östbye H, Wang H, Daniels R. Influenza A Virus Cell Entry, Replication, Virion Assembly and Movement. Front Immunol. 2018 Jul 20;9: 1581. doi: 10.3389/fimmu.2018.01581. PMID: 30079062; PMCID: PMC6062596.

3. Webster RG, Laver WG, Air GM, Schild GC. Molecular mechanisms of variation in influenza viruses. Nature. 1982 Mar 11;296: 115-121. doi: 10.1038/296115a0. PMID: 6174870.

4. Henritzi D, Petric PP, Lewis NS, Graaf A, Pessia A, Starick E, et al. Surveillance of European domestic pig populations identifies an emerging reservoir of potentially zoonotic swine influenza A viruses. Cell Host Microbe. 2020 Oct 7;28: 614-627.e6. doi: 10.1016/j.chom.2020.07.006. Epub 2020 Jul 27. PMID: 32721380.

5. Chauhan RP, Gordon ML. A systematic review analyzing the prevalence and circulation of influenza viruses in swine population worldwide. Pathogens. 2020 May 8;9: 355. doi: 10.3390/pathogens9050355. PMID: 32397138; PMCID: PMC7281378.

6. Mook P, Meerhoff T, Olsen SJ, Snacken R, Adlhoch C, Pereyaslov D, et al. Alternating patterns of seasonal influenza activity in the WHO European Region following the 2009 pandemic, 2010-2018. Influenza Other Respir Viruses. 2020 Mar;14:150-161. doi: 10.1111/irv.12703. Epub 2020 Jan 16. PMID: 31944604; PMCID: PMC7040975.

7. Anderson TK, Macken CA, Lewis NS, Scheuermann RH, van Reeth K, Brown IH, et al. A phylogeny-based global nomenclature system and automated annotation tool for H1 hemagglutinin genes from swine influenza A viruses. mSphere. 2016 Dec 28. doi: 10.1128/mSphere.00275-16.

8. Centers for Disease Control and Prevention (CDC). Swine influenza A (H1N1) infection in two children—Southern California, March–April 2009. MMWR Morb Mortal Wkly Rep. 2009 Apr 24;58: 400-402. PMID: 19390508.

9. Garten RJ, Davis CT, Russell CA, Shu B, Lindstrom S, Balish A, et al. Antigenic and genetic characteristics of swine-origin 2009 A(H1N1) influenza viruses circulating in humans. Science. 2009;325: 197–201.

10. Smith GJD, Vijaykrishna D, Bahl J, Lycett SJ, Worobey M, Pybus OG, et al. Origins and evolutionary genomics of the 2009 swine-origin H1N1 influenza A epidemic. Nature. 2009 Jun 25;459: 1122-1125. doi: 10.1038/nature08182. PMID: 19516283.

11. Guo F, Yang J, Pan J, Liang X, Shen X, Irwin DM, et al. Origin and Evolution of H1N1/pdm2009: a codon usage perspective. Front Microbiol. 2020 Jul 14;11: 1615. doi: 10.3389/fmicb.2020.01615. PMID: 32760376; PMCID: PMC7372903.

12. Webby RJ, Swenson SL, Krauss SL, Gerrish PJ, Goyal SM, Webster RG. Evolution of swine H3N2 influenza viruses in the United States. J Virol. 2000 Sep;74: 8243-8251. doi: 10.1128/jvi.74.18.8243-8251.2000. PMID: 10954521; PMCID: PMC116332.

13. Mena I, Nelson MI, Quezada-Monroy F, Dutta J, Cortes-Fernández R, Lara-Puente JH, et al. Origins of the 2009 H1N1 influenza pandemic in swine in Mexico. Elife. 2016 Jun 28;5: e16777. doi: 10.7554/eLife.16777. PMID: 27350259; PMCID: PMC4957980.

14. Howden KJ, Brockhoff EJ, Caya FD, McLeod LJ, Lavoie M, Ing JD, et al. An investigation into human pandemic influenza virus (H1N1) 2009 on an Alberta swine farm. Can Vet J. 2009 Nov;50: 1153-1161. PMID: 20119537; PMCID: PMC2764467.

15. Nelson MI, Vincent AL. Reverse zoonosis of influenza to swine: new perspectives on the human-animal interface. Trends Microbiol. 2015 Mar;23: 142-153. doi: 10.1016/j.tim.2014.12.002. Epub 2015 Jan 4. PMID: 25564096; PMCID: PMC4348213.

16. Ryt-Hansen P, Krog JS, Breum SØ, Hjulsager CK, Pedersen AG, Trebbien R, et al. Co-circulation of multiple influenza A reassortants in swine harboring genes from seasonal human and swine influenza viruses. Elife. 2021 Jul 27;10: e60940. doi: 10.7554/eLife.60940. PMID: 34313225; PMCID: PMC8397370.

17. Simon G, Larsen LE, Dürrwald R, Foni E, Harder T, Van Reeth K, et al. European Surveillance Network for Influenza in Pigs: surveillance programs, diagnostic tools and swine influenza virus subtypes identified in 14 European countries from 2010 to 2013. PLoS One. 2014 Dec 26;9: e115815. doi: 10.1371/journal.pone.0115815. PMID: 25542013; PMCID: PMC4277368.

18. Watson SJ, Langat P, Reid SM, Lam TTY, Cotten M, Kelly M, et al. Molecular epidemiology and evolution of influenza viruses circulating within European swine between 2009 and 2013 J Virol. 2015 Oct;89: 9920-9931. doi: 10.1128/JVI.00840-15. Epub 2015 Jul 22. PMID: 26202246; PMCID: PMC4577897.

19. Gao S, Anderson TK, Walia RR, Dorman KS, Janas-Martindale A, Vincent AL. The genomic evolution of H1 influenza A viruses from swine detected in the United States between 2009 and 2016. J Gen Virol. 2017 Aug;98: 2001-2010. doi: 10.1099/jgv.0.000885. Epub 2017 Jul 31. PMID: 28758634; PMCID: PMC5817270.

20. Liang H, Lam TT, Fan X, Chen X, Zeng Y, Zhou J, et al. Expansion of genotypic diversity and establishment of 2009 H1N1 pandemic-origin internal genes in pigs in China. J Virol. 2014 Sep;88: 10864-10874. doi: 10.1128/JVI.01327-14. Epub 2014 Jul 9. PMID: 25008935; PMCID: PMC4178866.

21. Sun H, Xiao Y, Liu J, Wang D, Li F, Wang C, et al. Prevalent Eurasian avian-like H1N1 swine influenza virus with 2009 pandemic viral genes facilitating human infection. Proc Natl Acad Sci U S A. 2020 Jul 21;117: 17204-17210. doi: 10.1073/pnas.1921186117. Epub 2020 Jun 29. PMID: 32601207; PMCID: PMC7382246.

22. Sobolev I, Kurskaya O, Leonov S, Kabilov M, Alikina T, Alekseev A, et al. Novel reassortant of H1N1 swine influenza virus detected in pig population in Russia. Emerg Microbes Infect. 2019;8: 1456-1464. doi: 10.1080/22221751.2019.1673136. PMID: 31603050; PMCID: PMC6818105.

23. Nasamran C, Janetanakit T, Chiyawong S, Boonyapisitsopa S, Bunpapong N, Prakairungnamthip D, et al. Persistence of pdm2009-H1N1 internal genes of swine influenza in pigs, Thailand. *Sci Rep*. 2020 Nov 16;10: 19847. doi: 10.1038/s41598-020-76771-2. PMID: 33199784; PMCID: PMC7669897.

24. Zell R, Groth M, Krumbholz A, Lange J, Philipps A, Dürrwald R. Novel reassortant swine H3N2 influenza A viruses in Germany. *Sci Rep*. 2020 Aug 31;10: 14296. doi: 10.1038/s41598-020-71275-5. PMID: 32868846; PMCID: PMC7458913.

25. Goecke NB, Hjulsager CK, Krog JS, Skovgaard K, Larsen LE. Development of a high-throughput real-time PCR system for detection of enzootic pathogens in pigs. J Vet Diagn Invest. 2020 Jan;32: 51-64. doi: 10.1177/1040638719890863. Epub 2019 Nov 21. PMID: 31752620; PMCID: PMC7003221.

26. Schwaiger T, Sehl J, Karte C, Schäfer A, Hühr J, Mettenleiter TC, et al. Experimental H1N1pdm09 infection in pigs mimics human seasonal influenza infections. PLoS One. 2019 Sep 20;14:e0222943. doi: 10.1371/journal.pone.0222943. PMID: 31539406; PMCID: PMC6754157.

27. Cimolai N, Taylor GP, Mah D, Morrison BJ. Definition and application of a histopathological scoring scheme for an animal model of acute *Mycoplasma pneumoniae* pulmonary infection. Microbiol Immunol. 1992;36:465-78. doi: 10.1111/j.1348-0421.1992.tb02045.x. PMID: 1513263.

28. Soerensen CM, Holmskov U, Aalbaek B, Boye M, Heegaard PM, Nielsen OL. Pulmonary infections in swine induce altered porcine surfactant protein D expression and localization to dendritic cells in bronchial-associated lymphoid tissue. Immunology. 2005 Aug;115: 526-535. doi: 10.1111/j.1365-2567.2005.02189.x. PMID: 16011521; PMCID: PMC1782188.

29. Fobian K, Fabrizio TP, Yoon SW, Hansen MS, Webby RJ, Larsen LE. New reassortant and enzootic European swine influenza viruses transmit efficiently through direct contact in the ferret model. J Gen Virol. 2015 Jul;96: 1603-1612. doi: 10.1099/vir.0.000094. Epub 2015 Feb 20. PMID: 25701826; PMCID: PMC4635450.

30. Ryt-Hansen P, Pedersen AG, Larsen I, Krog JS, Kristensen CS, Larsen LE. Acute Influenza A virus outbreak in an enzootic infected sow herd: Impact on viral dynamics, genetic and antigenic variability and effect of maternally derived antibodies

and vaccination. PLoS One. 2019 Nov 14;14:e0224854. doi: 10.1371/journal.pone.0224854. PMID: 31725751; PMCID: PMC6855628.

31. Ryt-Hansen P, Larsen I, Kristensen CS, Krog JS, Larsen LE. Limited impact of influenza A virus vaccination of piglets in an enzootic infected sow herd. Res Vet Sci. 2019 Dec;127: 47-56. doi: 10.1016/j.rvsc.2019.10.015. Epub 2019 Oct 31. PMID: 31677416.

32. De Vleeschauwer A, Atanasova K, Van Borm S, van den Berg T, Rasmussen TB, Uttenthal A, et al. Comparative pathogenesis of an avian H5N2 and a swine H1N1 influenza virus in pigs. PLoS One. 2009 Aug 17;4: e6662. doi: 10.1371/journal.pone.0006662. PMID: 19684857; PMCID: PMC2722722.

33. Kalyaanamoorthy S, Minh BQ, Wong TKF, von Haeseler A, Jermiin LS. ModelFinder: fast model selection for accurate phylogenetic estimates. Nat Methods. 2017 Jun;14: 587-589. doi: 10.1038/nmeth.4285. Epub 2017 May 8. PMID: 28481363; PMCID: PMC5453245.

34. Nguyen LT, Schmidt HA, von Haeseler A, Minh BQ. IQ-TREE: a fast and effective stochastic algorithm for estimating maximum-likelihood phylogenies. Mol Biol Evol. 2015 Jan;32: 268-274. doi: 10.1093/molbev/msu300. Epub 2014 Nov 3. PMID: 25371430; PMCID: PMC4271533.

35. Landis JR, Koch GG. The measurement of observer agreement for categorical data. *Biometrics* 1977 Mar;33: 159-174. PMID: 843571.

36. Fu Y, Durrwald R, Meng F, Tong J, Wu NH, Su A, et al. Infection studies in pigs and porcine airway epithelial cells reveal an evolution of A(H1N1)pdm09 influenza A viruses toward lower virulence. J Infect Dis. 2019 Apr 19;219: 1596-1604. doi: 10.1093/infdis/jiy719. PMID: 30776304; PMCID: PMC7107423.

37. Nogales A, Martinez-Sobrido L, Topham DJ, DeDiego ML. Functional evolution of the 2009 pandemic H1N1 influenza virus NS1 and PA in humans. J Virol. 2018 Sep 12;92: e01206-18. doi: 10.1128/JVI.01206-18. PMID: 30021892; PMCID: PMC6146824.

38. Amat JAR, Patton V, Chauché C, Goldfarb D, Crispell J, Gu Q, et al. Long-term adaptation following influenza A virus host shifts results in increased within-host viral fitness due to higher replication rates, broader dissemination within the respiratory epithelium and reduced tissue damage. PLoS Pathog. 2021 Dec 17;17(12):e1010174. doi: 10.1371/journal.ppat.1010174. PMID: 34919598; PMCID: PMC8735595.

39. Nogales A, Villamayor L, Utrilla-Trigo S, Ortego J, Martinez-Sobrido L, Dediego ML. Natural selection of H5N1 avian influenza A viruses with increased PA-X and NS1 shutoff activity. Viruses. 2021 Sep 3;13: 1760. doi: 10.3390/v13091760. PMID: 34578340; PMCID: PMC8472985.

40. Henningson JN, Rajao DS, Kitikoon P, Lorusso A, Culhane MR, Lewis NS, et al. Comparative virulence of wild-type H1N1pdm09 influenza A isolates in swine. Vet

Microbiol. 2015 Mar 23;176: 40-49. doi: 10.1016/j.vetmic.2014.12.021. Epub 2014 Dec 31. PMID: 25601799.

41. Brookes SM, Núñez A, Choudhury B, Matrosovich M, Essen SC, Clifford D, et al. Replication, pathogenesis and transmission of pandemic (H1N1) 2009 virus in non-immune pigs. PLoS One. 2010 Feb 5;5: e9068. doi: 10.1371/journal.pone.0009068. PMID: 20140096; PMCID: PMC2816721.

42. Mellau LSB, Nonga HE, Karimuribo ED. A slaughterhouse survey of lung lesions in slaughtered stocks at Arusha, Tanzania. Prev Vet Med. 2010 Nov 1;97: 77-82. doi: 10.1016/j.prevetmed.2010.08.008. Epub 2010 Sep 26. PMID: 20875689.

43. Siqueira FM, Pérez-Wohlfeil E, Carvalho FM, Trelles O, Schrank IS, Vasconcelos ATR, et al. Microbiome overview in swine lungs. PLoS One. 2017 Jul 18;12: e0181503. doi: 10.1371/journal.pone.0181503. PMID: 28719637; PMCID: PMC5515459.

44. Sarli G, D'annunzio G, Gobbo F, Benazzi C, Ostanello F. The role of pathology in the diagnosis of swine respiratory disease. Vet Sci. 2021 Oct 29;8: 256. doi: 10.3390/vetsci8110256. PMID: 34822629; PMCID: PMC8618091.

45. Albrecht RA, Liu WC, Sant AJ, Tompkins SM, Pekosz A, Meliopoulos V, et al. Moving forward: recent developments for the ferret biomedical research model. mBio. 2018 Jul 17;9: e01113-18. doi: 10.1128/mBio.01113-18. PMID: 30018107; PMCID: PMC6050969.

46. Belser JA, Eckert AM, Huynh T, Gary JM, Ritter JM, Tumpey TM, et al. A guide for the use of the ferret model for influenza virus infection. Am J Pathol. 2020 Jan;190: 11-24. doi: 10.1016/j.ajpath.2019.09.017. Epub 2019 Oct 23. PMID: 31654637; PMCID: PMC8264465.

47. Perrin TL, Oliphant JW. Pathologic histology of experimental virus influenza in ferrets. Public Health Reports. 1940;55: 1077–1086.

48. Jonsson CB, Camp JV, Wu A, Zheng H, Kraenzle JL, Biller AE, et al. Molecular imaging reveals a progressive pulmonary inflammation in lower airways in ferrets infected with 2009 H1N1 pandemic influenza virus. PLoS One. 2012;7: e40094. doi: 10.1371/journal.pone.0040094. Epub 2012 Jul 20. PMID: 22911695; PMCID: PMC3401186.

49. Munster VJ, Wit E de, Brand JM a van den, Herfst S, Schrauwen EJ a, Bestebroer TM, et al. Pathogenesis and transmission of swine-origin 2009 A(H1N1) influenza virus in ferrets. Science. 2009 Jul 24;325: 481-483. doi: 10.1126/science.1177127. Epub 2009 Jul 2. PMID: 19574348; PMCID: PMC4814155.

50. Belser JA, Gustin KM, Maines TR, Blau DM, Zaki SR, Katz JM, et al. Pathogenesis and transmission of triple-reassortant swine H1N1 influenza viruses isolated before the 2009 H1N1 pandemic. J Virol. 2011 Feb;85: 1563-1572. doi: 10.1128/JVI.02231-10. Epub 2010 Dec 1. PMID: 21123386; PMCID: PMC3028905.

51. Pulit-Penaloza JA, Brock N, Jones J, Belser JA, Jang Y, Sun X, et al. Pathogenesis and transmission of human seasonal and swine-origin A(H1) influenza viruses in the ferret model. Emerg Microbes Infect. 2022 Dec;11: 1452-1459. doi: 10.1080/22221751.2022.2076615. PMID: 35537045; PMCID: PMC9176692.

52. Marriott AC, Dove BK, Whittaker CJ, Bruce C, Ryan KA, Bean TJ, et al. Low dose influenza virus challenge in the ferret leads to increased virus shedding and greater sensitivity to oseltamivir. PLoS One. 2014 Apr 7;9: e94090. doi: 10.1371/journal.pone.0094090. PMID: 24709834; PMCID: PMC3978028.

53. Pulit-Penaloza JA, Jones J, Sun X, Jang Y, Thor S, Belser JA, et al. Antigenically diverse swine origin H1N1 variant influenza viruses exhibit differential ferret pathogenesis and transmission phenotypes. J Virol. 2018 May 14;92: e00095-18. doi: 10.1128/JVI.00095-18. PMID: 29540597; PMCID: PMC5952129.

54. Belser JA, Pulit-Penaloza JA, Maines TR. Ferreting out influenza virus pathogenicity and transmissibility: Past and future risk assessments in the ferret model. Cold Spring Harb Perspect Med. 2020 Jul 1;10: a038323. doi: 10.1101/cshperspect.a038323. PMID: 31871233; PMCID: PMC7328449.

55. Nissen JN, George SJ, Hjulsager CK, Krog JS, Nielsen XC, Madsen T v., et al. Reassortant influenza A(H1N1)pdm09 virus in elderly woman, Denmark, January 2021 Emerg Infect Dis. 2021 Dec;27: 3202-3205. doi: 10.3201/eid2712.211361. PMID: 34808097; PMCID: PMC8632190.

56. Andersen KM, Vestergaard LS, Nissen JN, George SJ, Ryt-Hansen P, Hjulsager CK, Krog JS, Skov MN, Alexandersen S, Larsen LE, Trebbien R. Severe human case of zoonotic infection with swine-origin influenza A virus, Denmark, 2021. Emerg Infect Dis. 2022 Dec;28: 2561-2564. doi: 10.3201/eid2812.220935. PMID: 36418004; PMCID: PMC9707568.

Figure Captions

Figure 1. Study design for the pig experiment. DPI = days post inoculation. The tissue specimens included in this paper are illustrated. Made by Helena Aagaard Glud in Biorender.com. Modified by permission.

Figure 2. **Study design for the ferret experiment.** DPI = days post inoculation. Made by Charlotte Kristensen in Biorender.com.

Figure 3. **Scatterplot of viral shedding as detected by nasal swabbing in pigs on days post inoculation (DPI) 1 to 3.** Each pig is represented by a dot colored according to their group. Black lines represent the median viral shedding of positive samples. The number of positive samples out of the total number of pigs in the group (n = 12) is presented above each cluster of dots. (*/***) denotes a significant difference in viral shedding between groups.

Figure 4. **Viral load in porcine lung tissues (LU1, LU4, LU9), nasal mucosa (NM), upper trachea (UT), and lower trachea (LT) collected at 3 DPI**. Black lines represent the median viral load in the different tissue specimens. The number of positive samples out of the total number of pigs in the groups (n = 8) is presented above each cluster of dots as a fraction.

Figure 5. The group median histopathological scores for each category for pigs at 3 DPI. The categories were as follows: peribronchial/peribronchiolar infiltrates (none, few [<10%], many [10%–50%], majority or all [>50%]), bronchial luminal exudate (none, minimal, heavy), and alveolar infiltrates (none, minimal, heavy) (see Table S2).

Figure 6. **Histopathological changes in infected pigs at 3 days post inoculation.** A) Lung tissue from an mxH1N1pdm09-infected pig at 3 DPI with a histopathological score of 5, showing bronchiolitis with exudation dominated by neutrophils and some mononuclear cells (arrow), patchy infiltration in the alveoli (arrowheads), and peribronchiolar infiltration by mononuclear cells (stars). B) Lung tissue from an swH1N1pdm09-infected pig at 3 DPI with a histopathological score of 7, showing bronchiolitis with massive

exudation of neutrophils and necrotic debris (arrow), infiltration of neutrophils in the alveoli (arrowhead), and marked peribronchiolar infiltration by mononuclear cells (stars). H&E stained.

Figure 7. **Lung tissue from a swH1N1pdm09-infected pig at 14 DPI**. Moderate hyperplasia of cytokeratin positive type II pneumocytes (arrowheads) is demonstrated by immunohistochemical staining for cytokeratin.

Figure 8. **Scatterplot of viral shedding as detected by nasal washes in ferrets.** A) Scatterplot of viral shedding as detected in nasal washes collected from inoculated ferrets at 2 days post inoculation (DPI). B) Scatterplot of viral shedding as detected in nasal washes collected from DC ferrets at 2, 5, 7, and 9 DPI. One 9-DPI sample from the swH1N1pdm09 group was missing. C) Scatterplot of viral shedding as detected in nasal washes collected from AT ferrets at 2, 5, 7, and 9 DPI. Black lines represent the median viral shedding for positive samples. The number of positive samples out of the total number of samples in the group is presented above each cluster of dots as a fraction.

Figure 9. Viral load in inoculated ferret lung tissues (LU1, LU4, LU9), nasal turbinates (NT), and trachea collected at 3 DPI. The number of positive samples out of the total number of ferrets in the group (n = 3) is presented above each cluster of dots as a fraction.

Supporting information

Text S1. Supporting information.

Figure S1. Phylogenetic relationship between inoculum strains. Maximum likelihood tree of nucleotide H1pdm09 segments of the inoculum strains (colored red, blue, and orange), a reference strain for the 2009 pandemic (A/California/07/2009, colored green), and reference strains whose origins are described in the Methods section. Node labels represent bootstrap values.

Figure S2. Total viral load of pigs on days 1, 2, 3 post inoculation (DPI) visualized as the median area under the curve (AUC). Comparison of the total viral loads on days 1, 2, and 3 days post inoculation (DPI), visualized as the median area under the curve (AUC), for the swH1N1pdm09, huH1N1pdm09, and mxH1N1pdm09 groups.

Figure S3. Dynamics of viral shedding in the pigs. Scatterplot of viral shedding detected in nasal swabs collected on days post inoculation (DPI) 1, 2, 3, 4, 7, 10, and 14. Black lines represent the median viral shedding for virus-positive samples. The number of virus-positive samples out of the total number of pigs in the group (n = 4) is shown above each cluster of dots. If no number is indicated, all pigs in that group were virus positive.

Figure S4. Macroscopic appearance of swH1N1pdm09, huH1N1pdm09 and mxH1N1pdm09. Macroscopic appearance of representative lungs collected from pigs 3 days after they were inoculated with different strains of IAV. Areas with atelectasis are marked with arrows. Pigs inoculated with mxH1N1pdm09 had more atelectasis than did pigs inoculated with huH1N1pdm09 or swH1N1pdm09.

Figure S5. Histopathological findings in lungs of control pigs at 3 days post inoculation. A) Lung tissue from a control pig at 3 DPI, showing organized bronchus-associated lymphoid tissue (BALT) (arrows) throughout. B) Lung tissue from a different control pig at 3 DPI, showing acute, mild bronchiolitis with infiltration of macrophages (arrows) and neutrophils (arrowheads). H&E stained.

Figure S6. **Histopathological findings in the nasal mucosa of infected pigs at 3 days post inoculation.** Nasal mucosa from an swH1N1pdm09-infected pig at 3 DPI, showing acute, moderate, suppurative, necrotizing rhinitis with exudation of neutrophils (arrowhead), necrosis (star), and desquamation of epithelial cells (arrow). Notice that only basal cells with intracellular edema remain. H&E stained.

Figure S7. **Histopathological findings in the tracheal tissues of infected pigs at 3 days post inoculation.** A) Trachea from an swH1N1pdm09-infected pig at 3 DPI, showing acute, moderate, suppurative, necrotizing tracheitis with exocytosis of neutrophils (arrowhead) and loss of cilia (arrow). H&E stained. B) Trachea from an mxH1N1pdm09-infected pig at 3 DPI, showing acute, mild, suppurative tracheitis with neutrophils

present in the lamina propria and lamina epithelialis (arrowheads). C) Trachea from an mxH1N1pdm09-infected pig at 14 DPI, showing hyperplasia of the tracheal epithelium and exocytosis of a few neutrophils. H&E stained. H&E stained.

Figure S8. **Histopathological findings in the lung tissues of infected pigs at 14 days post inoculation.** A) Lung tissue from an huH1N1pdm09-infected pig at 14 DPI, showing acute, mild bronchiolitis with macrophages (arrows) and a few neutrophils (arrowhead). B) Lung tissue from an mxH1N1pdm09-infected pig at 14 DPI. Note that the bronchiolar epithelium is missing (arrowhead). H&E stained.

Figure S9. Body temperatures in inoculated, direct-contact (DC) and aerosol transmission (AT) ferrets. A) The change in body temperature (in °C) from baseline (0 DPI) in inoculated ferrets (n = 3) at 2 DPI. The mean baseline temperatures in inoculated ferrets were 38.1°C, 38.4°C, and 38.4°C for the swH1N1pdm09, huH1N1pdm09, and mxH1N1pdm09 groups, respectively. B) The change in body temperature (in °C) from baseline (0 DPI) in DC ferrets (n = 3) at 2, 5, 7, and 9 DPI. The average baseline temperatures in DC ferrets were 38.6°C, 38.7°C, and 38.5°C for the swH1N1pdm09, huH1N1pdm09, and mxH1N1pdm09 groups, respectively. C) The change in body temperatures (in °C) from baseline (0 DPI) in AT ferrets (n = 9) at 2, 5, 7, and 9 DPI. The average baseline temperatures in AT ferrets were 38.3°C, 38.3°C, and 38.7°C for the swH1N1pdm09, huH1N1pdm09, and mxH1N1pdm09 groups, respectively. Ferrets that did not test positive for IAV at any time point during the study are marked with crosses. DPI = days post inoculation.

Figure S10. Body weight loss in inoculated, direct-contact (DC) and aerosol transmission (AT) ferrets. A) Percentage body weight loss in inoculated ferrets (n = 3) from 0 to 2 DPI. Black lines represent the median weight loss per group. B) Percentage body weight loss in DC ferrets (n = 3) from 0 to 2, 0 to 5, 0 to 7, and 0 to 9 DPI. Black lines represent the median weight loss per group. C) Percentage body weight loss in AT ferrets (n = 3) from 0 to 2, 0 to 5, 0 to 7, and 0 to 9 DPI. Black lines represent the median weight loss per group. Crosses in the scatterplot indicate ferrets that tested negative for IAV in nasal washes at any time point. DPI = days post inoculation.

Figure S11. **Total viral load of direct-contact (DC) and aerosol transmission (AT) ferrets on days post inoculation (DPI) 0, 2, 5, 7, and 9 visualized as the median area under the curve (AUC).** A) Comparison of the AUCs for the swH1N1pdm09, huH1N1pdm09, and mxH1N1pdm09 DC ferret groups. B) Comparison of the AUCs for the swH1N1pdm09, huH1N1pdm09, and mxH1N1pdm09 AC ferret groups.

Figure S12. **Histopathological changes in the lungs of inoculated ferrets**. A) Lung tissue from an mxH1N1pdm09-inoculated ferret at 2 DPI, showing acute, mild, suppurative bronchiolitis with scant exudation of neutrophils (arrowheads). B) Lung tissue from an swH1N1pdm09- inoculated ferret at 2 DPI, showing acute, mild, necrotizing bronchointerstitial pneumonia characterized by multifocal, suppurative, necrotizing bronchiolitis (arrow) and exudation to adjacent alveoli (arrowheads). Peribronchiolar and interstitial infiltration dominated by mononuclear cells (orange stars) is also present. H&E stained.

Figure S13. Histopathological changes in the nasal turbinates of inoculated ferrets Nasal turbinates from an mxH1N1pdm09-inoculated ferret at 2 DPI, showing acute, moderate, suppurative, necrotizing rhinitis characterized by infiltration of neutrophils (arrowheads) and mononuclear cells in the lamina propria and necrosis of the nasal epithelium. Notice that only the basal cells remain. H&E stained.

Table S1. Specimens collected for virological and histopathological analysis.

Table S2. **Histopathology scoring scheme.**

Table S3. Macroscopic evaluation of the porcine lungs. Necropsy date, gross lesions, distribution of atelectasis, macroscopic score for each lung lobe, and number of lobes affected for each pig. The macroscopic score in bold is the overall macroscopic score for that pig.

Table S4. **Morphological diagnoses of the lung, nasal mucosa, and tracheal lesions observed at 3 and 14 days post inoculation (DPI) and the number of affected pigs in each group**. HP = histopathological score.

Table S5. **Summary of results from inoculated ferrets.**

Table S6. Morphological diagnoses of lung lesions in inoculated ferrets at 3 days post inoculation (DPI) and in direct contact (DC) infected ferrets at 14 DPI. The number of affected ferrets in each group is shown.

S1 data. Excel spreadsheet containing summary statistics, ELISA results, viral load in porcine tissues, histopathological grading and inter-observer agreements. Data is presented in different sheets (XLSX).

Figures

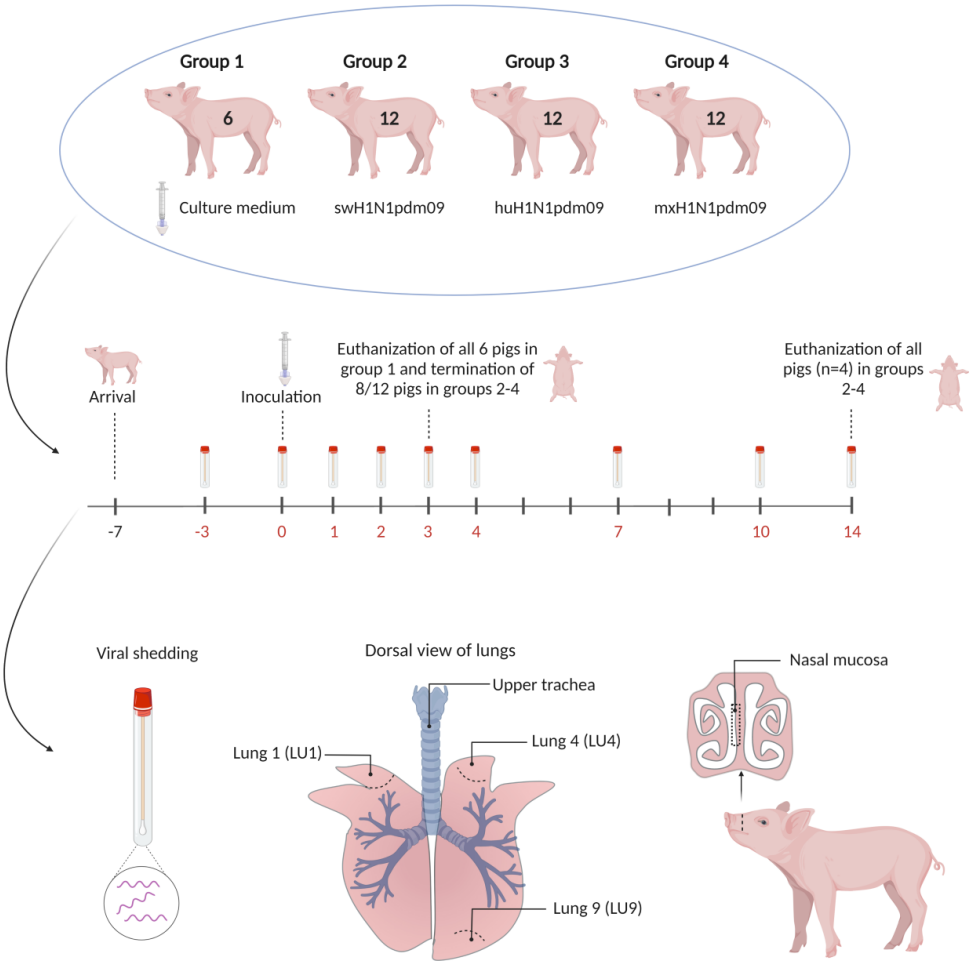

Figure 1. Study design for the pig experiment. DPI = days post inoculation. The tissue specimens included in this paper are illustrated. Made by Helena Aagaard Glud in Biorender.com. Modified by permission.

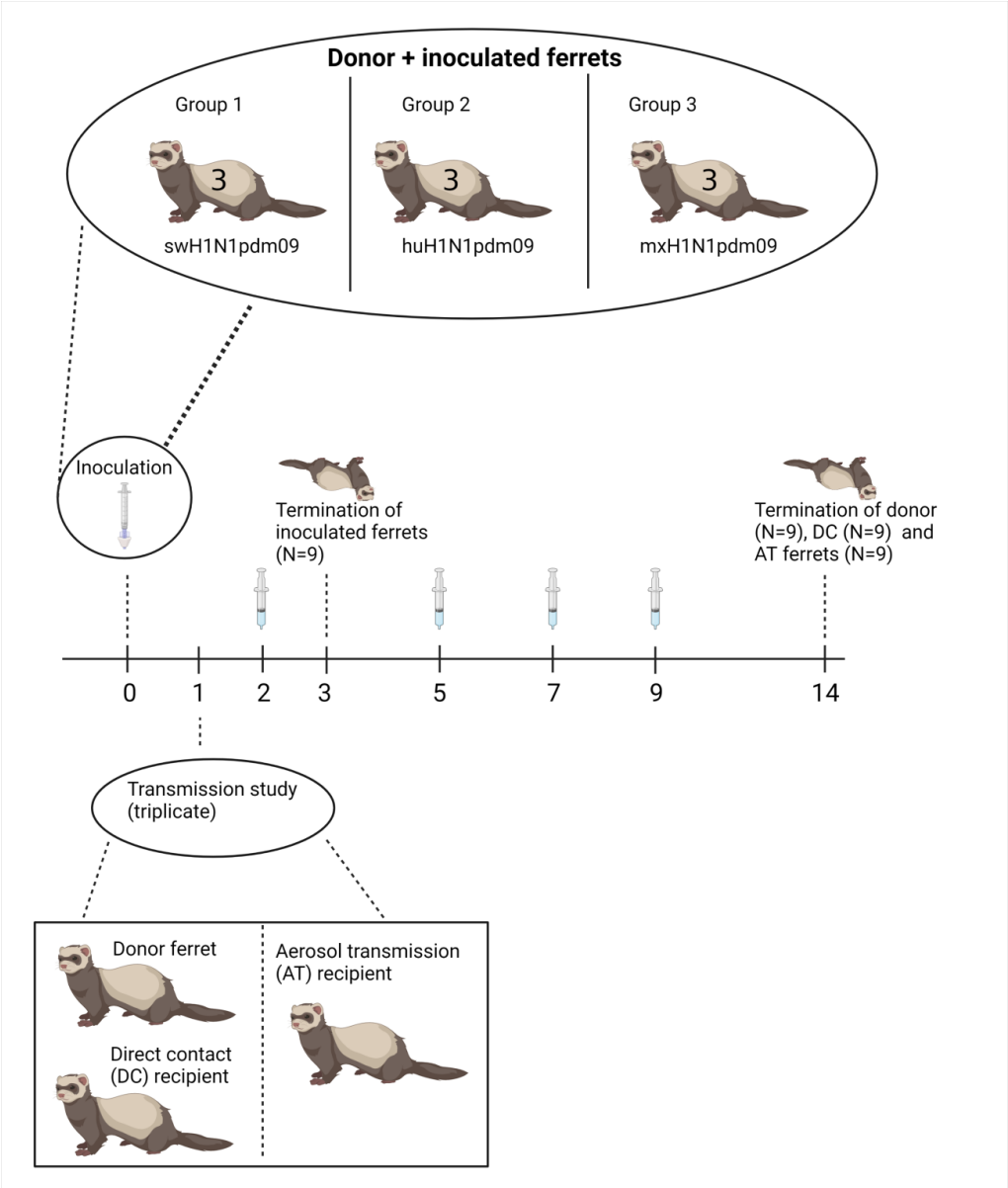

Figure 2. **Study design for the ferret experiment.** DPI = days post inoculation. Made by Charlotte Kristensen in Biorender.com.

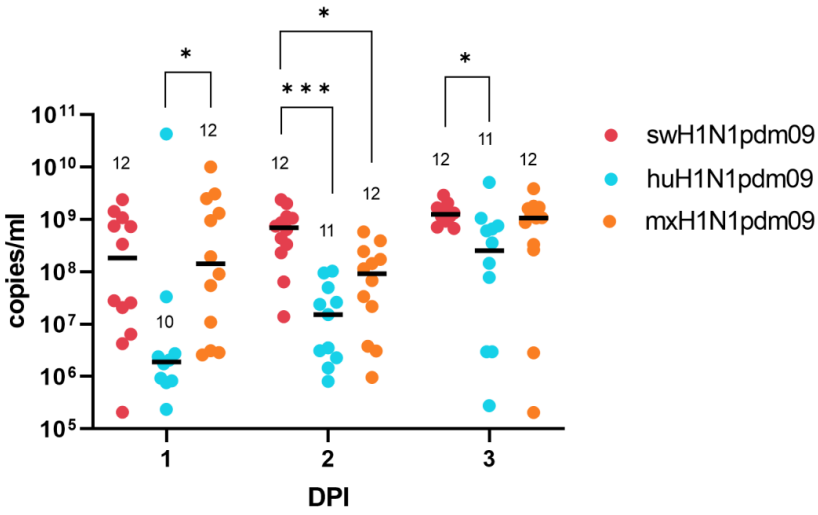

Figure 3. **Scatterplot of viral shedding as detected by nasal swabbing in pigs on days post inoculation (DPI) 1 to 3.** Each pig is represented by a dot colored according to their group. Black lines represent the median viral shedding of positive samples. The number of positive samples out of the total number of pigs in the group (n = 12) is presented above each cluster of dots. (*/***) denotes a significant difference in viral shedding between groups.

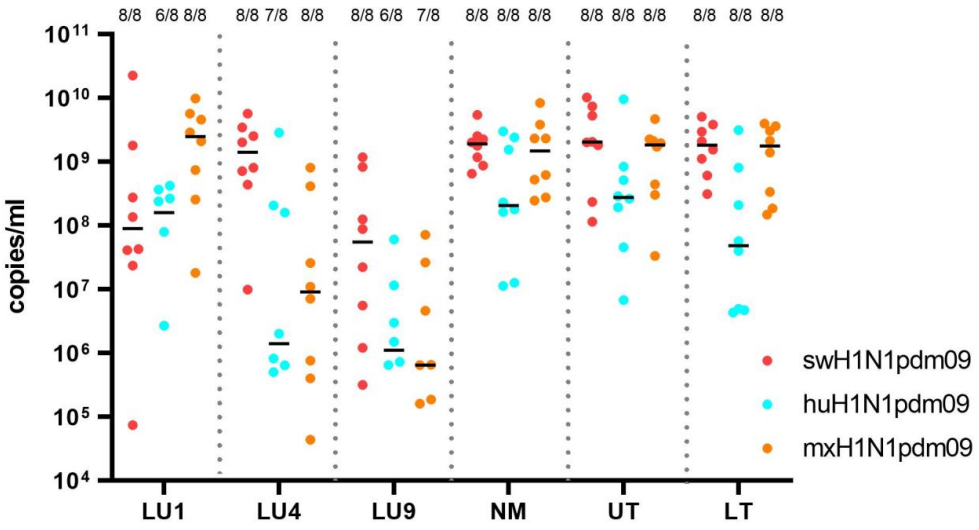

Figure 4. **Viral load in porcine lung tissues (LU1, LU4, LU9), nasal mucosa (NM), upper trachea (UT), and lower trachea (LT) collected at 3 DPI**. Black lines represent the median viral load in the different tissue specimens. The number of positive samples out of the total number of pigs in the groups (n = 8) is presented above each cluster of dots as a fraction.

Figure 5. The group median histopathological scores for each category for pigs at 3 DPI. The categories were as follows: peribronchial/peribronchiolar infiltrates (none, few [<10%], many [10%–50%], majority or all [>50%]), bronchial luminal exudate (none, minimal, heavy), and alveolar infiltrates (none, minimal, heavy) (see Table S2).

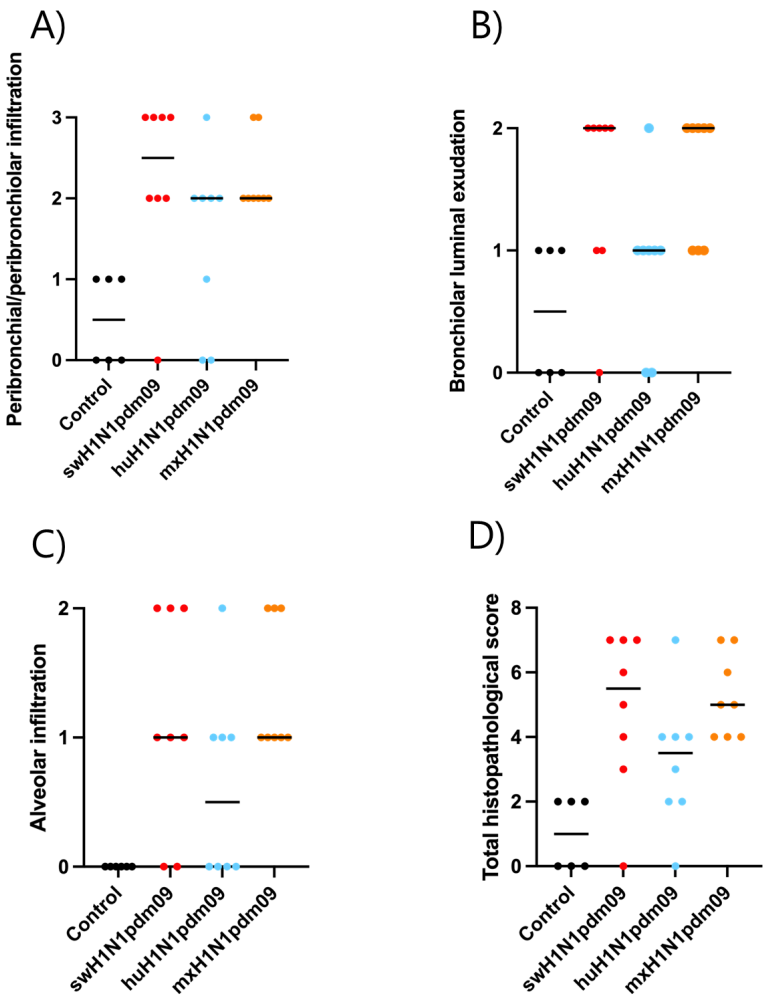

Figure 5. The group median histopathological scores for each category for pigs at 3 DPI. The categories were as follows: peribronchial/peribronchiolar infiltrates (none, few [<10%], many [10%–50%], majority or all [>50%]), bronchial luminal exudate (none, minimal, heavy), and alveolar infiltrates (none, minimal, heavy) (see Table S2).

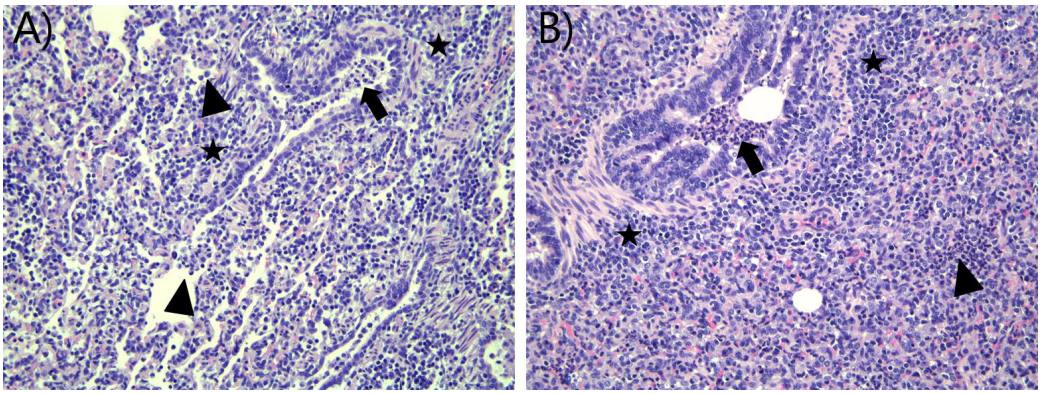

Figure 6. **Histopathological changes in infected pigs at 3 days post inoculation.** A) Lung tissue from an mxH1N1pdm09-infected pig at 3 DPI with a histopathological score of 5, showing bronchiolitis with exudation dominated by neutrophils and some mononuclear cells (arrow), patchy infiltration in the alveoli (arrowheads), and peribronchiolar infiltration by mononuclear cells (stars). B) Lung tissue from an swH1N1pdm09-infected pig at 3 DPI with a histopathological score of 7, showing bronchiolitis with massive exudation of neutrophils and necrotic debris (arrow), infiltration of neutrophils in the alveoli (arrowhead), and marked peribronchiolar infiltration by mononuclear cells (stars). H&E stained.

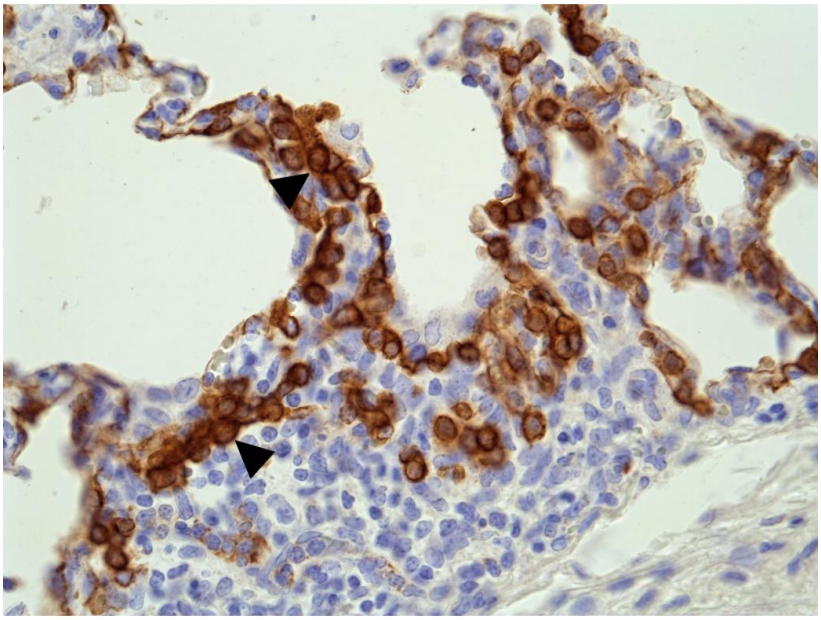

Figure 7. **Lung tissue from a swH1N1pdm09-infected pig at 14 DPI**. Moderate hyperplasia of cytokeratin positive type II pneumocytes (arrowheads) is demonstrated by immunohistochemical staining for cytokeratin.

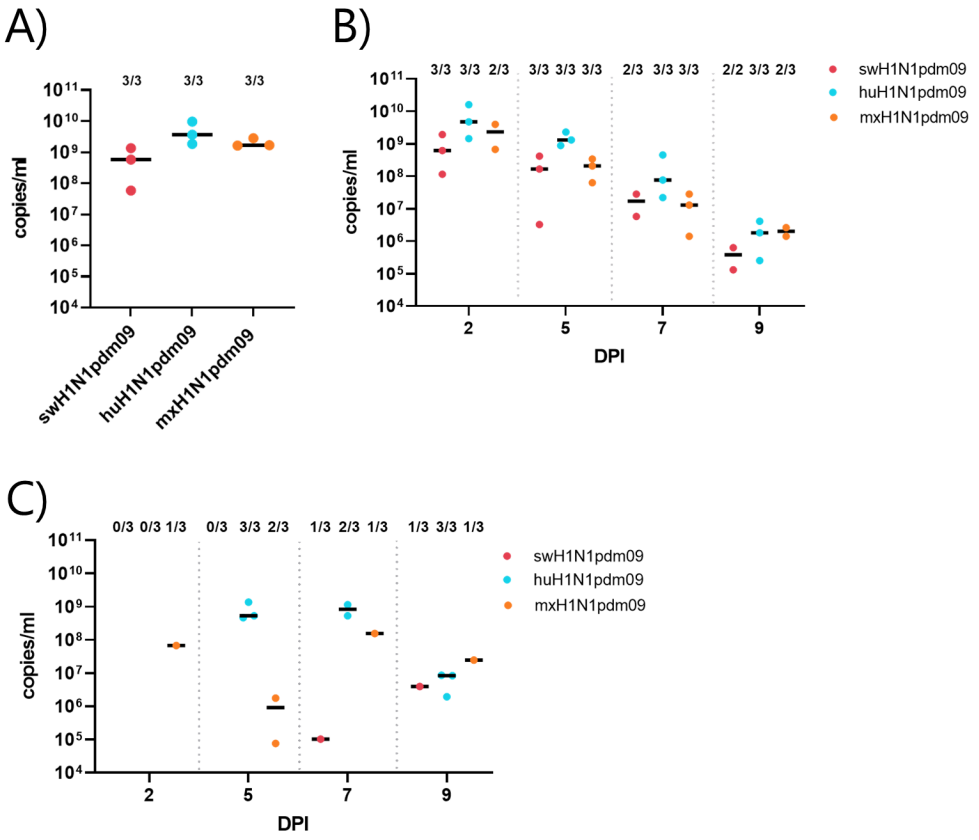

Figure 8. **Scatterplot of viral shedding as detected by nasal washes in ferrets.** A) Scatterplot of viral shedding as detected in nasal washes collected from inoculated ferrets at 2 days post inoculation (DPI). B) Scatterplot of viral shedding as detected in nasal washes collected from DC ferrets at 2, 5, 7, and 9 DPI. One 9-DPI sample from the swH1N1pdm09 group was missing. C) Scatterplot of viral shedding as detected in nasal washes collected from AT ferrets at 2, 5, 7, and 9 DPI. Black lines represent the median viral shedding for positive samples. The number of positive samples out of the total number of samples in the group is presented above each cluster of dots as a fraction.

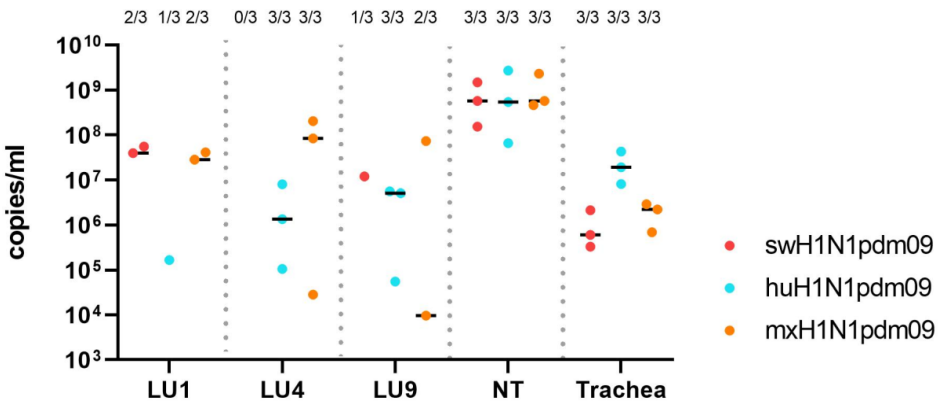

Figure 9. Viral load in inoculated ferret lung tissues (LU1, LU4, LU9), nasal turbinates (NT), and trachea collected at 3 DPI. The number of positive samples out of the total number of ferrets in the group (n = 3) is presented above each cluster of dots as a fraction.

4.3 Paper 3

Kinetics and magnitude of mucosal antiviral innate immune responses in nasopharyngeal swab specimens depends on host adaptation of influenza A virus

Helena Aagaard Glud, Anders Gorm Pedersen, Louise Brogaard, Chrysillis Hellemann Polhaus, Charlotte Kristensen, Ramona Trebbien, Lars Erik Larsen, and Kerstin Skovgaard

Corresponding Author: Helena Aagaard Glud, haaglu@dtu.dk

Manuscript in preparation

Kinetics and magnitude of mucosal antiviral innate immune responses in nasopharyngeal swab specimens depends on host adaptation of influenza A virus

Helena Aagaard Glud[1], Anders Gorm Pedersen[2], Louise Brogaard[1], Chrysillis Hellemann Polhaus[1], Charlotte Kristensen[3], Ramona Trebbien[4], Lars Erik Larsen[3], Kerstin Skovgaard[1]

[1]Department of Biotechnology and Biomedicine, Technical University of Denmark, Kongens Lyngby, Denmark

[2]Department of Health Technology, Technical University of Denmark, Kongens Lyngby, Denmark

[3]Department of Veterinary and Animal Sciences, University of Copenhagen, Copenhagen, Denmark

[4]Department of Virus and Microbiological Special Diagnostics, Statens Serum Institut, Copenhagen S, Denmark

Corresponding author: Helena Aagaard Glud, Department of Biotechnology and Biomedicine, Technical University of Denmark, Søltofts Plads, Building 224, 2800 Kongens Lyngby, Denmark. Phone: +4542404863. E-mail: haaglu@dtu.dk

Abstract

Four influenza pandemics have occurred during the past 100 years, and new variants of the influenza virus will continue to emerge. The pandemic potential of novel influenza strains is difficult to evaluate as we lack basic knowledge of immune dynamic differences between seasonal and pandemic influenza strains. Using non-invasive nasopharyngeal swabs, we investigated and compared the transcriptional antiviral innate immune response by high-throughput qPCR daily after experimental infection of pigs with three different strains of influenza A virus (IAV) including a swine-adapted, a human-adapted, and a "pre-pandemic" H1N1pdm09 isolate. A strong antiviral innate immune response was initiated in all infected groups, including an interferon-mediated response and upregulation of several cytokines and chemokines. The swine-adapted IAV induced a fast and strong expression of innate factors compared to the human-adapted IAV, while the pre-pandemic IAV induced a prolonged mucosal immune response in the infected pigs compared to the two other viruses. In addition, downregulation of mucins (*MUC5AC, MUC5B,* and *MUC12*) in the pigs infected with the swine-adapted IAV strain was observed. Overall, we demonstrate important differences in kinetics and expression levels of genes involved in the classical antiviral immune response and respiratory mucin production upon infection with human and swine IAV strains.

Importance

IAV evolves fast and has several mechanisms to do so, which results in many new IAV strains increasing the potential of creating a new pandemic. Viral and host markers important for host adaptation of IAV are poorly defined, which makes it challenging to evaluate the pandemic potential of novel IAV strains. In this study, the host response against three different H1N1pdm09 viruses with different degrees of host adaptation was assessed by high-throughput microfluidic qPCR.

Key words: Influenza virus, experimental infection, mucosal innate immunity, nasopharyngeal swabs, IAV adaptation

Introduction

Influenza A virus (IAV) is a zoonotic virus which causes respiratory illness worldwide. IAV causes annual seasonal epidemics and occasional global pandemics. The annual epidemics lead to approximately 3-5 million cases of severe illness, resulting in about 290,000-650,000 deaths each year[1]. The natural reservoir of IAV is aquatic birds, but IAV can infect many other species, such as humans, pigs, poultry, ferrets, and horses[2–5]. The wide host range and regular interaction between many of the host species highlights the risk of emergence of new reassorted influenza viruses with zoonotic and even pandemic potential. Indeed, the latest pandemic in 2009 originated from swine[6]. The pandemic potential of novel swine IAV strains is difficult to evaluate. Viral mutation rate and the range of susceptible host species have been demonstrated to be uncorrelated across many viruses[7], and high viral load does not always equal high clinical impacts ("Unpublished data", Kristensen C, Glud HA, Crumpton JC, Martiny K, Webb A, Ryt-Hansen P, et al.). This highlights the importance of investigating host factors in relation to IAV infection in the context of identifying IAV strains with higher zoonotic and pandemic potential.

IAV enters the respiratory airways through the nasal cavity, where the virus has to penetrate the airway mucus layer to reach and infect the underlying respiratory epithelial cells. Infection is initiated by binding of the viral surface protein hemagglutinin (HA) to host cell surface receptors. Human and swine IAVs prefer sialic acid (SA) linked to galactose by α-2,6 (SA-α2,6) linkage, while avian IAVs prefer SA-α2,3 as receptor[3,8,9]. The airway distribution of SA-α2,6 receptors is highly similar in humans and pigs, as is the mucin composition of the airway mucus and distribution of mucus-secreting goblet cells[10]. The airway mucus of mammals consists of two layers: a viscous gel-like layer situated on top of a periciliary liquid layer (PCL)[11]. The viscous gel-like layer consists of secreted mucins, mainly MUC5AC and MUC5B, secreted from goblet cells and mucous cells of the submucosal glands, respectively. These mucins are sialic acid bearing, and as a result, they can act as decoy receptors binding and facilitating the removal of

IAV by mucociliary clearance. The PCL consists of transmembrane mucins, such as MUC12, MUC15, and MUC20, presented on ciliated respiratory epithelial cells. The transmembrane mucins attract water resulting in reduced viscosity, facilitating ciliary beating essential for mucociliary clearance.

If IAV does manage to reach and infect the host cells, it is recognised by pattern recognition receptors (PRRs), including Toll-like receptors (TLRs) and retinoic acid-inducible gene I-like receptors (RLRs). Activation of the PRRs induces a signalling cascade where transcription factors, such as IFN-regulatory factors (IRFs) and nuclear factor-κB (NF-κB), are activated, resulting in the transcription and production of interferons (IFNs), pro-inflammatory cytokines, and chemokines[15,16,17]. Secreted IFNs stimulate the expression of hundreds of IFN-stimulated genes (ISGs) in the infected cell as well as in neighbouring cells. ISGs interfere with and restrict viral replication, while cytokines and chemokines recruit and activate immune cells[18,19]. However, the pro-inflammatory cytokine and chemokine response is also associated with the immunopathology observed during severe respiratory viral infections caused by IAV[20,21], SARS-CoV-2[22,23], and respiratory syncytial virus (RSV)[24,25]. IAV pathogenesis and disease severity are also influenced by other innate immune factors, including IFITM3 and IRF9[26,27], emphasising the importance of determining the specific innate host factors involved in IAV pathogenesis and deducing their mechanism of action.

Even though the nasal mucosa acts as the primary site of exposure to IAV infection and the vast majority of all infections are assumed to be contained by the innate immune system, viral recognition and innate immune responses in the nasal mucosa are poorly understood. Additionally, mucosal immune dynamics upon infection with human- and swine-adapted IAV have never been investigated. Here we aimed to study mucosal and innate immune factors centrally involved in IAV recognition and control, and how host adaptation of the infecting IAV strain affects these processes. To this end, nasopharyngeal specimens were collected daily from experimentally challenged pigs with swine-adapted (swH1N1pdm09), human-adapted (huH1N1pdm09), and “pre-pandemic” (mxH1N1pdm09) IAV

("Unpublished data", Kristensen C, Glud HA, Crumpton JC, Martiny K, Webb A, Ryt-Hansen P, et al.). Gene expression levels were analysed using high-throughput microfluidic qPCR.

Results

High-quality RNA extracted from swab samples

The nasal mucosal RNA samples were of high quality, with 260/280 absorbance ratios above 1.8 and a mean RNA integrity number (RIN) of 7[28]. High reproducibility was seen for cDNA replicates produced from the same RNA sample after data analysis using our primer assays optimised for medium to low RNA quality[29]. The mean and range of RNA concentration, purity, and integrity are listed in Supplementary Table 1.

Classical innate antiviral immune response characterised in non-invasive nasopharyngeal swab samples after IAV infection

A classical innate antiviral immune response was observed in the nasal mucosa of all three inoculated groups after IAV infection. The expression of 76 genes centrally involved in the antiviral innate immune response was investigated, and statistically significant changes in the expression of mucins, PRRs, transcription factors and adapter proteins, IFNs, ISGs, cytokines, and chemokines were seen at one or more time points after inoculation in all groups (Table 1). All statistically significantly upregulated and downregulated genes are summarised in Supplementary Table 2.

A rapid increase of important PRRs in the antiviral immune pathway, including *DDX58* (RIG-I), *IFIH1* (MDA5), *TLR7*, and *TLR8*, as well as downstream transcription factors (*IRF7*, *IRF9*, and *STAT1*), ISGs, and cytokines and chemokines, was seen in the nasopharyngeal swab samples at 1 day post inoculation (dpi) in response to all three IAV strains (Figure 1).

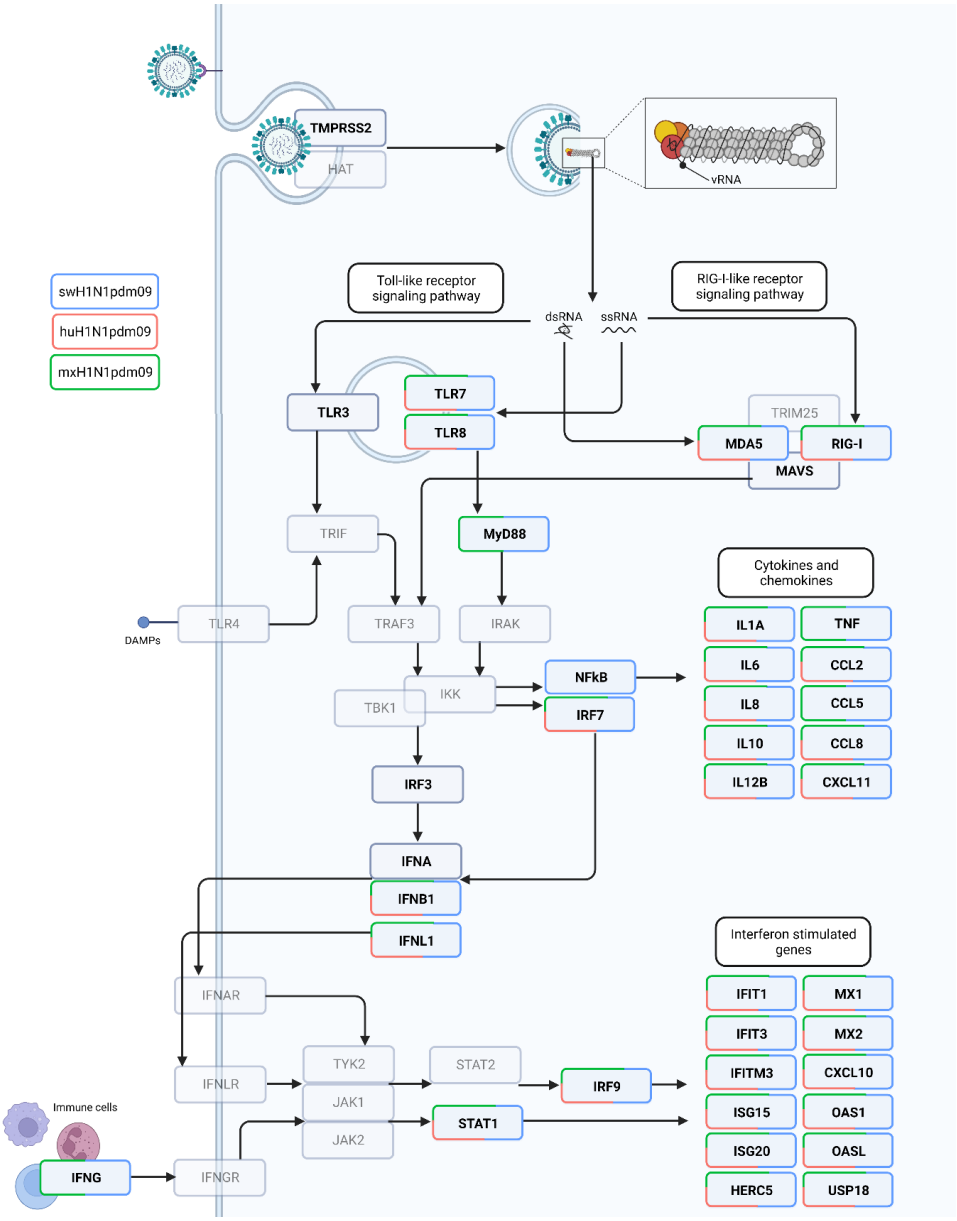

Figure 1: Many genes in the antiviral innate pathway are induced after infection with all IAV strains. Differentially expressed genes in the antiviral innate pathway at 1 day post inoculation in all infected groups highlighted by color (blue, swH1N1pdm09; light red, huH1N1pdm09; green, mxH1N1pdm09). No color (grey): not regulated in any groups. Transparent genes: not investigated in this study. Created with BioRender.com.

Type I IFN (*IFNB1*) and type III IFN (*IFNL1* (IL29)) were upregulated in all groups at 1 to 4 dpi, with *IFNB1* as the most highly differentially expressed of the two (Figure 2). ISGs were also highly expressed from 1 to 4 dpi, including genes from the IFN-induced protein with tetratricopeptide repeats (IFIT) family (*IFIT1* and *IFIT3*), the oligoadenylate synthetase (OAS) family (*OAS1* and *OASL*), *MX1/2*, and *CXCL10* (Figure 1 and Figure 2). Likewise, induction of important negative regulators of type I IFN and inflammation, namely *USP18*, *IL1RN*, and *IL10*, were observed after IAV inoculation (Supplementary Table 2). Cytokines (*IL12B*, *IL1A*, and *IL1B*) were upregulated at 1 to 7 dpi in all groups (Figure 3). Thus, a classical innate antiviral immune response after experimental IAV infection can be monitored daily in non-invasive nasopharyngeal swab samples.

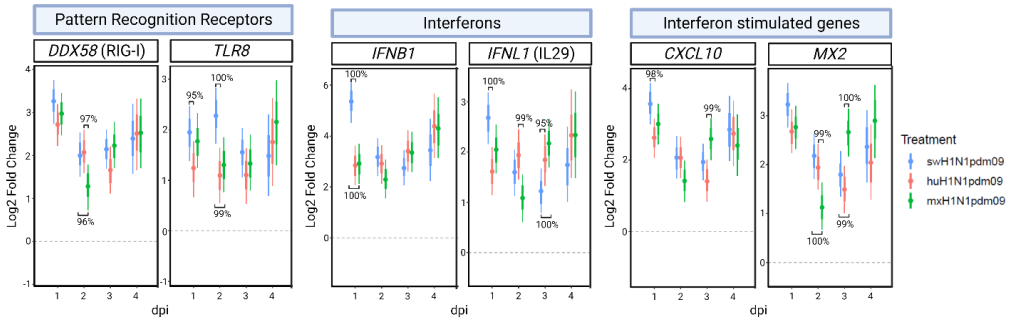

Figure 2: A classical innate antiviral immune response (pattern recognition receptors, interferons, and interferon stimulated genes) was initiated early after infection in all infected groups. A selection of significant differentially expressed genes in nasopharyngeal swab samples (blue, swH1N1pdm09; light red, huH1N1pdm09; green, mxH1N1pdm09). Data are shown as mean log2 fold change (dot) compared to baseline, the 60% credible interval (thick bar), and the 90% credible interval (thin bar). Significant differences between the infected groups (Posterior probability of >95%) are indicated with brackets. dpi = day post inoculation.

Rapid onset of the immune response against swH1N1pdm09 and prolonged response after mxH1N1pdm09 infection

The total number of statistically significant upregulated genes (+2-fold compared to baseline, posterior probability >95%) on each day after inoculation with the three strains is summarised in Table 1. Differential expression levels of single genes of interest can be seen in Supplementary Table 2.

The highest number of antiviral genes differentially expressed in the nasopharyngeal specimens after inoculation was found in the swH1N1pdm09 group at 1 dpi (n=52), followed by the mxH1N1pdm09 group (n=49) and the huH1N1pdm09 group (n=45) at 4 dpi (Table 1). In general, the immune response had a rapid onset in the swH1N1pdm09 group with high expression of PRRs, transcription factors and adapters, interferons, ISGs, cytokines, and chemokines at 1 dpi, followed by a decrease in expression until 14 dpi with the exception of 4 dpi where the expression levels were re-induced, though not to the same magnitude as at 1 dpi. However, pro and anti-inflammatory cytokines (*IL10*, *IL12B*, *IL17A*, *IL1A*, *IL1B*, *IL1RN*) had peak expression levels at 2 dpi (FC of 3.2-24.7) in the swH1N1pdm09 group (Figure 3). The expression of immune genes in the huH1N1pdm09 group had a similar expression pattern with re-induction at 4 dpi, though the response was dampened compared to the swH1N1pdm09 group with fewer differentially expressed genes and lower FC increase. This pattern of lower expression levels in antiviral innate pathways was seen both in the initial phase and further downstream (Figure 2 and Figure 3).

The immune response in the mxH1N1pdm09 group had a prolonged duration compared to the other two infected groups. PRRs, IFNB1, ISGs, cytokines, and chemokines were strongly expressed from 1 to 4 dpi (Figure 2 and Figure 3), with peak expression at 4 dpi. A decrease in gene expression levels was first seen at 7 dpi, therefore the re-induction of gene expression at 4 dpi seen in the other groups was not observed until 10 dpi, where substantially more genes were differentially expressed (Table 1) with high expression levels (Supplementary table 2). Especially cytokines (*IL10*, *IL12B*, *IL1A*, *IL1B*, *IL1RN,* and *IL6*) were highly expressed at 10 dpi (FC of 5.2-7.8) in the mxH1N1pdm09 group (Figure 3). Some of the

159 cytokines were still significant differentially expressed at 14 dpi (*IL1A* and *IL1RN*) together with other
160 pro- and anti-inflammatory proteins (*SELL, PTGS2* (COX-2)*,* and *TNFAIP3*)*.* Late expression of cytokines
161 was only observed for *IL6* in the other IAV inoculated groups at 10 dpi (and at 14 dpi in the
162 swH1N1pdm09 group), as well as *IL12B* for the huH1N1pdm09 group and *IL10* for the swH1N1pdm09
163 group. Thus, the expression pattern of the immune response in the mxH1N1pdm09 differed from the
164 two other IAV inoculated groups with a more sustained innate response (1 to 4 dpi) followed by a
165 prolonged response with high expression levels of immune genes at 10 and 14 dpi, this was especially
166 true for the cytokines.

167 There were other noteworthy differences between the groups, e.g. the differential expression of the
168 inflammatory marker *S100A7* was found solely in the mxH1N1pdm09 group at 3 dpi (FC of 3.6) and 14
169 dpi (FC of 3.3) and the absence of upregulation of the important transcription factor *NFKB1* at any time
170 point in the huH1N1pdm09 group. Lastly, downregulation of four genes was only shown in the
171 swH1N1pdm09 group (*C4A*, *CXCL9*, *IFNA1*, and *TLR3*) at 2 dpi and three of them (*CXCL9*, *IFNA1*, and
172 *TLR3*) at 4 dpi as well (Supplementary Table 2).

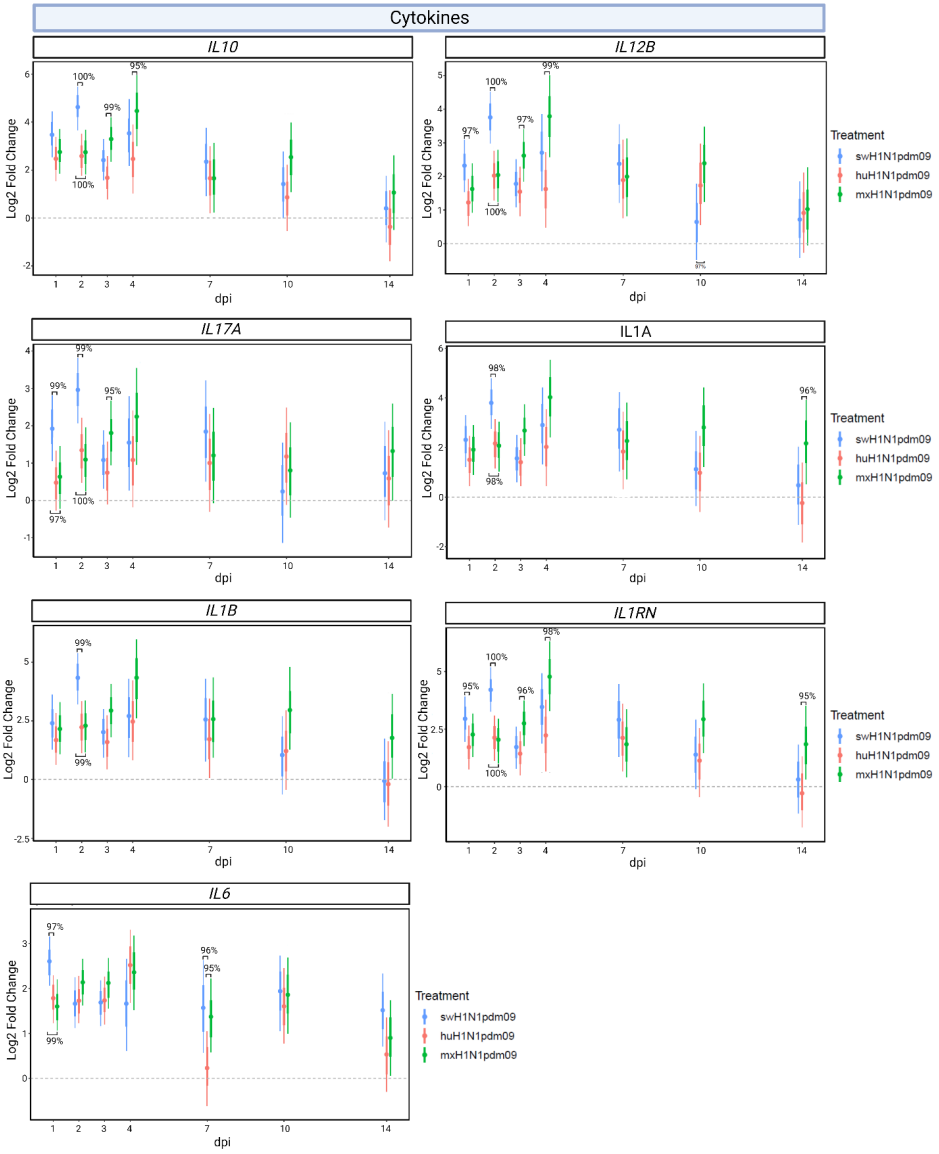

Figure 3: Cytokine expression was induced early after infection with all IAV strains but was prolonged during mxH1N1pdm09 infection. A selection of significant differentially expressed genes in nasopharyngeal swab samples (blue, swH1N1pdm09; light red, huH1N1pdm09; green, mxH1N1pdm09). Data are shown as mean log2 fold change (dot) compared to baseline, the 60% credible interval (thick bar), and the 90% credible interval (thin bar). Significant differences between the infected groups (Posterior probability of >95%) are indicated with brackets. dpi = day post inoculation.

The highest viral load was found after infection with swH1N1pdm09, while clinical signs were more severe in pigs infected with mxH1N1pdm09

Viral RNA load from nasopharyngeal swab samples, clinical signs, and histopathological changes of the nasal mucosa are reported in detail in Kristensen et al., in prep. Viral load peaked at 4 dpi in all infected groups. The highest viral load was observed in the swH1N1pdm09 group (2.10 × 10^9 copies/ml), followed by the mxH1N1pdm09 group (1.61 × 10^9 copies/ml) and lastly, the huH1N1pdm09 group (6.25 × 10^8 copies/ml) (All control pigs were negative) (Figure 4).

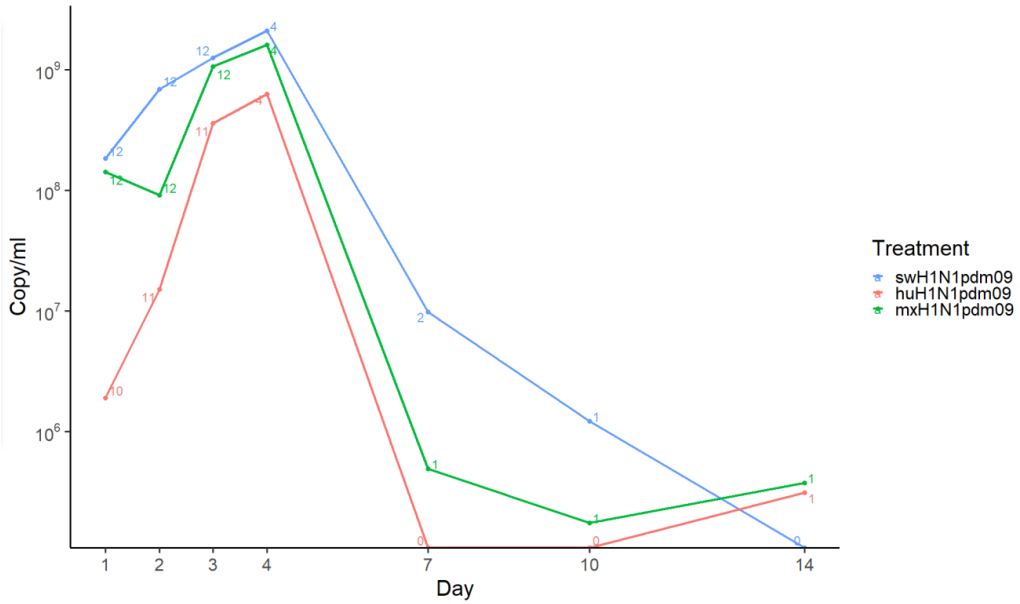

Figure 4: Highest viral load in swab samples after infection with swH1N1pdm09. Viral load quantified by qPCR in swab samples of all pigs from 1-14 days post inoculation (blue, swH1N1pdm09; light red, huH1N1pdm09; green, mxH1N1pdm09). The number of positive animals is indicated at each time point. Results obtained from Kristensen et al., in prep.

Gains in body weight and temperature were measured during the entire study. Fever (rectal temperature above 40°C) was observed in several pigs from the mxH1N1pdm09 group (5/12 pigs experienced fever at least one day during the study), together with the lowest weight gain compared to

193 the other infected groups. Fever was only observed in one and three pigs from the swH1N1pdm09 and
194 huH1N1pdm09, respectively. Inflammation was observed in nasal mucosa tissue in all inoculated pigs
195 with acute, moderate, suppurative, necrotising rhinitis with exudation of neutrophils. No inflammation
196 was found in control pigs ("Unpublished data", Kristensen C, Glud HA, Crumpton JC, Martiny K, Webb A,
197 Ryt-Hansen P, et al.).

198 **Downregulation of mucins after infection with swH1N1pdm09**

199 A distinctive difference in the innate immune response upon infection with the three different IAV
200 strains was the substantial downregulation of several mucins in the swH1N1pdm09 group. The main
201 secreted mucins, *MUC5AC* and *MUC5B*, were downregulated in the early period of infection (Figure 5
202 and Supplementary Table 2). The transmembrane mucin *MUC12* was significantly downregulated in the
203 swH1N1pdm09 group at 2, 3, and 7 dpi (FC of 0.23-0.44). In the other IAV inoculated groups,
204 downregulation of *MUC5AC* was only observed at 2 dpi (huH1N1pdm09: FC of 0.49 and mxH1N1pdm09:
205 FC of 0.45). *MUC5B* and *MUC12* were not significant differentially expressed in the other IAV inoculated
206 groups, except at 7 dpi in the huH1N1pdm09 group where they were significantly downregulated (Figure
207 5 and Supplementary Table 2).

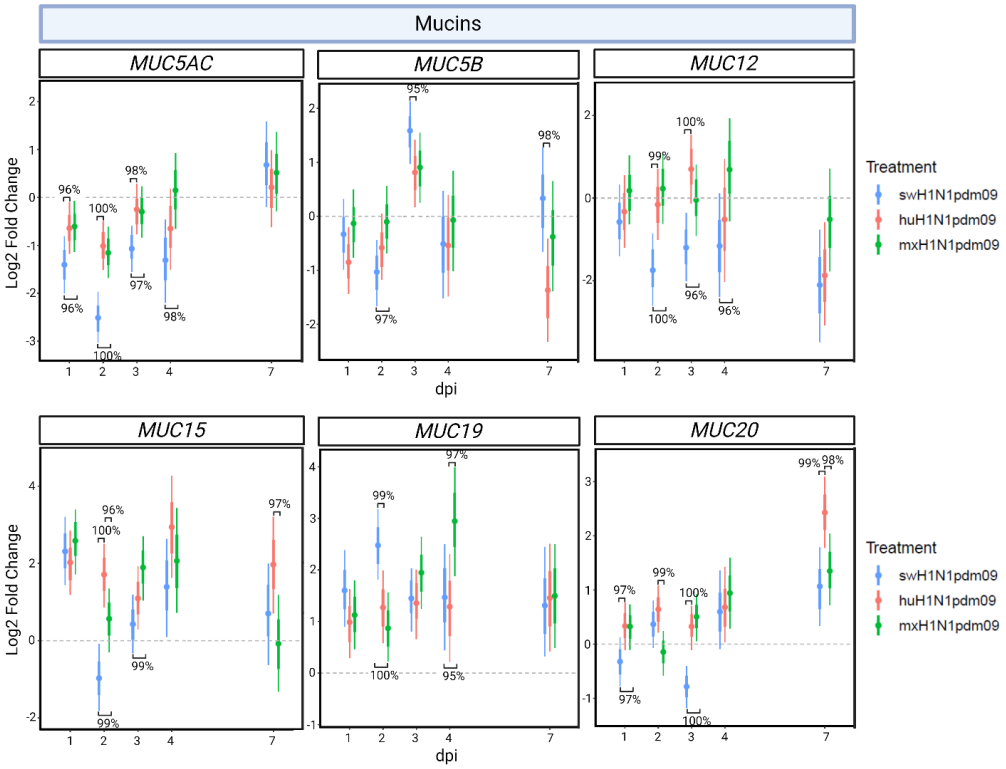

Figure 5: Infection with different IAV strains results in divergent mucin expression. A selection of significant differentially expressed genes in nasopharyngeal swab samples (blue, swH1N1pdm09; light red, huH1N1pdm09; green, mxH1N1pdm09). Data are shown as mean log2 fold change (dot) compared to baseline, the 60% credible interval (thick bar), and the 90% credible interval (thin bar). Significant differences (Posterior probability of >95%) are indicated with brackets. dpi = day post inoculation.

Other mucins, *MUC15*, *MUC19*, and *MUC20*, were significantly upregulated in all IAV inoculated groups at more than one time point (Figure 5). None of them were significantly downregulated.

Discussion

The innate immune response plays a key role in the host defence against invading pathogens, and although substantial and significant efforts have been made to elucidate the role of innate immunity in

response to IAV and other respiratory infections, viral recognition and innate responses in the nasal mucosa is still poorly understood. Particularly, the contribution of host factors in either facilitating or inhibiting viral infection at the site of first contact between host and pathogen when IAV crosses the species barrier remains to be investigated. In the present study, a classical antiviral innate immune response was demonstrated and explored over the course of infection and recovery in pigs infected with pre- and post-pandemic IAV, adapted to either humans or pigs. The mucosal innate immune response, including respiratory mucin production, was found to differ in kinetics and magnitude depending on host adaptation of the infecting IAV strain. The host response was surveyed at the site of infection by a non-invasive sampling method using nasopharyngeal swabs. The high RNA quality and reproducible qPCR results obtained by this sampling method prove its applicability for continuous monitoring of the local host response during infection, allowing in-depth investigation of the temporal dynamics of the mucosal antiviral innate immune response. The non-invasive sampling method could also be used to collect and study human mucosa during infection and recovery from viral respiratory pathogens, including IAV, SARS-CoV-2, and RSV.

A prompt onset of the innate immune response with peak expression of interferons, notably *IFNB1*, was seen already at 1 dpi in the swH1N1pdm09 group compared to a delayed response in the two other infected groups. In contrast to our results, a significantly lower expression of IFNs in porcine tracheal epithelial cells infected with a swine-adapted IAV was demonstrated during the first 12 hours after infection (hpi) compared to a human-adapted IAV[30]. However, the appreciable difference in the model systems (*in vitro* versus *in vivo*) likely accounts for this discrepancy. Further, the lack of a fully functional protective mucus layer in the monolayer cell culture presumably leads to more rapid infection compared to the nasal mucosa of pigs and humans. *In vivo*, sialic acid-coated mucins act as IAV decoy receptors, impeding viral transport through the mucus layers towards the respiratory cell surface[12], and the lack of mucins in an *in vitro* model could therefore be important for the results obtained. In the present study, a

decreased expression of both secreted and transmembrane mucins (*MUC5AC*, *MUC5B*, and *MUC12*) was observed in the nasal mucosa specimens at several time points after infection with the swine-adapted strain (swH1N1pdm09). Lower levels of mucins could potentially allow the swH1N1pdm09 IAV to reach and infect epithelial cells more rapidly, thereby inducing an innate immune response with an earlier onset than the two other IAV inoculated groups. Mucin expression in relation to IAV infection has only been described *in vivo* in mouse lungs[31,32] and only in a few *in vitro* studies in human epithelial cells[33,34]. Crossing the species barrier will most likely require adaptation to the host-specific mucus glycome and evolution of traits to evade or suppress mucosal clearance. It could be anticipated that viruses with high zoonotic potential have decreased affinity for abundant mucus glycosylation patterns, including sialic decoy receptors, in order to increase infectivity in a broad host range. A thorough *in vivo* analysis of mucin expression after IAV challenge has to our knowledge not been performed before, positioning the results presented here as an important foundation for future studies of mucosal virus-host interaction in both animals and humans.

The most rapid induction and highest magnitude of innate immune factors were observed in the swH1N1pdm09 group, followed by the mxH1N1pdm09 group and lastly, the huH1N1pdm09 group. These findings are consistent with the viral load measured in the same animals (Figure 4). Association between viral load and induction of the innate immune response has been documented previously in blue-winged teals infected with avian low-path H5N9 avian IAV strain[35]. Furthermore, higher viral load has also been associated with higher levels of ISGs (*MX1, MX2, ISG15,* and *OAS1*) in Covid-19 positive patients[36]. In general, the magnitude of the inflammatory immune response towards the human-adapted strain (huH1N1pdm09) was lower compared to the other groups of infected pigs. Lower cytokine expression and viral load in the huH1N1pdm09 group agree with the absence of transcription factor *NFKB1* upregulation during infection in this group[37–40]. Contrary to the huH1N1pdm09 group, the "pre-pandemic" mxH1N1pdm09 group induced a substantial and prolonged immune response. PRRs,

transcription factors, cytokines, and ISGs were highly expressed shortly after inoculation (1 to 4 dpi) and again at 10 dpi. Interferons (*IFNA1, IFNB1,* and *IFNL1*), cytokines (*IL17A, IL1A, IL1RN,* and *TNF*), and other pro- and anti-inflammatory proteins, such as *S100A7, SELL, PTGS2* (COX-2) and *TNFAIP3*, were even differentially expressed at day 14 when the infection was cleared in 11/12 pigs (Figure 4). These pro- and anti-inflammatory proteins could potentially be involved in tissue damage and immunopathology as previously reported after infection with the mxH1N1pdm09 isolate in the same group of pigs ("Unpublished data", Kristensen C, Glud HA, Crumpton JC, Martiny K, Webb A, Ryt-Hansen P, et al.). Indeed, severe IAV infection has been described to have a delayed activation of critical immune cells and a prolonged immune activation[41,42]. The differential expression of *S100A7* was seen only in the mxH1N1pdm09 group. Induction of *S100A7* has been demonstrated by others after IAV infection in a human lung alveolus model[43], but the precise role of this inflammatory protein during IAV infection is still unknown. Though, it has been demonstrated to induce the expression of many immune genes, such as *IFNB1*, *IFNL1*, *CCL5*, and *IFI6*[43]. Future studies of S100A7 after viral infection are warranted to evaluate its exact role in the antiviral response.

The higher viral load in the swH1N1pdm09 group (Figure 4) also agrees with the downregulation of *IFNA1* observed only in this group as IFN-α treatment has been demonstrated to reduce viral shedding in both guinea pigs and ferrets[44,45] and prevent infection in humans[46]. Inhibition of *IFNA1* production could be due to nonstructural protein 1 (NS1)-mediated immune evasion of IAV, as NS1 has been demonstrated to be a type I IFN antagonist[47–51]. At least two independent NS1 functions are involved in limiting host IFN production: i) inhibition of RIG-I and ii) inhibition of CPSF30, which mediate maturation of host mRNA[52–54]. NS1 has shown to inhibit RIG-I by several mechanisms: direct binding to RIG-I[55,56], by sequestering its activating ligand[47,57], or by binding to TRIM25 and/or RNF135 (Riplet)[58,59]. Rajsbaum and colleges[59] demonstrated that NS1 inhibits the RIG-I pathway in a species-specific manner. In HEK293T cells (human cell line) infected with human-, mouse-, avian-, and swine-adapted IAV, only NS1 proteins

291 from human-adapted IAV strains (H1N1 and H3N2) demonstrated binding to Riplet[59]. Thus, species-
292 specific binding of swine-adapted viral NS1 to swine Riplet could also be involved in the observed
293 downregulation of *IFNA1* in this study. A pairwise comparison and a phylogenetic analysis
294 (Supplementary Text S1 and S2) indicate higher similarity between the NS gene segments of the
295 huH1N1pdm09 and swH1N1pdm09 isolates (93.3%) compared to the mxH1N1pdm09 isolate (86.2% and
296 89.4%, respectively) (Supplementary Figure 1 and 2). Short-term circulation and less adaptation to pigs
297 of the "pre-pandemic" mxH1N1pdm09 strain was also suggested by Kristensen and colleagues
298 ("Unpublished data", Kristensen C, Glud HA, Crumpton JC, Martiny K, Webb A, Ryt-Hansen P, et al.) after
299 pig and ferret infection trials using the same isolates. The NS1 region between amino acids 175–210 is
300 important for CPSF30 binding[54,60,61]. Indeed, the substitution of aspartic acid (D) at position 189 and
301 valine (V) at position 194 leads to impaired inhibition of host gene expression by NS1[52]. The NS segment
302 of huH1N1pdm09 and swH1N1pdm09 has a substitution in position 189, whereas the mxH1N1pdm09
303 NS segment has substitutions in both positions (Supplementary Figure 3). Additionally, four amino acids
304 within the CPSF30 binding site of the NS segment from the mxH1N1pdm09 isolate differ from the other
305 strains (position 202, 206, 207, and 209). These differences could result in reduced binding of CPSF30
306 and consequently a less effective immune evasion of the "pre-pandemic" mxH1N1pdm09 isolate,
307 contributing to the prolonged immune response observed. Further studies are needed to resolve host-
308 NS1 interaction in viral adaptation and host tropism.

309 Overall, we have provided novel insight into the local antiviral and mucosal immune response towards
310 three different H1N1 IAV strains using a non-invasive sampling method. We propose that viral host
311 adaptation might involve shutdown of several mucins so the virus can reach and infect the epithelial
312 cells of the nasal mucosa more efficiently. The mucosal host response against swine-adapted IAV
313 (swH1N1pdm09) was rapid and activated a strong antiviral immune response, but host adaptation most
314 likely enabled the virus to evade or suppress important immune factors, such as mucins and *IFNA1*,

315 resulting in high viral load. The “pre-pandemic” (mxH1N1pdm09) strain induced a prolonged immune
316 response compared to the other strains. We speculate that this strain is fully prepared to cross the
317 species barrier and that several mechanisms might be involved in host tropism, including the mucosal
318 composition/structure and viral affinity for host-specific glycans on mucins as well as the ability to evade
319 the immune system, as proposed by NS1 in this study. The role of these host-pathogen interactions in
320 relation to the potential for zoonotic transmission warrants further attention in the effort to provide the
321 scientific community with improved tools for surveillance of zoonotic threats and prevention of future
322 pandemics.

323 ## Material and methods

324 ### Animal challenge

325 The study included 42 Danish Landrace Crossbred pigs (7 weeks old) confirmed IAV negative and
326 seronegative. Groups of minimum 5 animals are sufficient for statistical significance based on power
327 analysis from previous comparable data. More animals are desirable, but due to the 3R principle and
328 high cost, we strive to keep technical variation, including animal-to-animal variation, as low as possible
329 by using animals from the same litters. The pigs were allocated into four groups by minimisation
330 (ARRIVE guidelines), with sex and size as nuisance variables, to ensure a balance between the groups.
331 Each group (experimental unit) was housed in a separate isolation unit; groups 2-4 each included 12
332 pigs, and group 1 consisted of 6 pigs. All pigs were fed non-pelleted feed (Svinefoder 5 from NAG,
333 Helsinge, Denmark) and had *ad libitum* access to water. The pigs had an acclimatisation period of 1
334 week. On day 0 of the study, all pigs were sedated by intramuscular injection (0.1 mL/kg) of a Zoletil
335 mixture consisting of one Zoletil 50 Vet (without solvent) (Virbac, Mumbai, India) mixed with 6.25
336 Rompun (20 mg/mL) (Bayer AG, Leverkusen, Germany), 1.25 mL Ketaminol (100 mg/mL) (Merck Animal
337 Health, Rahway, New Jersey), and 2.50 mL Torbugesic (butorphanol tartrate) (10 mg/mL) (Zoetis,

Parsippany, New Jersey). Pigs in groups 2-4 were inoculated intranasally to simulate the natural route of IAV infection by a MAD Nasal Intranasal Mucosal Atomization Device (Teleflex, Wayne, Pennsylvania) containing 3 ml of 10^7 $TCID_{50}$/ml of A/Swine/Denmark/2017_10298/4_4p1/2017 (H1N1) (swH1N1pdm09), A/Denmark/238/2020 (H1N1) (huH1N1pdm09), and A/Swine/Mexico/AVX-39/2012 (H1N1) (mxH1N1pdm09), respectively. Group 1 was mock inoculated with the same MAD nasal device containing culture medium only (control). Nasopharyngeal swab samples were collected with FLOQSwabs (COPAN Diagnostics, Murrieta, California) from all animals just before inoculation (day 0) and at 1, 2, 3, 4, 7, 10, and 14 dpi and stored in DNA/RNA Shield (Zymo Research, Irvine, California) at -20°C. Group 1 (control) was located in the first isolation unit and was always sampled first. The pigs were evaluated daily and excluded if reaching the humane endpoints (fever >40.5°C for more than 2 days, severe respiratory difficulties, suppressed appetite in more than 2-3 days, followed by visible weight loss). None of the pigs reached the human endpoints, therefore all animals were included in the study. All 6 pigs in group 1 (control) and 8 pigs from each inoculated group (30 in total) were euthanised at 3 dpi, while the 4 remaining pigs from each inoculated group (12 in total) were euthanised at 14 dpi (Figure 6). Euthanisation was performed at 3 dpi to collect samples to investigate tissue-specific host innate antiviral immune response during IAV infection (not included in the present study).

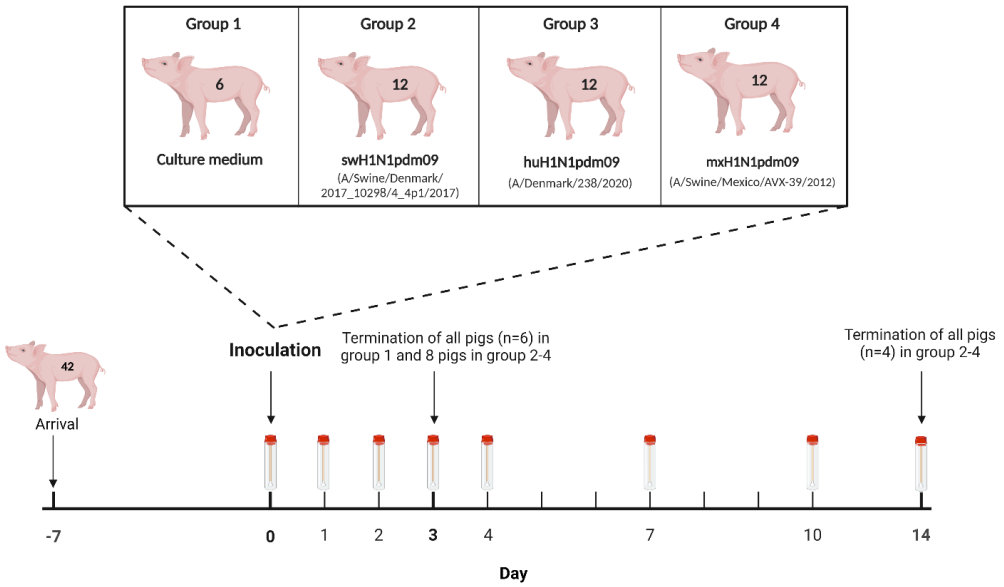

Figure 6: Overview of the experimental setup. Pigs were inoculated on day 0 of the study, group 1 with culture medium, group 2 with a swine-adapted IAV (swH1N1pdm09), group 3 with a human-adapted IAV (huH1N1pdm09), and group 4 with a "pre-pandemic" H1N1 isolate (mxH1N1pdm09). Nasopharyngeal swabs were collected before inoculation (0 dpi) and at 1, 2, 3, 4, 7, 10, and 14 days post inoculation. All pigs in group 1 (n=6) and 8 pigs from each inoculated group were euthanised at day 3 post inoculation, while the 4 remaining pigs from each inoculated group were euthanised at day 14 post inoculation.

The animal experiment was performed under biosafety level 2 conditions and under an animal study protocol approved by The Danish Animal Experimentation Council (protocol no. 2020-15-0201-00502).

RNA extraction

Total RNA was extracted from nasopharyngeal swab samples with the Quick-RNA Microprep Kit (Zymo Research, Irvine, California) according to the manufacturer's protocol. All steps were carried out at room temperature (RT). In brief, the FLOQSwab was removed, and 400 µl RNA lysis buffer was added to 400 µl sample, followed by addition of 800 µl absolute ethanol. The sample was transferred to a Zymo-Spin IC Column (supplied in kit) and centrifuged at 13,000 x g for 30 seconds. One washing step with RNA Wash

Buffer was performed prior to DNase treatment, where 40 µl DNase I Reaction Mix (5 µl DNase I and 35 µl DNA Digestion Buffer) was added directly to the column matrix and incubated for 15 minutes at RT. Before elution, three additional washing steps were performed (one with RNA Prep Buffer followed by two with RNA Wash Buffer) with centrifugation at 13,000 x g for 30 seconds, except the last wash where the centrifugation was performed for 2 minutes to prevent any carryover of buffers to the eluate. RNA was eluted in 15 µl RNase-free water. RNA purity and concentration were assessed using a NanoDrop ND-1000 spectrophotometer (Thermo Fisher Scientific, Waltham, Massachusetts). RNA quality was determined using the Agilent RNA 6000 Nano Kit on the Bioanalyzer 2100 system (Agilent Technologies, Santa Clara, California).

High-throughput qPCR

Using the QuantiTect Reverse Transcription Kit (QIAGEN, Hilden, Germany), 300 ng RNA was reverse transcribed into cDNA. Two separate cDNA reactions were performed for each RNA sample (technical replicates) to validate the qPCR data. An additional DNase treatment was performed prior to cDNA synthesis by adding 1.5 µl Wipeout Buffer to 1 µl RNA and 11.5 µl RNase-free water. The mix was incubated in a thermal cycler (Biometra TRIO 48) for 2 minutes at 42°C. Hereafter, 6 µl reverse transcription mix (reverse transcriptase, RT Buffer, RT Primer Mix, and RNase-free water mixed in a 1:1:4:2 ratio) was added to the RNA. Non-reverse transcription controls were included (reverse transcriptase replaced with water). Samples were incubated for 15 minutes at 42°C followed by 3 minutes at 95°C to inactivate the enzyme. Before pre-amplification, cDNA was diluted 1:10 in TE-buffer (VWR, Radnor, Pennsylvania). All porcine primers used in this study were designed using Primer3 (v. 0.4.0) (https://bioinfo.ut.ee/primer3-0.4.0/) and purchased from Merck Life Science A/S, Soeborg, Denmark. A thorough description of the primer design can be found in Supplementary Text S3. Sequences and qPCR efficiencies for all primers can be found in Supplementary Table 3. Target genes

were pre-amplified using TaqMan PreAmp Master Mix (Applied Biosystems, Waltham, Massachusetts). A 200 nM primer mix containing all selected primers included in this study was prepared. Primer mix (2.5 µl) was combined with 5 µl TaqMan PreAmp Master Mix and 2 µl TE Buffer (PanReac AppliChem, Barcelona, Spain) and added to 2.5 µl cDNA. Samples were incubated at 95°C for 10 minutes, followed by 20 cycles of 95°C for 15 seconds and 60°C for 4 minutes. Residual primers were digested by treatment with 4U of Exonuclease I (New England BioLabs, Ipswich, Massachusetts) by incubation at 37°C for 30 minutes, followed by 80°C for 15 minutes. Finally, pre-amplified and exonuclease-treated cDNA samples were diluted 1:10 in TE Buffer. High-throughput qPCR was carried out using 96.96 Dynamic Array IFC chips (Standard BioTools Inc., South San Francisco, California) running on the BioMark real-time platform (Standard BioTools Inc., South San Francisco, California). The following PCR protocol was used: 2 minutes at 50°C and 10 minutes at 95°C, followed by 35 PCR cycles with denaturation for 15 seconds at 95°C and annealing/elongation for 1 minute at 60°C.

qPCR data analysis

Data were coded prior to analysis in order to complete the analysis blinded to treatment. Amplification and melting curves were visually inspected using the Fluidigm Real-Time PCR Analysis software (v4.8.1). Primer efficiencies were calculated for each assay from two independent 5-fold dilution series. Data were pre-processed in GenEx7 (MultiD, Gothenburg, Sweden), including interplate calibration, correction for PCR efficiency, evaluation of (using the algorithms geNorm[62] and NormFinder[63]) and normalisation to reference genes, and averaging of technical replicates. Samples were excluded if more than 15% of the technical replicates exceeded the accepted criteria (>1.5 Cq difference). All data points were included (only 3 samples had a single replicate removed). A biologically relevant cut-off value of ±2-fold change in gene expression compared to baseline (all data before inoculation and data from the control group) was used. The change in gene expression level was considered statistically significant with a posterior probability of >95%.

Statistical Analysis

Software

The data analysis was performed in the R programming environment (version 4.2.1[64]) in RStudio (version 2022.12.0.353[65]). The R-packages tidyverse (version 1.3.2[66]) and bayesplot (version 1.9.0[67]) were used for data manipulation and plotting. Statistical models were specified and fitted using Stan[68] and RStan (RStan v2.26.13[69]). The R-package "loo" (version 2.5.1) was used to check model fit and for model comparison[70,71]. Further, model fit assessment was done using the bayesplot R-package to do posterior predictive checking[72].

For all Bayesian models (see description in Supplementary Text S4, we fit one model for each gene), we ran two independent Markov chain Monte Carlo (MCMC) chains for 10,000 iterations each, with 5,000 iterations warm-up, resulting in 10,000 post-warmup samples for each parameter. Convergence of MCMC runs was monitored by checking that there were no divergent transitions during sampling and that the potential scale reduction factor ("R-hat") was close to 1 at the end of the run for all model parameters.

Statistical model

We assume that, for a given gene and a given treatment, each day after inoculation has its own typical expression level that we are interested in estimating. Empirical measurements will be randomly distributed around this typical level. Specifically, we assume that the measurements are log-normally distributed around the typical value. This fits with the idea that expression changes are multiplicative (that transcription rates will typically increase or decrease by a certain percentage) and also fits very well with the empirical data, which are strictly positive and have a distribution with a longer tail to the right. Finally, we assume that, for each gene, there is a typical baseline expression, which we take to be the level in all measurements from control pigs (regardless of the day), and also in the day 0

measurements from non-control pigs. Again, we assume that measurements of baseline are log-normally distributed around the typical baseline value. The ratio between these levels (average expression level on a given day for a given treatment, divided by the average baseline level for that gene) indicates whether the gene is upregulated or downregulated.

More specifically, we take the logarithm of the gene expression values, standardise the data (see below), and then estimate the average of the log-transformed, standardised data as a measure of the typical level. To make the estimates more robust against outliers, we fit a generalised t-distribution to these log-transformed data. A t-distribution has fatter tails, so outliers do not pull the average up or down as easily as in the case of a normal distribution. For each gene, we also estimate the degrees of freedom (nu) and the spread (sigma) for the t-distribution. Larger values of nu will cause the t-distribution to be more similar to a normal distribution. Standardisation is done by subtracting the mean and dividing by the standard deviation (sd) (for all expression values for a gene across days and treatments). In this way, most values will lie in the range -2 to 2, which makes it simpler to set priors on the parameters (we can use the same priors for all genes regardless of their absolute expression levels).

Below is a description of the model parameters and their prior distributions. There is a total of 24 parameters for each investigated gene. Note that the parameters below correspond to the log-transformed and standardised data – the estimates must be back-transformed to learn about the original levels:

- Parameter 1: Average baseline expression. This is taken to be the level present in all measurements from control pigs and also from day-0 measurements from non-controls. Prior distribution on parameter: normal distribution with mean=0 and sd=1. This is a weakly informative, regularising prior.

- Parameters 2-22: Average expression levels for each of the 21 combinations of day and treatment (3 treatments, 7 days with measurements). Prior on these parameters was also normal (0,1).
- Parameter 23: Standard deviation (sigma) for t-distributions. Note that we only estimate one sigma parameter, which is then used for all the 22 t-distributions above. Constant variance is a consequence of the log-transformation – see below). Prior for parameter: half-normal (0,1).
- Parameter 24: Degrees of freedom (nu) of the t-distributions. Prior: gamma (2, 0.1). Note that we also use the same nu parameter for all 22 t-distributions.

The prior on nu follows a suggestion in Juárez and Steel (2010)[73], while the other priors follow the prior choice recommendations on the Stan GitHub page. Before settling on the described model, other models were explored as well (see Supplementary Text S5).

Analysis of fitted models

The goal of the analysis is to estimate the typical (average) expression levels for each combination of gene, treatment, and day. We do this using a Bayesian approach, which means we get a posterior distribution over the possible values of the parameters. Specifically, we get 10,000 MCMC samples from the Stan program for each parameter. We can calculate all the quantities we are interested in from these MCMC estimates: log2 fold change vs baseline for a given day, for example, can be calculated by first back-transforming the parameter estimates to their original scale (parameters correspond to data that has been log-transformed and standardised), and then dividing the estimated average level that day by the estimated average *baseline* level for that gene, and taking the log2 of that ratio. When we calculate that value for each of the 10,000 lines in our sample file, we automatically get a posterior distribution over the log-fold change as well (10,000 values we can calculate credible intervals, etc. from). The same approach can be used for comparisons between treatments (contrasts): we can divide

the estimate of the average level for treatment 1 on day 1, by the estimate for treatment 2 also on day 1, and take the log2, to obtain the posterior for that contrast.

Data Availability

All data generated or analysed during this study are included in this published article and its supplementary information files.

489 **References**

490 1. WHO. Fact Sheet Influenza (Seasonal). https://www.who.int/news-room/fact-
491 sheets/detail/influenza-(seasonal). Published 2018.

492 2. Alexander DJ. A review of avian influenza in different bird species. *Vet Microbiol*. 2000;**74**:3-13.
493 doi:10.1016/S0378-1135(00)00160-7

494 3. Trebbien R, Larsen LE, Viuff BM. Distribution of sialic acid receptors and influenza A virus of avian
495 and swine origin in experimentally infected pigs. *Virol J*. 2011;**8**(434):1-14. doi:10.1186/1743-
496 422X-8-434

497 4. Webster RG, Bean WJ, Gorman OT, Chambers TM, Kawaoka Y. Evolution and ecology of influenza
498 A viruses. *Microbiol Rev*. 1992;**56**(1):152-179. doi:10.1128/mr.56.1.152-179.1992

499 5. Xu Q, Wang W, Cheng X, Zengel J, Jin H. Influenza H1N1 A/Solomon Island/3/06 Virus Receptor
500 Binding Specificity Correlates with Virus Pathogenicity, Antigenicity, and Immunogenicity in
501 Ferrets. *J Virol*. 2010;**84**(10):4936-4945. doi:10.1128/jvi.02489-09

502 6. Mena et al. Origins of the 2009 H1N1 influenza pandemic in swine in Mexico. *Elife*. 2016;**5**:1-21.
503 doi:10.7554/eLife.16777

504 7. Glud HA, George S, Skovgaard K, Larsen LE. Zoonotic and reverse zoonotic transmission of viruses
505 between humans and pigs. *Apmis*. 2021;**129**(12):675-693. doi:10.1111/apm.13178

506 8. De Graaf M, Fouchier RAM. Role of receptor binding specificity in influenza A virus transmission
507 and pathogenesis. *EMBO J*. 2014;**33**(8):823-841. doi:10.1002/embj.201387442

508 9. Nicholls JM, Bourne AJ, Chen H, Guan Y, Peiris JM. Sialic acid receptor detection in the human
509 respiratory tract: Evidence for widespread distribution of potential binding sites for human and
510 avian influenza viruses. *Respir Res*. 2007;**8**(73):1-10. doi:10.1186/1465-9921-8-73

511 10. Starbæk et al. Animal Models for Influenza A Virus Infection Incorporating the Involvement of
512 Innate Host Defenses: Enhanced Translational Value of the Porcine Model. *ILAR J*.
513 2018;**59**(3):323-337. doi:10.1093/ilar/ily009

514 11. Widdicombe JH. Early studies on the surface epithelium of mammalian airways. *Am J Physiol -*
515 *Lung Cell Mol Physiol*. 2019;**317**:L486-L495. doi:10.1152/AJPLUNG.00240.2019

516 12. Chatterjee M, van Putten JPM, Strijbis K. Defensive Properties of Mucin Glycoproteins during
517 Respiratory Infections—Relevance for SARS-CoV-2. *MBio*. 2020;**11**(6):e02374-20.
518 doi:10.1128/mBio.02374-20

519 13. Wallace LE, Liu M, van Kuppeveld FJM, de Vries E, de Haan CAM. Respiratory mucus as a virus-
520 host range determinant. *Trends Microbiol*. 2021;**29**(11):983-992. doi:10.1016/j.tim.2021.03.014

521 14. Zanin M, Baviskar P, Webster R, Webby R. The Interaction between Respiratory Pathogens and
522 Mucus. *Cell Host Microbe*. 2016;**19**:159-168. doi:10.1016/j.chom.2016.01.001

523 15. Iwasaki A, Pillai PS. Innate immunity to influenza virus infection. *Nat Rev Immunol*. 2014;**14**:315-
524 328. doi:10.1038/nri3665

525 16. Mifsud EJ, Kuba M, Barr IG. Innate Immune Responses to Influenza Virus Infections in the Upper
526 Respiratory Tract. *Viruses*. 2021;**13**(2090):1-13. doi:10.3390/v13102090

17. Stanifer ML, Pervolaraki K, Boulant S. Differential Regulation of Type I and type III Interferon Signaling. *Int J Mol Sci*. 2019;**20**(1445):1-22. doi:10.3390/ijms20061445

18. Kelly et al. Comprehensive single cell analysis of pandemic influenza A virus infection in the human airways uncovers cell-type specific host transcriptional signatures relevant for disease progression and pathogenesis. *Front Immunol*. 2022;**13**(978824):1-22. doi:10.3389/fimmu.2022.978824

19. Sanders CJ, Doherty PC, Thomas PG. Respiratory epithelial cells in innate immunity to influenza virus infection. *Cell Tissue Res*. 2011;**343**(1):13-21. doi:10.1007/s00441-010-1043-z

20. de Jong et al. Fatal outcome of human influenza A (H5N1) is associated with high viral load and hypercytokinemia. *Nat Med*. 2006;**12**(10):1203-1207. doi:10.1038/nm1477

21. Gao et al. Cytokine and Chemokine Profiles in Lung Tissues from Fatal Cases of 2009 Pandemic Influenza A (H1N1): Role of the Host Immune Response in Pathogenesis. *Am J Pathol*. 2013;**183**(4):1258-1268. doi:10.1016/j.ajpath.2013.06.023

22. Wang et al. Definition and Risks of Cytokine Release Syndrome in 11 Critically Ill COVID-19 Patients with Pneumonia: Analysis of Disease Characteristics. *J Infect Dis*. 2020;**222**:1444-1451. doi:10.1093/infdis/jiaa387

23. Huang et al. Clinical features of patients infected with 2019 novel coronavirus in Wuhan, China. *Lancet*. 2020;**395**:497-506. doi:10.1016/S0140-6736(20)30183-5

24. Tabarani et al. Novel Inflammatory Markers, Clinical Risk Factors, and Virus Type Associated with Severe Respiratory Syncytial Virus Infection. *Pediatr Infect Dis J*. 2013;**32**(12):e437-e442. doi:10.1097/INF.0b013e3182a14407.Novel

25. McNamara PS, Flanagan BF, Hart CA, Smyth RL. Production of Chemokines in the Lungs of Infants with Severe Respiratory Syncytial Virus Bronchiolitis. *J Infect Dis*. 2005;**191**:1225-1232. doi:10.1086/428855

26. Hernandez et al. Life-threatening influenza pneumonitis in a child with inherited IRF9 deficiency. *J Exp Med*. 2018;**215**(10):2567-2585. doi:10.1084/JEM.20180628

27. Everitt et al. IFITM3 restricts the morbidity and mortality associated with influenza. *Nature*. 2012;**484**:519-525. doi:10.1038/nature10921

28. Fleige S, Pfaffl MW. RNA integrity and the effect on the real-time qRT-PCR performance. *Mol Aspects Med*. 2006;**27**(2-3):126-139. doi:10.1016/j.mam.2005.12.003

29. Barington K, Jensen HE, Skovgaard K. Forensic age determination of human inflicted porcine bruises inflicted within 10 h prior to slaughter by application of gene expression signatures. *Res Vet Sci*. 2018;**120**:47-53. doi:10.1016/j.rvsc.2018.08.007

30. Krishna et al. Differential Induction of Type I and Type III Interferons by Swine and Human Origin H1N1 Influenza A Viruses in Porcine Airway Epithelial Cells. *PLoS One*. 2015;**10**(9):1-20. doi:10.1371/journal.pone.0138704

31. Ehre et al. Overexpressing mouse model demonstrates the protective role of Muc5ac in the lungs. *Proc Natl Acad Sci U S A*. 2012;**109**(41):16528-16533. doi:10.1073/pnas.1206552109

32. Barbier et al. Influenza A Induces the Major Secreted Airway Mucin MUC5AC in a Protease-EGFR-

Extracellular Regulated Kinase-Sp1-Dependent Pathway. *Am J Respir Cell Mol Biol*. 2012;**47**(2):149-157. doi:10.1165/rcmb.2011-0405OC

33. Chen et al. Upregulation of cell-surface mucin MUC15 in human nasal epithelial cells upon influenza A virus infection. *BMC Infect Dis*. 2019;**19**(622):1-11. doi:10.1186/s12879-019-4213-y

34. Iverson et al. Membrane-Tethered Mucin 1 Is Stimulated by Interferon and Virus Infection in Multiple Cell Types and Inhibits Influenza A Virus Infection in Human Airway Epithelium. *MBio*. 2022;**13**(4). doi:10.1128/mbio.01055-22

35. Dolinski AC, Homola JJ, Jankowski MD, Robinson JD, Owen JC. Host Gene Expression Is Associated With Viral Shedding Magnitude in Blue-Winged Teals (Spatula Discors) Infected With Low-Path Avian Influenza Virus. *Comp Immunol Microbiol Infect Dis*. 2022;**90-91**:101909. doi:10.1016/j.cimid.2022.101909

36. Toro et al. Pin-Pointing the Key Hubs in the IFN-γ Pathway Responding to SARS-CoV-2 Infection. *Viruses*. 2022;**14**:2180. doi:10.3390/v14102180

37. Ehrhardt et al. The NF-kB inhibitor SC75741 efficiently blocks influenza virus propagation and confers a high barrier for development of viral resistance. *Cell Microbiol*. 2013;**15**(7):1198-1211. doi:10.1111/cmi.12108

38. Mazur et al. Acetylsalicylic acid (ASA) blocks influenza virus propagation via its NFkB-inhibiting activity. *Cell Microbiol*. 2007;**9**(7):1683-1694. doi:10.1111/j.1462-5822.2007.00902.x

39. Pinto et al. Inhibition of influenza virus-induced NF-kappaB and Raf/MEK/ERK activation can reduce both virus titers and cytokine expression simultaneously in vitro and in vivo. *Antiviral Res*. 2011;**92**:45-56. doi:10.1016/j.antiviral.2011.05.009

40. Kumar N, Xin Z, Liang Y, Ly H, Liang Y. NF-kB Signaling Differentially Regulates Influenza Virus RNA Synthesis. *J Virol*. 2008;**82**(20):9880-9889. doi:10.1128/JVI.00909-08

41. Wong et al. Severe Influenza Is Characterized by Prolonged Immune Activation: Results From the SHIVERS Cohort Study. *J Infect Dis*. 2018;**217**:245-256. doi:10.1093/infdis/jix571

42. Fox et al. Severe Pandemic H1N1 2009 Infection Is Associated with Transient NK and T Deficiency and Aberrant CD8 Responses. *PLoS One*. 2012;**7**(2):1-10. doi:10.1371/journal.pone.0031535

43. Bai et al. Mechanical control of innate immune responses against viral infection revealed in a human lung alveolus chip Haiqing. *Nat Commun*. 2022;**13**(1928):1-17. doi:10.1038/s41467-022-29562-4

44. Van Hoeven et al. Pathogenesis of 1918 Pandemic and H5N1 Influenza Virus Infections in a Guinea Pig Model: Antiviral Potential of Exogenous Alpha Interferon To Reduce Virus Shedding. *J Virol*. 2009;**83**(7):2851-2861. doi:10.1128/jvi.02174-08

45. Kugel et al. Intranasal Administration of Alpha Interferon Reduces Seasonal Influenza A Virus Morbidity in Ferrets. *J Virol*. 2009;**83**(8):3843-3851. doi:10.1128/jvi.02453-08

46. Gao et al. A randomized controlled trial of low-dose recombinant human interferons α-2b nasal spray to prevent acute viral respiratory infections in military recruits. *Vaccine*. 2010;**28**:4445-4451. doi:10.1016/j.vaccine.2010.03.062

47. Wang et al. Influenza A Virus NS1 Protein Prevents Activation of NF-κB and Induction of

Alpha/Beta Interferon. *J Virol*. 2000;**74**(24):11566-11573. doi:10.1128/jvi.74.24.11566-11573.2000

48. Talon et al. Activation of Interferon Regulatory Factor 3 Is Inhibited by the Influenza A Virus NS1 Protein. *J Virol*. 2000;**74**(17):7989-7996. doi:10.1128/jvi.74.17.7989-7996.2000

49. García-Sastre et al. Influenza A Virus Lacking the NS1 Gene Replicates in Interferon- Deficient Systems. *Virology*. 1998;**252**:324-330. doi:10.1006/viro.1998.9508

50. Tisoncik et al. The NS1 protein of influenza A virus suppresses interferon-regulated activation of antigen-presentation and immune-proteasome pathways. *J Gen Virol*. 2011;**92**:2093-2104. doi:10.1099/vir.0.032060-0

51. Solórzano et al. Mutations in the NS1 Protein of Swine Influenza Virus Impair Anti-Interferon Activity and Confer Attenuation in Pigs. *J Virol*. 2005;**79**(12):7535-7543. doi:10.1128/jvi.79.12.7535-7543.2005

52. Nogales A, Luis M-S, David J. T, Marta L. D. NS1 Protein Amino Acid Changes D189N and V194I Affect Interferon Responses, Thermosensitivity, and Virulence of Circulating H3N2 Human Influenza A Viruses. *J Virol*. 2017;**91**(5):e01930-16. doi:https://doi.org/ 10.1128/JVI.01930-16

53. Hale et al. Inefficient Control of Host Gene Expression by the 2009 Pandemic H1N1 Influenza A Virus NS1 Protein. *J Virol*. 2010;**84**(14):6909-6922. doi:10.1128/jvi.00081-10

54. Das et al. Structural basis for suppression of a host antiviral response by influenza a virus. *Proc Natl Acad Sci U S A*. 2008;**105**(35):13093-13098. doi:10.1073/pnas.0805213105

55. Mibayashi et al. Inhibition of Retinoic Acid-Inducible Gene I-Mediated Induction of Beta Interferon by the NS1 Protein of Influenza A Virus. *J Virol*. 2007;**81**(2):514-524. doi:10.1128/JVI.01265-06

56. Pichlmair et al. RIG-I-mediated antiviral responses to single- stranded RNA bearing 5'-phosphates. Science. *Science (80-)*. 2006;**314**:997-1001. doi:10.1126/science.1132998

57. Lu Y, Wambach M, Katze MG, Krug RM. Binding of the Influenza Virus NS1 Protein to Double-Stranded RNA Inhibits the Activation of the Protein Kinase That Phosphorylates the eIF-2 Translation Initiation Factor. *Virology*. 1995;**214**:222-228. doi:10.1006/viro.1995.9937

58. Gack et al. Influenza A Virus NS1 Targets the Ubiquitin Ligase TRIM25 to Evade Recognition by the Host Viral RNA Sensor RIG-I. *Cell Host Microbe*. 2009;**5**:439-449. doi:10.1016/j.chom.2009.04.006

59. Rajsbaum et al. Species-Specific Inhibition of RIG-I Ubiquitination and IFN Induction by the Influenza A Virus NS1 Protein. *PLoS Pathog*. 2012;**8**(11):e1003059. doi:10.1371/journal.ppat.1003059

60. Noah DL, Twu KY, Krug RM. Cellular antiviral responses against influenza A virus are countered at the posttranscriptional level by the viral NS1A protein via its binding to a cellular protein required for the 3' end processing of cellular pre-mRNAS. *Virology*. 2003;**307**:386-395. doi:10.1016/S0042-6822(02)00127-7

61. Li Y, Chen Z-Y, Wang W, Baker CC, Krug RM. The 3'-end-processing factor CPSF is required for the splicing of single-intron pre-mRNAS in vivo. *RNA*. 2001;**7**:920-931. doi:10.1017/S1355838201010226

62. Vandesompele et al. Accurate normalization of real-time quantitative RT-PCR data by geometric averaging of multiple internal control genes. *Genome Biol*. 2002;**3**(7):research0034.1–0034.12. doi:10.1007/s00603-018-1496-z

63. Andersen CL, Jensen JL, Ørntoft TF. Normalization of real-time quantitative reverse transcription-PCR data: A model-based variance estimation approach to identify genes suited for normalization, applied to bladder and colon cancer data sets. *Cancer Res*. 2004;**64**(15):5245-5250. doi:10.1158/0008-5472.CAN-04-0496

64. R Core Team. R: A language and environment for statistical computing. R Foundation for Statistical Computing. Vienna, Austria. https://www.r-project.org/. Published 2022.

65. Posit Team. RStudio: Integrated Development Environment for R. Posit Software, PBC. Boston, MA. http://www.posit.co/. Published 2022.

66. Wickham et al. Welcome to the Tidyverse. *J Open Source Softw*. 2019;**4**(43):1686. doi:10.21105/joss.01686

67. Gabry J, Mahr T. bayesplot: Plotting for Bayesian Models. R package version 1.9.0. https://mc-stan.org/bayesplot/. Published 2022.

68. Carpenter et al. Stan: A probabilistic programming language. *J Stat Softw*. 2017;**76**(1):1-32. doi:10.18637/jss.v076.i01

69. Stan Development Team. RStan: the R interface to Stan. R package version v2.26.13. http://mc-stan.org/. Published 2023.

70. Vehtari A, Gelman A, Gabry J. Practical Bayesian model evaluation using leave-one-out cross-validation and WAIC. *Stat Comput*. 2017;**27**:1413-1432. doi:10.1007/s11222-016-9696-4

71. Vehtari et al. loo: Efficient leave-one-out cross-validation and WAIC for Bayesian models. R package version 2.5.1. https://mc-stan.org/loo/. Published 2022.

72. Gabry J, Simpson D, Vehtari A, Betancourt M, Gelman A. Visualization in Bayesian workflow. *J R Stat Soc*. 2019;**182**:389-402. doi:10.1111/rssa.12378

73. Juárez MA, Steel MFJ. Model-Based Clustering of Non-Gaussian Panel Data Based on Skew-t Distributions. *J Bus Econ Stat*. 2010;**28**(1):52-66. doi:10.1198/jbes.2009.07145

672 **Acknowledgements**

673 The work presented in this study is part of the FluZooMark project supported by the Novo Nordisk
674 Foundation (grant NNF19OC0056326). We thank Sophie J. George for providing the phylogenetic
675 analysis. Karin Tarp and Betina Lyngfeldt Henriksen are kindly thanked for their technical assistance.
676

677 **Author Contributions**

678 H.A.G., C.K., R.T., L.E.L., and K.S. designed and performed the animal experiment. H.A.G. performed the
679 gene expression experiment and analysed the data, and A.G.P. conducted the statistical analysis. H.A.G.
680 wrote the manuscript, and K.S., L.B., and C.H.P. contributed to the interpretation of data for the
681 manuscript and substantially contributed to the editing process. All authors read and approved the
682 manuscript.

683 **Competing interests**

684 The authors declare no competing interests.

685

686 **Table 1: The total number of statistically significant upregulated genes for each IAV strain after inoculation.**

	1 dpi	2 dpi	3 dpi	4 dpi	7 dpi	10 dpi	14 dpi
Total number of genes regulated in swH1N1pdm09	52	44	39	45	29	16	7
Mucins (7)	2	1	2	3	2	3	1
Pattern recognition receptors (5)	4	4	3	3	2	1	0
Transcription factors + adapter proteins (8)	6	5	3	5	5	2	2
Interferons (4)	3	2	2	2	0	0	1
Interferon stimulated genes (14)	14	10	9	12	4	3	1
Cytokines and chemokines (17)	14	13	13	13	11	3	2
Others (21)	9	9	6	7	5	4	0
Total number of genes regulated in huH1N1pdm09	38	41	33	45	39	8	3
Mucins (7)	1	2	2	2	4	2	0
Pattern recognition receptors (5)	4	3	2	3	3	0	0
Transcription factors + adapter proteins (8)	3	3	2	3	4	1	1
Interferons (4)	2	2	3	3	3	1	1
Interferon stimulated genes (14)	12	12	8	13	10	1	1
Cytokines and chemokines (17)	11	13	10	14	7	2	0
Others (21)	5	6	6	7	7	1	0
Total number of genes regulated in mxH1N1pdm09	44	28	45	49	16	36	13
Mucins (7)	2	0	2	3	3	4	1
Pattern recognition receptors (5)	4	2	4	3	0	3	0
Transcription factors + adapter proteins (8)	4	2	5	6	1	5	1
Interferons (4)	3	2	2	2	0	2	3
Interferon stimulated genes (14)	12	5	11	12	0	8	0
Cytokines and chemokines (17)	13	12	14	16	9	11	4
Others (21)	6	5	7	6	3	3	4

687 76 different genes were investigated and separated into 6 categories: Mucins (7 genes), PRRs (5 genes), transcription factors
688 and adapter proteins (8 genes), IFNs (4 genes), ISGs (14 genes), cytokines and chemokines (17 genes), and others (21 genes). A
689 blue color gradient highlights high (dark blue) to low (light blue) numbers of upregulated genes. dpi = day post inoculation.

Supplementary Tables

Supplementary Table 1: Mean and range of RNA concentration, purity, and quality. RNA purity and concentration was assessed using a NanoDrop ND-1000 spectrophotometer (Thermo Fisher Scientific, Waltham, Massachusetts). RNA quality was determined using an Agilent 2100 Bioanalyzer (Agilent Technologies, Santa Clara, California).

	ng/µl	A_{260}/A_{280}	A_{260}/A_{230}	RIN
Mean	108.5	2.0	1.9	7.0
Range	41.9-253.5	1.9-2.1	0.1-2.3	2.0-9.7

Supplementary Table 2: Statistically significant upregulated genes in the swH1N1pdm09 group during the study period (+2-fold change (FC) in gene expression compared to baseline (all data before inoculation and data from the control group) with a posterior probability of >95%. Data which does not meet the criteria is excluded).

		Day 1 (n=12)			Day 2 (n=12)			Day 3 (n=12)			Day 4 (n=4)			Day 7 (n=4)			Day 10 (n=4)			Day 14 (n=4)		
Gene	Category	Fold change	Posterior probability	90% CI	Fold change	Posterior probability	90% CI	Fold change	Posterior probability	90% CI	Fold change	Posterior probability	90% CI	Fold change	Posterior probability	90% CI	Fold change	Posterior probability	90% CI	Fold change	Posterior probability	90% CI
BCL2	Other													2.01	1.00	[1.33;3.07]						
CCL2	Chemokine	12.53	1.00	[6.62;23.2]	12.03	1.00	[6.43;21.79]	4.59	1.00	[2.61;7.89]	6.24	1.00	[2.45;16.03]									
CCL5	Chemokine	5.01	1.00	[3.02;8.4]	8.44	1.00	[5.04;13.95]	2.20	1.00	[1.42;3.59]	5.91	1.00	[2.68;12.68]	4.61	1.00	[1.97;10.07]						
CCL8	Chemokine	6.68	1.00	[4.6;10.14]	2.58	1.00	[1.74;3.84]	2.39	1.00	[1.71;3.4]	2.06	0.98	[1.13;3.75]	2.54	0.99	[1.29;4.77]						
CD163	Other	6.53	1.00	[3.27;13.26]	18.97	1.00	[9.98;36.27]	8.32	1.00	[4.59;14.79]	6.63	1.00	[2.4;17.93]									
CXCL8 (IL8)	Chemokine	4.12	1.00	[2.1;8.68]	8.65	1.00	[4.54;16.12]	2.02	0.97	[1.13;3.8]	3.88	0.99	[1.48;9.94]	4.23	0.99	[1.57;11.46]						
CXCL10	Chemokine	11.86	1.00	[8.02;17.91]	4.19	1.00	[2.81;6.42]	3.86	1.00	[2.71;5.51]	7.25	1.00	[3.93;13.83]				2.24	0.98	[1.22;4.03]	2.51	0.99	[1.35;4.81]
CXCL11	Chemokine	3.95	1.00	[2.5;6.38]																		
DDX58 (RIG-I)	PRR	9.57	1.00	[6.71;13.48]	4.00	1.00	[2.85;5.79]	4.42	1.00	[3.24;6.05]	5.26	1.00	[3;9.17]	2.17	0.98	[1.17;3.89]	2.31	0.99	[1.35;4.07]			
EIF2AK2 (PKR)	ISG	3.23	1.00	[2.62;3.98]	2.44	1.00	[1.92;3.08]	2.36	1.00	[1.96;2.84]	2.21	1.00	[1.54;3.08]									
GBP1	ISG	2.41	1.00	[1.74;3.37]																		
GBP2	ISG	2.22	1.00	[1.65;3.03]																		
GZMB	Other	2.32	1.00	[1.73;3.2]										4.16	1.00	[2.48;6.7]	2.86	1.00	[1.71;4.78]			
HERC5	ISG	4.49	1.00	[3.55;5.75]	2.53	1.00	[1.96;3.24]	2.66	1.00	[2.13;3.32]	2.40	1.00	[1.63;3.45]									
IFI44	ISG	3.21	1.00	[2.59;3.95]	2.49	1.00	[2.04;3.09]	2.75	1.00	[2.29;3.3]	2.44	1.00	[1.8;3.38]									
IFIH1 (MDA5)	PRR	5.04	1.00	[3.69;6.82]	4.13	1.00	[2.96;5.64]	2.66	1.00	[1.99;3.58]	3.24	1.00	[2;5.32]	2.15	0.99	[1.34;3.64]						
IFIT1	ISG	7.34	1.00	[5.16;10.57]	3.61	1.00	[2.48;5.25]	3.52	1.00	[2.46;4.96]	4.01	1.00	[2.29;6.99]									
IFIT3	ISG	9.35	1.00	[6.18;13.69]	3.65	1.00	[2.43;5.41]	3.79	1.00	[2.67;5.41]	4.36	1.00	[2.37;7.95]	2.01	0.96	[1.03;3.92]	2.13	0.97	[1.14;4.07]			
IFITM3	ISG	2.10	1.00	[1.74;2.52]							2.59	1.00	[1.98;3.48]									
IFNB1	Interferon	40.94	1.00	[23.11;68.49]	9.04	1.00	[5.38;15.07]	6.69	1.00	[4.19;10.87]	10.81	1.00	[4.7;25.46]									
IFNG	Interferon	2.64	1.00	[1.86;3.73]																2.18	1.00	[1.31;3.48]
IFNL1 (IL29)	Interferon	6.41	1.00	[4.46;9.06]	3.02	1.00	[2.19;4.12]	2.33	1.00	[1.74;3.18]	3.35	1.00	[2.02;5.65]									
IL10	Cytokine	11.06	1.00	[5.81;21.74]	24.66	1.00	[12.69;44.24]	5.34	1.00	[2.97;9.82]	11.53	1.00	[4.5;30.81]	5.07	1.00	[1.89;13.53]	2.67	0.95	[1;6.82]			
IL12B	Cytokine	4.98	1.00	[2.92;8.57]	13.48	1.00	[7.88;22.92]	3.42	1.00	[2.14;5.69]	6.50	1.00	[2.97;14.45]	5.18	1.00	[2.33;11.73]						
IL17A	Cytokine	3.77	1.00	[2.09;7]	7.75	1.00	[4.2;14.03]	2.13	0.99	[1.25;3.66]	2.93	0.98	[1.21;6.91]	3.59	0.99	[1.42;9.24]						
IL1A	Cytokine	4.95	1.00	[2.34;9.91]	13.87	1.00	[6.81;27.66]	2.97	1.00	[1.52;5.66]	7.43	1.00	[2.51;21.41]	6.56	1.00	[2.07;19.13]						
IL1B	Cytokine	5.31	1.00	[2.46;12.36]	20.16	1.00	[9.27;42.04]	4.07	1.00	[1.91;8.06]	6.50	0.99	[1.95;20.2]	5.94	0.99	[1.72;19.65]						
IL1RN	Cytokine	7.71	1.00	[3.86;15.01]	18.46	1.00	[9.56;36.06]	3.29	1.00	[1.73;6.1]	10.97	1.00	[3.69;30.35]	7.47	1.00	[2.46;21.88]						
IL6	Cytokine	6.09	1.00	[4.19;8.93]	3.17	1.00	[2.18;4.75]	3.22	1.00	[2.24;4.54]	3.15	1.00	[1.53;6.31]	2.98	0.99	[1.5;6.2]	3.82	1.00	[2.08;6.62]	2.85	1.00	[1.64;5.02]
IRF1	Transcription factor	2.37	1.00	[1.66;3.49]	4.11	1.00	[2.9;5.85]				2.99	1.00	[1.75;5.32]	2.49	1.00	[1.36;4.37]						
IRF7	Transcription factor	7.48	1.00	[5.22;10.61]	4.92	1.00	[3.47;6.97]	3.72	1.00	[2.45;5.74]	6.96	1.00	[4.12;12.3]	2.08	0.98	[1.15;3.62]	2.34	0.99	[1.4;4.06]	2.30	0.99	[1.34;3.88]
IRF9	Transcription factor	2.15	1.00	[1.58;3]	4.65	1.00	[3.46;6.35]	3.72	1.00	[2.88;4.89]	5.92	1.00	[3.8;9.31]	3.99	1.00	[2.49;6.74]	3.18	1.00	[1.97;4.92]	4.34	1.00	[2.77;6.96]
ISG15	ISG	11.58	1.00	[7.63;17.67]	4.69	1.00	[3.07;7.37]	5.01	1.00	[3.4;7.34]	7.49	1.00	[3.86;14.57]									
ISG20	ISG	5.54	1.00	[3.86;8.15]	4.77	1.00	[3.27;6.96]	2.76	1.00	[1.97;3.89]	5.47	1.00	[3.13;9.76]	2.45	0.99	[1.31;4.46]						
MUC15	Mucin	4.98	1.00	[2.72;9.19]							2.62	0.96	[1.07;6.2]									
MUC19	Mucin	3.04	1.00	[1.87;5.21]	5.57	1.00	[3.51;9.05]	2.73	1.00	[1.75;4.07]	2.77	0.99	[1.37;5.65]	2.49	0.98	[1.26;5.46]	2.01	0.95	[1.02;4]			
MUC20	Mucin													2.10	0.99	[1.27;3.46]	2.31	1.00	[1.44;3.64]			
MUC5AC	Mucin																2.15	0.98	[1.22;3.89]	2.05	0.98	[1.17;3.6]
MUC5B	Mucin							3.00	1.00	[1.97;4.36]												
MX1	ISG	7.58	1.00	[5.57;10.58]	3.93	1.00	[2.85;5.39]	4.50	1.00	[3.35;5.95]	5.04	1.00	[3.01;8.46]	2.26	0.99	[1.29;3.83]	2.33	1.00	[1.43;3.83]			
MX2	ISG	9.37	1.00	[6.77;12.74]	4.53	1.00	[3.28;6.17]	3.46	1.00	[2.55;4.83]	5.14	1.00	[3.13;8.63]				2.43	1.00	[1.44;3.94]	2.23	1.00	[1.36;3.66]
MYD88	Adaptor protein	2.16	1.00	[1.54;3.1]	3.93	1.00	[2.82;5.58]				2.96	1.00	[1.71;5.07]	2.46	0.99	[1.43;4.47]						
NFKB1	Transcription factor	2.29	1.00	[1.62;3.32]	5.45	1.00	[3.91;7.81]	2.35	1.00	[1.73;3.18]	3.47	1.00	[2;5.94]	2.26	0.99	[1.3;3.88]						
OAS1	ISG	6.55	1.00	[4.02;10.79]	6.66	1.00	[4.1;10.92]	3.46	1.00	[2.24;5.41]	7.65	1.00	[3.6;16.21]	2.49	0.96	[1.05;5.92]						
OASL	ISG	4.25	1.00	[3.03;5.9]							3.47	1.00	[2.07;5.64]									
PTGS2	Other	2.61	1.00	[1.62;4.19]	5.92	1.00	[3.75;9.67]	3.33	1.00	[2.18;5.17]	3.58	1.00	[1.72;7.7]	3.29	1.00	[1.54;6.63]	2.20	0.97	[1.1;4.47]			
SELL	Other	6.67	1.00	[3.24;14.6]	23.29	1.00	[11.71;48.25]	4.53	1.00	[2.22;8.8]	9.74	1.00	[3.14;27.75]	7.80	1.00	[2.6;24.72]	3.14	0.96	[1.08;9.37]			
SLA1	Other	2.11	0.96	[1.05;4.29]	2.17	0.96	[1.06;4.34]															
STAT1	Transcription factor	2.11	1.00	[1.78;2.51]																		
SAA2	Other	4.33	1.00	[2.23;8.67]	11.64	1.00	[6.29;22.48]	6.48	1.00	[3.72;11.9]	5.26	1.00	[1.93;14.23]									
TAP1	Other	2.15	1.00	[1.73;2.69]	2.06	1.00	[1.67;2.6]				2.13	1.00	[1.53;3.02]									
TGFB	Other				2.64	1.00	[2.08;3.35]															
TLR7	PRR	4.47	1.00	[3.55;5.69]	2.00	1.00	[1.59;2.51]															
TLR8	PRR	3.86	1.00	[2.62;5.53]	4.86	1.00	[3.33;7.09]	2.94	1.00	[2.08;4.11]	2.80	1.00	[1.62;4.94]									
TNF	Cytokine	5.12	1.00	[2.78;10.05]	19.68	1.00	[10.29;37.37]	3.47	1.00	[1.87;6.23]	9.51	1.00	[3.52;26.08]	9.31	1.00	[3.34;25.4]						
TNFAIP3	Other	7.28	1.00	[3.81;13.89]	18.08	1.00	[9.61;32.5]	3.75	1.00	[2.02;6.58]	11.81	1.00	[4.61;32.16]	7.67	1.00	[2.76;21]	3.02	0.97	[1.17;7.54]			
USP18	Other	5.80	1.00	[4.32;7.65]	2.35	1.00	[1.74;3.13]	2.70	1.00	[2.09;3.46]	3.17	1.00	[2.06;4.97]									
Total number of genes regulated			52			44			39			45			29			16			7	

Supplementary Table 2: Statistically significant upregulated genes in the huH1N1pdm09 group during the study period (+2-fold change (FC) in gene expression compared to baseline (all data before inoculation and data from the control group) with a posterior probability of >95%. Data which does not meet the criteria is excluded).

		Day 1 (n=12)			Day 2 (n=12)			Day 3 (n=12)			Day 4 (n=4)			Day 7 (n=4)			Day 10 (n=4)			Day 14 (n=4)		
Gene	Category	Fold change	Posterior probability	90% CI	Fold change	Posterior probability	90% CI	Fold change	Posterior probability	90% CI	Fold change	Posterior probability	90% CI	Fold change	Posterior probability	90% CI	Fold change	Posterior probability	90% CI	Fold change	Posterior probability	90% CI
CCL2	Chemokine	5.90	1.00	[3.11;11.21]	5.42	1.00	[2.91;9.85]	2.65	1.00	[1.43;4.9]	4.87	1.00	[1.93;12.75]									
CCL5	Chemokine										3.01	0.99	[1.37;6.6]									
CCL8	Chemokine	2.40	1.00	[1.63;3.57]	2.33	1.00	[1.6;3.41]				4.37	1.00	[2.43;8.24]									
CD163	Other	4.05	1.00	[2.06;8.12]	3.67	1.00	[1.85;7.22]	4.28	1.00	[2.25;8.26]	7.41	1.00	[2.53;21.36]									
CXCL8 (IL8)	Chemokine	3.72	1.00	[1.99;7.04]	4.07	1.00	[2.16;7.81]	2.07	0.97	[1.08;3.85]	3.25	0.97	[1.26;9.18]									
CXCL10	Chemokine	6.16	1.00	[4.18;8.92]	4.18	1.00	[2.85;6.27]	2.65	1.00	[1.79;4.04]	6.67	1.00	[3.56;12.61]	2.94	1.00	[1.57;5.56]						
CXCL11	Chemokine	3.00	1.00	[1.97;4.7]	2.60	1.00	[1.69;4.15]				6.92	1.00	[3.39;13.47]									
DDX58 (RIG-I)	PRR	6.57	1.00	[4.66;9.12]	4.21	1.00	[3;6.03]	3.16	1.00	[2.17;4.61]	5.68	1.00	[3.16;10]	2.90	1.00	[1.64;5.13]						
EIF2AK2 (PKR)	ISG	2.49	1.00	[2.07;3.03]	2.20	1.00	[1.8;2.71]				2.04	1.00	[1.33;3.03]									
GBP1	ISG										2.08	0.99	[1.24;3.5]	2.58	1.00	[1.55;4.14]						
GZMB	Other										2.22	0.99	[1.32;3.72]	2.82	1.00	[1.66;4.82]						
HERC5	ISG	3.58	1.00	[2.87;4.51]	2.76	1.00	[2.19;3.49]				2.83	1.00	[1.98;4.27]	2.02	1.00	[1.38;2.92]						
IFI44	ISG	2.78	1.00	[2.32;3.42]	2.36	1.00	[1.95;2.89]				2.32	1.00	[1.67;3.19]									
IFIH1 (MDA5)	PRR	3.29	1.00	[2.49;4.46]	3.11	1.00	[2.29;4.15]				3.12	1.00	[1.91;5.1]	2.45	1.00	[1.53;3.96]						
IFIT1	ISG	4.50	1.00	[3.22;6.4]	3.50	1.00	[2.49;4.98]	2.17	1.00	[1.45;3.23]	3.80	1.00	[2.08;6.86]	2.74	1.00	[1.58;4.92]						
IFIT3	ISG	6.30	1.00	[4.26;9.25]	4.18	1.00	[2.77;6.2]	2.59	1.00	[1.7;3.92]	7.38	1.00	[3.91;14.02]	4.35	1.00	[2.33;8.14]	2.14	0.97	[1.09;4.2]			
IFITM3	ISG	2.29	1.00	[1.92;2.72]	2.31	1.00	[1.9;2.81]				2.27	1.00	[1.67;3.07]									
IFNA1	Interferon							2.08	1.00	[1.42;3.13]										2.89	1.00	[1.57;5.12]
IFNB1	Interferon	7.21	1.00	[4.19;12.27]	7.58	1.00	[4.39;12.5]	10.61	1.00	[6.12;18.52]	20.87	1.00	[8.84;50.96]	3.61	0.99	[1.62;8.82]	2.52	0.96	[1.02;6]			
IFNG	Interferon										2.07	0.99	[1.24;3.58]	2.14	0.99	[1.31;3.54]						
IFNL1 (IL29)	Interferon	3.06	1.00	[2.21;4.27]	3.83	1.00	[2.75;5.48]	3.58	1.00	[2.51;5.09]	5.04	1.00	[2.81;9.44]	2.07	0.99	[1.25;3.4]						
IL10	Cytokine	5.54	1.00	[2.9;10.39]	5.97	1.00	[3.16;11.42]	3.19	1.00	[1.72;5.98]	5.48	1.00	[2.04;14.84]	3.15	0.97	[1.16;7.93]						
IL12B	Cytokine	2.34	1.00	[1.45;3.81]	4.07	1.00	[2.45;6.78]	2.92	1.00	[1.77;4.87]	3.08	0.99	[1.4;6.61]	3.72	1.00	[1.7;8.51]	3.32	0.99	[1.48;7.85]			
IL17A	Cytokine				2.53	0.99	[1.39;4.64]															
IL18	Cytokine										2.19	0.96	[1.08;4.61]									
IL1A	Cytokine	2.84	0.99	[1.38;5.54]	4.47	1.00	[2.23;9.01]	2.65	0.99	[1.29;5.21]	4.11	0.98	[1.34;11.67]	3.57	0.97	[1.26;10.88]						
IL1B	Cytokine	3.23	1.00	[1.57;7.16]	4.69	1.00	[2.2;10.12]	3.02	0.99	[1.37;6.66]	5.53	0.99	[1.78;18.66]	3.30	0.95	[1.05;10.9]						
IL1RN	Cytokine	3.28	1.00	[1.69;6.31]	4.37	1.00	[2.19;8.5]	2.70	0.99	[1.42;5.25]	4.68	0.99	[1.6;13.69]	4.34	0.99	[1.6;12.11]						
IL6	Cytokine	3.43	1.00	[2.36;4.9]	3.32	1.00	[2.36;4.85]	3.32	1.00	[2.31;4.8]	5.75	1.00	[3.21;9.89]				3.04	1.00	[1.72;5.49]			
IRF1	Transcription factor													2.09	0.99	[1.26;3.6]						
IRF7	Transcription factor	4.19	1.00	[3.01;5.87]	3.21	1.00	[2.23;4.56]	2.78	1.00	[1.9;4.04]	3.62	1.00	[2.07;6.42]	2.39	0.99	[1.41;4.45]						
IRF9	Transcription factor	4.18	1.00	[3.15;5.54]	5.66	1.00	[4.24;7.5]	5.26	1.00	[3.94;7.03]	2.93	1.00	[1.82;4.69]	3.71	1.00	[2.35;5.77]	3.26	1.00	[2.11;5.09]	3.45	1.00	[2.23;5.44]
ISG15	ISG	6.24	1.00	[4.22;9.41]	3.99	1.00	[2.59;5.89]	2.75	1.00	[1.74;4.32]	6.68	1.00	[3.46;12.44]	3.05	1.00	[1.62;5.82]						
ISG20	ISG	3.40	1.00	[2.33;4.73]	3.02	1.00	[2.09;4.36]	2.18	1.00	[1.53;3.17]	3.14	1.00	[1.79;5.63]	2.30	0.99	[1.34;4.07]						
MUC15	Mucin	4.05	1.00	[2.28;7.19]	3.27	1.00	[1.82;5.68]	2.14	0.99	[1.23;3.81]	7.66	1.00	[3.1;19.26]	3.92	0.99	[1.63;9.18]						
MUC19	Mucin				2.42	1.00	[1.5;3.98]	2.56	1.00	[1.59;4.02]	2.44	0.98	[1.17;4.96]	2.73	0.99	[1.35;5.69]	2.32	0.97	[1.11;4.56]			
MUC20	Mucin													5.36	1.00	[3.43;8.54]	2.20	1.00	[1.41;3.47]			
MUC4	Mucin													3.66	1.00	[2.37;5.78]						
MX1	ISG	5.28	1.00	[3.86;7.13]	3.30	1.00	[2.41;4.53]	2.65	1.00	[1.89;3.79]	3.64	1.00	[2.23;6.05]	2.60	1.00	[1.62;4.36]						
MX2	ISG	6.39	1.00	[4.73;8.77]	3.84	1.00	[2.82;5.34]	2.81	1.00	[2.01;3.92]	4.12	1.00	[2.44;7.03]	2.61	1.00	[1.57;4.3]				2.21	0.99	[1.31;3.85]
MYD88	Adaptor protein				2.16	1.00	[1.54;3.1]				2.15	0.99	[1.27;3.86]	2.56	1.00	[1.5;4.24]						
OAS1	ISG	5.43	1.00	[3.43;8.59]	5.81	1.00	[3.63;9.29]	2.73	1.00	[1.7;4.43]	6.38	1.00	[2.85;13.59]	3.63	1.00	[1.74;7.6]						
OASL	ISG	4.71	1.00	[3.47;6.51]	2.85	1.00	[2.06;3.93]	2.12	1.00	[1.58;2.96]	4.51	1.00	[2.72;7.45]	2.51	1.00	[1.5;4.13]						
PTGS2	Other				2.96	1.00	[1.85;4.76]	2.90	1.00	[1.83;4.67]	2.58	0.99	[1.3;5.29]	2.68	0.99	[1.28;5.5]	2.36	0.96	[1.1;5.1]			
SELL	Other	2.57	0.98	[1.19;5]	4.79	1.00	[2.34;10.35]	2.82	0.99	[1.34;5.61]	4.72	0.99	[1.6;13.89]	4.16	0.98	[1.35;12.09]						
SLA1	Other													3.66	0.98	[1.33;10.03]						
SLA2	Other													2.14	1.00	[1.53;2.97]						
STAT1	Transcription factor	2.08	1.00	[1.75;2.44]																		
SAA2	Other	2.73	0.99	[1.46;5.38]	3.40	1.00	[1.77;6.4]	2.71	1.00	[1.47;5.23]	3.15	0.97	[1.16;8.37]									
TAP1	Other													2.49	1.00	[1.81;3.49]						
TLR7	PRR	2.63	1.00	[2.05;3.37]																		
TLR8	PRR	2.37	1.00	[1.6;3.42]	2.14	1.00	[1.46;3.12]	2.15	1.00	[1.46;3.1]	3.38	1.00	[1.86;6.17]	2.53	0.99	[1.37;4.51]						
TNF	Cytokine				3.88	1.00	[2.03;7.58]	2.62	0.99	[1.42;4.97]	3.04	0.97	[1.21;7.92]	2.97	0.97	[1.13;7.94]						
TNFAIP3	Other	2.86	1.00	[1.53;5.24]	4.37	1.00	[2.32;7.92]	2.79	1.00	[1.5;5.14]	4.65	1.00	[1.76;12.44]	3.57	0.99	[1.44;9.33]						
USP18	Other	4.31	1.00	[3.29;5.68]	2.93	1.00	[2.2;3.93]	2.26	1.00	[1.68;2.94]	3.93	1.00	[2.51;6.1]	2.44	1.00	[1.6;3.74]						
Total number of genes regulated			38			41			33			45			39			8			3	

Supplementary Table 2: Statistically significant upregulated genes in the mxH1N1pdm09 group during the study period (+2-fold change (FC) in gene expression compared to baseline (all data before inoculation and data from the control group) with a posterior probability of >95%. Data which does not meet the criteria is excluded).

		Day 1 (n=12)			Day 2 (n=12)			Day 3 (n=12)			Day 4 (n=4)			Day 7 (n=4)			Day 10 (n=4)			Day 14 (n=4)		
Gene	Category	Fold change	Posterior probability	90% CI	Fold change	Posterior probability	90% CI	Fold change	Posterior probability	90% CI	Fold change	Posterior probability	90% CI	Fold change	Posterior probability	90% CI	Fold change	Posterior probability	90% CI	Fold change	Posterior probability	90% CI
CCL2	Chemokine	6.41	1.00	[3.36;11.88]	3.57	1.00	[1.94;6.64]	5.54	1.00	[3.07;10.63]	4.43	0.99	[1.71;11.02]									
CCL5	Chemokine	2.19	1.00	[1.4;3.61]	2.43	1.00	[1.49;4.03]	2.85	1.00	[1.73;4.81]	7.30	1.00	[3.49;15.79]				2.75	0.98	[1.24;6.09]			
CCL8	Chemokine	3.58	1.00	[2.43;5.21]				2.60	1.00	[1.74;3.95]	3.90	1.00	[2.05;7.29]									
CD163	Other	5.06	1.00	[2.64;9.99]	5.26	1.00	[2.68;10.37]	9.22	1.00	[4.75;18.11]	7.73	1.00	[2.94;22.92]									
CXCL8 (IL8)	Chemokine	3.60	1.00	[1.87;6.71]	4.12	1.00	[2.12;7.79]	5.69	1.00	[2.94;10.62]	9.35	1.00	[3.49;23.36]	3.54	0.98	[1.35;9.69]	5.01	0.99	[1.87;14.42]			
CXCL10	Chemokine	8.06	1.00	[5.44;11.84]	2.67	1.00	[1.78;3.95]	6.03	1.00	[4.02;8.95]	5.30	1.00	[2.95;9.73]	2.35	0.99	[1.31;4.5]	2.12	0.97	[1.07;4.01]			
CXCL11	Chemokine	3.73	1.00	[2.42;5.94]				2.43	1.00	[1.56;3.71]	3.48	1.00	[1.77;6.74]									
DDX58 (RIG-I)	PRR	7.86	1.00	[5.53;11]	2.44	1.00	[1.66;3.45]	4.68	1.00	[3.28;6.86]	5.73	1.00	[3.25;10]				2.51	1.00	[1.39;4.34]			
EIF2AK2 (PKR)	ISG	2.83	1.00	[2.33;3.44]				2.46	1.00	[1.97;3.11]	3.58	1.00	[2.64;5.07]									
GZMB	Other	2.65	1.00	[1.92;3.6]										2.27	1.00	[1.39;3.74]						
HERC5	ISG	3.96	1.00	[3.14;4.99]				3.29	1.00	[2.52;4.34]	3.25	1.00	[2.29;4.77]				2.20	1.00	[1.48;3.29]			
IFI44	ISG	2.76	1.00	[2.27;3.36]				3.04	1.00	[2.38;3.88]	3.32	1.00	[2.4;4.65]									
IFIH1 (MDA5)	PRR	4.08	1.00	[3.08;5.52]				3.64	1.00	[2.67;5.07]	5.91	1.00	[3.63;9.54]				2.78	1.00	[1.68;4.68]			
IFIT1	ISG	5.59	1.00	[3.92;7.82]				4.39	1.00	[3.02;6.48]	5.67	1.00	[3.21;9.66]				2.67	0.99	[1.5;4.9]			
IFIT3	ISG	8.38	1.00	[5.61;12.38]				5.54	1.00	[3.7;8.48]	7.37	1.00	[3.84;13.9]				2.92	1.00	[1.57;5.54]			
IFITM3	ISG	2.34	1.00	[1.95;2.8]							2.50	1.00	[1.89;3.36]									
IFNA1	Interferon																			2.14	0.97	[1.11;3.97]
IFNB1	Interferon	7.56	1.00	[4.4;12.95]	4.89	1.00	[2.94;8.4]	10.16	1.00	[6.02;17.8]	19.56	1.00	[8.79;45.78]				3.20	0.98	[1.36;8.3]	2.55	0.96	[1.04;6.22]
IFNG	Interferon	2.00	1.00	[1.46;2.84]																		
IFNL1 (IL29)	Interferon	4.13	1.00	[2.98;5.82]	2.12	1.00	[1.53;2.93]	4.50	1.00	[3.23;6.34]	5.03	1.00	[2.8;9.2]				2.44	0.99	[1.44;4.26]	2.18	0.99	[1.29;3.59]
IL10	Cytokine	6.71	1.00	[3.63;13.07]	6.68	1.00	[3.53;12.75]	9.80	1.00	[5.09;18.27]	21.98	1.00	[8.02;61.13]	3.16	0.97	[1.19;8.74]	5.75	1.00	[2.12;15.77]			
IL12B	Cytokine	3.08	1.00	[1.89;5.22]	4.12	1.00	[2.38;6.93]	6.16	1.00	[3.61;10.53]	13.84	1.00	[5.99;32.03]	3.96	1.00	[1.77;8.71]	5.24	1.00	[2.38;11.13]			
IL15	Cytokine										2.28	1.00	[1.55;3.37]									
IL17A	Cytokine				2.14	0.98	[1.19;3.87]	3.50	1.00	[1.92;6.37]	4.74	1.00	[1.95;11.65]							2.51	0.95	[1.01;6.02]
IL18	Cytokine										3.68	1.00	[1.77;7.26]				2.35	0.97	[1.1;4.92]			
IL1A	Cytokine	3.75	1.00	[1.87;7.46]	4.23	1.00	[2.05;8.21]	6.37	1.00	[3.19;13.36]	16.19	1.00	[5.36;46.26]	4.77	0.99	[1.66;14.08]	7.05	1.00	[2.35;21.36]	4.55	0.98	[1.44;15.03]
IL1B	Cytokine	4.47	1.00	[2.14;9.82]	4.89	1.00	[2.25;10.39]	7.69	1.00	[3.51;16.85]	20.35	1.00	[6.15;62.82]	5.93	0.99	[1.91;20.49]	7.77	1.00	[2.44;27.86]			
IL1RN	Cytokine	4.79	1.00	[2.45;9.01]	4.10	1.00	[2.03;7.73]	6.74	1.00	[3.4;13.35]	27.10	1.00	[9.75;78.32]	3.58	0.98	[1.34;10.27]	7.64	1.00	[2.75;22.23]	3.59	0.97	[1.25;11.34]
IL6	Cytokine	3.03	1.00	[2.1;4.59]	4.39	1.00	[3.09;6.32]	4.35	1.00	[2.95;6.4]	5.13	1.00	[2.87;9.03]	2.59	1.00	[1.5;4.67]	3.62	1.00	[2;6.42]			
IRF1	Transcription factor							2.32	1.00	[1.63;3.38]	5.56	1.00	[3.13;9.4]				2.06	0.98	[1.21;3.65]			
IRF7	Transcription factor	4.93	1.00	[3.55;6.93]	2.25	1.00	[1.58;3.21]	4.01	1.00	[2.79;5.88]	5.31	1.00	[2.93;9.94]				2.73	0.99	[1.53;5.12]			
IRF9	Transcription factor	5.08	1.00	[3.82;6.82]	5.04	1.00	[3.76;6.71]	3.82	1.00	[2.89;5.19]	5.66	1.00	[3.53;8.85]	3.31	1.00	[2.11;5.15]	4.06	1.00	[2.6;6.53]	3.40	1.00	[2.12;5.35]
ISG15	ISG	8.35	1.00	[5.62;12.49]	2.37	1.00	[1.56;3.64]	4.88	1.00	[3.08;7.43]	6.38	1.00	[3.48;12.18]				2.58	0.99	[1.32;5.07]			
ISG20	ISG	4.17	1.00	[2.88;5.96]	2.09	1.00	[1.45;3.06]	3.86	1.00	[2.63;5.59]	7.96	1.00	[4.55;14.3]				2.16	0.99	[1.25;3.87]			
MUC15	Mucin	5.97	1.00	[3.29;10.47]				3.73	1.00	[2.07;6.49]	4.18	0.99	[1.66;10.79]				2.96	0.98	[1.17;6.94]			
MUC19	Mucin	2.18	1.00	[1.38;3.46]				3.87	1.00	[2.38;6.26]	7.67	1.00	[3.69;15.82]	2.83	0.99	[1.41;5.65]	4.56	1.00	[2.12;9.9]	2.68	0.98	[1.27;5.96]
MUC20	Mucin													2.54	1.00	[1.65;4.12]	2.93	1.00	[1.78;4.84]			
MUC4	Mucin																2.16	1.00	[1.35;3.33]			
MX1	ISG	6.05	1.00	[4.48;8.24]	2.06	1.00	[1.48;2.84]	4.63	1.00	[3.28;6.42]	4.55	1.00	[2.72;7.64]				2.22	0.99	[1.32;3.77]			
MX2	ISG	6.79	1.00	[4.99;9.19]	2.19	1.00	[1.6;3.11]	6.33	1.00	[4.51;8.84]	7.44	1.00	[4.39;12.36]				2.01	0.98	[1.19;3.39]			
MYD88	Adaptor protein	2.08	1.00	[1.47;2.87]				2.57	1.00	[1.84;3.66]	4.83	1.00	[2.76;8.43]				2.59	1.00	[1.48;4.52]			
NFKB1	Transcription factor							2.37	1.00	[1.68;3.32]	5.78	1.00	[3.34;10.37]				2.36	0.99	[1.39;4.1]			
OAS1	ISG	5.31	1.00	[3.41;8.4]	2.93	1.00	[1.8;4.74]	4.82	1.00	[2.89;8.04]	13.87	1.00	[6.77;30.17]				3.17	0.99	[1.5;6.79]			
OASL	ISG	4.95	1.00	[3.61;6.79]				2.53	1.00	[1.83;3.49]	2.51	1.00	[1.56;4.15]									
PTGS2	Other				2.90	1.00	[1.74;4.62]	5.02	1.00	[3.04;8.01]	5.82	1.00	[2.82;12.22]	2.60	0.99	[1.29;5.26]	4.61	1.00	[2.16;10.33]	2.92	0.99	[1.33;6.35]
S100A7	Other							3.56	1.00	[1.98;6.71]										3.33	0.98	[1.25;8.69]
SELL	Other	3.73	1.00	[1.82;7.69]	2.82	0.99	[1.39;6.09]	6.92	1.00	[3.34;15.19]	11.72	1.00	[3.93;38.43]				5.26	0.99	[1.85;18.1]	3.78	0.97	[1.22;13.29]
STAT1	Transcription factor	2.36	1.00	[2.02;2.81]							2.08	1.00	[1.59;2.73]									
SAA2	Other	3.42	1.00	[1.85;6.59]	3.15	1.00	[1.59;6.15]	5.14	1.00	[2.76;9.97]	7.29	1.00	[2.7;19.13]									
TGFB	Other									[1.81;2.94]	2.07	1.00	[1.43;3.04]									
TLR7	PRR	2.74	1.00	[2.18;3.53]				2.31	1.00	[1.75;3.73]												
TLR8	PRR	3.42	1.00	[2.38;5.03]	2.48	1.00	[1.71;3.61]	2.51	1.00	[3.64;13.07]	4.45	1.00	[2.47;7.89]				2.25	0.99	[1.24;3.98]			
TNF	Cytokine	2.82	1.00	[1.57;5.3]	4.39	1.00	[2.34;8.25]	6.63	1.00	[3.66;12.89]	35.61	1.00	[13.08;94.04]	5.39	1.00	[2.09;14.33]	5.34	1.00	[1.93;14.14]	3.07	0.96	[1.12;8.5]
TNFAIP3	Other	4.11	1.00	[2.21;7.67]	4.51	1.00	[2.43;8.54]	6.72	1.00	[2.56;4.61]	24.04	1.00	[8.99;60.89]	3.91	0.99	[1.56;10.28]	6.05	1.00	[2.25;16.35]	3.33	0.97	[1.23;9.35]
USP18	Other	4.82	1.00	[3.72;6.53]				3.44	1.00		3.71	1.00	[2.42;5.75]									
Total number of genes regulated			44			28			45			49			16			36			13	

Supplementary Table 2: Statistically significant upregulated genes in all inoculated groups during the study period (-2-fold change (FC) in gene expression compared to baseline (all data before inoculation and data from the control group) with a posterior probability of >95%. Data which does not meet the criteria is excluded).

		swH1N1pdm09														
		Day 1 (n=12)			Day 2 (n=12)			Day 3 (n=12)			Day 4 (n=4)			Day 7 (n=4)		
Gene	Category	Fold change	Posterior probability	90% CI	Fold change	Posterior probability	90% CI	Fold change	Posterior probability	90% CI	Fold change	Posterior probability	90% CI	Fold change	Posterior probability	90% CI
C4A	Other				0.33	1.00	[0.22;0.51]									
CXCL9	Chemokine				0.29	1.00	[0.2;0.43]				0.35	1.00	[0.2;0.66]			
IFNA1	Interferon				0.37	1.00	[0.26;0.55]				0.44	0.99	[0.24;0.76]			
MUC12	Mucin				0.30	1.00	[0.17;0.56]	0.44	0.99	[0.25;0.78]				0.23	0.99	[0.09;0.59]
MUC5AC	Mucin	0.38	1.00	[0.25;0.57]	0.18	1.00	[0.13;0.26]	0.48	1.00	[0.35;0.66]	0.40	0.99	[0.22;0.73]			
MUC5B	Mucin				0.49	1.00	[0.32;0.74]									
TLR3	PRR				0.22	1.00	[0.17;0.3]				0.46	1.00	[0.3;0.73]			
Total number of genes regulated			1			7			2			4			1	
		huH1N1pdm09														
MUC12	Mucin													0.28	0.99	[0.12;0.67]
MUC5AC	Mucin				0.49	1.00	[0.35;0.71]									
MUC5B	Mucin													0.39	0.99	[0.2;0.76]
Total number of genes regulated			-			1			-			-			2	
		mxH1N1pdm09														
MUC5AC	Mucin				0.45	1.00	[0,32;0,66]									
Total number of genes regulated			-			1			-			-			-	

Supplementary Table 3: qPCR primer sequences and experimentally determined PCR efficiencies for all reported genes in the present study.

Gene name	Forward primer	Reverse Primer	PCR eff. (%)
B2M (Reference)	TGAAGCACGTGACTCTCGAT	CTCTGTGATGCCGGTTAGTG	101
BCL2	CCCTGTGGATGACTGAGTACC	AACCACACATGCACCTACCC	112
C4A	CTACAACCCCGAGCACAAAT	GACATCAGCCGAGCACAAT	102
CCL2	CTTCTGCACCCAGGTCCTT	CGCTGCATCGAGATCTTCTT	104
CCL5	CTCCATGGCAGCAGTCGT	AAGGCTTCCTCCATCCTAGC	103
CCL8	GCCAGATTCAGTCTCCATCC	AGGGGATCTTTCCATTGACC	92
CD163	CACATGTGCCAACAAAATAAGAC	CACCACCTGAGCATCTTCAA	104
CTNNB1	CCAGGATGATCCCAGCTATC	CCCATCAACTGGATAGTCAGC	105
CXCL10	CCCACATGTTGAGATCATTGC	GCTTCTCTCTGTGTTCGAGGA	104
CXCL11	CACCCAAGTAACAACTGTGACAA	TTGGGATTTAGGCATCTTCG	101
CXCL8 (IL8)	TTGCCAGAGAAATCACAGGA	TGCATGGGACACTGGAAATA	104
CXCL9	TTAAACAATTTGCCCCAAGC	TGTTTGATCCCCATTCTTCA	95
DDX58 (RIG-I)	TTGCTCAGTGCAATCTGGTC	CTTCCTCTGCCTCTGGTTTG	103
EIF2AK2 (PKR)	AGAACTTCTTCACATATGTCGCAC	ATACATCTAAGACGCCAGCCTT	98
GAPDH (Putative reference)	ACCCAGAAGACTGTGGATGG	AAGCAGGGATGATGTTCTGG	106
GBP1	AAGCAGATCGAAGTGGAACG	ATTTGCATCTCCTCCAGCAT	97
GBP2	GCTGAGCAAGAGAGGGTTCTT	CCTTCTTGAATCCCTGTTCG	98
GZMB	CCAGGACCAGGATAATCGAA	GGGTGACGTTGATTGAGCTT	113
HERC5	TGAAGACGACGACTTTGGAA	TGACGTCACTTCCATGAGGA	100
HMGB1	CAAGGCCCGTTATGAAAGAG	ATCTGCAGCGGTGTTATTCC	105
IFI44	ATTGCTCACTCACGTGGACA	GCTTGAGTTTCACAGGCACA	107
IFIH1 (MDA5)	TCGGATTTTGGAACTCAACC	TCTTTGCGATTTCCGTCTCT	98
IFIT1	GGCCATTTTGTCTGAATGCT	TCAGGGCAAAGAGAGCCTTA	98
IFIT3	GAACAGCCCTTCAGGCATAG	TCCATTTCCTCAGTGCCTTC	93
IFITM3	ACCACGGTGATCAACATCCG	AGCACCAGTTCATGAAGAGGG	105
IFNA1	TACTCAGCTGCAATGCCATC	CTCCTCATTTGTGCCAGGAG	107
IFNB1	AGCACTGGCTGGAATGAAAC	TCCAGGATTGTCTCCAGGTC	102
IFNG	CCATTCAAAGGAGCATGGAT	TTCAGTTTCCCAGAGCTACCA	108
IFNL1 (IL29)	ATGGGCCAGTTCCAATCTC	CTGCAGCTCCAGTTCTTCAGT	108
IL10	TACAACAGGGGCTTGCTCTT	GCCAGGAAGATCAGGCAATA	104
IL12B	GACCAGAAAGAGCCCAAAAAC	AGGTGAAACGTCCGGAGTAA	110
IL15	CGTCATTTTGCAAGAGTCCA	TGGACGATAAACTGCTGTTTGC	102
IL17A	AATCAGGGAGTTCCCCTCTC	GTCCCGGGTGATGTTGTAAT	115
IL18	CAATTGCATCAGCTTTGTGG	TCCAGGTCCTCATCGTTTTC	96
IL1A	TGTGCTAAATAACCTGGATGAGG	GGTTCGTCTTCGTTTTGAGC	100
IL1B	TCTCTCACCCCTTCTCCTCA	GACCCTAGTGTGCCATGGTT	98
IL1RN	TGCCTGTCCTGTGTCAAGTC	GTCCTGCTCGCTGTTCTTTC	101
IL6	CCTCTCCGGACAAAACTGAA	TCTGCCAGTACCTCCTTGCT	101
IRF1	TGAAGCTGCAACAGATGAGG	CTTCCCATCCACGTTTGTCT	102

IRF3	GCTACACCCTCTGGTTCTGC	GAGACACATGGGGACAACCT	98
IRF7	GTGTGCTCCTGTACGGGTCT	CTGCAGCAGCTTCTCTGTGT	103
IRF9	CATTCAGACTTGGGGAGCAG	AAAGGGGCCTCAGTGGTAAC	111
ISG15	AGTTCTGGCTGACTTTCGAGG	GGTGCACATAGGCTTGAGGT	106
ISG20	AGATCCTGCAGCTCCTGAAA	TGCTCATGTTCTCCTTCAGC	103
KPNA2	GTTGTGAAGACAGGGGTCGT	TGAACTGCCGATTGTGACTC	97
KPNB1	GAGCTAAGGGAAGGCTGCTT	ATCACATCCGGGTGTACGTT	107
MAVS	ATCTCGCTGACGAAGTGTCC	GCCTCAGCAGGAGTAGATGG	106
MUC12	CGCAGCCAGGAATACAATTT	AGATTCTGGCCTTCCCAGAT	143
MUC15	CCCCCAAGAAGAGAACAGAA	GGAAGCACCCAGAATAGCAC	94
MUC19	CAAGGACAACTCTGCCAACA	GGGGAATATCTGCCAGTTGA	97
MUC20	CCCCTACCACTGTTCCAAGA	CTTCTGGGGAGACCACACTC	106
MUC4	CCGGAACAGACAAGTGGAAC	GGAACTCCGAGATGACTTTCC	102
MUC5AC	CCCAGATCTGCAGCACCTAC	GTAACACAGGCCACCTGCTT	104
MUC5B	GGACAACTGCACGGAGTACC	CCTTTTTCCGGAGGATGC	96
MX1	CCATCATTAAGAAGCAGGTCAGTG	AACATCTGTGAAGGCGAGCC	104
MX2	ACCAAGGGCCTGAATATGCT	ACGGGCTGTACAGGTTGTTC	109
MYD88	CCAGACTAAGTTTGCACTCAGC	AGGATGCTGGGGAACTCTTT	100
NFKB1	CCCTGTGAAGACCACCTCTC	ATCCCGGAGCTCGTCTATTT	109
OAS1	AAGAAACCCAGGCCTGTGATTC	TAGTGCCCCTTCTACCAGCT	109
OASL	TGCGACTGGTAAAACACTGG	CCCAGGCATAGATGGTCAGT	101
PPIA (Reference)	CAAGACTGAGTGGTTGGATGG	TGTCCACAGTCAGCAATGGT	105
PRPF8	TCCTTCCCAAGAATGTGCTC	ACAGGTACCCTGCAATTTGG	104
PTGS2	GAACTTACAGGAGAGAAGGAAATGG	TTTCTACCAGAAGGGCAGGA	103
S100A7	ACGACAGTGACACCATGGAC	TGTCACAGGCACTGAGGAAG	104
SELL	CCAAGAGAGCCCTCTGTTACAC	CCCGTAGTACCCTGCATCAC	104
SLA1	GGGTCCCCACTCCCTAAG	ACGTAGCCGACTTCGATGA	111
SLA2	CGCCTCGACACAGAATCTC	AGCAGAATGAGGATGGCTTG	96
STAT1	CCTTGCAGAATAGAGAACATGATAC	CCTTTCTCTTGTTGTCAAGCATT	101
SAA2	TGGAGAGCCTACTCGGACAT	CCTTTGGGCAGCATCATAGT	104
TAP1	CCAGCAATGGAGGAAGTCAT	CCTCTGTGTCGTAGCCTTGC	104
TGFB1	GCAAGGTCCTGGCTCTGTA	TAGTACACGATGGGCAGTGG	98
TLR3	ATTGTGCAAAAGATTCAAGGTG	TCTTCGCAAACAGAGTGCAT	106
TLR7	GGAAATAGCATCAGCCAAGCTC	TTCCAGGTTGCGTAGCTCTT	107
TLR8	GCAAAGACCACCACCAACTT	ATCCGTCAGTCTGGGAATTG	111
TMPRSS2	ATGGGCTACCGGAATAGCTT	TGTTGGCACTTTTGTTCAGC	118
TNF	CCCCCAGAAGGAAGAGTTTC	CGGGCTTATCTGAGGTTTGA	104
TNFAIP3	CCCAGCTTTCTCTCATGGAC	TTGGTTCTTCTGCCGTCTCT	104
USP18	CAATGACTCCAATGTCTGTTGG	AGCGGAAGCTGTGATTTCC	101
XPO1	CCCTCATCTACAAGATGCTCAAG	CCTCAGATGTTCCTTGAATGC	106
YWHAZ (Reference)	GCTGCTGGTGATGATAAGAAGG	AGTTAAGGGCCAGACCCAAT	103

Supplementary Figures

	1	2	3
huH1N1 NS (+1)	1	93.29	86.22
swH1N1 NS (+1)	2	93.29	89.40
mxH1N1 NS (+1)	3	86.22	89.40

Supplementary Figure 1: A pairwise comparison of the NS sequences of the three IAV strains included in the study.
High similarity between the huH1N1pdm09 and swH1N1pdm09 isolates (93.3%) compared to the mxH1N1pdm09 isolate (86.2% and 89.4%, respectively). The pairwise comparison was performed using CLC Main Workbench version 22.0.2 (QIAGEN, Hilden, Germany).

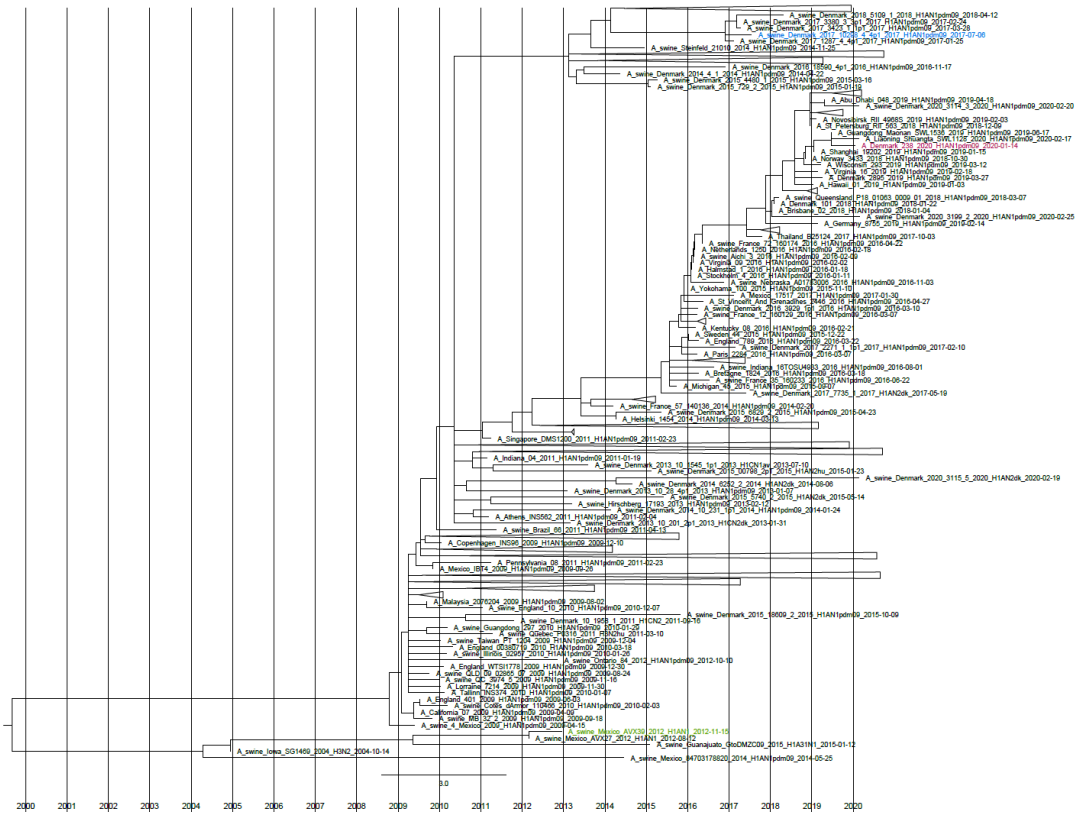

Supplementary Figure 2: Time-scaled phylogenetic tree estimated from segment 8 (NS) nucleotide sequences of inoculum strains and genetic relatives. Inoculum strains are indicated by colour, blue: A/swine/Denmark/2017_10298_4_4p1/2017 (swH1N1pdm09), light red: A/Denmark/238/2020 (huH1N1pdm09) and Green: A/swine/Mexico/AVX-39/2012 (mxH1N1pdm09). Clades are classified based on host species and collapsed clades displayed as triangles contain other descendants from A(H1N1)pdm09. Rooting was determined as best root-to-tip regression.

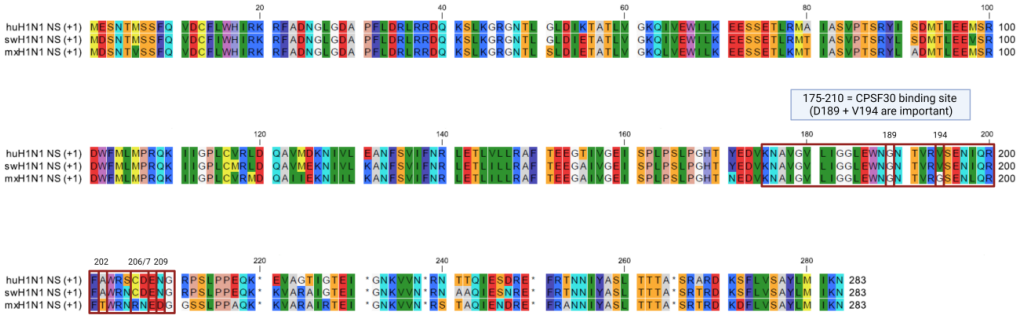

Supplementary Figure 3: Sequence alignment of the amino acid sequences of the NS segment of the three IAV strains included in the study. Important amino acid locations are marked with a red square. The alignment was performed using CLC Main Workbench Version 22.0.2 (QIAGEN, Hilden, Germany). Nucleotide sequences were translated into proteins prior to sequence alignment.

Supplementary Text

Text S1: Pairwise comparison

A pairwise comparison was performed on the NS sequences using CLC Main Workbench version 22.0.2 (QIAGEN, Hilden, Germany) to measure the percentage identity. NS sequences from inoculum strains was obtained from a full-genome sequencing performed prior to this study by Kristensen and colleges ("Unpublished data", Kristensen C, Glud HA, Crumpton JC, Martiny K, Webb A, Ryt-Hansen P, et al.).

Text S2: Phylogenetic analysis

Time-resolved phylogenetic tree based on nucleotide sequences of segment 8 (NS) coding region was estimated by TreeTime using a strict molecular clock inferred with general time reversible (GTR) substitution model[1]. Input alignment contained three inoculum strains and their closest genetic relatives identified by BLAST programs in GISAID EpiFlu™ Database and NCBI nucleotide databases. Input tree was reconstructed with IQ-TREE using substitution and rate heterogeneity models GTR+G2 with bootstrap replicates set to 1000 and maximum number of iterations stopping at 2500[2]. Trees were formatted using FigTree v1.4.4 (The University of Edinburgh, Scotland) and time scale was offset by time of oldest node with scale factor 0.99.

Text S3: Primer design

All porcine primers used in this study were designed using Primer3 (v. 0.4.0) (https://bioinfo.ut.ee/primer3-0.4.0/) and purchased from Merck Life Science A/S, Soeborg, Denmark. Sequences used for primer design were obtained from public databases (Ensembl (http://www.ensembl.org/index.html) or NCBI (https://www.ncbi.nlm.nih.gov/)). In Primer3, product

size range was set to 70-100 nucleotides, primer melting temperature was set to minimum 59°C, optimal 60°C, and maximum 61°C. The thermodynamic parameters were based on Breslauer et al., 1986[3]. Primers were designed to overlap an intron, if possible, otherwise primer pairs were designed on each side of an exon junction. BLAST searches (https://blast.ncbi.nlm.nih.gov/Blast.cgi) were performed to ensure primer specificity.

Text S4: Description of statistical analysis

We have used Bayesian methods to analyze the gene expression data. The main idea in Bayesian statistical modeling is to use probabilities to quantify uncertainty, and the outcome of a Bayesian statistical analysis is a so-called joint posterior probability distribution over possible parameter values, which summarizes all information that we can infer about the model given the observed data and our prior knowledge[4]. Parameter values with higher posterior probabilities are those that are more likely to be the true values. The posterior distribution can be used to investigate many different hypotheses. For instance, one can compute the probability that a parameter has a value above or below some threshold value, or the probability that it lies in a given interval. It is also possible to compare parameters, and compute for instance the probability that parameter 1 is larger than parameter 2. These probabilities quantify our degree of belief in the investigated hypotheses (an example of a model parameter in this paper could for instance be the average expression level for some gene on a given day after inoculation with IAV). A high degree of certainty about a parameter value corresponds to a narrow posterior distribution, while a wide posterior means we are less certain of the value. We can also compute various summaries of the posterior distribution, such as the posterior mean or a credible interval (credible intervals are regions that have some specified probability of containing the true parameter value and can be thought of as Bayesian confidence intervals). To compute a posterior distribution over possible

parameter values, we first need to specify a prior probability distribution, which expresses what we know about possible parameter values before analyzing the data set. The prior can be based on the posterior from a previous analysis, or it can be more weakly informative and essentially work to regularize the parameter estimation to avoid outlying data points having too much influence on the parameter estimate.

Most often, the posterior distribution is determined using an approximate method called Markov chain Monte Carlo (MCMC) sampling[5]. The result of MCMC is a file with typically hundreds or thousands of lines that each contain one sample from the posterior for all the model parameters. The empirical distribution of one parameter (one column) from this file is an estimate of the parameter's posterior distribution, and it is from these samples that various summaries can be computed (e.g., posterior mean or 90% credible interval). Based on MCMC samples it is also very simple to investigate statistical hypotheses about derived measures: one can simply compute the derived parameter for each line in the sample file, and the resulting set of values then constitute a posterior distribution for that derived parameter (In this paper we for instance use this approach to determine the posterior distribution for the log fold change for gene expression relative to baseline).

Text S5: Exploration of alternative models

Before settling on the model described above, we explored a number of other models. As expected we found that log-transforming data improved model fit significantly, compared to fitting a normal or t-distribution directly to the raw expression data.

We also found that individual pigs do not appear to have a consistently higher or lower values, and that using hierarchical models (with measurements nested inside pigs) did not improve model fit. This was

also apparent by inspecting plots of the original data where the levels for individual pigs often cross each other over the 7 days.

We use the same sigma and nu parameters for all 22 estimated means for a given gene (1 baseline value + 7 measurement days x 3 treatments). This was found to give better fits than when we estimated individual sigma and nu parameters for each mean, and was also expected for theoretical reasons after log transformation: before log transformation the mean and standard deviation for a given gene were found to be roughly proportional, and under those circumstances log transformation is expected to stabilize the variance to be approximately constant[6].

We also experimented with various time-series models for the purpose of regularizing variation across days (for instance: if many days in a row have a log fold change = 0, then we may be less convinced by a single day that has a slightly higher value than 0). The best-fitting time-series model was a simple model with local linear trend, but the fit was quite similar to the chosen model and parameter estimates were also very close, and we therefore chose to use the simpler model described in the paper.

References

1. Sagulenko P, Puller V, Neher RA. TreeTime: Maximum-likelihood phylodynamic analysis. *Virus Evol*. 2018;4(1):vex042. doi:10.1093/ve/vex042
2. Nguyen LT, Schmidt HA, Von Haeseler A, Minh BQ. IQ-TREE: A Fast and Effective Stochastic Algorithm for Estimating Maximum-Likelihood Phylogenies. *Mol Biol Evol*. 2015;32(1):268-274. doi:10.1093/molbev/msu300
3. Breslauer KJ, Frank R, Blocker H, Marky LA. Predicting DNA duplex stability from the base sequence. *Proc Natl Acad Sci U S A*. 1986;83:3746-3750. doi:10.1073/pnas.83.11.3746
4. Gelman A, Carlin JB, Stern HS, Dunson DB, Vehtari A, Rubin DB. *Bayesian Data Analysis*. 3rd ed. Chapman and Hall/CRC; 2013.
5. Gelfand AE, Smith AFM. Sampling-based approaches to calculating marginal densities. *J Am Stat Assoc*. 1990;85(410):398-409. doi:10.1080/01621459.1990.10476213
6. Bartlett MS. The Use of Transformations. *Biometrics*. 1947;3(1):39. doi:10.2307/3001536

4.4 Paper 4

Analysis of Influenza A Virus-Induced Transcriptional Changes and Modulation of Host Metabolism in Pig Tracheal Tissue

Helena Aagaard Glud, Betina Lyngfeldt Henriksen, Charlotte Kristensen, Yaolei Zhang, Louise Brogaard, Chrysillis Hellemann Polhaus, Ramona Trebbien, Lars Erik Larsen, and Kerstin Skovgaard

Corresponding Author: Helena Aagaard Glud, haaglu@dtu.dk

Manuscript in preparation

Analysis of Influenza A Virus-Induced Transcriptional Changes and Modulation of Host Metabolism in Pig Tracheal Tissue

H. A. Glud[1], B. L. Henriksen[1], C. Kristensen[2], Y. Zhang[3], L. Brogaard[1], C. H. Polhaus[1], R. Trebbien[4], L. E. Larsen[3], K. Skovgaard[1]

[1]Department of Biotechnology and Biomedicine, Technical University of Denmark, Kongens Lyngby, Denmark

[2]Department of Veterinary and Animal Sciences, University of Copenhagen, Copenhagen, Denmark

[3]Qingdao Key Laboratory of Marine Genomics, BGI-Qingdao, Qingdao, China

[4]Department of Virus and Microbiological Special Diagnostics, Statens Serum Institut, Copenhagen S, Denmark

Corresponding author: Helena Aagaard Glud, haaglu@dtu.dk

Abstract

Influenza A virus (IAV) is a global respiratory disease, which each year leads to approximately 3-5 million cases of severe illness, resulting in about 290,000-650,000 deaths. Furthermore, four devastating global IAV pandemics have occurred in the past 100 years. IAV infections have been studied for years, but little is known regarding the local host immune response in tracheal tissue after infection. In this study, pigs were experimentally inoculated with swine- or human-adapted IAV (H1N1) to conduct an in-depth transcriptional analysis of the host response in tracheal tissue. Tracheal tissue samples were investigated by RNA sequencing, and results were validated by microfluidic high-throughput qPCR. Additionally, a histopathological examination of selected samples was conducted to evaluate immune cell infiltration and IAV infection. A classical innate antiviral immune response was induced after infection with both swine- and human-adapted IAV, including upregulation of genes related to viral infections and recognition, where especially interferon stimulated genes were induced. A more significant number of highly regulated immune genes was observed after infection with the swine-adapted compared to the human-adapted IAV strain. Furthermore, several genes involved in nucleotide host metabolism, the pyrimidine metabolism, were found to be regulated in pigs infected with the swine-adapted IAV strain compared to the human-adapted IAV strain. Thus, it could be speculated that with adaptation, IAV develops the ability to regulate host nucleotide metabolism to improve viral replication.

Key words: Influenza A virus, RNA-seq, immune regulation, host metabolism, host adaptation

Introduction

Influenza A virus (IAV) is a zoonotic virus which can infect a wide range of avian and mammalian species[1–4]. IAV causes respiratory illness worldwide with annual seasonal epidemics and even global pandemics, of which four have occurred over the past 100 years[5,6]. Annual epidemics are estimated to result in 3-5 million cases of severe illness and 290,000-650,000 deaths each year[7]. IAV pandemics have emerged due to zoonotic transmission of IAV with avian and swine origin and subsequent reassortment events[8,9]. New IAV strains with pandemic potential will continue to emerge through mutation and genetic reassortment. In order to estimate if a new strain has zoonotic potential, we need more knowledge of how the host immune response reacts to both host-adapted IAV strains and non-adapted IAV strains (i.e. adapted to a different host than that being infected).

During IAV infection, the antiviral innate immune response is activated through pattern-recognition receptors (PRRs), such as Toll-like receptors (TLRs) and retinoic acid-inducible gene I-like receptors (RLRs). Upon recognition by PRRs, production of interferons (IFNs), pro-inflammatory cytokines, and chemokines is initiated. Type I and III IFNs stimulate the production of interferon stimulated genes (ISGs), which interfere with and restrict viral replication, while cytokines and chemokines recruit and activate immune cells[10,11,12]. The immune response in tracheal tissue after IAV infection has not been studied widely. Most studies have focused on T cell (CD8+ and γδ T cells) infiltration of tracheal tissue after IAV infection in small animal models[13–15], including their production of IFN-γ and IL-17A[14]. Chemokines involved in recruiting T cells (CXCL9/10 and CXCL12)[14,15] and promoting IL-17A expression (IL-23, IL-1β, and IL-6) were observed to be upregulated in tracheal lavage after infection in mice[14]. Ciliary activity has been investigated *ex vivo* by tracheal explants isolated from mice and *in vivo* in mice showing either increased[16] or decreased activity[17] after viral infection, respectively. Innate immune responses to avian IAV in chicken tracheal tissue have shown to trigger IFN-mediated responses, mainly related to type I[18]. This response was also found in *ex vivo* tracheal explants from chickens, but most of

62 the antiviral response got masked by the response to the tissue damage introduced during excision[18].
63 Additionally, the tracheal antiviral response has been shown to differ in kinetics and magnitude in
64 regard to age, with a shortened and dampened response in younger chickens[19]. Given the low
65 translational value for human biomedical research of the animal models previously employed for the
66 study of the tracheal host response to IAV infection, it would be pertinent to conduct such investigations
67 in the highly relevant pig animal model, given its advantages in this context[20].

68 IAV needs to replicate efficiently in the host cell to produce new progeny virus and spread to a new
69 susceptible host, but viruses do not have their own metabolism, so they have to rely on the host for all
70 necessary components for viral propagation[21,22]. Several viruses, such as adenovirus, human
71 cytomegalovirus, herpesvirus-1, dengue virus, zika virus, vaccinia virus, hepatitis C virus, poliovirus and
72 IAV, have been described to alter host cell metabolism upon infection, including glycolysis, nucleotide
73 synthesis, and lipid synthesis[21,22]. Glycolysis provides ATP and biosynthetic intermediates needed to
74 drive cellular metabolisms, including nucleotide and lipid synthesis[23]. Thus, during viral infection there is
75 a strong demand for glucose to drive cellular metabolic pathways to produce biomolecules and energy
76 essential for viral replication. Indeed, higher glucose uptake has been demonstrated by MDCK[24] and
77 NHBE[25] cells after IAV infection and in pediatric cancer patient lungs (tumor-free lungs) after IAV
78 infection[25]. Furthermore, increased IAV infection (viral protein accumulation and number of infected
79 cells) is correlated with higher glucose concentration in MDCK cells[26]. Nucleotides, including pyrimidines
80 (cytosine, thymine, and uracil) and purines (adenine and guanine), can be synthesised by two routes.
81 One is the salvage pathway, where preformed pyrimidine/purine nucleosides and nucleobases are
82 recycled to form pyrimidines/purines, which is the primary supply of nucleotides in resting or fully
83 differentiated cells. Producing nucleotides via this pathway requires less energy consumption than
84 producing the nucleotides from scratch by *de novo* synthesis[27,28], which is the other possible pathway for
85 nucleotide synthesis. However, some virus-infected cells (human cytomegalovirus and SARS-CoV-2)

promote *de novo* synthesis of pyrimidine nucleotides due to high requirements of nucleotides during virus replication[29,30]. In addition to nucleotides, host lipids are involved in viral replication as IAV acquires a host-derived lipid envelope during budding. Indeed, IAV alters the host cell lipid composition during infection of human lung epithelial cells and mice[31]. Thus, IAV seems to be able to alter host metabolism to optimise the environment in the infected cells for its own benefit. However, the antiviral innate immune response and host genes involved in a pro-viral host cell metabolism after IAV infection have, to our knowledge, not been studied previously in tracheal tissue.

In this study, an in-depth analysis of the swine tracheal transcriptional response to a swine- and human-adapted IAV was studied 3 days after experimental inoculation of pigs. Transcriptional response to the infection in tracheal tissue samples was investigated by RNA sequencing (RNA-seq), and results were validated by microfluidic high-throughput qPCR. To estimate immune cell infiltration and IAV infection, histopathological examination of selected samples was conducted.

Materials and methods

Experimental design

In this study, 22 seven-weeks-old Danish Landrace Crossbred pigs confirmed IAV negative and seronegative were included. The pigs were allocated into three groups and housed in separate isolation units. They were acclimatised for one week, fed non-pelleted feed (NAG Svinefoder 5), and had *ad libitum* access to water. Group 1 (control) consisted of 6 pigs, and groups 2 and 3 each included 8 pigs. The pigs were sedated before inoculation, group 1 was mock inoculated intranasally by a MAD nasal device (Nasal Intranasal Mucosal Atomization Device, Teleflex, Pennsylvania, USA, cat. no. MAD100) containing culture medium only, while group 2 and 3 were inoculated with 3 ml of 10^7 $TCID_{50}$/ml of a

swine-adapted strain, A/Swine/Denmark/3974/2017 (H1N1) (swH1N1pdm09), and a human-adapted strain, A/Denmark/238/2020 (H1N1) (huH1N1pdm09) ("Unpublished data", Kristensen C, Glud HA, Crumpton JC, Martiny K, Webb A, Ryt-Hansen P, et al.), respectively. Euthanisation was performed 3 days post inoculation, and tracheal tissue was collected and stored in RNA*later* (Thermo Fisher Scientific, Waltham, Massachusetts) at -20°C until RNA extraction.

The animal experiment was performed under biosafety level 2 conditions and under an animal study protocol approved by The Danish Animal Experimentation Council (protocol no. 2020-15-0201-00502).

RNA extraction

Trachea samples were homogenised in QIAzol Lysis reagent (QIAGEN, Hilden, Germany) using gentleMACS Mtubes (Miltenyi Biotec, Bergisch Gladbach, Germany). Total RNA was extracted using the miRNeasy mini kit (QIAGEN, Hilden, Germany) and treated with an RNase-free DNase set (QIAGEN, Hilden, Germany) according to the manufacturer's instructions. RNA quantity and purity were estimated using the Nanodrop ND-1000 spectrophotometer (Thermo Fisher Scientific, Waltham, Massachusetts) and the RNA integrity number was assessed by the Agilent RNA 6000 Nano Kit on the Bioanalyzer 2100 system (Agilent Technologies, Santa Clara, California).

RNA sequencing libraries were constructed with a non-stranded and PolyA selection method according to the manufacturer's specifications (BGI Genomics, Shenzhen, China). Paired-end reads with a length of 100 bp were sequenced using the DNBSEQ platform. The raw reads were filtered, which included adaptor removal, removal of contamination and low-quality reads.

RNA-seq data analysis

Clean reads were mapped to the pig genome (Sscrofa11.1, NCBI accession: GCA_000003025.6) using HISAT2[32]. RSEM[33] was used to annotate transcripts to prepare a transcript reference for subsequent

calculation of gene expression levels. The clean reads were mapped to this reference to quantify the gene expression using Bowtie2[34]. RSEM[33] was used to estimate the gene expression levels based on fragments per kilobase of exon per million fragments mapped (FPKM) for subsequent analysis of the differentially expressed genes (DEGs). DEGs were identified between different comparison groups by DESeq2[35]. The p-values of the DEGs were corrected for multiple testing using Benjamini-Hochberg false discovery rate (FDR)[36]. Finally, DEGs were defined with an expression fold change ±2 (log2 fold change ±1) and FDR (q-value) < 0.05. DEGs were functionally enriched by alignment to the Kyoto Encyclopedia of Genes and Genome (KEGG)[37] databases using enrichKEGG[38,39] with an FDR (q-value) cutoff of 0.05.

Validation of RNA-seq data

A subset of 93 genes (including six potential reference genes for data normalisation) with annotations from a statistical analysis of the RNA-seq was selected for validation using high-throughput quantitative reverse transcription polymerase chain reaction (RT-qPCR). Primers for the selected genes are shown in Supplementary Table 1. Primer design and subsequent cDNA and pre-amplification synthesis were performed as described before ("Unpublished data", Glud HA, Pedersen AG, Brogaard B, Polhaus CH, Kristensen C, Trebbien R, et al.). High-throughput qPCR was carried out using 96.96 Dynamic Array IFC chips (Standard BioTools Inc., South San Francisco, California) on the BioMark real-time platform using a previously described PCR protocol ("Unpublished data", Glud HA, Pedersen AG, Brogaard B, Polhaus CH, Kristensen C, Trebbien R, et al.).

Histopathology and IAV staining

Histological evaluations were performed on three pigs from the control group and two pigs from each inoculated group. Swine tracheal tissues for histopathology were fixed in 10% neutral-buffered formalin for a week. Formalin-fixed tissue was embedded in paraffin wax and sliced into 2–3 µm sections. Sections were stained with hematoxylin and eosin (H&E). Immunohistochemical staining targeting IAV

was performed by deparaffinizing formalin-fixed section before wash with TBS (pH 7.6) twice for 5 minutes. The washing step was performed after each step described below. Blocking for endogenous peroxidase was performed by adding 3% H_2O_2 to the sections for 10 minutes. Antigen retrieval was performed by adding 0.018 gram proteinase (Merck Life Science A/S, Soeborg, Denmark) in 100 ml TBS to the sections for 5 minutes. Sections were additionally blocked with Ultra V block (AH diagnostics, Tilst, Denmark) and anti-influenza A (NP) antibody (diluted 1:100,000 in 1% BSA/TBS) (HYB 340-05, SSI-antibodies, Copenhagen S, Denmark) and stored overnight at 4°C. UltraVision ONE HRP-Polymer (TL-125-HLJ, AH diagnostics, Tilst, Denmark) was added for 30 minutes, and the staining was visualised by adding DAB substrate (Cell Marque, Rocklin, California) for 10 minutes. The sections were counterstained by Mayer's hematoxylin (VWR, Radnor, Pennsylvania). An isotype control (X0931, Agilent Technologies, Santa Clara, California) (diluted in 1% BSA/TBS to the same protein concentration as the anti-influenza A (NP) antibody) was used as a negative control.

Quantification of IAV by real-time RT-qPCR

The PCR assay used to detect IAV was an in-house modified version of an RT-qPCR assay targeting the matrix gene (M-gene) using the SensiFast Probe No-ROX One-Step Mix kit (Meridian Bioscience, Cincinnati, Ohio) as described before ("Unpublished data", Kristensen C, Glud HA, Crumpton JC, Martiny K, Webb A, Ryt-Hansen P, et al.). Quantification was based on a 10-fold dilution series of the target sequence with known copy numbers.

Results

Sequencing data description

From the 22 samples, approximately 2000 million clean paired-end reads with a length of 100 bp were generated. On average, 88.85 million (72.95-94.55 million) clean reads were obtained for each sample. Among the samples, 94.8-97.0% of the clean reads were mapped to the reference genome (Sscrofa11.1, NCBI accession: GCA_000003025.6). Moreover, 90.6-93.7% of the clean reads were uniquely mapped (Supplementary Table 2).

Infection with the swH1N1pdm09 strain induces a strong tracheal antiviral immune response

Comparing the swH1N1pdm09 group with the control group, 244 differentially expressed genes (DEGs) were identified using RNA-seq. Approximately 8 times as many DEGs were upregulated than downregulated (216 upregulated and 28 downregulated). Data from all DEGs are summarised in Supplementary Table 3.

Hierarchical clustering (using Pearson Correlation Coefficient) of gene expression is shown in a heatmap in Figure 1 for the top 20 significantly upregulated and downregulated genes. Two major groups were identified, one including all the control pigs and two pigs from the infected group (Pig 9 and 10), while the second cluster included the remaining infected pigs. ISGs were highly expressed in the cluster including infected pigs only (*IFI6, OASL, MX2, XAF1, ISG15, OAS1, IFIT1, IFIT3, RSAD2* (Viperin), and *MX1*), as well as PRRs (*ZBP1, DHX58* (LGP2), and *DDX58* (RIG-I)). Of the top 20 upregulated genes, *IFI6* was the only ISG upregulated in the two infected pigs, which clustered together with the control pigs (Figure 1).

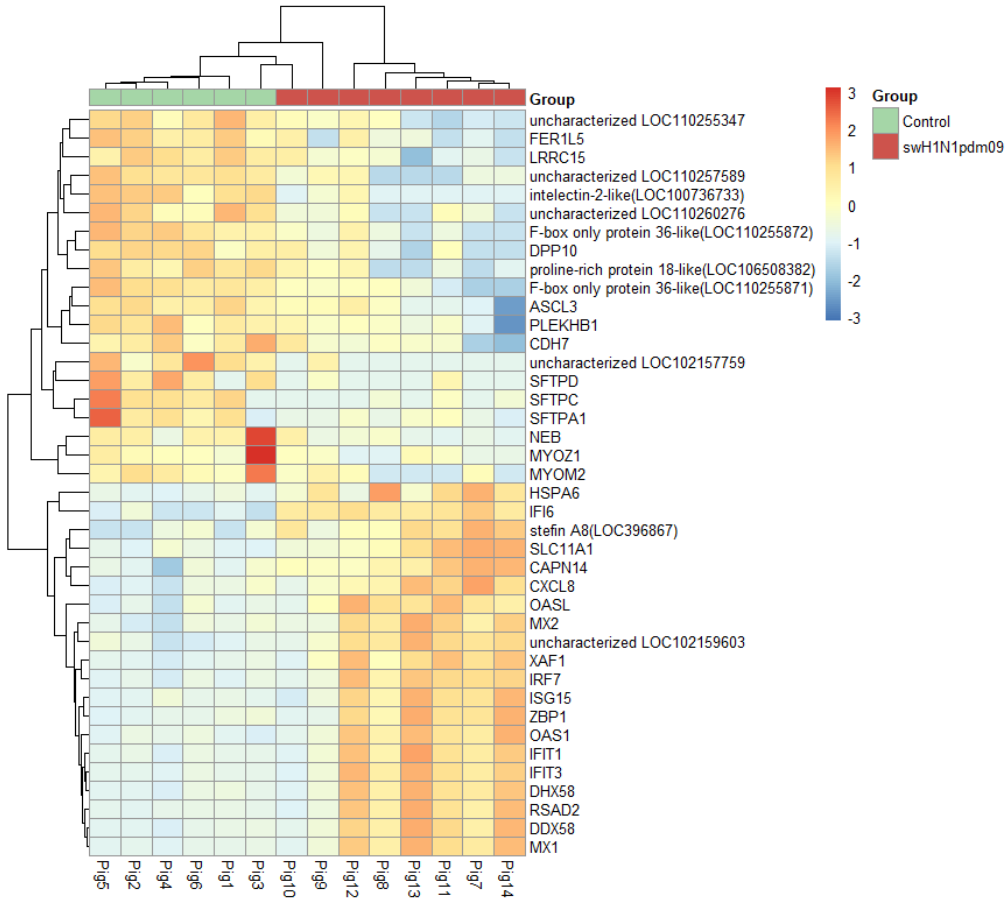

Figure 1: Interferon stimulated genes make up the majority of genes in the top 20 differentially expressed genes in the group inoculated with the swH1N1pdm09 strain compared to control pigs. Heatmap showing top 20 differentially expressed genes (up- and downregulated) comparing the control group (green) with the swH1N1pdm09 group (red). The color key from blue to red indicates low to high gene expression, respectively.

198 *IFI6* was the highest upregulated gene (fold change = 4.82), followed by *OASL* (fold change = 3.64), *IFIT3*
199 (fold change = 3.31), and *RSAD2* (Viperin) (fold change = 3.30) (Supplementary Table 3). The only gene in
200 the top 10 highest upregulated genes which was not an ISG or involved in their activation was *CAPN14*
201 (Calpain 14), a cysteine protease involved in, e.g. apoptosis. Genes encoding protein components of the
202 cytoskeleton (*NEB* (nebulin), *MYOM2* (myomesin 2), *MYOZ1* (myozenin 1), and *MYBPC1* (myosin binding
203 protein C1)) and surfactant proteins (A1, C, and D) were among the most downregulated genes (Figure 1
204 and Supplementary Table 3).

205 KEGG enrichment analysis was performed to identify the biological pathways associated with the DEGs.
206 Of the 244 DEGs, 121 were identified in 49 pathways. The top 10 significantly enriched pathways (based
207 on q-value) are highlighted in Figure 2. Most identified genes were involved in the cytokine-cytokine
208 receptor interaction and included important antiviral genes such as *TNF, IL1A, IL1B, IL6, IL19, CXCL8*, and
209 *CXCL10*. Pathways involved in response to RNA viruses, including SARS-CoV-2 and IAV, were highly
210 significantly enriched (q-value of 1.03×10^{-6} and 1.91×10^{-8}, respectively), and viral protein interaction
211 with cytokines and cytokine receptors were also included in the top 10 pathways (Figure 2).

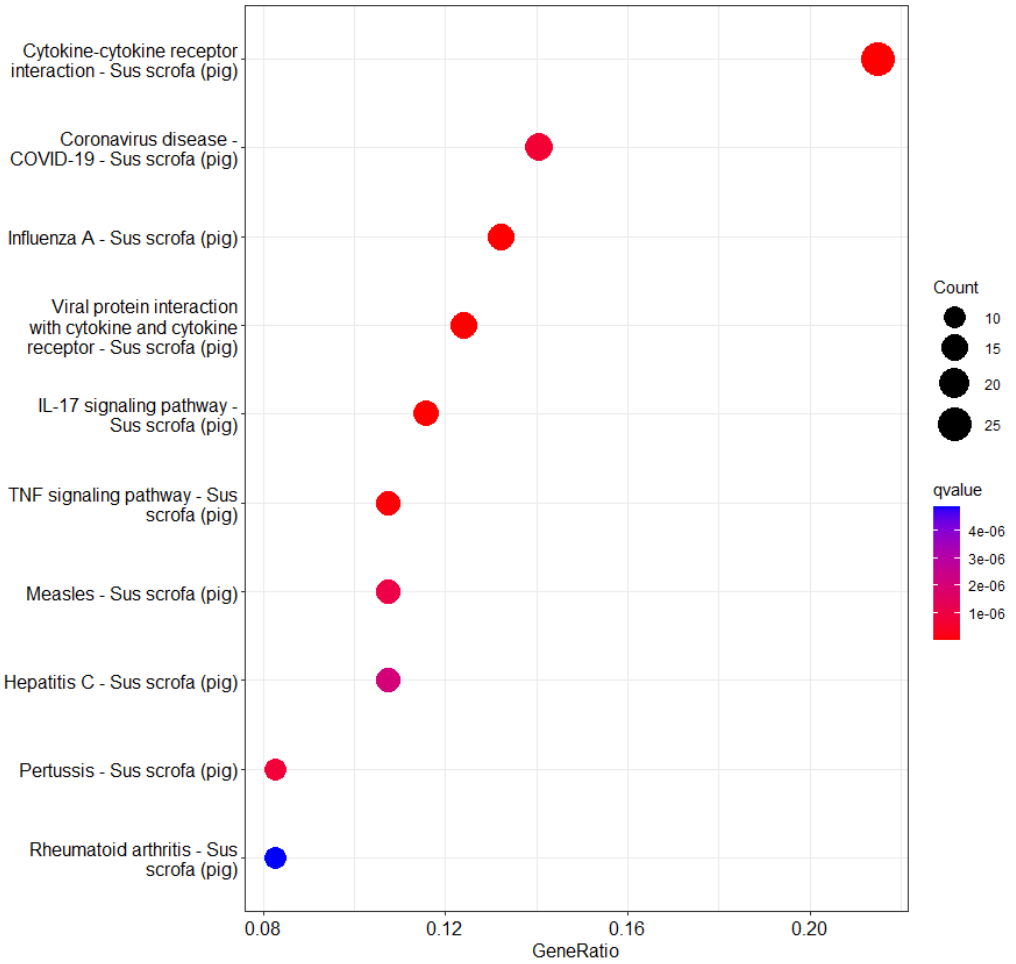

Figure 2: Upregulation of pathways involved in viral infections and antiviral immune responses in pigs infected with swH1N1pdm09. KEGG enrichment bubble diagram of DEGs in the swH1N1pdm09 relative to control indicates the ratio of enriched DEGs to the total number of identified genes in a certain pathway. Circles indicate the number of genes in the corresponding pathway, and color depicts the q-value.

Infection with a human-adapted strain (huH1N1pdm09) mainly affects the expression of interferon stimulated genes

In contrast to the swH1N1pdm09, only 28 differentially expressed genes were identified after infection with the human-adapted IAV (huH1N1pdm09) compared to the control group (17 upregulated and 11

222 downregulated). Hierarchical clustering (using Pearson Correlation Coefficient) of gene expression for all
223 DEGs is shown in Figure 3. Two major groups were identified, clustering the control pigs in one cluster
224 and the infected pigs in another cluster. ISGs were highly expressed in the cluster including the infected
225 pigs (*ISG15, IFI6, ISG12(A), BST2* (Tetherin)*, OAS1, RSAD2* (Viperin)*, IFIT1, MX2, MX1, IFI44, RTP4, XAF1*)
226 (Figure 3), of which *IFI6* was the highest upregulated gene (fold change = 5.58) (Supplementary Table 3).
227 Again, only one gene in the top 10 highest upregulated genes was not an ISG or involved in their
228 activation. In this case, the gene was part of the angiopoietin-like protein family, *ANGPTL4,* which is
229 involved in the regulation of glucose homeostasis and lipid metabolism.

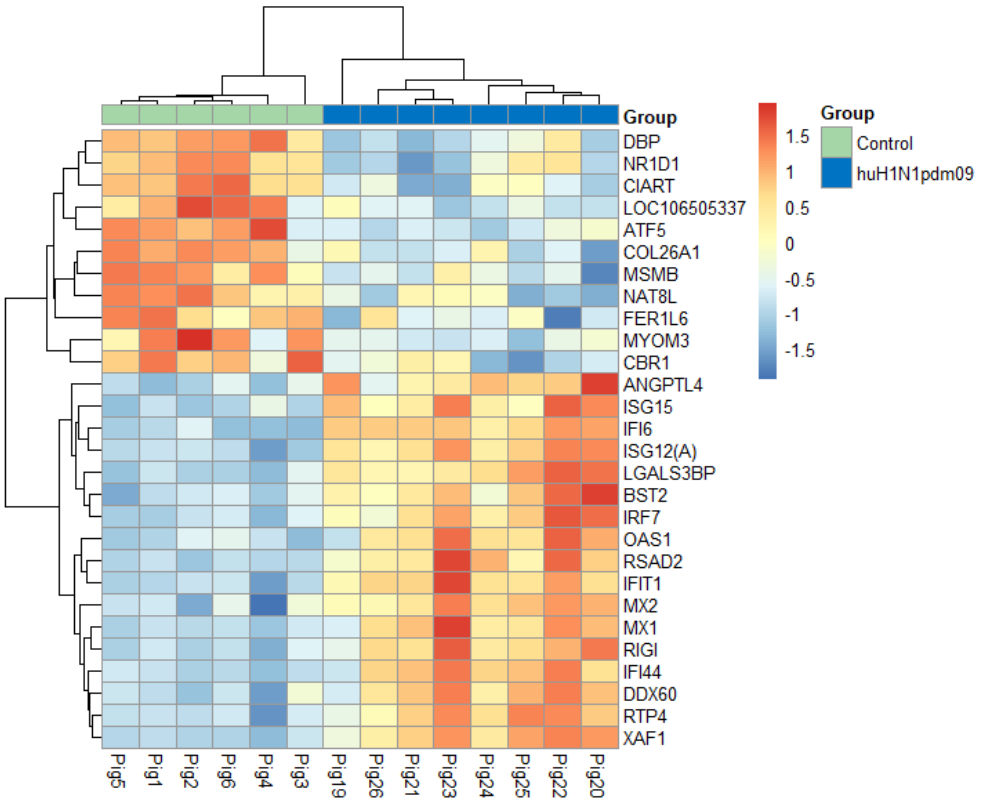

230

231 **Figure 3: Interferon stimulated genes were highly expressed in the group inoculated with the huH1N1pdm09 strain**
232 **compared to control pigs.** Heatmap showing all differentially expressed genes (up- and downregulated) comparing the control
233 group (green) with the huH1N1pdm09 group (blue). The color key from blue to red indicates low to high gene expression,
234 respectively.

235 A KEGG enrichment analysis was performed, and 14 of the 28 DEGs were identified to be significantly

236 enriched (q-value < 0.05) in 10 pathways (Figure 4). All pathways including upregulated genes were

237 related to the recognition and infection of RNA viruses and herpes simplex virus. Genes involved in

238 circadian rhythm were downregulated (*NR1D1* and *DBP*) (Supplementary Table 3).

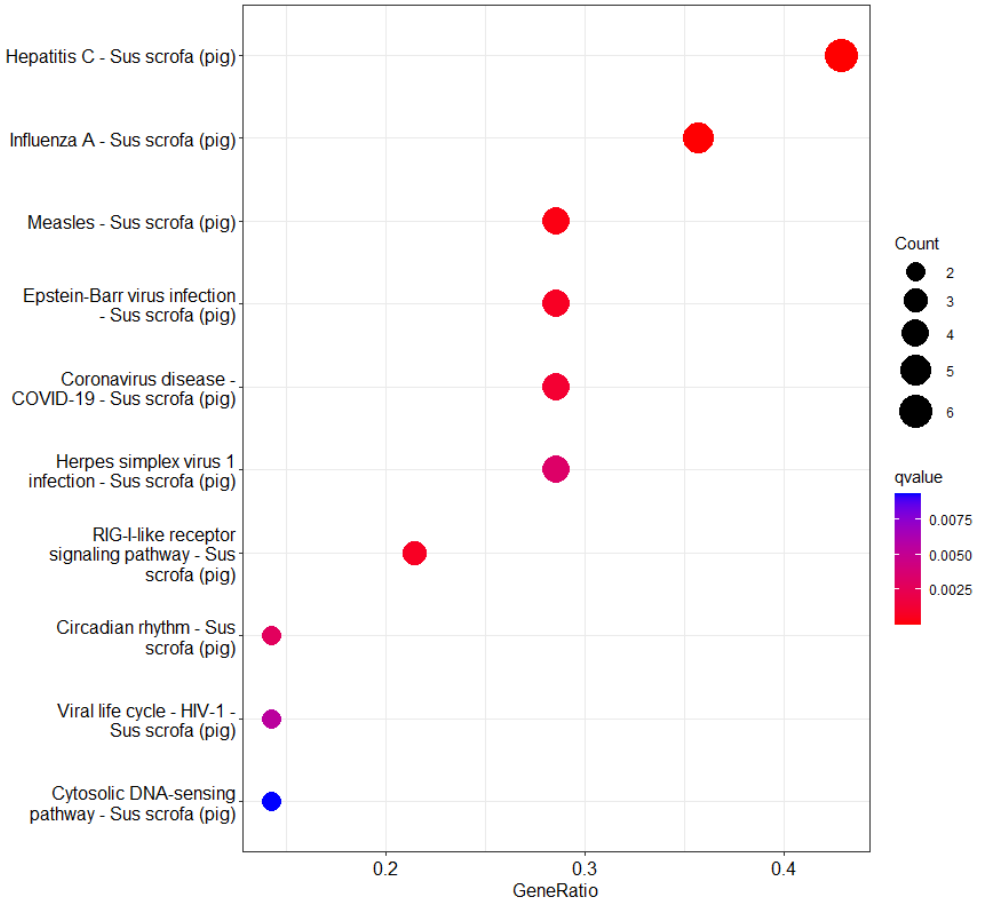

Figure 4: Upregulation of pathways involved in viral infections and recognition in pigs infected with huH1N1pdm09. KEGG enrichment bubble diagram of DEGs in the huH1N1pdm09 relative to control indicates the ratio of enriched DEGs to the total number of identified genes in a certain pathway. Circles indicate the number of genes in the corresponding pathway, and color depicts the q-value.

Host adaptation might involve regulation of genes associated with pyrimidine metabolism

A total of 255 genes were differentially expressed during swH1N1pdm09 infection, huH1N1pdm09 infection, or both. Of these, 17 DEGs were common for both infections (*DDX58* (RIG-I), *RSAD2* (Viperin), *MX2, MX1, OAS1, ANGPTL4, IRF7, ISG15, IFIT1, ISG12(A), DDX60, BST2, IFI44, XAF1, LGALS3BP, RTP4,* and *IFI6*), while 11 genes (one was uncharacterised) were only differentially expressed after infection with

the huH1N1pdm09 strain (*CBR1, CIART, NR1D1, FER1L6, COL26A1, NAT8L, MSMB, ATF5, DBP,* and *MYOM3*). The 17 shared DEGs were all upregulated in both infections, while the 11 genes regulated in the huH1N1pdm09 group only were all downregulated compared to control pigs. In contrast, many genes were uniquely differentially expressed in the swH1N1pdm09 group (Figure 5). This indication of highly distinct host responses in the two inoculated groups of pigs motivated further comparison between the two inoculated groups directly.

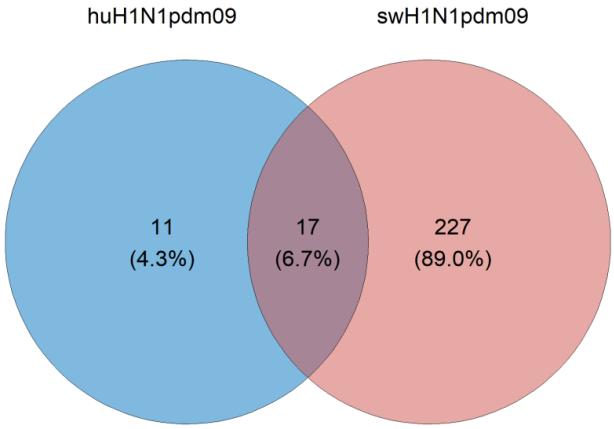

Figure 5: Venn Diagram comparing the differentially expressed genes in the two infected groups compared to the control group. In total, 17 genes are shared between the groups, while 11 genes were unique for the huH1N1pdm09 group and 227 genes were unique for the swH1N1pdm09 group.

When comparing the huH1N1pdm09 group to the swH1N1pdm09 group, 52 differentially expressed genes were identified (13 upregulated and 39 downregulated). Hierarchical clustering (using Pearson Correlation Coefficient) of gene expression for all DEGs between the two inoculated groups identified two major groupings. One group clustered six out of eight pigs infected with the swH1N1pdm09 strain, the other clustered all the pigs infected with the huH1N1pdm09 strain and two pigs from the swH1N1pdm09 group (Pig 9 and 10) (Figure 6), which are the same two pigs who clustered together

with the control group (Figure 1). Only one antiviral immune gene was expressed higher in the huH1N1pdm09 group, *CXCL9*, which is a chemoattractant for immune cells. In contrast, cytokines and chemokines (*IL19, IL20,* and *CXCL13*) and ISGs (*IFIT3* and *RSAD2*) were downregulated in the huH1N1pdm09 group compared to the swH1N1pdm09 group (Figure 6). Thus, the immune response seems to be less induced in the pigs infected with the human-adapted strain (huH1N1pdm09) compared to the swine-adapted strain (swH1N1pdm09).

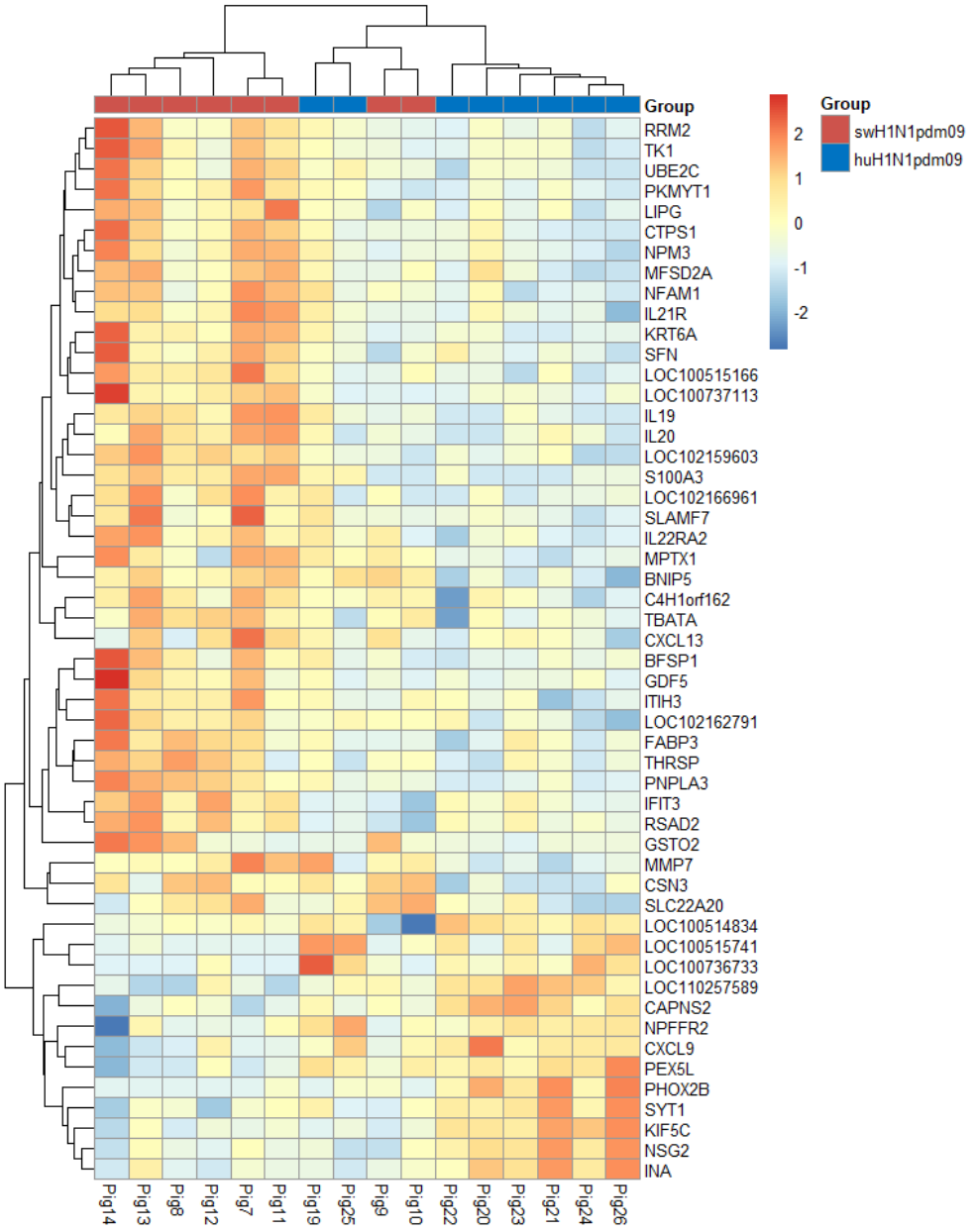

Figure 6: Heatmap showing all differentially expressed genes (up- and downregulated) comparing the huH1N1pdm09 group (blue) with the swH1N1pdm09 group (red). The color key from blue to red indicates low to high gene expression, respectively.

KEGG enrichment analysis was performed again, and 26 DEGs were identified to be significantly enriched (q-value < 0.05) in 6 pathways revealing differences in innate immune response pathways (cytokine-cytokine receptor interaction, JAK-STAT signalling pathway, and viral protein interaction with cytokine and cytokine receptor). In addition, genes involved in the nucleotide metabolism, more specifically the pyrimidine metabolism (*RRM2* (ribonucleotide reductase regulatory subunit M2), *CTPS1* (CTP synthase 1), and *TK1* (thymidine kinase 1)), were reduced after infection with huH1N1pdm09 strain compared to swH1N1pdm09 strain (Figure 7).

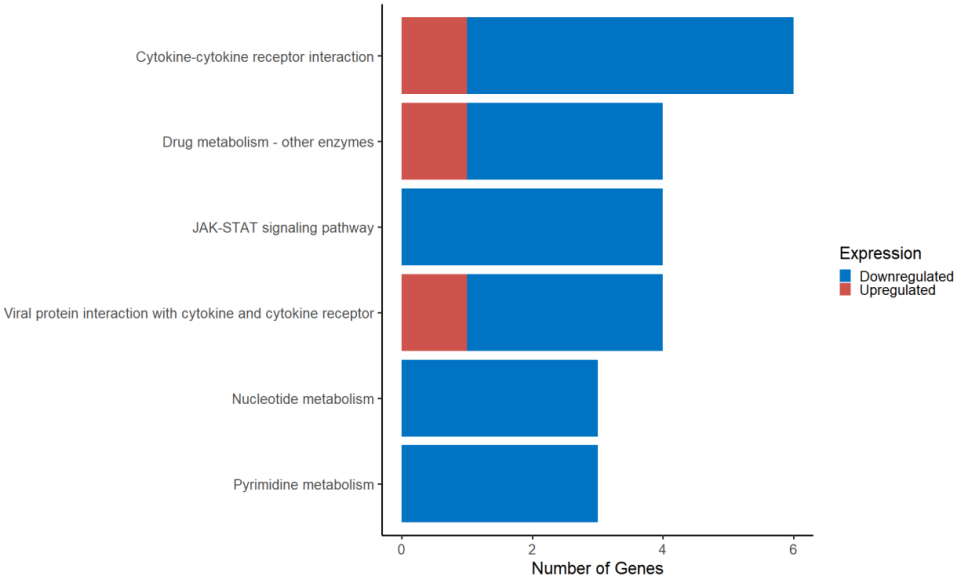

Figure 7: Enriched pathways were composed of downregulation in nucleotide metabolism in the huH1N1pdm09 group compared to the swH1N1pdm09 group. KEGG enrichment bar diagram of DEGs in the huH1N1pdm09 relative to swH1N1pdm09. Bars indicate the number of genes, and colors indicate upregulated genes (red) and downregulated genes (blue).

Validation of RNA-seq results with qPCR

To verify the results of the RNA-seq, a total of 93 genes were selected for high-throughput qPCR. As shown in Figure 8, the expression levels of *IFI6, IFIT1, ISG15, XAF1, MX1, MX2, OAS1,* and *RSAD2* were

found to be significantly upregulated in the two infected groups compared to control by both RNA-seq (q-value < 0.00003) and qPCR (p-value < 0.005) (Figure 8). The qPCR results showed that the expression levels of the selected genes were consistent with the RNA-seq, though with the tendency of fold changes being of a greater magnitude for some genes when investigated with qPCR. Based on the qPCR validation, the results from the RNA-seq were reliable.

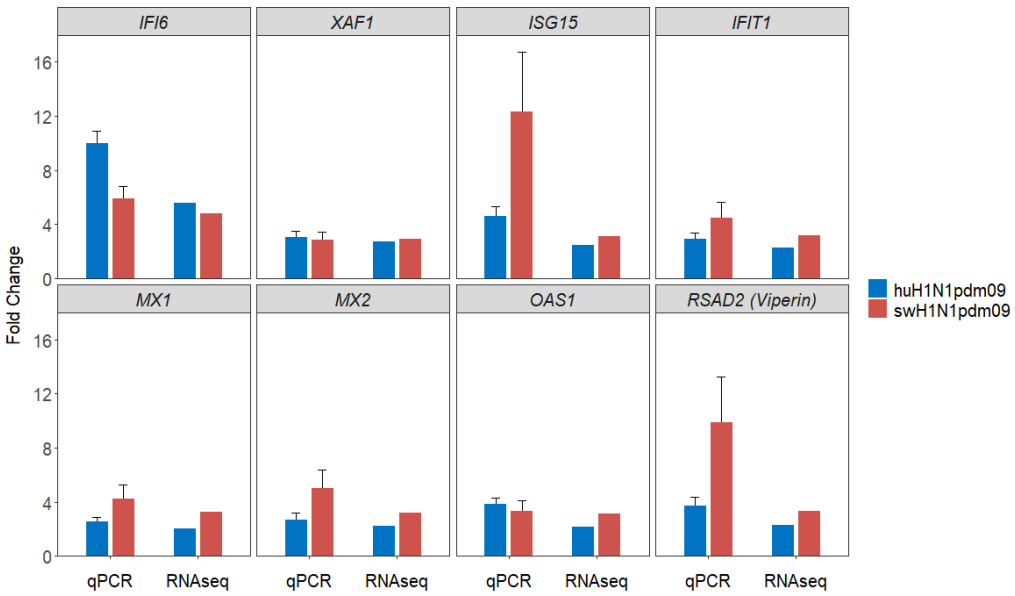

Figure 8: Validation of relevant differentially expressed genes by qPCR. Fold change levels estimated by RNA-seq and qPCR of selected differentially expressed antiviral genes in the IAV inoculated groups (huH1N1pdm09, blue; swH1N1pdm09, red. n = 8) relative to mock inoculated controls (n = 6). SEM is depicted by error bars.

Investigation of genes related to pyrimidine metabolism

RNA-seq results motivated a further investigation of genes associated with pyrimidine metabolism during IAV infection. As such, a selection of genes within the pyrimidine metabolism pathway was included in the qPCR analysis. In agreement with the RNA-seq results, *RRM2*, *CTPS1*, and *TK1* were significantly downregulated in the pigs infected with the huH1N1pdm09 strain compared to the pigs

infected with the swH1N1pdm09 strain (Figure 9). Further, *NME1, NME2* and *UCK2* were significantly slightly downregulated (Figure 9). UCK2 catalyses the first step in the salvage pathway, the phosphorylation of the nucleosides uridine and cytidine, while NME1 and NME2 balance the intracellular pool of nucleotide diphosphates and triphosphates.

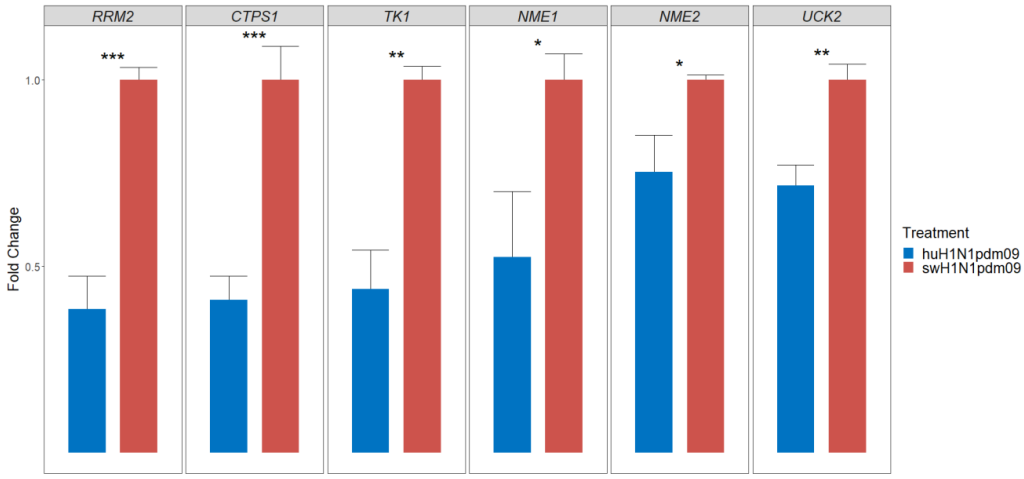

Figure 9: Investigation of genes involved in pyrimidine metabolism. Fold change levels of genes involved in the pyrimidine metabolism in the group inoculated with the huH1N1pdm09 strain (blue) relative to swH1N1pdm09 (red). The swH1N1pdm09 group mean was scaled to one. SEM is depicted by error bars. * $p < 0.05$, ** $p < 0.01$, and *** $p < 0.001$ (Student's *t*-test).

Infiltration of mononuclear cells and IAV-positive cells identified in the swH1N1pdm09 group by histopathological examination

During the histopathological examination of tracheal sections, acute, multifocal, mild to moderate, necrotising tracheitis characterised by single cell necrosis of the epithelial cells and mild to moderate infiltration of mononuclear cells in lamina propria was observed in the pigs infected with the swH1N1pdm09 strain. No lesions were observed in the control group or those infected with the huH1N1pdm09 strain (Figure 10). Though mild edema between lamina epithelialis and lamina propria was observed in one tracheal section from a pig infected with huH1N1pdm09, this finding was not representative of the whole section (data not shown).

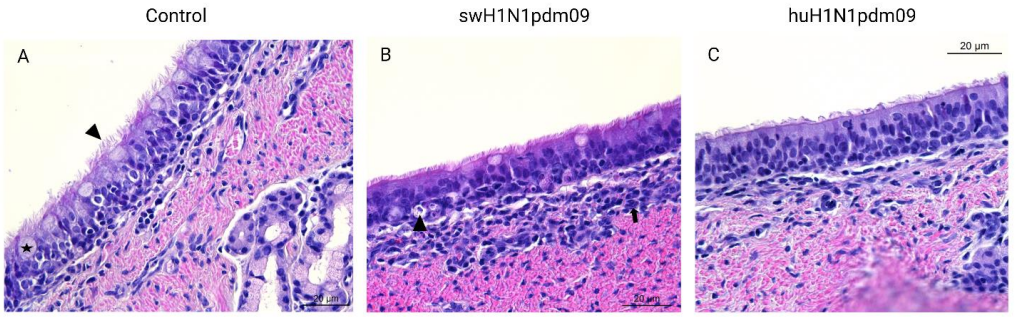

Figure 10: Tracheal lesions were only observed in pigs infected with swH1N1pdm09. Hematoxylin and eosin (H&E) staining of swine tracheal tissues from the control (n=3), swH1N1pdm09 (n=2), and huH1N1pdm09 (n=2) groups. A) Goblet cells (star) and cilia (arrowhead) are present in the control group. B) Single cell necrosis (arrowhead) of tracheal epithelial cells and mild infiltration of mononuclear cells in lamina propria (arrow) in the swH1N1pdm09 group. C) No changes were observed in the huH1N1pdm09 group compared to control pigs.

The tracheal sections were also investigated for IAV-positive cells. No IAV-positive cells were found in the control and huH1N1pdm09 groups, while several positive cells were found in the pigs infected with the swH1N1pdm09 (Figure 11).

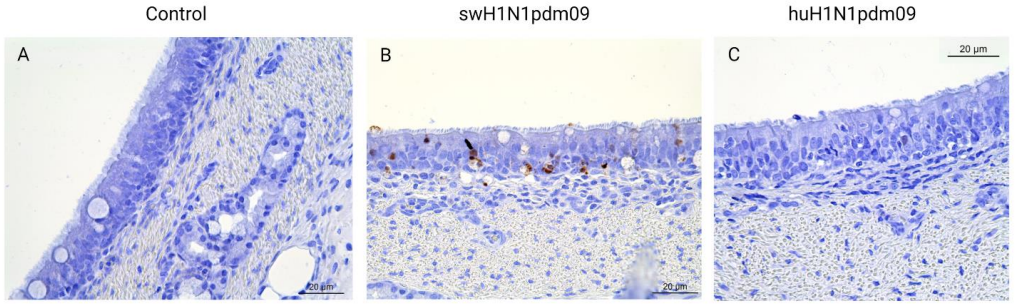

Figure 11: Immunohistochemical detection of IAV-positive cells. The presence of IAV-positive cells (brown) was investigated by immunohistochemical staining of swine tracheal tissues from the control (n=3), swH1N1odm09 (n=2), and huH1N1pdm09 (n=2) groups. A) No IAV-positive cells in the control group. B) IAV-positive cells were present in the epithelium (brown) in the pigs from the swH1N1pdm09 group. C) No IAV-positive cells in the huH1N1pdm09 group.

The difference in IAV quantity between the infected groups was also investigated by viral RNA (M-gene) load quantified by qPCR (Figure 12). A higher viral load was found in the swH1N1pdm09 group with a mean viral load of 2.19×10^9 copies/ml compared to 5.33×10^8 copies/ml in the huH1N1pdm09 group (p-value of 0.004). In agreement with the heatmaps, the two pigs (Pig 9 and 10) clustering together with

control pigs and pigs infected with the human-adapted strain (huH1N1pdm09) had the lowest viral loads within the swH1N1pdm09 group (Figure 12).

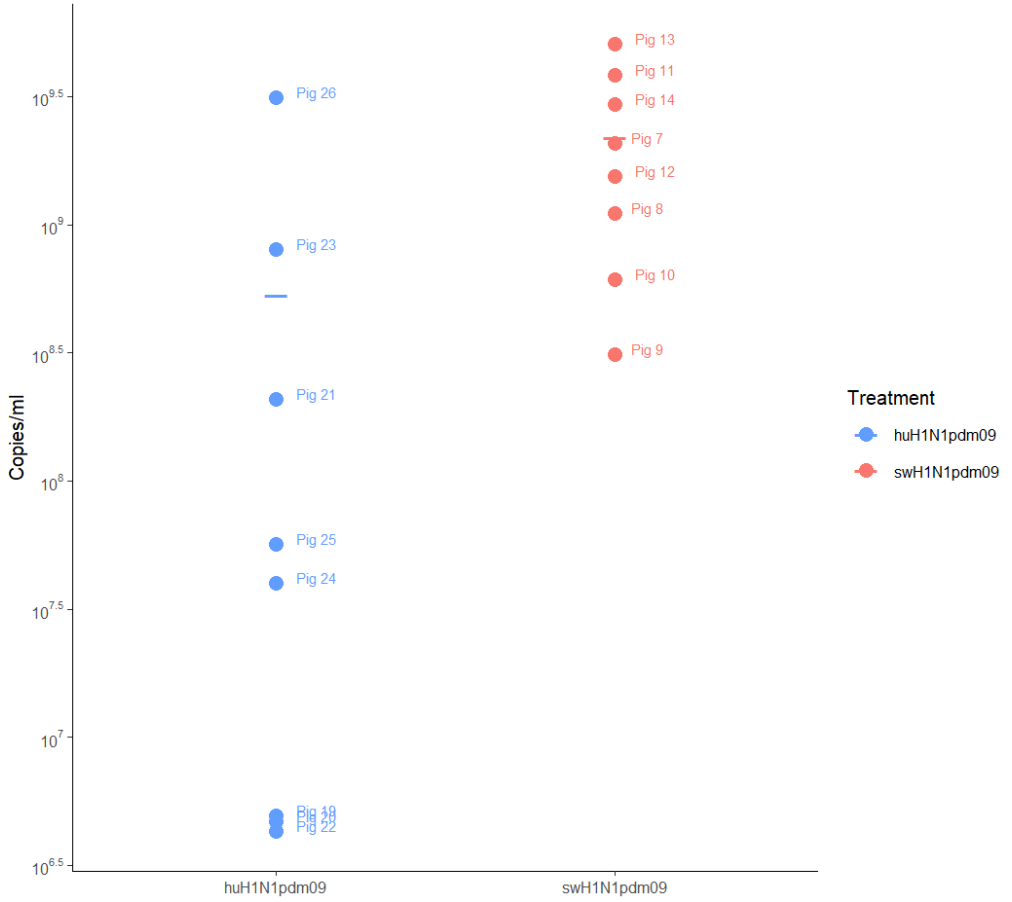

Figure 12: Higher viral load in the swH1N1pdm09 group compared to the huH1N1pdm09 group. Viral load quantified by RT-qPCR in trachea samples from the two infected groups 3 days post inoculation (blue, huH1N1pdm09; light red, swH1N1pdm09). All control pigs were negative.

Discussion

Studying host responses to IAV infection in tracheal tissue *in vivo* in the pig model can provide results with high translational value for human IAV infection[20]. A classical antiviral response in tracheal tissue from pigs was observed when infected with both a swine-adapted H1N1 (swH1N1pdm09) and a human-

adapted H1N1 (huH1N1pdm09) compared to mock inoculated control pigs, mainly through activation of several ISGs (*RSAD2, MX2, MX1, OAS1, ISG15, IFIT1, ISG12(A), BST2, IFI44, XAF1, RTP4,* and *IFI6*). *IFI6* was highly induced in both infected groups, indicating that it has an important function in the antiviral immune response regardless of how well the infectious IAV strain is adapted to the host. Indeed, *IFI6* has been demonstrated to be highly upregulated in human lung epithelial cells (A549) when infected with several different IAV H1N1 strains and even when infected with different subtypes as well, including avian H5N2, H5N3, and H9N2[40]. The function of IFI6 has been described in relation to other viral infections. It has been described to inhibit hepatitis B virus transcription and replication[41] and hepatitis C virus entry and replication[42]. However, in the case of IAV and SARS-CoV-2, it has been demonstrated to dampen the innate immune response, most likely by negatively affecting RIG-I activation either directly or through dsRNA binding[43]. IFI6 modulation of the innate immune response also affects IAV replication, as blocking IFI6 expression in human lung cells leads to lower IAV titers compared to IFI6 expressing control cells[43]. On the other hand, another study showed that IFI6 could be correlated with the infiltration of immune cells (mainly Type 17 T helper cells and Natural killer cells) in blood from Covid-19 and influenza patients[44]. Thus, IFI6 might have several roles during IAV infection, and the exact mechanism needs to be studied further.

One gene, *CAPN14*, was significantly upregulated only in the swH1N1pdm09 group. CAPN14 has been associated with apoptosis, as it induces impairment of epithelial barriers[45,46]. To our knowledge, CAPN14 expression has not been demonstrated before in tracheal tissue, and CAPN14 has not been associated with IAV infection, but inhibition of other calpains, including CAPN1 and CAPN2, have been demonstrated to decrease both H3N2 and hypervirulent H5N1 IAV infections *in vitro* in human bronchial epithelial cells and *in vivo* in mice[47]. Thus, the upregulation of *CAPN14* in the swH1N1pdm09 group could be involved in the higher viral load and immune regulation observed compared to both control and huH1N1pdm09 infected pigs, potentially due to a disruptive effect on the airway epithelial barriers.

Indeed, higher viral load identified by RT-qPCR (Figure 12) and a higher degree of single cell necrosis and IAV-positive cells were observed during histopathological examination of pigs from the swH1N1pdm09 group compared to the huH1N1pdm09 group (Figure 10). Though, expression of *ZBP1*, an activator of apoptosis and necroptosis after IAV infection[48], is likewise induced and could contribute to the histopathological changes as well. Apoptosis could be induced by IAV to avoid being recognised by the host innate immune response, but it could also be an important function of the innate immune response to kill the infected cell. The exact mechanism of CAPN14 in IAV infection needs to be studied further.

Genes involved in pyrimidine metabolism (*RRM2*, *CTPS1*, and *TK1*) were highly expressed in the swH1N1pdm09 group compared to huH1N1pdm09 infected animals. RRM2 and TK1 catalyse nucleotides into deoxynucleotides for DNA replication and repair[49,50], while CTPS1 takes part in RNA synthesis[27,28]. The RRM2 domain of SRSF5 (pre-mRNA splicing factor) has been demonstrated to bind IAV mRNA (M-gene) and promote splicing and M2 production *in vitro* and *in vivo*, facilitating viral replication[51]. Further, the RRM2 domain of GRSF1 (mitochondrial RNA binding factor) has been described to be responsible for NP and NS1 mRNA binding *in vitro* in order to stimulate their production[52]. Thus, RRM2 could have an important function in promoting viral replication. To our knowledge, TK1 has not been described in relation to IAV infection before, but as the function of TK1 is to maintain sufficient deoxythymidine triphosphate (dTTP) for DNA replication and repair[50], it can be speculated that IAV induces TK1 to sustain host cell viability of the infected cells to ensure sufficient time for viral replication. This mechanism could also be connected to RRM2 since it is also involved in DNA synthesis. Another aspect could be that the host mRNA transcription is dampened by a shift towards DNA synthesis by TK1 and RRM2 expression. In addition, CTPS1 is a CTP synthase in the pyrimidine pathway, which catalyses the formation of cytidine triphosphate (CTP) from uridine triphosphate (UTP) in an ATP-dependent manner[28]. CTP is formed subsequent to the *de novo* or salvage pathway and acts as a substrate in the synthesis of RNA[27,28]. CTP is essential for influenza transcription as it has been described that IAV, as well

405 as influenza B virus, mRNA elongation will be stalled in the lack of CTP[53,54]. Further, it has been
406 suggested that CTPS1 inhibit IFN induction during SARS-CoV-2 infection, though the work has yet to be
407 evaluated by the medical community[55]. The exact mechanisms of how IAV regulates components in the
408 pyrimidine pathway have to be investigated, but it can be proposed that with adaptation, the
409 swH1N1pdm09 strain has acquired strategies to promote its own replication.

410 On the other hand, other factors linked to host metabolism were downregulated after infection with the
411 swH1N1pdm09 strain compared to the control group, exemplified by the reduction of genes coding for
412 cytoskeleton elements (*NEB, MYOM2, MYOZ1*, and *MYBPC1*). However, downregulation of these genes
413 could be an advantage for IAV in order to disrupt mucociliary clearance as airway cilia are affected by
414 the microtubule cytoskeleton network in order to be situated in the correct structure for proper
415 mucociliary clearance[56]. Potentially, downregulating components composing the cytoskeleton could lead
416 to less efficient mucociliary clearance of newly released viral progeny. Further, mucociliary clearance
417 requires energy in the form of ATP for ciliary movement[57], therefore, inhibition of mucociliary clearance
418 would not only lead to reduced clearance of new viral progeny but also increase the energy pool for viral
419 replication. In agreement with this hypothesis, a decrease in mucociliary velocity in tracheas of mice
420 after IAV infection was demonstrated by Pittet and Colleagues[17]. However, *ex vivo* ciliary activity in mice
421 trachea was shown to be enhanced after IAV infection in a TLR3-dependent manner[16]. Thus, the effect
422 on mucociliary clearance through IAV interaction with cytoskeleton elements needs to be studied
423 further.

424 To conclude, when pigs were infected with a human-adapted IAV strain (huH1N1pdm09), a sufficient
425 host immune response was induced with upregulation of genes related to viral infection and
426 recognition, where especially ISGs were induced. Infection with a host-adapted virus (swH1N1pdm09)
427 induced a much stronger immune response, with more activated immune genes with higher expression
428 levels compared to infection with a human-adapted IAV strain (huH1N1pdm09). However, this response

could also be connected to the higher viral load within this group. Though, it is also hypothesised that an adapted IAV strain has evolved immune evasion strategies to favour viral replication by both upregulating and downregulating host metabolic factors.

Acknowledgements

The work presented in this study is part of the FluZooMark project supported by the Novo Nordisk Foundation (grant NNF19OC0056326). Karin Tarp is kindly thanked for her technical assistance.

Competing interests

The authors declare no competing interests.

References

1. Alexander DJ. A review of avian influenza in different bird species. *Vet Microbiol*. 2000;74:3-13. doi:10.1016/S0378-1135(00)00160-7

2. Trebbien R, Larsen LE, Viuff BM. Distribution of sialic acid receptors and influenza A virus of avian and swine origin in experimentally infected pigs. *Virol J*. 2011;8(434):1-14. doi:10.1186/1743-422X-8-434

3. Webster RG, Bean WJ, Gorman OT, Chambers TM, Kawaoka Y. Evolution and ecology of influenza A viruses. *Microbiol Rev*. 1992;56(1):152-179. doi:10.1128/mr.56.1.152-179.1992

4. Xu Q, Wang W, Cheng X, Zengel J, Jin H. Influenza H1N1 A/Solomon Island/3/06 Virus Receptor Binding Specificity Correlates with Virus Pathogenicity, Antigenicity, and Immunogenicity in Ferrets. *J Virol*. 2010;84(10):4936-4945. doi:10.1128/jvi.02489-09

5. Kim H, Webster RG, Webby RJ. Influenza Virus: Dealing with a Drifting and Shifting Pathogen. *Viral Immunol*. 2018;31(2):174-183. doi:10.1089/vim.2017.0141

6. Shao W, Li X, Goraya MU, Wang S, Chen JL. Evolution of Influenza A Virus by Mutation and Re-Assortment. *Int J Mol Sci*. 2017;18:1650. doi:10.3390/ijms18081650

7. WHO. Fact Sheet Influenza (Seasonal). https://www.who.int/news-room/fact-sheets/detail/influenza-(seasonal). Published 2018.

8. Kawaoka Y, Krauss S, Webster RG. Avian-to-Human Transmission of the PB1 Gene of Influenza A Viruses in the 1957 and 1968 Pandemics. *J Virol*. 1989;63(11):4603-4608.

9. Garten RJ, Davis CT, Russell CA, et al. Antigenic and Genetic Characteristics of Swine-Origin 2009 A(H1N1) Influenza Viruses Circulating in Humans. *Science (80-)*. 2009;325:197-202.

10. Iwasaki A, Pillai PS. Innate immunity to influenza virus infection. *Nat Rev Immunol*. 2014;14:315-328. doi:10.1038/nri3665

11. Mifsud EJ, Kuba M, Barr IG. Innate Immune Responses to Influenza Virus Infections in the Upper Respiratory Tract. *Viruses*. 2021;13(2090):1-13. doi:10.3390/v13102090

12. Stanifer ML, Pervolaraki K, Boulant S. Differential Regulation of Type I and type III Interferon Signaling. *Int J Mol Sci*. 2019;20(1445):1-22. doi:10.3390/ijms20061445

13. Lambert Emo K, Hyun YM, Reilly E, et al. Live Imaging of Influenza Infection of the Trachea Reveals Dynamic Regulation of CD8+ T Cell Motility by Antigen. *PLoS Pathog*. 2016;12(9):e1005881. doi:10.1371/journal.ppat.1005881

14. Palomino-Segura M, Latino I, Farsakoglu Y, Gonzalez SF. Early production of IL-17A by γδ T cells in the trachea promotes viral clearance during influenza infection in mice. *Eur J Immunol*. 2020;50:97-109. doi:10.1002/eji.201948157

15. Lim K, Hyun Y, Lambert-emo K, et al. Neutrophil trails guide influenza- specific CD8 + T cells in the airways. *Science (80-)*. 2015;349(6252):aaa4352. doi:10.1126/science.aaa4352

16. Kamiya Y, Fujisawa T, Katsumata M, et al. Influenza A virus enhances ciliary activity and mucociliary clearance via TLR3 in airway epithelium. *Respir Res*. 2020;21(282):1-13. doi:10.1186/s12931-020-01555-1

17. Pittet LA, Hall-Stoodley L, Rutkowski MR, Harmsen AG. Influenza Virus Infection Decreases Tracheal Mucociliary Velocity and Clearance of Streptococcus pneumoniae. *Am J Respir Cell Mol Biol*. 2010;42:450-460. doi:10.1165/rcmb.2007-0417OC

18. Reemers SS, Groot Koerkamp MJ, Holstege FC, van Eden W, Vervelde L. Cellular host transcriptional responses to influenza A virus in chicken tracheal organ cultures differ from responses in in vivo infected trachea. *Vet Immunol Immunopathol*. 2009;132:91-100. doi:10.1016/j.vetimm.2009.04.021

19. Reemers SS, Leenen D Van, Groot MJ, et al. Early host responses to avian influenza A virus are prolonged and enhanced at transcriptional level depending on maturation of the immune system. *Mol Immunol*. 2010;47:1675-1685. doi:10.1016/j.molimm.2010.03.008

20. Starbæk SMR, Brogaard L, Dawson HD, et al. Animal Models for Influenza A Virus Infection Incorporating the Involvement of Innate Host Defenses: Enhanced Translational Value of the Porcine Model. *ILAR J*. 2018;59(3):323-337. doi:10.1093/ilar/ily009

21. Thaker SK, Ch'ng J, Christofk HR. Viral hijacking of cellular metabolism. *BMC Biol*. 2019;17(59):1-15. doi:10.1186/s12915-019-0678-9

22. Sanchez EL, Lagunoff M. Viral activation of cellular metabolism. *Virology*. 2015;479-480:609-618. doi:10.1016/j.virol.2015.02.038

23. Liu G, Summer R. Cellular Metabolism in Lung Health and Disease. *Annu Rev Physiol*. 2019;81:403-428. doi:10.1146/annurev-physiol-020518-114640

24. Ritter JB, Wahl AS, Freund S, Genzel Y, Reichl U. Metabolic effects of influenza virus infection in cultured animal cells: Intra- and extracellular metabolite profiling. *BMC Syst Biol*. 2010;4(61):1-22. doi:10.1186/1752-0509-4-61

25. Smallwood HS, Duan S, Morfouace M, et al. Targeting Metabolic Reprogramming by Influenza Infection for Therapeutic Intervention. *Cell Rep*. 2017;19:1640-1653. doi:10.1016/j.celrep.2017.04.039

26. Kohio HP, Adamson AL. Glycolytic control of vacuolar-type ATPase activity: A mechanism to regulate influenza viral infection. *Virology*. 2013;444:301-309. doi:10.1016/j.virol.2013.06.026

27. Sepúlveda CS, García CC, Damonte EB. Inhibitors of Nucleotide Biosynthesis as Candidates for a Wide Spectrum of Antiviral Chemotherapy. *Microorganisms*. 2022;10:1631. doi:10.3390/microorganisms10081631

28. Evans DR, Guy HI. Mammalian Pyrimidine Biosynthesis: Fresh Insights into an Ancient Pathway. *J Biol Chem*. 2004;279(32):33035-33038. doi:10.1074/jbc.R400007200

29. Qin C, Rao Y, Yuan H, et al. SARS-CoV-2 couples evasion of inflammatory response to activated nucleotide synthesis. *PNAS*. 2022;119(26):e2122897119. doi:10.1073/pnas.2122897119

30. Renee S, Ortiz-riaño E, Martínez-sobrido L, Munger J. Cytomegalovirus-mediated activation of pyrimidine biosynthesis drives UDP-sugar synthesis to support viral protein glycosylation. *PNAS*. 2014;111(50):18019–18024 MICROBIOLOGY. doi:10.1073/pnas.1415864111

31. Tanner LB, Chng C, Guan XL, Lei Z, Rozen SG, Wenk MR. Lipidomics identifies a requirement for peroxisomal function during influenza virus replication. *J Lipid Res*. 2014;55:1357-1365.

doi:10.1194/jlr.M049148

32. Pertea M, Kim D, Pertea GM, Leek JT, Salzberg SL. Transcript-level expression analysis of RNA-seq experiments with HISAT, StringTie and Ballgown. *Nat Protoc*. 2016;11(9):1650-1667. doi:10.1038/nprot.2016.095

33. Li B, Dewey CN. RSEM: accurate transcript quantification from RNA-Seq data with or without a reference genome. *BMC Bioinformatics*. 2011;12(323):1-16. doi:https://doi.org/10.1186/1471-2105-12-323

34. Langmead B, Salzberg SL. Fast gapped-read alignment with Bowtie 2. *Nat Methods*. 2012;9(4):357-359. doi:10.1038/nmeth.1923

35. Love MI, Huber W, Anders S. Moderated estimation of fold change and dispersion for RNA-seq data with DESeq2. *Genome Biol*. 2014;15(550):1-21. doi:10.1186/s13059-014-0550-8

36. Benjamini Y, Yekutieli D. The control of the false discovery rate in multible testing under dependency. *Ann Stat*. 2001;29(4):1165-1188.

37. Yi Y, Fang Y, Wu K, Liu Y, Zhang W. KEGG: Kyoto Encyclopedia of Genes and Genomes. *Nucleic Acids Res*. 2020;28(1):27-30. doi:10.3892/ol.2020.11439

38. Yu G, Wang LG, Han Y, He QY. clusterProfiler: an R Package for Comparing Biological Themes Among Gene Clusters. *Omi A J Integr Biol*. 2012;16(5):284-287. doi:10.1089/omi.2011.0118

39. Wu T, Hu E, Xu S, et al. clusterProfiler 4.0: A universal enrichment tool for interpreting omics data. *Innov*. 2021;2(3):100141. doi:10.1016/j.xinn.2021.100141

40. Zhou A, Dong X, Liu M, Tang B. Comprehensive Transcriptomic Analysis Identifies Novel Antiviral Factors Against Influenza A Virus Infection. *Front Immunol*. 2021;12:632798. doi:10.3389/fimmu.2021.632798

41. Sajid M, Ullah H, Yan K, et al. The Functional and Antiviral Activity of Interferon Alpha-Inducible IFI6 Against Hepatitis B Virus Replication and Gene Expression. *Front Immunol*. 2021;12:634937. doi:10.3389/fimmu.2021.634937

42. Meyer K, Kwon YC, Liu S, Hagedorn CH, Ray RB, Ray R. Interferon-α inducible protein 6 impairs EGFR activation by CD81 and inhibits hepatitis C virus infection. *Sci Rep*. 2015;5:9012. doi:10.1038/srep09012

43. Villamayor L, Rivero V, López-García D, et al. Interferon alpha inducible protein 6 is a negative regulator of innate immune responses by modulating RIG-I activation. *Front Immunol*. 2023;14:1105309. doi:10.3389/fimmu.2023.1105309

44. Sun Z, Ke L, Zhao Q, et al. The use of bioinformatics methods to identify the effects of SARS-CoV-2 and in fl uenza viruses on the regulation of gene expression in patients. *Front Immunol*. 2023;14:1098688. doi:10.3389/fimmu.2023.1098688

45. Kottyan LC, Davis BP, Sherrill JD, et al. Genome-wide association analysis of eosinophilic esophagitis provides insight into the tissue specificity of this allergic disease. *Nat Genet*. 2014;46(8):895-900. doi:10.1038/ng.3033

46. Davis BP, Stucke EM, Khorki ME, et al. Eosinophilic esophagitis-linked calpain 14 is an IL-13-induced protease that mediates esophageal epithelial barrier impairment. *JCI Insight*.

2016;1(4):e86355. doi:10.1172/jci.insight.86355

47. Blanc F, Furio L, Moisy D, et al. Targeting host calpain proteases decreases influenza A virus infection. *Am J Physiol - Lung Cell Mol Physiol*. 2016;310(7):L689-L699. doi:10.1152/ajplung.00314.2015

48. Thapa RJ, Ingram JP, Ragan KB, et al. DAI Senses Influenza A Virus Genomic RNA and Activates RIPK3-Dependent Cell Death. *Cell Host Microbe*. 2016;20:674-681. doi:10.1016/j.chom.2016.09.014

49. Stubbe J, Van der Donk WA. Ribonucleotide reductases: radical enzymes with suicidal tendencies. *Chem Biol*. 1995;2(12):793-801.

50. Bitter EE, Townsend MH, Erickson R, Allen C, O'Neill KL. Thymidine kinase 1 through the ages: a comprehensive review. *Cell Biosci*. 2020;10(138):1-16. doi:10.1186/s13578-020-00493-1

51. Li Q, Jiang Z, Ren S, et al. SRSF5-Mediated Alternative Splicing of M Gene is Essential for Influenza A Virus Replication: A Host-Directed Target Against Influenza Virus. *Adv Sci*. 2022;9:2203088. doi:10.1002/advs.202203088

52. Kash JC, Cunningham DM, Smit MW, et al. Selective Translation of Eukaryotic mRNAs: Functional Molecular Analysis of GRSF-1, a Positive Regulator of Influenza Virus Protein Synthesis. *J Virol*. 2002;76(20):10417-10426. doi:10.1128/jvi.76.20.10417-10426.2002

53. Kouba T, Drncová P, Cusack S. Structural snapshots of actively transcribing influenza polymerase. *Nat Struct Mol Biol*. 2019;26:460-470. doi:10.1038/s41594-019-0232-z

54. Kouba T, Dubankova A, Drncova P, et al. Direct observation of backtracking by influenza A and B polymerases upon consecutive incorporation of the nucleoside analog T1106. *Cell Rep*. 2023;42:111901. doi:10.1016/j.celrep.2022.111901

55. Rao Y, Wang T-Y, Qin C, et al. Targeting CTP Synthetase 1 to Restore Interferon Induction and Impede Nucleotide Synthesis in SARS-CoV-2 Infection. *bioRxiv*. 2021. doi:10.1101/2021.02.05.429959

56. Vladar EK, Bayly RD, Sangoram AM, Scott MP, Axelrod JD. Microtubules Enable the Planar Cell Polarity of Airway Cilia. *Curr Biol*. 2012;22(23):2203-2212. doi:10.1016/j.cub.2012.09.046

57. Wanner A, Salathé M, O'riordan TG. Mucociliary Clearance in the Airways. *Am J Respir Crit Care Med*. 1996;154:1868-1902.

Supplementary Table 1: qPCR primer sequences and experimentally determined PCR efficiencies for all reported genes in the present study. Newly designed primer assays were designed in at least dublicates and indicated by numbers in brackets. *IFI6 primer assay was included twice.

Gene name	Forward primer	Reverse Primer	PCR eff. (%)
ACTB (Reference)	CTACGTCGCCCTGGACTTC	GCAGCTCGTAGCTCTTCTCC	108
ANGPTL4 (1)	CAGACTCAGCTCAAGGCTCA	TCTCAAGTGCTGCTTCTCCA	118
ANGPTL4 (2)	CTCTCTGGTGGTTGGTGGTT	CGAGGGATGGAATGGAAGTA	96
B2M (Putative reference)	TGAAGCACGTGACTCTCGAT	CTCTGTGATGCCGGTTAGTG	104
BFSP1	TTGAGAACGAAGGCAACAGA	CTCCATGGCTCGCTGTGTA	99
BNIP5	AGCTGGACAGAGCCTCAGAA	GCTCCTCTGCATCTTGGAGT	105
BST2	GGAGATGGAGAAGACGCAAA	CCTCCTGCAGCTTCTGATTC	96
CAD (1)	CCCCAGATGAAGTGGATGAG	ACTCTCCCACCACCAGTCCT	106
CAD (2)	AAAGAAGCCACAGCTGGAAA	GAAGCCCAGGGAGACAGAG	109
CAPN14	ATCTGGCACCGTGAGTATCC	GACCGGTGAGTGTCTTGCTT	108
CBR1 (1)	AACCTCAAGCAGAGTGGTGAA	ATTCAGGGCTGCACTCGTTA	112
CBR1 (2)	CCAGTTGGACAATCCCACA	ATTTCGGGTTCCCATGAAGT	101
CCL2	CTTCTGCACCCAGGTCCTT	CGCTGCATCGAGATCTTCTT	109
CDA (1)	AGAAGGCCATCTCAGAAGGAT	GCATGGCGAAATAAAATCATC	106
CDA (2)	GCAGGCAAGTCATGAGAGAGT	TGGATGGTCCTGACAACGTA	111
CIART (1)	TCCTCATATAGCTGCCCAGAA	GGCTTGGAAAATGCTTGGT	96
CIART (2)	AGCTGCCCAGAAGTCATCAT	GGATAACTGTGGTGGCTTGG	112
CMPK1 (1)	CGATGTCTTGAGAGGGGAAA	GGTTTGAATTCTCTTTTCCAAGC	99
CMPK1 (2)	TGAAGAAATGGGGAAAGTCAA	GCCTTCTTTGTCAAAAATCTTCA	100
CMPK2 (1)	CCAGAGAGGAGGTTGAGCTG	CATCCGCTGGTAGGACACTT	104
CMPK2 (2)	GGATGCCACAGGTAAAACCA	CAGGTGGCGACTTTAGGAGA	105
CSN3	TGCCTATCCTGGCATTAACA	CACAGCGCGTTAGTTTTTCC	86
CTPS1 (1)	TGGCAGTGGTTGAGTTTTCA	ATGACCACAGGGTGACTGGT	106
CTPS1 (2)	CCATCAACCACAAGTTGGAA	CTCCTCCTGCAAGGTGCTT	113
CTPS2 (1)	TGGAGAAATATGGCTGACAGG	GAGCTTGGTGTACTTGCCAAC	110
CTPS2 (2)	GCCATCAACCACAAGTTGAA	GTCCTCAGTTTCGGTGGTCT	113
CXCL10	CCCACATGTTGAGATCATTGC	GCTTCTCTCTGTGTTCGAGGA	107
CXCL13 (1)	GATTCAAATCTGGCCTCCTG	GCTTTGAGGGTTCAAGCAGA	110
CXCL13 (2)	GATCTCTGCTTCTCGTGCTG	CTTCGGAGGCATTGACACTT	104
CXCL8 (IL8)	GAAGAGAACTGAGAAGCAACAACA	TTGTGTTGGCATCTTTACTGAGA	104
CXCL9	TTAAACAATTTGCCCCAAGC	TGTTTGATCCCCATTCTTCA	104
DBP (1)	CCAGCCAATCATGAAGAAGG	CTTGGCTGCCTCGTTATTCT	100
DBP (2)	GGAAGATCCAGGTACCAGAGG	TTGGCTGCCTCGTTATTCTT	103
DDX58 (RIG-I)	TTGCTCAGTGCAATCTGGTC	CTTCCTCTGCCTCTGGTTTG	98
DDX60	GGAACTCAGATGGTGATTTGCT	GCCTGAGAGCTACTGATACCG	99
DHODH (1)	GCTCTCAGTGGTGGAACACA	TCCCCAGGTTTATTCCCAGT	109
DHODH (2)	TGCTGGAAGTGAGAGTCCTG	TTCCCCGTGCTTATCAAATC	110
DHX58 (LGP2)	GAGTACCAGGCCAAGATCCA	CTTCTGCTGCCGACTCTTCT	96
DTYMK (1)	CTGGAGGCGGTACCTTCA	AAGGCGTATCTGTCCACGAC	106
DTYMK (2)	CCCTGGTCGTGGACAGATAC	CACCAGTCCAGGGAAAAGTT	106
FABP3 (1)	TCAAGCTGGGAGTGGAGTTT	GTGGACAAGTTTGCCTCCAT	98
FABP3 (2)	TGGAAGCTAGTGGACAGCAA	GGTAGGCTTGGTCATGTTGG	101
GAPDH (Reference)	ACCCAGAAGACTGTGGATGG	AAGCAGGGATGATGTTCTGG	104
GDF5 (1)	AACAGCAGCGTGAAGTTGG	CTTCCTGACTGCAGGACCTC	106
GDF5 (2)	CCCATCAGCATCCTCTTCAT	AAGACTCCACGACCATGTCC	106
GRSF1 (1)	GCCAATGCCCAAGACATTAT	CTGGAGCTATATTCCATGGTGA	98

GRSF1 (2)	GGGGTTACTGCCAGGAGTC	GGCAGTTCATACTCAGGGAGA	102
GSTO2	GCTGGATGTATATGGAATAGCTGAC	AGACTGTGGGGTCCTGCTT	114
HPRT1 (Reference)	ACACTGGCAAAACAATGCAA	TGCAACCTTGACCATCTTTG	101
IFI44	ATTGCTCACTCACGTGGACA	GCTTGAGTTTCACAGGCACA	105
IFI6	AAGGCGGTATCGCTCTTCTT	GAGCTGCTGTTGTCCTCAGA	105
*IFI6**	AAGGCGGTATCGCTCTTCTT	GAGCTGCTGTTGTCCTCAGA	104
IFIH1 (MDA5)	CAGTGTGCTAGCCTGCTCTG	GCAGTGCCTTGTTTCCTCTC	105
IFIT1	GGCCATTTTGTCTGAATGCT	TCAGGGCAAAGAGAGCCTTA	102
IFIT3	GAACAGCCCTTCAGGCATAG	TCCATTTCCTCAGTGCCTTC	98
IFNA	TACTCAGCTGCAATGCCATC	CTCCTCATTTGTGCCAGGAG	103
IFNL1 (IL29)	ATGGGCCAGTTCCAATCTC	CTGCAGCTCCAGTTCTTCAGT	102
IL1A	TGTGCTAAATAACCTGGATGAGG	GGTTCGTCTTCGTTTTGAGC	107
IL1B	TCTCTCACCCCTTCTCCTCA	GACCCTAGTGTGCCATGGTT	97
IL1RN	TGCCTGTCCTGTGTCAAGTC	GTCCTGCTCGCTGTTCTTTC	100
IL20 (1)	GCCAGAGATGAAATCATTGACA	AGCACTGATCTGCAGGCTTT	105
IL20 (2)	GGAATTCGAAATGGATTTTCAG	CTTCTTCAAGATTCTGATGTCAATG	94
IL22RA2	GCTTGTACCAGCAACAGCAG	GAACTCTTGAATACCCCAGCA	106
IL6	CCTCTCCGGACAAAACTGAA	TCTGCCAGTACCTCCTTGCT	107
IRF7	GTGTGCTCCTGTACGGGTCT	CTGCAGCAGCTTCTCTGTGT	106
ISG12(A) (1)	GCCTGGCTTCCAAGATACTG	AGCCCTGCTGAAGGAAGTC	107
ISG12(A) (2)	ATCTAGCCTGGGATCCTTGC	GCCTTGGCTCCTAGTGAAGA	103
ISG15	AGTTCTGGCTGACTTTCGAGG	GGTGCACATAGGCTTGAGGT	106
ITIH3 (1)	GATGAAGACCCAGGCACAGT	TCCTGGCTGCTTCTCTTCTC	117
ITIH3 (2)	ACTCCTGAGAACATCCAAAAGG	CCGTCATTGATGTTGGTCATT	114
KIF5C (1)	GCTTCCAGGATAAGGAGAAGG	GGTGGCTCTCCATCTGTTGT	111
KIF5C (2)	ACAGTGACGATGGAGGAGGA	GGACGAGCTGTTTGTGAACTT	105
KRT6A (1)	GGAGATTGCCACCTACAGGA	TGGACTGCACCACAGAGATG	108
KRT6A (2)	GCTGAGGCTGAGTCCTGGTA	GTGTTGCGCAGGTCATCTC	105
LIPG (1)	TGGACTCAACGACATCTTGG	CGCTCATGCTCACACTTCAT	102
LIPG (2)	ACGATGAGTGGCATGTTTGA	CCACAACATTGGCTCCTTTC	105
MFSD2A	GCACATACACCTTGGGCTTT	GATTGTGGCTGAGAGCATGA	106
MMP7 (1)	GGGAGGAGATGCTCACTTTG	GCCAAGTTCATGAGTTGCAG	108
MMP7 (2)	GTTAGCTGGGGAATTGCTGA	AGGCATGAGCCAGTGTGTTT	113
MSMB (1)	CCCGCTCATCACAATGAAAT	TGAAATAGCACTGGGAGTTGC	110
MSMB (2)	TGCAACTCCCAGTGCTATTTC	AGTTCAGCGGGTGTGAGACT	105
MX1	CCATCATTAAGAAGCAGGTCAGTG	AACATCTGTGAAGGCGAGCC	98
MX2	ACCAAGGGCCTGAATATGCT	ACGGGCTGTACAGGTTGTTC	111
MYOM3 (1)	CCTCTGCAGTGGAAGGTCAC	AAGCGGGTTTCTTTCTTGGT	105
MYOM3 (2)	CTGTGCTGCCTGTTTTCAGA	TCAGTAGCCTCCCATCTTGG	96
NEB	GCTGCAGAGCGATGTTGA	ATTTCCAAGGACCCAAAAGG	105
NFAM1	AGACACAGGGTACCGAGAGC	GGAGCCTGCATCTGTTTCTT	113
NME1 (1)	TGGTGACGTACATGCATTCAG	CCAAGCATCACTCGACCTG	115
NME1 (2)	AGTCGGCAGAAACATCATCC	GGTGAAACCACAAGCCAATC	102
NME2 (1)	TCGTTGCCTTGAAGTTCCTT	CCGGTCTTTCAGGTCAATGT	104
NME2 (2)	CTTCTTCCCGGGACTGGT	ATCACTCGGCCTGTCTTCAC	108
NME3 (1)	CTGCTGCGGGAGCACTAC	CCGAGCCCATGTACTTCAC	118
NME3 (2)	CGCCTGGTGAAGTACATGG	GAAGCGCGAACAACGTCTA	119
NME4 (1)	CATCCGCGGAGACTTCAG	GGCCCCTTCCACAGAGTC	104
NME4 (2)	GGGTTGTCCCTCCTGGAC	TCTCAAAGCGCTGGATCAC	99
NME6 (1)	ACAACCCATGGCTCTGATTC	GGGCTCCTCTTCCTCATACC	112

NME6 (2)	TAGCCCCAGATTCAATTCGT	TGGCTGAAACCACAGAATCA	114
NME7 (1)	GGCCAGCAAACACTGCTAA	CTTTCCCAGCAGTCCTTCAC	106
NME7 (2)	TCATCAGTCAAGGCCCTTTT	CATCATCTCTTAAAATCTCCATAGCA	96
NPM3 (1)	AGGAGATTGCAGTCCCTGTG	GGAGCTGGAAGTCATCCAAA	102
NPM3 (2)	CGGCACCAGATTGTTACTATGA	TTCCTCCTCACTCCCCTCTT	100
NR1D1 (1)	TTCCGTGATCTTTCTCAGCA	GGTCCTTCACGTTGAACAGC	112
NR1D1 (2)	ACCTTTGAGGTGCTGATGGT	CTGCAGGCTGTAGGTGGTG	112
OAS1	AAGAAACCCAGGCCTGTGATTC	TAGTGCCCCTTCTACCAGCT	109
OASL	TGCGACTGGTAAAACACTGG	CCCAGGCATAGATGGTCAGT	111
PEX5L	GCTCATCTAGAACGGGATCAA	CACCACTCAGTTCTGGCTGA	105
PPIA (Reference)	CAAGACTGAGTGGTTGGATGG	TGTCCACAGTCAGCAATGGT	105
RRM2 (1)	TTGGCAAGGTCTTCAGAGTAGAG	GAAGTTTGTCTTCCCCTCCA	100
RRM2 (2)	CGGATAGAACAGGAGTTCCTCA	TCTGCCACGAACTCGATGTA	116
RRM2 (3)	CGTGCGGATAGAACAGGAGT	TCTGCCACGAACTCGATGTA	106
RRM2 (4)	CCTGACCTTTTCCAACGAAC	GCTCCGAAGGCTTGTGTAAC	105
RSAD2 (1)	AAAGACGTGTCCTGCTTGGT	GCCCGTTTCTACAGTTCAGG	106
RSAD2 (2)	CCAAAAACTGAGGACGTGGT	CTTCCACATTGAAGCGATTG	93
S100A3	GCCAGTCCTCTGGAGCAG	GCAGAGCTTGTGCTTGTCC	105
SFN (1)	AACCTGCTCTCAGTGGCCTA	TACTGGACAGGACCCTCCAC	109
SFN (2)	ACAAGAATGTGGTGGGTGGT	CTTCTCTTCCGAGCCTTCCT	108
SRSF5 (1)	CAGACCTCGAAATGATAGACGA	TAAATTCTCAACTATAAGCCGATTTTC	97
SRSF5 (2)	TGCGGATGCACATAGACCT	GCATTCTTTAAATCACCATAAGAGG	97
STAT1	CACGAAGGTGATGAACATGG	TCTTTCAGTTGCAGGTGTCG	99
SYT1 (1)	GGTCATTCTGGAGGCAAAGA	CTTCAGCCTCTTGCCATTCT	98
TBATA	AGGAGTTGCTGATCCTGGAG	GAGCCAAAACTGGATAGCATTC	105
THRSP (1)	CCAGTTCCACCTGCATTTCT	TCACCTCCTCAGCTTTCAGG	108
THRSP (2)	AAAACGATGGGGCTGAGAAT	CAGGTGGAACTGGGCTTCTA	108
TK1 (1)	GACGGGACCTTCCAGAGG	TCAGCTTCACCACGCTCTC	117
TK1 (2)	AAGGGCAGTTTTTCCCTGAC	ACAATCACGGTCTTGCCTTC	108
TK2 (1)	TTCACAGCGCAAGATACGTT	CTCCCTTTGATGAGCCACTC	106
TK2 (2)	GCCCAAGTGGAGGAATGTC	GTACGTCTGCAGCGTGAGG	105
TNF	CCCCCAGAAGGAAGAGTTTC	CGGGCTTATCTGAGGTTTGA	105
UBE2C (1)	TCGATAGCCCTCTGAACACA	CCTGCTTGGAGTAGGTTTCCT	108
UBE2C (1)	CAGCCGGCACAGTATATGAA	GGCGTGAGGAACTTCACTGT	113
UCK1 (1)	GCCTTGAAGGGACAGTACAATTT	GTGTCAGCGTCCTGTGCAT	111
UCK1 (2)	GAGCGGCAAGTCAACTGTC	GCTGCCTGTGGTCTACTTCA	108
UCK2 (1)	CGAAGGGAAAACAGTCCAGA	GGTAACCGTCTCCTCCTTCC	100
UCK2 (2)	CTCTTCGTGGACACAGATGC	CTCCCTCTTTCGCTGATGTC	108
UCKL1 (1)	ATCATTTTCGAGGGCATCAT	GGAGTCCGTGTCCACAAAG	108
UCKL1 (2)	CACGGCACACAGTCCAAG	ATTCTGGCCACAGTGGTCTT	114
UMPS (1)	AAAAGCAGTATGCAGGTGGTG	GGCACCACATGAGCATTTACTA	103
UMPS (2)	ACACTGAGGCAGCAGTGAGA	CTCGGGAGCCAGAAATAAAA	100
XAF1	ATTCCAGCTCCTGAAAGCAA	GGACAGCATCTACCCAGGTG	102
YWHAZ (Reference)	GCTGCTGGTGATGATAAGAAGG	AGTTAAGGGCCAGACCCAAT	105
ZBP1	CCCAGAGGATGCAGAGCTT	GGTTATCAAATGCCAGGTGC	108

Supplementary Table 2: Statistics for reads mapping to reference genome (Sscrofa11.1, NCBI accession: GCA_000003025.6).

Pig	Total Clean reads	Total Clean Bases	Q20(%)	Total Mapping Ratio (%)	Uniquely Mapping Ratio (%)
1	93,017,450	9,301,745,000	96.28	96.35	91.62
2	92,781,534	9,278,153,400	96.04	96.4	92.16
3	92,607,366	9,260,736,600	95.95	96.24	92.74
4	72,948,272	7,294,827,200	95.29	96.31	92.8
5	90,312,686	9,031,268,600	96.1	96.23	92.18
6	92,159,984	9,215,998,400	95.69	95.86	91.54
7	94,547,290	9,454,729,000	95.6	95.75	91.77
8	78,054,052	7,805,405,200	94.8	94.77	90.58
9	75,695,336	7,569,533,600	95.39	96.31	91.87
10	91,368,948	9,136,894,800	95.27	96.3	93.29
11	85,046,536	8,504,653,600	95.39	96.31	92.76
12	89,096,070	8,909,607,000	95.36	96.41	92.05
13	76,359,076	7,635,907,600	95.17	95.61	91.61
14	92,786,030	9,278,603,000	95.88	96.35	93.46
19	92,553,154	9,255,315,400	95.75	96.32	92.63
20	91,797,872	9,179,787,200	95.39	96.05	92.67
21	92,370,054	9,237,005,400	95.73	96.07	93.26
22	93,209,902	9,320,990,200	96.34	96.96	93.35
23	92,320,856	9,232,085,600	95.73	96.02	92.08
24	92,148,930	9,214,893,000	95.5	96.34	93.7
25	92,550,798	9,255,079,800	95.53	95.93	92.88
26	90,863,612	9,086,361,200	95.97	96.1	93.18

Supplementary Table 3: List of 244 differentially expressed genes in the pigs infected with the swH1N1pdm09 strain compared to mock inoculated control pigs.

GeneID	Description	Symbol	Log2 Fold Change	Relative Fold Change	Padj (q-value)	Expression
110261124	interferon alpha inducible protein 6(IFI6)	IFI6	2.27	4.82	1.48E-36	Up
595119	2'-5'-oligoadenylate synthetase like(OASL)	OASL	1.86	3.64	7.54E-06	Up
100154248	interferon induced protein with tetratricopeptide repeats 3(IFIT3)	IFIT3	1.73	3.31	3.44E-05	Up
396752	radical S-adenosyl methionine domain containing 2(RSAD2)	RSAD2	1.72	3.30	6.18E-05	Up
102159603	uncharacterized LOC102159603(LOC102159603)	LOC102159603	1.71	3.28	3.44E-05	Up
397128	MX dynamin like GTPase 1(MX1)	MX1	1.71	3.26	3.44E-05	Up
396893	myxovirus (influenza virus) resistance 2 (mouse)(MX2)	MX2	1.68	3.22	6.18E-05	Up
396723	RNA sensor RIG-I(RIGI)	RIGI	1.68	3.20	5.45E-05	Up
100515433	calpain 14(CAPN14)	CAPN14	1.66	3.17	1.11E-04	Up
397570	2'-5'-oligoadenylate synthetase 1(OAS1)	OAS1	1.66	3.16	6.18E-05	Up
100153038	interferon-induced protein with tetratricopeptide repeats 1(IFIT1)	IFIT1	1.65	3.15	6.71E-05	Up
100145895	ISG15 ubiquitin like modifier(ISG15)	ISG15	1.65	3.14	1.24E-04	Up
396880	C-X-C motif chemokine ligand 8(CXCL8)	CXCL8	1.60	3.04	2.09E-04	Up
100037289	interferon regulatory factor 7(IRF7)	IRF7	1.56	2.95	3.44E-05	Up
396906	heat shock protein family A (Hsp70) member 6(HSPA6)	HSPA6	1.56	2.94	2.09E-04	Up
100524520	DExH-box helicase 58(DHX58)	DHX58	1.54	2.91	8.43E-05	Up
102159947	XIAP associated factor 1(XAF1)	XAF1	1.54	2.91	3.44E-05	Up
396867	stefin A8(LOC396867)	LOC396867	1.54	2.90	4.31E-04	Up
100144524	Z-DNA binding protein 1(ZBP1)	ZBP1	1.52	2.87	4.00E-04	Up
396764	solute carrier family 11 member 1(SLC11A1)	SLC11A1	1.51	2.86	5.80E-04	Up
100518083	HECT and RLD domain containing E3 ubiquitin protein ligase 5(HERC5)	HERC5	1.50	2.83	1.11E-04	Up
396900	alveolar macrophage-derived chemotactic factor-II(AMCF-II)	AMCF-II	1.50	2.83	6.66E-04	Up
102158401	collagen alpha-1(I) chain-like(LOC102158401)	LOC102158401	1.50	2.83	6.71E-05	Up
100623872	cytidine/uridine monophosphate kinase 2(CMPK2)	CMPK2	1.50	2.83	1.47E-04	Up
397316	ficolin (collagen/fibrinogen domain containing) 1(FCN1)	FCN1	1.50	2.82	7.54E-04	Up
733603	serum amyloid A-3 protein(SAA3)	SAA3	1.48	2.80	8.58E-04	Up
396777	ubiquitin specific peptidase 18(USP18)	USP18	1.48	2.78	7.98E-05	Up
100153902	putative ISG12(a) protein(ISG12(A))	ISG12 (A)	1.47	2.77	4.42E-09	Up
397094	interleukin 1 alpha(IL1A)	IL1A	1.47	2.76	1.06E-03	Up
100152038	oncostatin M(OSM)	OSM	1.45	2.74	1.20E-03	Up

100155467	interferon induced protein with tetratricopeptide repeats 2(IFIT2)	IFIT2	1.44	2.72	5.98E-04	Up
595128	2'-5'-oligoadenylate synthetase 2(OAS2)	OAS2	1.43	2.69	1.06E-03	Up
100625050	epithelial stromal interaction 1(EPSTI1)	EPSTI1	1.42	2.67	4.17E-04	Up
100155953	serpin family A member 11(SERPINA11)	SERPINA11	1.41	2.67	1.70E-03	Up
100738056	transmembrane protease serine 11G-like(LOC100738056)	LOC100738056	1.41	2.66	1.71E-03	Up
396972	galectin 9(LGALS9)	LGALS9	1.41	2.66	6.71E-05	Up
100625797	kelch domain containing 8A(KLHDC8A)	KLHDC8A	1.41	2.66	1.06E-03	Up
100153822	nuclear factor, interleukin 3 regulated(NFIL3)	NFIL3	1.41	2.66	2.09E-04	Up
397590	prostaglandin-endoperoxide synthase 2(PTGS2)	PTGS2	1.41	2.65	1.71E-03	Up
100518788	osteoclast associated Ig-like receptor(OSCAR)	OSCAR	1.41	2.65	1.37E-03	Up
100525680	serum amyloid A-2 protein(SAA2)	SAA2	1.40	2.63	1.63E-03	Up
100517333	MEFV innate immunity regulator, pyrin(MEFV)	MEFV	1.40	2.63	2.01E-03	Up
102162068	NFAT activating protein with ITAM motif 1(NFAM1)	NFAM1	1.39	2.62	7.54E-04	Up
100511370	hematopoietic SH2 domain containing(HSH2D)	HSH2D	1.39	2.62	7.20E-05	Up
100861588	interleukin 17C(IL17C)	IL17C	1.39	2.62	1.00E-03	Up
493186	suppressor of cytokine signaling 3(SOCS3)	SOCS3	1.39	2.61	2.25E-03	Up
100628112	interleukin 1 receptor type 2(IL1R2)	IL1R2	1.37	2.59	2.33E-03	Up
100518612	MFSD2 lysolipid transporter A, lysophospholipid(MFSD2A)	MFSD2A	1.36	2.57	1.37E-03	Up
110258214	basic salivary proline-rich protein 4-like(LOC110258214)	LOC110258214	1.35	2.55	7.42E-04	Up
396601	triggering receptor expressed on myeloid cells 1(TREM1)	TREM1	1.34	2.53	3.34E-03	Up
767627	V-set pre-B cell surrogate light chain 1(VPREB1)	VPREB1	1.34	2.53	2.01E-03	Up
110260994	carcinoembryonic antigen-related cell adhesion molecule 21-like(LOC110260994)	LOC110260994	1.34	2.52	3.09E-03	Up
493187	interleukin 27(IL27)	IL27	1.33	2.52	2.90E-03	Up
414374	C-C motif chemokine receptor 1(CCR1)	CCR1	1.33	2.51	2.81E-03	Up
100622336	colony stimulating factor 3 receptor(CSF3R)	CSF3R	1.33	2.51	3.46E-03	Up
414904	chemokine (C-X-C motif) ligand 2(CXCL2)	CXCL2	1.32	2.50	2.82E-03	Up
100155736	lipase G, endothelial type(LIPG)	LIPG	1.32	2.50	1.19E-03	Up
100157276	ADAM metallopeptidase with thrombospondin type 1 motif 4(ADAMTS4)	ADAMTS4	1.32	2.49	4.21E-03	Up
397031	CD163 molecule(CD163)	CD163	1.32	2.49	2.58E-03	Up
448855	interferon stimulated exonuclease gene 20(ISG20)	ISG20	1.32	2.49	4.17E-04	Up
100302088	bone marrow stromal cell antigen 2(BST2)	BST2	1.31	2.49	1.20E-03	Up
100152729	S100 calcium binding protein A2(S100A2)	S100A2	1.31	2.48	1.76E-03	Up
100127488	S100 calcium binding protein A8(S100A8)	S100A8	1.30	2.46	4.66E-03	Up

100525523	interferon induced protein 44(IFI44)	IFI44	1.30	2.46	5.43E-04	Up
396865	chitinase 3 like 1(CHI3L1)	CHI3L1	1.29	2.45	5.41E-03	Up
110255273	H2B clustered histone 18(H2BC18)	H2BC18	1.29	2.45	2.34E-03	Up
100624191	leukocyte immunoglobulin-like receptor subfamily A member 6(LOC100624191)	LOC100624191	1.29	2.44	2.22E-03	Up
397623	sialic acid binding Ig like lectin 1(SIGLEC1)	SIGLEC1	1.29	2.44	2.81E-03	Up
110256385	receptor transporter protein 4(RTP4)	RTP4	1.28	2.44	1.30E-03	Up
100512873	antileukoproteinase(LOC100512873)	LOC100512873	1.28	2.44	5.56E-03	Up
100152206	C2 calcium-dependent domain-containing protein 4A(LOC100152206)	LOC100152206	1.28	2.43	1.63E-03	Up
100152253	syntaxin 11(STX11)	STX11	1.28	2.42	4.01E-03	Up
110257486	solute carrier organic anion transporter family member 4A1(SLCO4A1)	SLCO4A1	1.28	2.42	1.33E-03	Up
100511550	mast cell expressed membrane protein 1(MCEMP1)	MCEMP1	1.27	2.42	4.84E-03	Up
396866	stefin A1(LOC396866)	LOC396866	1.26	2.40	7.14E-03	Up
100515166	keratin, type I cytoskeletal 13(LOC100515166)	LOC100515166	1.26	2.39	4.66E-03	Up
102166944	metallothionein-1E-like(LOC102166944)	LOC102166944	1.26	2.39	6.90E-03	Up
397106	interleukin 10(IL10)	IL10	1.25	2.38	2.59E-03	Up
100514753	ubiquitin conjugating enzyme E2 L6(UBE2L6)	UBE2L6	1.25	2.38	2.01E-03	Up
100156489	transglutaminase 1(TGM1)	TGM1	1.24	2.37	8.68E-03	Up
100127358	interferon-induced transmembrane protein 1(IFITM1)	IFITM1	1.24	2.37	1.71E-03	Up
110258600	basic salivary proline-rich protein 2-like(LOC110258600)	LOC110258600	1.24	2.36	2.44E-03	Up
100514482	anterior gradient 2, protein disulphide isomerase family member(AGR2)	AGR2	1.23	2.34	4.43E-03	Up
100628141	membrane spanning 4-domains A7(MS4A7)	MS4A7	1.23	2.34	9.92E-03	Up
100737113	keratin, type I cytoskeletal 17(LOC100737113)	LOC100737113	1.23	2.34	1.04E-02	Up
100517891	mucosal pentraxin 1(MPTX1)	MPTX1	1.22	2.33	1.02E-02	Up
100525175	placenta associated 8(PLAC8)	PLAC8	1.22	2.33	4.95E-03	Up
100515653	paired immunoglobin like type 2 receptor alpha(PILRA)	PILRA	1.21	2.32	1.01E-02	Up
100522695	interleukin 20(IL20)	IL20	1.21	2.32	9.16E-03	Up
102164569	neuregulin 1(NRG1)	NRG1	1.21	2.32	5.15E-03	Up
100516287	testis expressed 50(TEX50)	TEX50	1.21	2.32	2.93E-03	Up
102163655	uncharacterized LOC102163655(LOC102163655)	LOC102163655	1.21	2.32	1.62E-03	Up
100158037	DExD/H-box helicase 60(DDX60)	DDX60	1.21	2.32	2.01E-03	Up
100316849	ZFP36 ring finger protein(ZFP36)	ZFP36	1.21	2.32	1.06E-03	Up
494019	C-X-C motif chemokine ligand 10(CXCL10)	CXCL10	1.21	2.32	1.20E-02	Up
100525346	PVR cell adhesion molecule(PVR)	PVR	1.21	2.32	3.71E-03	Up

100101927	interferon induced with helicase C domain 1(IFIH1)	IFIH1	1.21	2.31	1.20E-03	Up
100736623	signal-regulatory protein beta-1-like(LOC100736623)	LOC100736623	1.20	2.30	1.18E-02	Up
110256379	nmrA-like family domain-containing protein 1(LOC110256379)	LOC110256379	1.20	2.30	1.03E-02	Up
100310802	STEAP4 metalloreductase(STEAP4)	STEAP4	1.20	2.29	4.40E-03	Up
100124654	C-X-C motif chemokine receptor 2(CXCR2)	CXCR2	1.19	2.28	1.25E-02	Up
100523811	matrix metallopeptidase 8(MMP8)	MMP8	1.19	2.28	1.36E-02	Up
100526085	HCK proto-oncogene, Src family tyrosine kinase(HCK)	HCK	1.19	2.28	1.62E-03	Up
100157298	SAM domain, SH3 domain and nuclear localization signals 1(SAMSN1)	SAMSN1	1.18	2.27	1.34E-02	Up
100736831	TNF superfamily member 9(TNFSF9)	TNFSF9	1.18	2.27	1.36E-02	Up
100153948	poly(ADP-ribose) polymerase family member 14(PARP14)	PARP14	1.18	2.27	3.39E-04	Up
414378	iodothyronine deiodinase 3(DIO3)	DIO3	1.18	2.27	1.49E-02	Up
397303	lipopolysaccharide binding protein(LBP)	LBP	1.18	2.26	1.54E-02	Up
100625277	uridine phosphorylase 1(UPP1)	UPP1	1.18	2.26	4.43E-03	Up
110257977	double-stranded RNA-specific adenosine deaminase-like(LOC110257977)	LOC110257977	1.17	2.26	1.55E-02	Up
110258215	progesterone receptor-like(LOC110258215)	LOC110258215	1.17	2.26	1.36E-02	Up
100037944	chitinase 3 like 2(CHI3L2)	CHI3L2	1.17	2.26	1.60E-02	Up
106505478	uncharacterized LOC106505478(LOC106505478)	LOC106505478	1.17	2.25	3.31E-03	Up
100626657	HECT and RLD domain containing E3 ubiquitin protein ligase family member 6(HERC6)	HERC6	1.17	2.24	3.09E-03	Up
397278	phorbol-12-myristate-13-acetate-induced protein 1(PMAIP1)	PMAIP1	1.17	2.24	4.00E-04	Up
100737989	lipase H(LIPH)	LIPH	1.16	2.24	8.71E-03	Up
100524399	G protein-coupled receptor 87(GPR87)	GPR87	1.16	2.24	6.87E-03	Up
733625	stratifin(SFN)	SFN	1.16	2.24	1.55E-02	Up
100521017	plasminogen activator, urokinase receptor(PLAUR)	PLAUR	1.16	2.24	7.18E-03	Up
100154994	serpin family B member 10(SERPINB10)	SERPINB10	1.16	2.23	7.42E-03	Up
100516039	C-C motif chemokine 23(LOC100516039)	LOC100516039	1.16	2.23	1.36E-02	Up
110260086	nuclear protein 1, transcriptional regulator(NUPR1)	NUPR1	1.16	2.23	1.41E-03	Up
397668	amphiregulin(AREG)	AREG	1.16	2.23	1.78E-02	Up
100511665	macrophage scavenger receptor 1(MSR1)	MSR1	1.16	2.23	2.03E-04	Up
574058	CD274 molecule(CD274)	CD274	1.16	2.23	1.80E-02	Up
100626468	solute carrier family 2 member 3(SLC2A3)	SLC2A3	1.15	2.22	2.81E-03	Up
100154319	superoxide dismutase 2(SOD2)	SOD2	1.15	2.22	1.06E-02	Up
100516458	TNF superfamily member 18(TNFSF18)	TNFSF18	1.15	2.21	2.01E-02	Up
100157144	dual specificity phosphatase 5(DUSP5)	DUSP5	1.14	2.21	7.76E-03	Up

100622156	TNF alpha induced protein 3(TNFAIP3)	TNFAIP3	1.14	2.21	7.08E-03	Up
100517204	transcription factor EC(TFEC)	TFEC	1.14	2.21	1.33E-03	Up
100738704	TNFAIP3 interacting protein 3(TNIP3)	TNIP3	1.14	2.20	1.94E-02	Up
553951	C-C motif chemokine ligand 20(CCL20)	CCL20	1.14	2.20	1.93E-02	Up
100620969	epiregulin(EREG)	EREG	1.13	2.20	2.04E-02	Up
110255823	uncharacterized LOC110255823(LOC110255823)	LOC110255823	1.13	2.19	2.05E-02	Up
110257759	UPF0329 protein ECU05_1680/ECU11_0050-like(LOC110257759)	LOC110257759	1.13	2.19	2.04E-02	Up
100187727	cadherin 3(CDH3)	CDH3	1.13	2.19	2.60E-03	Up
100156932	H2B clustered histone 14(H2BC14)	H2BC14	1.13	2.19	1.91E-02	Up
102158679	carcinoembryonic antigen-related cell adhesion molecule 5-like(LOC102158679)	LOC102158679	1.13	2.19	7.50E-03	Up
100621090	growth arrest and DNA damage inducible beta(GADD45B)	GADD45B	1.12	2.18	1.16E-02	Up
110255988	mast cell immunoglobulin like receptor 1(MILR1)	MILR1	1.12	2.18	1.12E-03	Up
397628	angiopoietin like 4(ANGPTL4)	ANGPTL4	1.12	2.17	2.07E-02	Up
100125829	mucin 13, cell surface associated(MUC13)	MUC13	1.12	2.17	1.84E-03	Up
110257903	granulocyte-macrophage colony-stimulating factor receptor subunit alpha-like(LOC110257903)	LOC110257903	1.12	2.17	1.57E-02	Up
100156127	H2B clustered histone 6(H2BC6)	H2BC6	1.12	2.17	2.18E-02	Up
106510322	uncharacterized LOC106510322(LOC106510322)	LOC106510322	1.12	2.17	2.18E-02	Up
110255217	interferon lambda-3-like(LOC110255217)	LOC110255217	1.11	2.16	2.07E-02	Up
100626110	TRAF interacting protein(TRAIP)	TRAIP	1.11	2.16	2.90E-03	Up
100511886	fibroblast growth factor binding protein 1(FGFBP1)	FGFBP1	1.11	2.16	2.49E-02	Up
397564	heparin binding EGF like growth factor(HBEGF)	HBEGF	1.11	2.16	1.71E-03	Up
100624161	G0/G1 switch 2(G0S2)	G0S2	1.11	2.16	2.42E-02	Up
110257911	uncharacterized LOC110257911(LOC110257911)	LOC110257911	1.11	2.16	2.64E-02	Up
100156146	ADAM metallopeptidase domain 8(ADAM8)	ADAM8	1.11	2.16	1.78E-02	Up
397588	eukaryotic translation initiation factor 2 alpha kinase 2(EIF2AK2)	EIF2AK2	1.10	2.15	2.81E-03	Up
396724	oxidized low density lipoprotein receptor 1(OLR1)	OLR1	1.10	2.14	1.05E-02	Up
110255948	galectin 3 binding protein(LGALS3BP)	LGALS3BP	1.10	2.14	9.07E-04	Up
100524379	peptidyl arginine deiminase 3(PADI3)	PADI3	1.10	2.14	2.11E-02	Up
733644	Rh family C glycoprotein(RHCG)	RHCG	1.10	2.14	2.17E-02	Up
100622162	transient receptor potential cation channel subfamily V member 5(TRPV5)	TRPV5	1.10	2.14	2.31E-02	Up
100520876	sorting nexin 10(SNX10)	SNX10	1.10	2.14	2.81E-03	Up
397122	interleukin 1 beta(IL1B)	IL1B	1.09	2.14	1.65E-02	Up
397086	tumor necrosis factor(TNF)	TNF	1.09	2.13	2.93E-02	Up

100737399	TNF receptor superfamily member 8(TNFRSF8)	TNFRSF8	1.09	2.13	8.31E-03	Up
396873	transcobalamin 1(TCN1)	TCN1	1.09	2.13	2.44E-02	Up
100152200	BCL2 interacting protein 5(BNIP5)	BNIP5	1.09	2.13	4.40E-03	Up
396915	endothelin 1(EDN1)	EDN1	1.09	2.13	3.02E-02	Up
100525396	growth-regulated protein homolog gamma-like(LOC100525396)	LOC100525396	1.09	2.12	3.07E-02	Up
110261664	H3 clustered histone 12(H3C12)	H3C12	1.09	2.12	2.64E-02	Up
100519098	sterile alpha motif domain-containing protein 9(LOC100519098)	LOC100519098	1.08	2.12	2.64E-03	Up
100525349	transmembrane protein 156(TMEM156)	TMEM156	1.08	2.11	1.59E-02	Up
100522887	caspase-13(LOC100522887)	LOC100522887	1.08	2.11	6.44E-03	Up
100512496	ras related dexamethasone induced 1(RASD1)	RASD1	1.08	2.11	1.41E-03	Up
100514823	NLR family pyrin domain containing 3(NLRP3)	NLRP3	1.08	2.11	1.91E-02	Up
396862	TIMP metallopeptidase inhibitor 1(TIMP1)	TIMP1	1.08	2.11	2.89E-02	Up
100126285	free fatty acid receptor 2(FFAR2)	FFAR2	1.07	2.10	3.49E-02	Up
397195	adrenomedullin(ADM)	ADM	1.07	2.10	1.62E-03	Up
102158335	uncharacterized LOC102158335(LOC102158335)	LOC102158335	1.06	2.09	1.88E-02	Up
100626247	interferon-induced transmembrane protein 1-like(LOC100626247)	LOC100626247	1.06	2.09	4.43E-03	Up
100151816	interferon induced protein with tetratricopeptide repeats 5(IFIT5)	IFIT5	1.06	2.08	2.90E-03	Up
100738744	H2B clustered histone 19(H2BC19)	H2BC19	1.06	2.08	2.97E-02	Up
397158	5-hydroxytryptamine receptor 7(HTR7)	HTR7	1.05	2.08	1.92E-02	Up
102161418	interferon-induced transmembrane protein 1-like(LOC102161418)	LOC102161418	1.05	2.07	1.76E-02	Up
100622812	dual specificity phosphatase 2(DUSP2)	DUSP2	1.05	2.07	3.17E-02	Up
396648	heat shock protein 70.2(HSP70.2)	HSP70.2	1.05	2.07	4.31E-03	Up
100622710	leukocyte immunoglobulin-like receptor subfamily B member 3(LOC100622710)	LOC100622710	1.05	2.07	3.70E-02	Up
100152428	ATP binding cassette subfamily C member 13(ABCC13)	ABCC13	1.04	2.06	2.83E-02	Up
397346	matrix metallopeptidase 13(MMP13)	MMP13	1.04	2.06	3.28E-02	Up
100049692	serglycin(SRGN)	SRGN	1.04	2.05	2.11E-02	Up
110261673	H4 clustered histone 8(H4C8)	H4C8	1.04	2.05	2.44E-02	Up
100627962	chromosome 4 C1orf162 homolog(C4H1orf162)	C4H1orf162	1.04	2.05	3.54E-02	Up
102161654	tyrosine-protein phosphatase non-receptor type substrate 1(LOC102161654)	LOC102161654	1.04	2.05	6.54E-03	Up
100515345	C-X-C chemokine receptor type 2(LOC100515345)	LOC100515345	1.04	2.05	3.94E-02	Up
100625728	complement C3a receptor 1(C3AR1)	C3AR1	1.04	2.05	2.95E-02	Up
100627227	nucleophosmin/nucleoplasmin 3(NPM3)	NPM3	1.03	2.05	2.94E-02	Up
100187577	LDL receptor related protein 8(LRP8)	LRP8	1.03	2.05	1.02E-02	Up

100736799	BPI fold containing family B member 6(BPIFB6)	BPIFB6	1.03	2.05	3.47E-02	Up
100152215	cyclin dependent kinase inhibitor 1A(CDKN1A)	CDKN1A	1.03	2.04	4.75E-03	Up
100518075	peptidyl-prolyl cis-trans isomerase E-like(LOC100518075)	LOC100518075	1.03	2.04	4.69E-02	Up
100517285	leukocyte immunoglobulin-like receptor subfamily A member 6(LOC100517285)	LOC100517285	1.03	2.04	3.91E-02	Up
397508	selectin E(SELE)	SELE	1.03	2.04	4.71E-02	Up
448981	complement C2(C2)	C2	1.02	2.03	2.25E-03	Up
100519082	interferon-induced transmembrane protein 1(LOC100519082)	LOC100519082	1.02	2.03	5.16E-03	Up
100739264	hes family bHLH transcription factor 4(HES4)	HES4	1.02	2.03	2.14E-02	Up
100522855	hexokinase 3(HK3)	HK3	1.02	2.03	3.17E-02	Up
100124383	complement factor B(CFB)	CFB	1.02	2.03	1.58E-02	Up
399500	interleukin 6(IL6)	IL6	1.02	2.03	3.02E-02	Up
106504105	purinergic receptor P2X 1(P2RX1)	P2RX1	1.02	2.03	4.20E-02	Up
106507710	uncharacterized LOC106507710(LOC106507710)	LOC106507710	1.02	2.03	1.58E-02	Up
106508640	uncharacterized LOC106508640(LOC106508640)	LOC106508640	1.02	2.02	4.97E-02	Up
100515919	cathepsin L(CTSL)	CTSL	1.01	2.02	4.38E-02	Up
100519694	proline-serine-threonine phosphatase interacting protein 2(PSTPIP2)	PSTPIP2	1.01	2.02	3.46E-02	Up
100516257	pleckstrin(PLEK)	PLEK	1.01	2.02	3.70E-02	Up
100524951	aconitate decarboxylase 1(ACOD1)	ACOD1	1.01	2.01	2.74E-02	Up
396892	pepsinogen 5, group I (pepsinogen A)(PGA5)	PGA5	1.01	2.01	4.33E-02	Up
100038024	interleukin 19(IL19)	IL19	1.00	2.00	3.94E-02	Up
448812	insulin like growth factor binding protein 3(IGFBP3)	IGFBP3	1.00	2.00	1.34E-02	Up
414905	troponin C2, fast skeletal type(TNNC2)	TNNC2	-1.00	0.50	2.95E-02	Down
110260219	gasdermin-D-like(LOC110260219)	LOC110260219	-1.01	0.50	3.01E-02	Down
100302021	claudin 8(CLDN8)	CLDN8	-1.02	0.49	2.29E-02	Down
102158352	uncharacterized LOC102158352(LOC102158352)	LOC102158352	-1.02	0.49	3.70E-02	Down
100515999	secretoglobin family 3A member 1(SCGB3A1)	SCGB3A1	-1.03	0.49	3.58E-02	Down
110258406	uncharacterized LOC110258406(LOC110258406)	LOC110258406	-1.03	0.49	4.64E-02	Down
100523187	myosin binding protein C1(MYBPC1)	MYBPC1	-1.03	0.49	4.15E-02	Down
100516058	glycoprotein hormone subunit alpha 2(GPHA2)	GPHA2	-1.04	0.49	2.07E-02	Down
110260276	uncharacterized LOC110260276(LOC110260276)	LOC110260276	-1.05	0.48	3.91E-02	Down
100156376	cadherin 7(CDH7)	CDH7	-1.05	0.48	3.91E-02	Down
397198	surfactant protein D(SFTPD)	SFTPD	-1.06	0.48	3.49E-02	Down
100523824	myomesin 2(MYOM2)	MYOM2	-1.06	0.48	3.52E-02	Down

100157195	dipeptidyl peptidase like 10(DPP10)	DPP10	-1.07	0.48	1.59E-02	Down
100627869	fer-1 like family member 5(FER1L5)	FER1L5	-1.08	0.47	1.66E-02	Down
100513608	pleckstrin homology domain containing B1(PLEKHB1)	PLEKHB1	-1.10	0.47	1.69E-02	Down
100518920	achaete-scute family bHLH transcription factor 3(ASCL3)	ASCL3	-1.11	0.46	2.11E-02	Down
574060	myozenin 1(MYOZ1)	MYOZ1	-1.14	0.46	1.87E-02	Down
110255347	uncharacterized LOC110255347(LOC110255347)	LOC110255347	-1.14	0.45	2.94E-03	Down
100627664	leucine rich repeat containing 15(LRRC15)	LRRC15	-1.14	0.45	2.44E-03	Down
102157759	uncharacterized LOC102157759(LOC102157759)	LOC102157759	-1.20	0.44	1.02E-02	Down
110255872	F-box only protein 36-like(LOC110255872)	LOC110255872	-1.22	0.43	1.01E-02	Down
397503	surfactant protein A1(SFTPA1)	SFTPA1	-1.24	0.42	9.15E-03	Down
733580	surfactant protein C(SFTPC)	SFTPC	-1.28	0.41	2.90E-03	Down
100515976	nebulin(NEB)	NEB	-1.35	0.39	2.81E-03	Down
106508382	proline-rich protein 18-like(LOC106508382)	LOC106508382	-1.40	0.38	1.60E-03	Down
110257589	uncharacterized LOC110257589(LOC110257589)	LOC110257589	-1.45	0.37	1.24E-04	Down
110255871	F-box only protein 36-like(LOC110255871)	LOC110255871	-1.50	0.35	5.01E-04	Down
100736733	intelectin-2-like(LOC100736733)	LOC100736733	-1.58	0.33	3.12E-04	Down

Supplementary Table 3: List of 28 differentially expressed genes in the pigs infected with the huH1N1pdm09 strain compared to mock inoculated control pigs.

GeneID	Description	Symbol	Log2 Fold Change	Relative Fold Change	Padj (q-value)	Expression
110261124	interferon alpha inducible protein 6(IFI6)	IFI6	2.48	5.59	4.43E-44	Up
100153902	putative ISG12(a) protein(ISG12(A))	ISG12(A)	1.49	2.82	3.46E-17	Up
102159947	XIAP associated factor 1(XAF1)	XAF1	1.44	2.71	3.36E-12	Up
100145895	ISG15 ubiquitin like modifier(ISG15)	ISG15	1.29	2.44	5.75E-07	Up
397628	angiopoietin like 4(ANGPTL4)	ANGPTL4	1.23	2.35	3.22E-06	Up
396752	radical S-adenosyl methionine domain containing 2(RSAD2)	RSAD2	1.20	2.29	3.09E-07	Up
100153038	interferon-induced protein with tetratricopeptide repeats 1(IFIT1)	IFIT1	1.18	2.27	8.65E-11	Up
110256385	receptor transporter protein 4(RTP4)	RTP4	1.17	2.24	3.25E-08	Up
396893	myxovirus (influenza virus) resistance 2 (mouse)(MX2)	MX2	1.14	2.21	5.75E-07	Up
396723	RNA sensor RIG-I(RIGI)	RIGI	1.12	2.17	8.69E-08	Up
100037289	interferon regulatory factor 7(IRF7)	IRF7	1.10	2.15	3.02E-07	Up
397570	2'-5'-oligoadenylate synthetase 1(OAS1)	OAS1	1.10	2.15	2.72E-05	Up
100525523	interferon induced protein 44(IFI44)	IFI44	1.08	2.11	9.05E-08	Up
100158037	DExD/H-box helicase 60(DDX60)	DDX60	1.05	2.07	4.89E-06	Up
110255948	galectin 3 binding protein(LGALS3BP)	LGALS3BP	1.05	2.06	7.47E-10	Up
397128	MX dynamin like GTPase 1(MX1)	MX1	1.04	2.05	3.13E-06	Up
100302088	bone marrow stromal cell antigen 2(BST2)	BST2	1.01	2.01	4.83E-05	Up
397143	carbonyl reductase 1(CBR1)	CBR1	-1.01	0.50	9.04E-05	Down
100156195	circadian associated repressor of transcription(CIART)	CIART	-1.02	0.49	1.70E-08	Down
641342	nuclear receptor subfamily 1 group D member 1(NR1D1)	NR1D1	-1.05	0.48	1.77E-04	Down
100620175	fer-1 like family member 6(FER1L6)	FER1L6	-1.09	0.47	1.77E-04	Down
106505337	uncharacterized LOC106505337(LOC106505337)	LOC106505337	-1.14	0.45	8.23E-05	Down
100519542	collagen type XXVI alpha 1 chain(COL26A1)	COL26A1	-1.15	0.45	2.64E-05	Down
102158081	N-acetyltransferase 8 like(NAT8L)	NAT8L	-1.16	0.45	4.52E-05	Down
396852	microseminoprotein beta(MSMB)	MSMB	-1.20	0.44	1.10E-06	Down
100523675	activating transcription factor 5(ATF5)	ATF5	-1.22	0.43	1.36E-07	Down
100524747	D-box binding PAR bZIP transcription factor(DBP)	DBP	-1.35	0.39	3.89E-09	Down
102166275	myomesin 3(MYOM3)	MYOM3	-1.36	0.39	9.29E-08	Down

Supplementary Table 3: List of 52 differentially expressed genes in the pigs infected with the huH1N1pdm09 strain compared to the pigs infected with the swH1N1pdm09 strain.

GeneID	Description	Symbol	Log2 Fold Change	Relative Fold Change	Padj (q-value)	Expression
100513599	synaptotagmin 1(SYT1)	SYT1	1.21	2.32	3.62E-02	Up
100738087	neuronal vesicle trafficking associated 2(NSG2)	NSG2	1.15	2.21	3.69E-02	Up
100736733	intelectin-2-like(LOC100736733)	LOC100736733	1.11	2.16	3.76E-02	Up
100515741	UDP-glucuronosyltransferase 2B31(LOC100515741)	LOC100515741	1.11	2.16	3.69E-02	Up
100153400	internexin neuronal intermediate filament protein alpha(INA)	INA	1.10	2.14	4.40E-02	Up
100622938	paired like homeobox 2B(PHOX2B)	PHOX2B	1.10	2.14	4.40E-02	Up
100524828	peroxisomal biogenesis factor 5 like(PEX5L)	PEX5L	1.07	2.10	3.62E-02	Up
100622102	kinesin family member 5C(KIF5C)	KIF5C	1.06	2.09	3.69E-02	Up
110257589	uncharacterized LOC110257589(LOC110257589)	LOC110257589	1.05	2.07	4.40E-02	Up
100518072	calpain small subunit 2(CAPNS2)	CAPNS2	1.04	2.06	3.77E-02	Up
100514834	uncharacterized LOC100514834(LOC100514834)	LOC100514834	1.02	2.03	4.60E-02	Up
100135681	C-X-C motif chemokine ligand 9(CXCL9)	CXCL9	1.02	2.03	3.62E-02	Up
100524634	neuropeptide FF receptor 2(NPFFR2)	NPFFR2	1.02	2.02	4.60E-02	Up
102162791	uncharacterized LOC102162791(LOC102162791)	LOC102162791	-1.00	0.50	3.69E-02	Down
100152200	BCL2 interacting protein 5(BNIP5)	BNIP5	-1.02	0.49	3.76E-02	Down
110255958	thymidine kinase 1(TK1)	TK1	-1.02	0.49	3.77E-02	Down
100286809	protein kinase, membrane associated tyrosine/threonine 1(PKMYT1)	PKMYT1	-1.03	0.49	3.98E-02	Down
100155736	lipase G, endothelial type(LIPG)	LIPG	-1.03	0.49	3.69E-02	Down
100154248	interferon induced protein with tetratricopeptide repeats 3(IFIT3)	IFIT3	-1.03	0.49	4.65E-02	Down
102164968	keratin 6A(KRT6A)	KRT6A	-1.03	0.49	4.63E-02	Down
399532	fatty acid binding protein 3(FABP3)	FABP3	-1.03	0.49	4.76E-02	Down
100518612	MFSD2 lysolipid transporter A, lysophospholipid(MFSD2A)	MFSD2A	-1.03	0.49	4.72E-02	Down
100157235	inter-alpha-trypsin inhibitor heavy chain 3(ITIH3)	ITIH3	-1.05	0.48	3.50E-02	Down
100518723	interleukin 21 receptor(IL21R)	IL21R	-1.05	0.48	4.40E-02	Down
100316853	ribonucleotide reductase regulatory subunit M2(RRM2)	RRM2	-1.05	0.48	3.69E-02	Down
102162068	NFAT activating protein with ITAM motif 1(NFAM1)	NFAM1	-1.06	0.48	4.40E-02	Down
100157925	S100 calcium binding protein A3(S100A3)	S100A3	-1.06	0.48	4.89E-02	Down
100514149	solute carrier family 22 member 20(SLC22A20)	SLC22A20	-1.07	0.48	4.60E-02	Down
100154053	SLAM family member 7(SLAMF7)	SLAMF7	-1.07	0.48	4.65E-02	Down
100153133	ubiquitin conjugating enzyme E2 C(UBE2C)	UBE2C	-1.07	0.48	3.69E-02	Down

100524265	C-X-C motif chemokine ligand 13(CXCL13)	CXCL13	-1.09	0.47	4.55E-02	Down
396752	radical S-adenosyl methionine domain containing 2(RSAD2)	RSAD2	-1.10	0.47	4.40E-02	Down
445511	casein kappa(CSN3)	CSN3	-1.10	0.47	4.14E-02	Down
100521759	beaded filament structural protein 1(BFSP1)	BFSP1	-1.10	0.47	4.12E-02	Down
100038024	interleukin 19(IL19)	IL19	-1.12	0.46	3.69E-02	Down
100627227	nucleophosmin/nucleoplasmin 3(NPM3)	NPM3	-1.13	0.46	3.69E-02	Down
100525292	CTP synthase 1(CTPS1)	CTPS1	-1.14	0.45	3.39E-02	Down
100517891	mucosal pentraxin 1(MPTX1)	MPTX1	-1.14	0.45	3.72E-02	Down
733625	stratifin(SFN)	SFN	-1.15	0.45	3.69E-02	Down
102166961	uncharacterized LOC102166961(LOC102166961)	LOC102166961	-1.16	0.45	3.69E-02	Down
100513324	interleukin 22 receptor subunit alpha 2(IL22RA2)	IL22RA2	-1.17	0.44	3.69E-02	Down
100512730	thyroid hormone responsive(THRSP)	THRSP	-1.17	0.44	3.62E-02	Down
100524769	thymus, brain and testes associated(TBATA)	TBATA	-1.17	0.44	3.50E-02	Down
100522695	interleukin 20(IL20)	IL20	-1.20	0.44	3.62E-02	Down
100520988	growth differentiation factor 5(GDF5)	GDF5	-1.26	0.42	3.50E-02	Down
100627962	chromosome 4 C1orf162 homolog(C4H1orf162)	C4H1orf162	-1.27	0.41	3.39E-02	Down
102159603	uncharacterized LOC102159603(LOC102159603)	LOC102159603	-1.30	0.41	1.35E-02	Down
100737113	keratin, type I cytoskeletal 17(LOC100737113)	LOC100737113	-1.36	0.39	1.80E-02	Down
397411	matrix metallopeptidase 7(MMP7)	MMP7	-1.47	0.36	1.52E-04	Down
100049690	patatin like phospholipase domain containing 3(PNPLA3)	PNPLA3	-1.55	0.34	1.86E-03	Down
100152209	glutathione S-transferase omega 2(GSTO2)	GSTO2	-1.56	0.34	1.86E-03	Down
100515166	keratin, type I cytoskeletal 13(LOC100515166)	LOC100515166	-1.65	0.32	1.36E-04	Down

4.5 Paper 5

Innate antiviral responses in porcine nasal mucosal explants inoculated with influenza A virus are comparable with responses in respiratory tissues after viral infection

Sofie M. R. Starbæk, Malene Rask Andersen, Louise Brogaard, Anna Spinelli, Victoria Rapson, **Helena Aagaard Glud**, Lars Erik Larsen, Peter M. H. Heegaard, Hans Nauwynck, and Kerstin Skovgaard

Corresponding Author: Kerstin Skovgaard, kesk@dtu.dk

Published in Immunobiology (2022) 127: 152192.

doi.org/10.1016/j.imbio.2022.152192

Immunobiology 227 (2022) 152192

Contents lists available at ScienceDirect

Immunobiology

journal homepage: www.elsevier.com/locate/imbio

Innate antiviral responses in porcine nasal mucosal explants inoculated with influenza A virus are comparable with responses in respiratory tissues after viral infection

Sofie M.R. Starbæk [a,1], Malene Rask Andersen [b,1], Louise Brogaard [a,2], Anna Spinelli [a], Victoria Rapson [a], Helena Aagaard Glud [a], Lars E. Larsen [c], Peter M.H. Heegaard [a,d], Hans Nauwynck [e], Kerstin Skovgaard [a,*]

[a] Department of Biotechnology and Biomedicine, Technical University of Denmark, Kgs. Lyngby, Denmark
[b] National Veterinary Institute, Technical University of Denmark, Kgs. Lyngby, Denmark
[c] Department of Veterinary and Animal Sciences, University of Copenhagen, Frederiksberg, Denmark
[d] Department of Health Technology, Technical University of Denmark, Kgs. Lyngby, Denmark
[e] Faculty of Veterinary Medicine, Ghent University, Belgium

ARTICLE INFO

Keywords:
Ex vivo
Gene expression
Influenza A virus
Innate immune response
Porcine mucosal explant
Pig
Influenza infection model

ABSTRACT

Nasal mucosal explant (NEs) cultured at an air–liquid interface mimics *in vivo* conditions more accurately than monolayer cultures of respiratory cell lines or primary cells cultured in flat-bottom microtiter wells. NEs might be relevant for studies of host-pathogen interactions and antiviral immune responses after infection with respiratory viruses, including influenza and corona viruses.

Pigs are natural hosts for swine influenza A virus (IAV) but are also susceptible to IAV from humans, emphasizing the relevance of porcine NEs in the study of IAV infection. Therefore, we performed fundamental characterization and study of innate antiviral responses in porcine NEs using microfluidic high-throughput quantitative real-time PCR (qPCR) to generate expression profiles of host genes involved in inflammation, apoptosis, and antiviral immune responses in mock inoculated and IAV infected porcine NEs.

Handling and culturing of the explants *ex vivo* had a significant impact on gene expression compared to freshly harvested tissue. Upregulation (2–43 fold) of genes involved in inflammation, including *IL1A* and *IL6*, and apoptosis, including *FAS* and *CASP3*, and downregulation of genes involved in viral recognition (MDA5 (*IFIH1*)), interferon response (*IFNA*), and response to virus (*OAS1*, *IFIT1*, *MX1*) was observed. However, by comparing time-matched mock and virus infected NEs, transcription of viral pattern recognition receptors (RIG-I (*DDX58)*, MDA5 (*IFIH1*), *TLR3*) and type I and III interferons (*IFNB1*, *IL28B (IFNL3)*) were upregulated 2–16 fold in IAV-infected NEs. Furthermore, several interferon-stimulated genes including *MX1*, *MX2*, *OAS*, *OASL*, *CXCL10*, and *ISG15* was observed to increase 2–26 fold in response to IAV inoculation. NE expression levels of key genes involved in antiviral responses including *IL28B* (*IFNL3*), *CXCL10*, and *OASL* was highly comparable to expression levels found in respiratory tissues including nasal mucosa and lung after infection of pigs with the same influenza virus isolate.

1. Introduction

Influenza A virus (IAV) is a zoonotic respiratory pathogen of global importance in veterinary and human health. Although aquatic birds are the natural reservoir for IAV, other species such as humans and pigs can be hosts. IAV belongs to the *Orthomyxoviridae* family and is a single-stranded, negative-sense RNA virus with a characteristic segmented genome. The surface glycoproteins hemagglutinin (HA) and

* Corresponding author at: Kerstin Skovgaard, Department of Biotechnology and Biomedicine, Technical University of Denmark, Søltofts Plads, Building 224, 2800 Kgs. Lyngby, Denmark.
E-mail address: kesk@dtu.dk (K. Skovgaard).
[1] Shared first authorship.
[2] Current affiliation: Department of Veterinary and Animal Sciences, University of Copenhagen, Frederiksberg, Denmark.

https://doi.org/10.1016/j.imbio.2022.152192
Received 9 August 2021; Received in revised form 15 February 2022; Accepted 19 February 2022
Available online 22 February 2022

neuraminidase (NA) determine the virus subtype (Yoon et al., 2014).

IAV infection in mammals is in general restricted to the respiratory tract. IAV enters the hosts through the nasal cavity, where they encounter the mucosal surface as the first barrier towards infection (Starbæk et al., 2018). Infection of host cells is subsequently mediated through attachment of HA to sialic acid(SA)-coated surface glycoproteins of the respiratory epithelium. The configuration of the SA-linkage is considered a major determinant of IAV host specificity, as avian IAV prefer binding to α2,3-linked SAs, while mammalian IAV generally prefer α2,6-linked SAs (Webster et al., 1992; Byrd-Leotis et al., 2017).

Nasal mucosal explants (NEs) cultured at an air–liquid interface resemble the *in vivo* situation more accurately than cells grown in 2D flasks or culture plates. NEs maintain tissue complexity and cell–cell interactions including apical tight junctions, intermediate junctions, and desmosomes of the nasal mucosa of healthy individuals (Denney and Ho, 2018). Furthermore, porcine NEs are easily acquired from slaughterhouses and have been shown to remain viable and exhibit minimal changes in morphology, ciliary beating, and number of apoptotic cells for up to 72 h of cultivation at an air–liquid interface (Glorieux et al., 2007; Tulinski et al., 2013). Porcine NEs therefore represent a highly relevant viral infection model for studies of host-pathogen interactions and pathogenesis. Importantly, using NEs as a replacement for live animals is in accordance with the 3R principle, seeking to reduce the number of animals included in a given study (Tannenbaum and Bennett, 2015).

NE models to study bacterial and viral infection have been established for humans (Jang et al., 2005; Glorieux et al., 2011; Cantero et al., 2013), pigs (Van Poucke et al., 2010), horses (Vairo et al., 2013), cattle (Niesalla et al., 2009; Steukers et al., 2012), sheep (Mazzetto et al., 2020) and ferrets (Roberts et al., 2011). Porcine NEs are low cost and easily available, and both human and porcine NEs have been used in studies of respiratory viruses (Pol et al., 1991; Jang et al., 2005; Glorieux et al., 2007; Van Poucke et al., 2013; Frydas and Nauwynck, 2016), three-dimensional modelling of virus invasion (Glorieux et al., 2009), elucidation of virulence factors of pandemic influenza (Pena et al., 2012), and for comparative analysis of innate immune responses after infection with SARS-CoV-2 and IAV (Alfi et al., 2021). However, to the best of our knowledge, innate immune factors centrally involved in IAV recognition and control have not been studied in porcine nasal explants before.

The similarity of the anatomy (e.g. epithelial cell distribution) of the upper respiratory system including the nasal cavity of pigs and humans has recently been reviewed by us and others (Rajao and Vincent, 2015; Iwatsuki-horimoto et al., 2017; Starbæk et al., 2018). Distribution and quantities of mucus–producing goblet cells and ciliated epithelial cells are highly similar, as is the distribution of SA-coated viral receptors in nasal cavities of pigs and humans, thus rendering porcine NEs a promising model also for human respiratory infections (Spicer et al., 1983; Wallace et al., 1994; Shinya et al., 2006; Zhang et al., 2009; Trebbien et al., 2011).

The antiviral immune response to IAV infection is initiated by recognition of the viral pathogen by pattern recognition receptors (PRR) of the host cells in the nasal mucosa and along the respiratory tract. PRRs such as RIG-I (*DDX58*), TLR3, and MDA5 (*IFIH1*) will detect viral RNA in the host cell cytoplasm and activate the expression of type I and III interferons (IFNs), which induce the expression of a wide range of antiviral interferon-stimulated genes (ISGs) in infected and neighboring cells (Kato et al., 2006; Pichlmair et al., 2006; Brogaard et al., 2018). The local production of ISGs at the site of infection establishes an antiviral state, where components like MX1, OAS1, OASL, and CXCL10 are important for controlling the IAV replication and production of infectious viral progeny during the first days of disease (Skovgaard et al., 2013; Delgado-Ortega et al., 2014; Kim et al., 2015; Brogaard et al., 2018).

To examine the utility of porcine NEs for the study of host responses to IAV infection, 69 NEs isolated from 11 different pigs were used in this study to analyze the transcriptional response to culturing and to IAV exposure.

2. Materials and methods

2.1. Animals

Data presented in this study originates from three independent trials, comprising 69 NEs collected from 11 different pigs (cross-bred Landrace × Yorkshire × Duroc) (Table 1). Animals were acquired from farms of high health status without prior history of respiratory infections. No IAV-specific antibodies were detected in serum samples from the animals prior to the experiment using a commercial ELISA Kit (IDEXX) following the manufacturer's instructions.

Trial 1: 11 NEs were obtained from each of three 6-weeks old piglets (total no. of explants = 33), provided from a herd located in Holbæk, Denmark. The pigs were treated with broad-spectrum antibiotics (200 mg Alamycin containing oxytetracycline, ScanVet, Fredensborg) daily, from three days before euthanasia. At euthanasia, the animals were anesthetized by intramuscular injection of 0.1 ml/kg Zoletil 50 VET (tiletamine 25 mg/ml, zolazepam 25 mg/ml) and euthanized by intracardiac injection of 20 % sodium pentobarbital (KELA, 150 mg/kg).

Trial 2: 12 NEs were obtained from each of two 6-weeks old piglets at Ghent University (total no. of explants = 24). Animals were obtained, treated, and euthanized as described by Glorieux et al. (2007).

Trial 3: Two NEs from each of six 6-weeks old piglets were included in this study (total no. of explants = 12). These animals originated from the same farm as trial 1. Euthanasia was performed as described in trial 1, but animals were not treated with antibiotics prior to euthanasia.

All work has been carried out in accordance with the EU Directive 2010/63/EU for animal experiments.

Gene expression data from nasal mucosal tissue and lung tissue were included for benchmarking our nasal mucosal explants to respiratory tissue isolated from IAV infected pigs (Brogaard et al., 2018; Starbæk et al. in prep). The same A/swine/Denmark/12687/2003 (H1N2) isolate was used for inoculation in all included studies. Lung samples from cross-bred Large White × German Landrace challenged by aerosol exposure were obtained 72 hpi (infected n = 6 and control n = 5) and nasal mucosal tissue from Göttingen Minipigs inoculated by an

Table 1
Sampling and inoculation of nasal mucosal explants. Trial 1 was conducted at the National Veterinary Institute, Technical University of Denmark and included three 6-weeks old pigs, from each of which 11 nasal mucosal explants (NEs) were isolated. Trial 2 included two 6-weeks old pigs from each of which 12 NEs were isolated. This trial was performed at Ghent University, Belgium. Trial 3 was conducted at the National Veterinary Institute, Denmark and included six 6–week old pigs from each of which two explants were isolated. Hours post inoculation (hpi).

Trial	Number of pigs	Number of NEs	Sampling time (hpi)	Number of NEs/time point	Inoculation
1	3	33 (11/pig)	−20	3	3 mock
			0	3	3 mock
			1	9	3 mock + 6 IAV
			24	9	3 mock + 6 IAV
			48	9	3 mock + 6 IAV
2	2	24 (12/pig)	1	8	4 mock + 4 IAV
			24	8	4 mock + 4 IAV
			48	8	4 mock + 4 IAV
3	6	12 (2/pig)	24	6	6 mock
			48	6	6 mock

intranasal mucosal atomisation device were obtained 4 days post infection (infected n = 7 and control n = 5). Further details have been described in (Brogaard et al., 2018; Starbæk et al. in prep respectively).

2.2. Isolation, culture, inoculation, and sampling of nasal mucosal explants

NEs from all trials were isolated and cultured as described by Glorieux et al. (2007) with minor modifications. Briefly, after euthanasia snouts were sawn off the skull in front of the eyes and stripped of skin and muscle tissue. The snouts were split open and mucosa was stripped from the underlying cartilage in the nasal cavity (septum and conchae) and divided into 0.25 cm^2 squares and placed with the epithelium surface upwards on modified cell strainers (VWR) (trial 1 and 3) or stainless-steel supports (trial 2), dimensioned to support the NEs at an air–liquid interface. At this time point (−20 h post inoculation (hpi)), three NEs (trial 1) were harvested and stored in RNAlater (Qiagen). NEs were supplied with serum-free culture medium from the basal side. The NEs were cultured for approximately 20 h at 37 °C and 5% CO_2, before three NEs (trial 1) were collected (0 hpi), divided into two pieces, one half was stored in RNAlater at −20 °C and the other in PBS at −80 °C. The NEs were inoculated with 0.6 ml virus suspension containing 10^4 (trial 2) and 10^5 (trial 1) $TCID_{50}$ of A/swine/Denmark/12687/2003 (H1N2) or virus-free growth medium (mock) (trial 1, 2, and 3) and incubated for 1 h at 37 °C and 5 % CO_2. After inoculation, the explants were washed three times in pre-heated culture medium (37 °C) and placed at an air–liquid interface in fresh pre-heated culture medium (37 °C) (Fig. 1). The culture medium consisted of 1:1 RPMI (Gibco) and DMEM (Gibco) supplemented by 0.1 μg/ml gentamicin (Gibco) and 100 U/ml penicillin and 0.1 mg/ml streptomycin (Gibco) (trial 1 and 2). In trial 3, the amounts of penicillin and streptomycin was increased to 1000 U/ml and 1 mg/ml respectively, gentamicin was increased to 0.5 mg/ml and finally 5 μg/ml amphotericin B "Fungizone" was added to compensate for the lack of pre-euthanasia antibiotic treatment in these piglets compared to the method described by Glorieux et al. (2007). The virus growth medium varied slightly in trypsin concentration (1 μg/ml trypsin TPCK (Sigma-Aldrich) (trial 1 and 3) vs. 0.4 μl/ml (trial 2)). Furthermore, 1 % BME vitamins were added to medium in trial 1 and 3.

NEs were harvested at 1 hpi, 24 hpi, and 48 hpi, one piece stored in RNAlater at −20 °C and the other in PBS at −80 °C (trial 1 and 3). NEs from trial 2 were preserved in one piece in RNAlater. NEs from trial 3 were not inoculated with IAV and were only used in combination with uninfected NEs from trial 1 to study gene expression as a consequence of the *ex vivo* conditions after mock inoculation. Number of pigs and NEs,

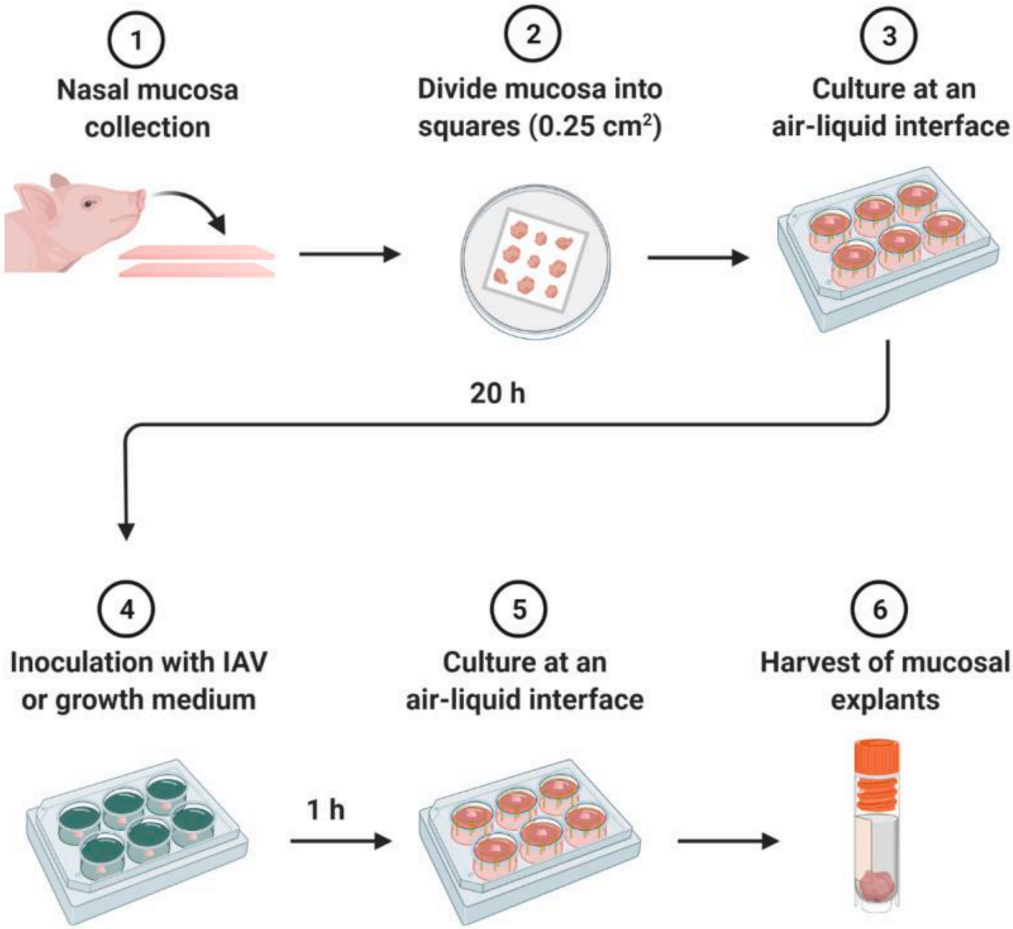

Fig. 1. Schematic representation of the experimental setup. Nasal mucosal isolation (1), air–liquid interface culture procedure (2–3),inoculation with IAV (4), and further cultivation and harvest (5-6). The figure was created with BioRender.com.

as well as treatment and time of harvesting in each trial is summarized in Table 1.

2.3. Viability of cells in nasal mucosal explants and bacterial contamination

The extend of apoptosis was assessed in NEs of trial 2 by termal deoxynucleotidyl transferase dUTP nick end labelling (TUNEL) assay as described by Glorieux et al. (2007). Matrix-assisted laser desorption/ionization time-of-flight mass spectrometry (MALDI-TOF MS) was used to check for bacterial contamination of growth medium before and after NE cultivation as previously described (Nonnemann et al., 2019).

2.4. Reverse transcription (RT)-qPCR analysis

Total RNA was extracted from NEs stabilized in RNAlater as described previously (Barington et al., 2018). Briefly, explants were homogenized in QIAzol Lysis reagent (Qiagen) using gentleMACS M-tubes (Miltenyi Biotec). RNA was extracted using the miRNeasy mini kit (Qiagen) and treated with RNase-free DNase set (Qiagen) according to the manufacturer's instructions. RNA quantity, purity, and integrity were estimated using the Nanodrop ND-1000 spectrophotometer (Saveen and Werner AB) and the Agilent Bioanalyzer (Agilent Technologies), respectively. 500 ng total RNA was used for the cDNA synthesis (QuantiTect Reverse Transcription Kit (Qiagen)) and an additional DNase treatment was included. Two cDNA replicates were prepared for each RNA sample and –RT controls (reverse transcriptase replaced with water) were included in the reverse transcription. Pre-amplification was performed using TaqMan PreAmp Master Mix (Applied Biosystems). A pool of 200 nM qPCR primer mix was prepared by combining primer pairs used in the subsequent qPCR. 5 µl TaqMan PreAmp Master Mix, 2.5 µl 200 nM qPCR primer mix and 2.5 µl cDNA was incubated at 95 °C for 10 min followed by cycles of 95 °C for 15 s and 60 °C for 4 min. Residual primers were digested by adding 16 U of Exonuclease I (New England BioLabs) and incubating at 37 °C for 30 min followed by 80 °C for 15 min.

Microfluidic high-throughput qPCR was performed on a BioMark HD real-time instrument (Fluidigm) as previously described (Brogaard et al., 2018). A number of reference genes were included in the panel of genes to allow normalization of the data. Two different dynamic arrays were used in the present study (GE 96.96 and GE 192.24) combining 96 samples with 96 primer assays and 192 samples with 24 primer assays generating 9216 or 4608 parallel qPCR reactions in a single run, respectively. Primer names, sequences, and length of amplicons used in the present study can be seen in Supplementary Table S1.

After qPCR, data was manually curated using Fluidigm Real-Time PCR Analysis software 3.0.2 (Fluidigm), followed by data pre-processing as previously described (Barington et al., 2018) in GenEx5 (MultiD Analyses AB). GeNorm (Vandesompele et al., 2002) and NormFinder (Andersen et al., 2004) were used to identify the most stable reference genes (using the GenEx5 software). All putative reference genes included (*GAPDH*, *HPRT1*, *RPL13A*, *PPIA*, *YWHAZ*, and *TBP*) were validated as appropriate for normalization and used for data normalization. Relative gene expression levels were calculated after transforming normalized Cq values to relative quantities scaled to the sample in the data set which had the lowest expression of the gene in question. P-values to determine statistical significance of differences in gene expression levels were calculated for mock inoculated explants on LOG2 transformed data using ANOVA, after testing for normal distribution of the data and correcting for multiple testing using Benjamini-Hochberg false discovery rate.

2.5. Virus replication

Tissue culture infectious dose ($TCID_{50}$) was determined as described by Van Poucke et al. (2010) of homogenized NEs, however, the incubation was reduced to three days (trial 1 and 3). Briefly, MDCK cells were inoculated with ten-fold serial dilutions of homogenized NEs collected 24 hpi and 48 hpi and incubated at 37 °C with 5 % CO_2 for three days. Virus replication was confirmed by immunocytochemistry of the MDCK cells, fixed in 99% ethanol and stained using an in-house polyclonal rabbit anti-swine IAV antibody, followed by horse radish peroxidase (HRP) conjugated anti-rabbit immunoglobulins and streptavidin HRP conjugate. The staining was developed by precipitated polymerized ethylcarbazole and inspected using an inverted light microscope. $TCID_{50}$ was calculated by the Reed and Muench approach. For trial 2, viral replication was confirmed by determining $TCID_{50}$ of the NE culture supernatants. MDCK cells seeded in 96-well plates were inoculated in quadruplicate with 10-fold serial dilutions (ranging from 10^0 to 10^{-7}) of NE culture supernatant collected at 24 hpi and 48 hpi, and incubated at 37 °C with 5 % CO_2 for three days. Induction of cytopathic effect (CPE) was recorded and $TCID_{50}$ was calculated by the Reed and Muench approach. Influenza RNA levels in NEs were determined as described above by RT-qPCR targeting the influenza matrix protein gene with the following primers (Nagy et al., 2010); Forward Sequence (5′ to 3′) GGCCCCCTCAAAGCCGA and Reverse Sequence (5′ to 3′) CGTCTACGYTGCAGTCC as well as in-house primers targeting the HA gene. The level of initial viral RNA (average of matrix protein assay and HA assay) from the inoculum was measured at 1 hpi, and was scaled to 1 in order to measure any relative increase from this time point.

3. Results

3.1. Gene expression changes during ex vivo explant culture

Changes in gene expression as a consequence of *ex vivo* culturing were studied for 82 genes involved in inflammation, apoptosis, and antiviral immune responses (Supplementary Table S1) in mock inoculated porcine NEscollected at necropsy (–20 hpi), after 20 h of acclimatization (0 hpi), and at 24 hpi and 48 hpi. Multivariate analysis (principal component analysis (PCA)) of gene expression data, from a total of 24 explants across the four time points, identified three clusters of NE samples having comparable gene expression profiles (Fig. 2, top panel). NEs collected at necropsy (-20 hpi) form one cluster (green), those collected following 20 h of *ex vivo* acclimatization (time 0 hpi) form a second cluster (yellow), while the third cluster is constituted of NE samples collected at both 24 and 48 hpi (red and dark red). Thus, despite of differences in trial 1 and 3, 24 hpi and 48 hpi was clearly separated from earlier time points. RNA quality, shown as RNA integrity numbers (RIN), was not affected by the duration of culturing (Fig. 2, bottom panel).

Quantification of specific mRNA changes resulting from culturing by itself revealed a significant regulation of 24 genes after correction for multiple testing (see Supplementary Table S2). These genes were mainly involved in inflammation or response to inflammation. However, genes involved in apoptosis and response to viral infection were also regulated (see Supplementary Table S2 and Fig. 2, bottom panel). Importantly, several key genes involved in innate antiviral immune response including viral PRRs (MDA5 (*IFIH1*) and *TLR8*), Type I IFNs (*IFNA* and *IFNB1*), and ISGs (*OAS1*, *MX1* and *RNASEL*) were significantly down-regulated 2–10 fold during culturing. Genes involved in inflammatory response such as *IL1A* and *IL6* were on the contrary upregulated 4 to 44 fold (Fig. 2, bottom panel) after culturing. Furthermore, the acute-phase protein serum amyloid A (SAA) was also found to be significantly upregulated at all three time points following culturing.

3.2. Gene expression changes in mucosal explants exposed to influenza A virus during culture

The response to IAV exposure in explants grown at an air liquid interface were analyzed for genes involved in antiviral immune responses and compared to time-matched mock controls. Expression of

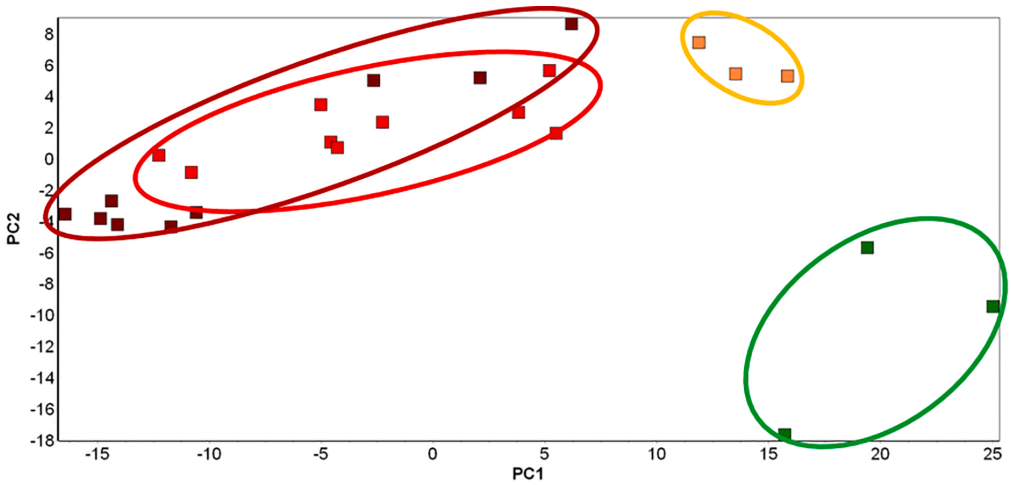

	Genes involved in inflammation					Genes involved in antiviral response				Reference genes			RIN values	Number of mock inoculated animals/explants
	IL1A	*IL6*	*SAA*	*CCL20*	*CXCL2*	*MDA5*	*IFNA*	*IRF7*	*MX1*	*PPIA*	*TBP*	*YWHAZ*		
-20 hours	1.0	1.0	1.0	1.0	1.0	1.0	1.0	1.0	1.0	1.0	1.0	1.0	8.8	3/3
SEM	0.1	0.9	0.5	0.2	0.7	0.2	0.2	0.5	0.4	0.1	0.0	0.1	0.5	
0 hours	9.6	43.5	4.1	8.7	13.4	1.1	0.4	0.5	0.6	1.2	0.8	1.2	8.3	3/3
SEM	1.9	2.2	1.1	1.4	1.7	0.1	0.1	0.2	0.1	0.1	0.1	0.1	0.4	
24 hours	8.8	9.8	4.6	10.2	10.2	0.7	0.2	0.2	0.2	1.2	1.0	1.3	8.6	9/9
SEM	1.0	1.1	0.8	2.2	1.3	0.1	0.0	0.1	0.1	0.1	0.0	0.1	0.2	
48 hours	7.1	10.9	5.5	12.5	4.8	0.5	0.3	0.1	0.2	1.3	1.0	1.2	9.0	9/9
SEM	1.0	4.5	1.7	7.3	0.8	0.1	0.1	0.0	0.1	0.1	0.1	0.1	0.2	
P-value	6.30E-07	4.64E-05	1.18E-02	1.18E-02	5.43E-04	1.15E-02	2.38E-03	9.38E-03	5.00E-04	NS	NS	NS	NS	

Fig. 2. Gene expression analysis of mock inoculated control mucosal explants from trial 1 and 3. Top panel: Principal component analysis (PCA) of gene expression data from 82 genes involved in inflammation and antiviral immune response. Green: Nasal mucosa collected directly from the pig at euthanasia (-20 hpi), Orange: Nasal mucosa explants after 20 h acclimatization in the culture system (0 hpi), Red: Nasal mucosa cultured in virus free medium, sampled 24 hpi, Dark red: Nasal mucosa cultured in virus free medium, sampled 48 hpi. PC = Principal component. Bottom panel: Changes of expression in genes involved in inflammation, antiviral immune response and reference genes. Expression data are scaled to the mean values of −20 hpi explants (scaled to 1). SEM = Standard error of mean; RIN = RNA Integrity Number; NS = not significant. P–values to determine statistical significance of differences in gene expression levels over time were calculated using ANOVA.

several pattern recognition receptors including RIG-I (*DDX58*), MDA5 (*IFIH1*), *TLR3*, and the downstream regulatory factor *IRF7* was upregulated in virus inoculated NEs compared to the mock inoculated NEs at 24 hpi (Fig. 3).

Likewise, the expression of *MX1* and *MX2* was upregulated following IAV inoculation at 24 hpi. Type I IFN (*IFNB1*) and type III IFN (*IL28B* (*IFNL3*)), several ISGs (*ISG15*, *IFITM1*, *IFITM3*, *OAS1*, *OASL*, *EIF2AK2*), and the chemokines *CXCL10* and *CXCL2* were found to be upregulated between 3 and 26 fold in IAV infected NEs at 48 h after viral exposure, compared to mock inoculated NEs harvested at the same time point (Table 2). Increased expression of both IFNs and ISGs from 24 h to 48 h after IAV infection is seen in all investigated antiviral genes compared to

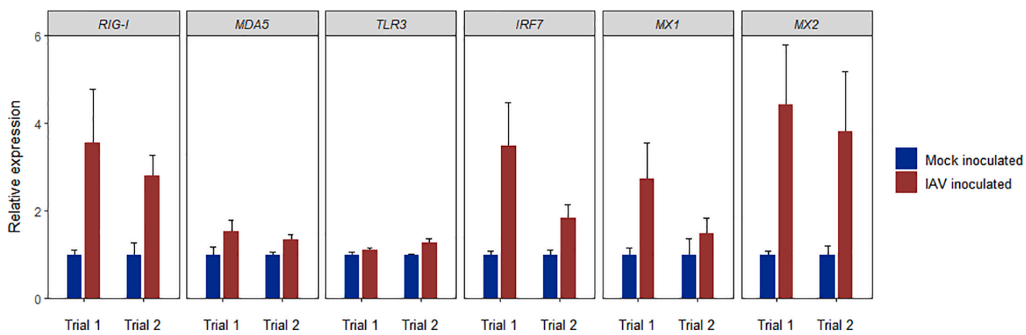

Fig. 3. Relative expression of the pattern recognition receptors RIG-I (*DDX58*), MDA5 (*IFIH1*), *TLR3,* and transcription factor *IRF7* as well as the ISGs *MX1* and *MX2*, 24 h after mock inoculation (blue, scaled to 1) or viral inoculation (red) of porcine NEs. Relative expression is presented as mean relative expression ± SEM. Descriptive statistics were used due to small group size. Trial 1 infected n = 6, control n = 3 and trial 2 infected n = 4, control n = 4.

Table 2
Differential expression of antiviral genes from mock and virus inoculated explants 24 h and 48 h after inoculation (trial 2). Data is presented as mean relative expression ± SEM in brackets. Differentially expression of more than two folds in the NE are shown in bold. Descriptive statistics were used due to small group size.

Gene	Explant mock 24 h	Explant inoculated 24 h	Explant mock 48 h	Explant inoculated 48 h
CCL2	1 (0.1)	1.1 (0.1)	**1 (0.1)**	**2.0 (0.3)**
CXCL10	**1 (0.2)**	**3.9 (1.5)**	**1 (0.2)**	**17.7 (4.8)**
IFNB1	1 (0.1)	1.2 (0.4)	**1 (0.2)**	**3.3 (1.1)**
IL28B (IFNL3)	**1 (0.3)**	**5.4 (3.5)**	**1 (0.2)**	**15.7 (5.4)**
ISG15	**1 (0.2)**	**2.1 (0.5)**	**1 (0.1)**	**9.1 (0.8)**
IFITM1	1 (0.2)	1.2 (0.1)	**1 (0.1)**	**2.7 (0.6)**
IFITM3	1 (0.1)	1.2 (0.2)	**1 (0.1)**	**3.5 (0.6)**
OASL	**1 (0.4)**	**2.0 (0.7)**	**1 (0.3)**	**9.1 (1.5)**
OAS1	**1 (0.1)**	**4.9 (1.6)**	**1 (0.1)**	**25.8 (4.3)**
EIF2AK2	1 (0.2)	1.8 (0.4)	**1 (0.1)**	**4.8 (0.4)**

their time matched controls (Table 2).

In order to compare changes in expression of antiviral genes in explants of the present study with respiratory tissue from experimentally IAV infected pigs (Brogaard et al., 2018; Starbæk et al. in prep.), selected data of gene expression is illustrated in Fig. 4. Comparable changes in expression of key innate antiviral genes including *IL28B* (*IFNL3*), *OASL*, and *CXCL10* were seen between cultured NEs 24 h after viral exposure and nasal mucosal tissue and lung tissue isolated from pigs three to four days after infection with the same influenza isolate, A/swine/Denmark/12687/2003 (H1N2) (Fig. 4).

Infectious viral titer and viral RNA levels are seen in Table 3. Virus replication could only be detected in trial 2, at 24 and 48 hpi. Viral RNA was detected in infected NEs by qPCR, and increased over time, but at different rates in trial 1 and 2.

Low to moderate levels of apoptotic cells were detected by TUNEL assay. However, no distinct association was found between the extend of apoptotic cells and cultivation time or infection status of the NEs (data not shown). In contrast, several genes associated with apoptosis including *FAS*, *FOS* and *CASP3* were upregulated 2–4 fold at the three time points following −20 hpi. (Table S2). No bacterial contamination was found in the growth medium of explants using MALDI-TOF MS.

4. Discussion

The local innate immune response to infection by IAV is a highly complex process orchestrated by numerous respiratory epithelial cells and epithelium-associated immune cells. The process of viral

Table 3
Viral replication determined by infectious dose 50% endpoint (TCID50) in MDCK cells, calculated using Reed and Muench method (Reed and Muench, 1938) and RNA expression measured by RT-qPCR. qPCR data is expressed as mean relative expression ± SEM compared to 1 h post inoculation, nvd = no virus detected.

	Infectious viral titer (TCID50)		Viral RNA (relative quantities)		
Experiment	24 h	48 h	1 h PI	24 h PI	48 h PI
NE trial 1	nvd	nvd	1 (0.2)	2.5 (1.3)	3.4 (2.6)
NE trial 2	5.9 (log10 TCID50/ml)	7.1 (log10 TCID50/ml)	1 (0.5)	146 (137)	487 (127)

recognition and activation of signalling pathways leading to type I and III IFN production and subsequent upregulation of antiviral ISGs is paramount for the early control and elimination of any IAV infection (Bowie and Unterholzner, 2008; Starbæk et al., 2018). The epithelium of the nasal mucosa is composed of ciliated cells, secretory cells, and basal cells attached to each other by tight junctions and immune cells, notably resident macrophages and dendritic cells (Knight and Holgate, 2003; Jahnsen et al., 2004; Beule, 2010). This highly multifaceted respiratory environment can be approximated using nasal explants grown at an air–liquid interface for a limited time period (Glorieux et al., 2007; Van Poucke et al., 2010). After isolation, culturing, and inoculation of porcine NEs, we were able to study the molecular antiviral immune response to IAV at the site of infection, in time-matched mock and virus infected explants up to 48 h after viral exposure.

In the present study no decrease in RNA quality or significant correlation of number of apoptotic cells over time was seen in response to *ex vivo* culturing, which is in accordance with previous results obtained with this model, showing no or little apoptosis and necrosis up to 96 h of *ex vivo* culturing (Glorieux et al., 2007; Van Poucke et al., 2010). Not surprisingly, the environmental change from *in vivo* to *ex vivo* resulted in increased expression of several pro-inflammatory genes, such as *IL1A* and *IL6* and genes associated with apoptosis including *FAS* and *CASP3*. In addition, genes involved in viral pathogen recognition, IFN signalling, and several ISGs were found to be regulated over time during cultivation in the absence of virus. Most of these genes were downregulated. These important and opposite effects on the gene expression of pro-inflammatory as opposed to antiviral immune genes solely brought about by the change in environment, strongly highlight the importance of including and standardizing data to time and handling matched mock controls when studying molecular antiviral immune responses to IAV infection in NEs.

Following IAV inoculation, the expression of several PRRs important

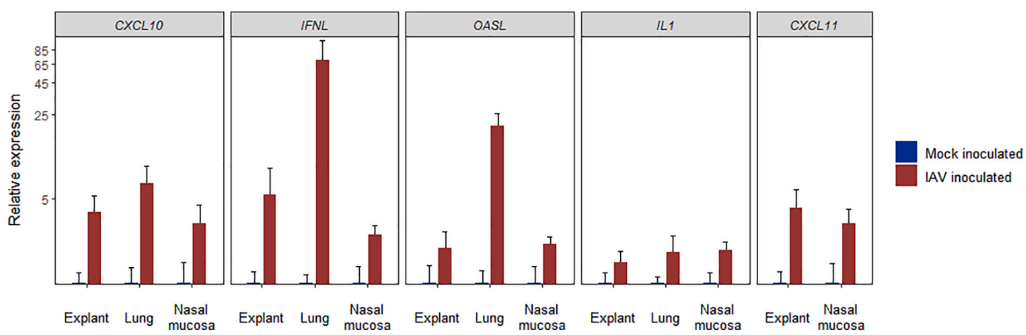

Fig. 4. Comparable expression of key innate antiviral genes within cultured explants at 24 h post inoculation compared with *in vivo* nasal mucosal tissue and lung tissue isolated from pigs infected with the same IAV isolate. Lung data was obtained 3 days post IAV infection (control n = 5 and infected n = 6). Nasal mucosal tissue was collected 4 days post inoculation (control n = 5 and infected n = 7). Relative expression is presented as mean expression ± SEM. Please note the log2 scale on the Y-axis. Descriptive statistics were used due to small group size.

for detection of viral RNA was induced in NEs, including RIG-I (*DDX58*) and MDA5 (*IFIH1*). We have previously studied the innate immune response in lungs of IAV infected pigs inoculated with the same viral isolate used in the present study, A/swine/Denmark/12687/2003 (H1N2) (Skovgaard et al., 2013; Brogaard et al., 2018). Although the change in gene expression depends on cell composition of the tissue and number of infecting virus particles, gene expression patterns in NEs, nasal mucosa, and lung tissue show comparable patterns of expression for selected antiviral genes. The moderate to high upregulation of *IL28B* (*IFNL3*), *OASL*, and *CXCL10* seen in this study was in accordance with previously reported regulation in lung tissue (Brogaard et al., 2018) as well as nasal mucosal tissue isolated from pigs infected with the same IAV isolate (Starbæk et al. in prep.).

A strong but transient IFN response is of great importance during viral infection. In the present study, *IFNB1* was upregulated in IAV infected NEs 48 h after virus exposure compared to mock inoculated NEs harvested at the same time point. Upregulation of *IFNB1* was also found in human nasal epithelial cells 24 h and 48 h after exposure to human H3N2 by Tan et al. (2018). Type III interferon (IFN-λ) has been shown to be among the primary interferons produced by epithelial and dendritic cells in response to IAV infections of the upper respiratory tract (Jewell et al., 2010; Yan et al., 2016; Klinkhammer et al., 2018; Tan et al., 2018). In the present study, *IL28B (IFNL3)* was found to be upregulated in infected NEs at both 24 hpi and 48 hpi. The results of both type I and III IFNs mirrors previously results obtained from *in vivo* infected pig lungs and nasal mucosal tissue with the same viral isolate (Brogaard et al., 2018; Starbæk et al. in prep) as well as in human nasal epithelial cells in response to H3N2 IAV infection (Yan et al., 2016; Tan et al., 2018).

MX1 and *MX2* were upregulated after viral inoculation in both trial 1 and 2. *MX1* is a homolog to the mouse *Mx1* involved in inhibition of viral transcription in the nucleus (Dreiding et al., 1985; Verhelst et al., 2012), whereas the porcine *MX1* is found in the cytoplasm, where it interferes with transport of viral particles to the nucleus, hence inhibiting viral replication (Palm et al., 2010). Upregulation of *MX1* has previously been reported in human nasal epithelial cells infected with H1N1 (Kim et al., 2015) and in human blood samples from individuals infected with influenza virus (Andres-Terre et al., 2015). Upregulation of *MX2* has previously been reported in IAV infected porcine lung explants, both in case of single–infection with a H1N1 swine IAV and co–infection with swine IAV (H1N1) and porcine reproductive and respiratory syndrome virus (PRRSV) (Dobrescu et al., 2014) and after infection with H3N2 swine IAV (Delgado-Ortega et al., 2014). However, the *MX2* gene has to our knowledge, not previously been reported to be involved in response to IAV infection of the upper respiratory system in pigs, and its relevance in porcine nasal mucosal tissue remains to be studied in detail.

Other interferon stimulated genes important for influenza viral restriction early after infection, including *CXCL10*, *OAS1*, *OASL*, and *ISG15*, were found to be highly upregulated in NEs 48 hpi. *CXCL10* has previously been found upregulated in human nasal epithelial cells after infection with human H3N2 (Tan et al., 2018) and *CXCL10* and *OAS1* have been reported to participate in control of infection through suppression of transcription or replication of IAV in human nasal epithelium (Kim et al., 2015). Furthermore, OAS becomes catalytically active in the epithelial cell cytosol upon binding of viral double stranded RNA (dsRNA) during the IAV replication cycle. This activation promotes OAS mediated degradation of viral RNA through RNase L activity and in turn inhibits viral replication (Min and Krug, 2006; Drappier and Michiels, 2015).

Replication of IAV in NEs has previously been reported (Van Poucke et al., 2010). Viral RNA measured by qPCR increased modestly in trial 1 compared to trial 2, and no infectious virus was detected in trial 1. However, reduced viral replication seemed to have only minor effects on the magnitude of antiviral immune responses measured in NEs. Comparing the patterns of gene regulation between trial 1 and 2 for key antiviral genes revealed no systematic differences. Future studies are needed to address the difference in viral replication in order to obtain more reproducible results.

In general, the use of NEs provides easily accessible, cheap samples, and limited space requirements compared to a similar *in vivo* setup with live pigs. However, it of course comes with some limitations; The NEs are removed from the organism and its natural environment. The tissue lacks the lymph system and influx of immune cells and other immune-related components. Future studies should hold more biological replicates in order to allow statistical analysis on all data. Furthermore, the experimental settings should be standardized completely between different trials so pigs and NEs are treated under the same conditions and inoculated with the same amount of virus particles. The lack of antibiotic treatment in trial 3 was compensated by using time-matched controls to adjust for a possible difference in the baseline. The presence of other respiratory viruses was not examined, however, nasal explants were isolated from pigs acquired from farms of high health status without prior history of respiratory infections. Therefore, the presence of other respiratory virus cannot be excluded, but it would reflect a natural environment in the nasal mucosa. Virus enters host cells from the apical side of epithelial cells in the airways. In order to mimic nature more closely, virus could be administered on top of the NEs i.e. from the apical side of the cells instead of immersing NEs into virus suspension. Furthermore, it could be speculated, that the incubation temperature should be decreased a few degrees to mimic the nature of a slightly colder environment of the snout/nose. Finally, the TUNEL assay detects DNA fragmentation, which occurs in the late phase of apoptosis. Assays detecting early stage apoptosis, such as caspase activation assay, should be used in future studies.

High similarity of human and pig respiratory epithelium anatomy and antiviral immune proteins (Dawson et al., 2013; Starbæk et al., 2018) suggests that porcine NEs could be a relevant 3R compliant model for the study of early innate host defence against both swine and human adapted IAV. In conclusion, we have shown that NEs are an important valid method for the study of the innate antiviral immune response after IAV infection, though gene expression changes solely as a consequence of *ex vivo* culturing. However, by careful analysis of time and handling matched mock control samples, transcriptional analysis of the innate antiviral immune response is indeed possible and comparable to responses measured in nasal mucosal tissue and lung tissue isolated from IAV infected pigs.

Funding

The work presented in this article is part of the FluZooMark project supported by Novo Nordisk Foundation (grant NNF19OC0056326).

CRediT authorship contribution statement

Sofie M.R. Starbæk: Conceptualization, Data curation, Formal analysis, Investigation, Methodology, Project administration, Validation, Vizualization, Writing - origional draft, Writing - review & editing. **Malene Rask Andersen:** Data curation, Formal analysis, Investigation, Methodology, Writing – original draft, Writing – review & editing. **Louise Brogaard:** Data curation, Formal analysis, Methodology, Writing – review & editing. **Anna Spinelli:** Formal analysis, Methodology, Writing – review & editing. **Victoria Rapson:** Formal analysis, Methodology, Writing – review & editing. **Helena Aagaard Glud:** Formal analysis, Methodology, Visualization, Writing – review & editing. **Lars E. Larsen:** Funding acquisition, Methodology, Writing – review & editing. **Peter M.H. Heegaard:** Methodology, Writing – review & editing. **Hans Nauwynck:** Methodology, Writing – review & editing. **Kerstin Skovgaard:** Conceptualization, Formal analysis, Funding acquisition, Methodology, Project administration, Supervision, Writing – review & editing.

Declaration of Competing Interest

The authors declare that they have no known competing financial interests or personal relationships that could have appeared to influence the work reported in this paper.

Acknowledgements

We thank Bettina Nonnemann (Department of Health Technology, Technical University of Denmark) for practical support of quality control (MALDI-TOF MS) throughout this study. We also thank Karin Tarp (Department of Biotechnology and Biomedicine, Technical University of Denmark) for technical assistance for performing qPCR.

Appendix A. Supplementary data

Supplementary data to this article can be found online at https://doi.org/10.1016/j.imbio.2022.152192.

References

Alfi, O.r., Yakirevitch, A., Wald, O., Wandel, O., Izhar, U., Oiknine-Djian, E., Nevo, Y., Elgavish, S., Dagan, E., Madgar, O., Feinmesser, G., Pikarsky, E., Bronstein, M., Vorontsov, O., Jonas, W., Ives, J., Walter, J., Zakay-Rones, Z., Oberbaum, M., Panet, A., Wolf, D.G., Heise, M.T., 2021. Human nasal and lung tissues infected ex vivo with SARS-CoV-2 provide insights into differential tissue-specific and virus-specific innate immune responses in the upper and lower respiratory tract. J. Virol. 95 (14).

Andersen, C.L., Jensen, J.L., Ørntoft, T.F., 2004. Normalization of real-time quantitative reverse transcription-PCR data: a model-based variance estimation approach to identify genes suited for normalization, applied to bladder and colon cancer data sets. Cancer Res. 64 (15), 5245–5250. https://doi.org/10.1158/0008-5472.CAN-04-0496.

Andres-Terre, M., McGuire, H., Pouliot, Y., Bongen, E., Sweeney, T., Tato, C., Khatri, P., 2015. Integrated, multi-cohort analysis identifies conserved transcriptional signatures across multiple respiratory viruses. Immunity 43 (6), 1199–1211. https://doi.org/10.1016/j.immuni.2015.11.003.

Barington, K., Skovgaard, K., Henriksen, N.L., Johansen, A.S.B., Jensen, H.E., 2018. The intensity of the inflammatory response in experimental porcine bruises depends on time, anatomical location and sampling site. J. Forensic Leg. Med. 58, 130–139. https://doi.org/10.1016/j.jflm.2018.06.005.

Beule, A.G., 2010. Physiology and pathophysiology of respiratory mucosa of the nose and the paranasal sinuses. GMS Curr. Top. Otorhinolaryngol. – Head Neck Surg. 9, 1–24. https://doi.org/10.3205/cto000071.

Bowie, A.G., Unterholzner, L., 2008. Viral evasion and subversion of pattern-recognition receptor signalling. Nat. Rev. Immunol. 8 (12), 911–922. https://doi.org/10.1038/nri2436.

Brogaard, L., Larsen, L.E., Heegaard, P.M.H., Anthon, C., Gorodkin, J., Dürrwald, R., Skovgaard, K., Renukaradhya, G.J., 2018. IFN-λ and microRNAs are important modulators of the pulmonary innate immune response against influenza A (H1N2) infection in pigs. PLoS ONE 13 (4), e0194765. https://doi.org/10.1371/journal.pone.0194765.

Byrd-Leotis, L., Cummings, R.D., Steinhauer, D.A., 2017. The interplay between the host receptor and influenza virus hemagglutinin and neuraminidase. Int. J. Mol. Sci. 18, 1–22. https://doi.org/10.3390/ijms18071541.

Cantero, D., Cooksley, C., Jardeleza, C., Bassiouni, A., Jones, D., Wormald, P.-J., Vreugde, S., 2013. A human nasal explant model to study Staphylococcus aureus biofilm in vitro. Int. Forum Allergy Rhinol. 3 (7), 556–562. https://doi.org/10.1002/alr.21146.

Dawson, H.D., Loveland, J.E., Pascal, G., Gilbert, J.GR., Uenishi, H., Mann, K.M., Sang, Y., Zhang, J., Carvalho-Silva, D., Hunt, T., Hardy, M., Hu, Z., Zhao, S.-H., Anselmo, A., Shinkai, H., Chen, C., Badaoui, B., Berman, D., Amid, C., Kay, M., Lloyd, D., Snow, C., Morozumi, T., Cheng, R.-Y., Bystrom, M., Kapetanovic, R., Schwartz, J.C., Kataria, R., Astley, M., Fritz, E., Steward, C., Thomas, M., Wilming, L., Toki, D., Archibald, A.L., Bed'Hom, B., Beraldi, D., Huang, T.-H., Ait-Ali, T., Blecha, F., Botti, S., Freeman, T.C., Giuffra, E., Hume, D.A., Lunney, J.K., Murtaugh, M.P., Reecy, J.M., Harrow, J.L., Rogel-Gaillard, C., Tuggle, C.K., 2013. Structural and functional annotation of the porcine immunome. BMC Genomics 14 (1). https://doi.org/10.1186/1471-2164-14-332.

Delgado-Ortega, M., Melo, S., Punyadarsaniya, D., Ramé, C., Olivier, M., Soubieux, D., Marc, D., Simon, G., Herrler, G., Berri, M., Dupont, J., Meurens, F., 2014. Innate immune response to a H3N2 subtype swine influenza virus in newborn porcine trachea cells, alveolar macrophages, and precision-cut lung slices. Vet. Res. 45 (1) https://doi.org/10.1186/1297-9716-45-42.

Denney, L., Ho, L.-P., 2018. The role of respiratory epithelium in host defence against influenza virus infection. Biomed. J. 41 (4), 218–233. https://doi.org/10.1016/j.bj.2018.08.004.

Dobrescu, I., Levast, B., Lai, K., Delgado-Ortega, M., Walker, S., Banman, S., Townsend, H., Simon, G., Zhou, Y., Gerdts, V., Meurens, F., 2014. In vitro and ex vivo analyses of co-infections with swine influenza and porcine reproductive and respiratory syndrome viruses. Vet. Microbiol. 169 (1-2), 18–32. https://doi.org/10.1016/j.vetmic.2013.11.037.

Drappier, M., Michiels, T., 2015. Inhibition of the OAS/RNase L pathway by viruses. Curr. Opin. Virol. 15, 19–26. https://doi.org/10.1016/j.coviro.2015.07.002.

Dreiding, P., Staeheli, P., Haller, O., 1985. Interferon-induced protein Mx accumulates in nuclei of mouse cells expressing resistance to influenza viruses. Virology 140 (1), 192–196.

Frydas, I.S., Nauwynck, H.J., 2016. Replication characteristics of eight virulent and two attenuated genotype 1 and 2 porcine reproductive and respiratory syndrome virus (PRRSV) strains in nasal mucosa explants. Vet. Microbiol. 182, 156–162. https://doi.org/10.1016/j.vetmic.2015.11.016.

Glorieux, S., Bachert, C., Favoreel, H.W., Vandekerckhove, A.P., Steukers, L., Rekecki, A., Van den Broeck, W., Goossens, J., Croubels, S., Clayton, R.F., Nauwynck, H.J., Geraghty, R.J., 2011. Herpes simplex virus type 1 penetrates the basement membrane in human nasal respiratory mucosa. PLoS ONE 6 (7), e22160. https://doi.org/10.1371/journal.pone.0022160.

Glorieux, S., Favoreel, H.W., Meesen, G., de vos, W., Van den Broeck, W., Nauwynck, H. J., 2009. Different replication characteristics of historical pseudorabies virus strains in porcine respiratory nasal mucosa explants. Vet. Microbiol. 136 (3-4), 341–346. https://doi.org/10.1016/j.vetmic.2008.11.005.

Glorieux, S., Van den Broeck, W., van der Meulen, K.M., Van Reeth, K., Favoreel, H.W., Nauwynck, H.J., 2007. In vitro culture of porcine respiratory nasal mucosa explants for studying the interaction of porcine viruses with the respiratory tract. J. Virol. Methods 142 (1-2), 105–112. https://doi.org/10.1016/j.jviromet.2007.01.018.

Iwatsuki-Horimoto, K., Nakajima, N., Shibata, M., Takahashi, K., Sato, Y., Kiso, M., Yamayoshi, S., Ito, M., Enya, S., Otake, M., Kangawa, A., da Silva Lopes, T.J., Ito, H., Hasegawa, H., Kawaoka, Y., Schultz-Cherry, S., 2017. The microminipig as an animal model for influenza A virus infection. J. Virol. 91 (2) https://doi.org/10.1128/JVI.01716-16.

Jahnsen, F.L., Gran, E., Haye, R., Brandtzaeg, P., 2004. Human nasal mucosa contains antigen-presenting cells of strikingly different functional phenotypes. Am. J. Respir. Cell Mol. Biol. 30 (1), 31–37. https://doi.org/10.1165/rcmb.2002-0230OC.

Jang, Y.J., Lee, S.H., Kwon, H.-J., Chung, Y.-S., Lee, B.-J., 2005. Development of rhinovirus study model using organ culture of turbinate mucosa. J. Virol. Methods 125 (1), 41–47. https://doi.org/10.1016/j.jviromet.2004.12.004.

Jewell, N.A., Cline, T., Mertz, S.E., Smirnov, S.V., Flaño, E., Schindler, C., Grieves, J.L., Durbin, R.K., Kotenko, S.V., Durbin, J.E., 2010. Lambda interferon is the predominant interferon induced by influenza A virus infection in vivo. J. Virol. 84 (21), 11515–11522. https://doi.org/10.1128/JVI.01703-09.

Kato, H., Takeuchi, O., Sato, S., Yoneyama, M., Yamamoto, M., Matsui, K., Uematsu, S., Jung, A., Kawai, T., Ishii, K.J., Yamaguchi, O., Otsu, K., Tsujimura, T., Koh, C.-S., Reis e Sousa, C., Matsuura, Y., Fujita, T., Akira, S., 2006. Differential roles of MDA5 and RIG-I helicases in the recognition of RNA viruses. Nature 441 (7089), 101–105. https://doi.org/10.1038/nature04734.

Kim, S., Kim, M.-J., Park, D.Y., Chung, H.J., Kim, C.-H., Yoon, J.-H., Kim, H.J., 2015. Mitochondrial reactive oxygen species modulate innate immune response to influenza A virus in human nasal epithelium. Antiviral Res. 119, 78–83. https://doi.org/10.1016/j.antiviral.2015.04.011.

Klinkhammer, J., Schnepf, D., Ye, L., Schwaderlapp, M., Gad, H.H., Hartmann, R., Garcin, D., Mahlakõiv, T., Staeheli, P., 2018. IFN-λ prevents influenza virus spread from the upper airways to the lungs and limits virus transmission. Elife 7. https://doi.org/10.7554/eLife.33354.

Knight, D.A., Holgate, S.T., 2003. The airway epithelium: Structural and functional properties in health and disease. Respirology 8 (4), 432–446. https://doi.org/10.1046/j.1440-1843.2003.00493.x.

Mazzetto, E., Bortolami, A., Fusaro, A., Mazzacan, E., Maniero, S., Vascellari, M., Beato, M.S., Schiavon, E., Chiapponi, C., Terregino, C., Monne, I., Bonfante, F., 2020. Replication of influenza D viruses of bovine and swine origin in ovine respiratory explants and their attachment to the respiratory tract of bovine, sheep, goat, horse, and swine. Front. Microbiol. 11 https://doi.org/10.3389/fmicb.2020.01136.

Min, J.-Y., Krug, R.M., 2006. The primary function of RNA binding by the influenza A virus NS1 protein in infected cells: Inhibiting the 2'-5' oligo (A) synthetase/RNase L pathway. Proc. Natl. Acad. Sci. 103 (18), 7100–7105. https://doi.org/10.1073/pnas.0602184103.

Nagy, A., Vostinakova, V., Pirchanova, Z., Cernikova, L., Dirbakova, Z., Mojzis, M., Jirincova, H., Havlickova, M., Dan, A., Ursu, K., Vilcek, S., Hornickova, J., 2010. Development and evaluation of a one-step real-time RT-PCR assay for universal detection of influenza A viruses from avian and mammal species. Arch. Virol. 155 (5), 665–673. https://doi.org/10.1007/s00705-010-0636-x.

Niesalla, H.S., Dale, A., Slater, J.D., Scholes, S.F.E., Archer, J., Maskell, D.J., Tucker, A. W., 2009. Critical assessment of an in vitro bovine respiratory organ culture system: A model of bovine herpesvirus-1 infection. J. Virol. Methods 158 (1-2), 123–129. https://doi.org/10.1016/j.jviromet.2009.02.001.

Nonnemann, B., Lyhs, U., Svennesen, L., Kristensen, K.A., Klaas, I.C., Pedersen, K., 2019. Bovine mastitis bacteria resolved by MALDI-TOF mass spectrometry. J. Dairy Sci. 102 (3), 2515–2524. https://doi.org/10.3168/jds.2018-15424.

Palm, M., Garigliany, M.-M., Cornet, F., Desmecht, D., 2010. Interferon-induced Sus scrofa Mx1 blocks endocytic traffic of incoming influenza A virus particles. Vet. Res. 41 (3), 29. https://doi.org/10.1051/vetres/2010001.

Pena, L., Vincent, A.L., Loving, C.L., Henningson, J.N., Lager, K.M., Lorusso, A., Perez, D. R., 2012. Restored PB1-F2 in the 2009 pandemic H1N1 influenza virus has minimal effects in swine. J. Virol. 86 (10), 5523–5532.

Pichlmair, A., Schulz, O., Tan, C.P., Näslund, T.I., Liljeström, P., Weber, F., Reis e Sousa, C., 2006. RIG-I-mediated antiviral responses to single-stranded RNA bearing 5′-phosphates. Science 314 (5801), 997–1001.

Pol, J.M.A., Quint, W.G.V., Kok, G.L., Broekhuysen-Davies, J.M., 1991. Pseudorabies virus infections in explants of porcine nasal mucosa. Res. Vet. Sci. 50 (1), 45–53. https://doi.org/10.1016/0034-5288(91)90052-P.

Rajao, D.S., Vincent, A.L., 2015. Swine as a model for influenza A virus infection and immunity. ILAR J. 56 (1), 44–52. https://doi.org/10.1093/ilar/ilv002.

Reed, L.J., Muench, H., 1938. A simple method of estimating fifty per cent endpoints. Am. J. Epidemiol. 27, 493–497. https://doi.org/10.1093/oxfordjournals.aje.a118408.

Roberts, K.L., Shelton, H., Scull, M., Pickles, R., Barclay, W.S., 2011. Lack of transmission of a human influenza virus with avian receptor specificity between ferrets is not due to decreased virus shedding but rather a lower infectivity in vivo. J. Gen. Virol. 92, 1822–1831. https://doi.org/10.1099/vir.0.031203-0.

Shinya, K., Ebina, M., Yamada, S., Ono, M., Kasai, N., Kawaoka, Y., 2006. Influenza virus receptors in the human airway. Nature 440 (7083), 435–436. https://doi.org/10.1038/440435a.

Skovgaard, K., Cirera, S., Vasby, D., Podolska, A., Breum, S.Ø., Dürrwald, R., Schlegel, M., Heegaard, P.MH., 2013. Expression of innate immune genes, proteins and microRNAs in lung tissue of pigs infected experimentally with influenza virus (H1N2). Innate Immun. 19 (5), 531–544. https://doi.org/10.1177/1753425912473668.

Spicer, S.S., Schulte, B.A., Thomopoulos, G.N., 1983. Histochemical properties of the respiratory tract epithelium in different species. Am. Rev. Respir. Dis. 128, 20–26. https://doi.org/10.1164/arrd.1983.128.2P2.S20.

Starbæk, S.M.R., Brogaard, L., Dawson, H.D., Smith, A.D., Heegaard, P.M.H., Larsen, L.E., Jungersen, G., Skovgaard, K., 2018. Animal models for Influenza A virus infection incorporating the involvement of innate host defenses: enhanced translational value of the porcine model. ILAR J. 59 (3), 323–337. https://doi.org/10.1093/ilar/ily009.

Steukers, L., Vandekerckhove, A.P., Broeck, W. Van Den, Glorieux, S., Nauwynck, H.J., (2012). Kinetics of BoHV-1 dissemination in an in vitro culture of bovine upper respiratory tract mucosa explants. ILAR J. 53, 43–54. doi:10.1093/ilar.53.1.43.

Tan, K.S., Yan, Y., Koh, W.L.H., Li, L., Choi, H., Tran, T., Sugrue, R., Wang, D.Y., Chow, V.T., 2018. Comparative transcriptomic and metagenomic analyses of influenza virus-infected nasal epithelial cells from multiple individuals reveal specific nasal-initiated signatures. Front. Microbiol. 9 https://doi.org/10.3389/fmicb.2018.02685.

Tannenbaum, J., Bennett, B.T., 2015. Russell and Burch's 3Rs then and now: The need for clarity in definition and purpose. J. Am. Assoc. Lab. Anim. Sci. 54, 120–132.

Trebbien, R., Larsen, L.E., Viuff, B.M., 2011. Distribution of sialic acid receptors and influenza A virus of avian and swine origin in experimentally infected pigs. Virol. J. 8, 434. https://doi.org/10.1186/1743-422X-8-434.

Tulinski, P., Fluit, A.C., van Putten, J.P.M., de Bruin, A., Glorieux, S., Wagenaar, J.A., Duim, B., Smith, T.C., 2013. An ex vivo porcine nasal mucosa explants model to study MRSA colonization. PLoS ONE 8 (1), e53783. https://doi.org/10.1371/journal.pone.0053783.

Vairo, S., Van Den Broeck, W., Favoreel, H., Scagliarini, A., Nauwynck, H., 2013. Development and use of a polarized equine upper respiratory tract mucosal explant system to study the early phase of pathogenesis of a European strain of equine arteritis virus. Vet. Res. 44, 1–9. https://doi.org/10.1186/1297-9716-44-22.

Van Poucke, S., Uhlendorff, J., Wang, Z., Billiau, V., Nicholls, J., Matrosovich, M., Van Reeth, K., 2013. Effect of receptor specificity of A/Hong Kong/1/68 (H3N2) influenza virus variants on replication and transmission in pigs. Influenza Other Respi. Viruses 7 (2), 151–159. https://doi.org/10.1111/j.1750-2659.2012.00376.x.

Van Poucke, S.G., Nicholls, J.M., Nauwynck, H.J., Van Reeth, K., 2010. Replication of avian, human and swine influenza viruses in porcine respiratory explants and association with sialic acid distribution. Virol. J. 7, 1–14. https://doi.org/10.1186/1743-422X-7-38.

Vandesompele, J., De Preter, K., Pattyn, F., Poppe, B., Van Roy, N., De Paepe, A., et al., (2002). Accurate normalization of real-time quantitative RT-PCR data by geometric averaging of multiple internal control genes. Genome Biol. 3, research0034.1–0034.11. doi:10.1613/jair.4265.

Verhelst, J., Parthoens, E., Schepens, B., Fiers, W., Saelens, X., 2012. Interferon-inducible protein Mx1 inhibits influenza virus by interfering with functional viral ribonucleoprotein complex assembly. J. Virol. 86 (24), 13445–13455.

Wallace, P., Kennedy, J.R., Mendicino, J., 1994. Transdifferentiation of outgrowth cells and cultured epithelial cells from swine trachea. Vitr. Cell. Dev. Biol. - Anim. 30 (3), 168–180. https://doi.org/10.1007/BF02631440.

Webster, R.G., Bean, W.J., Gorman, O.T., Chambers, T.M., Kawaoka, Y., 1992. Evolution and ecology of influenza A viruses. Microbiol. Rev. 56 (1), 152–179. https://doi.org/10.1128/mr.56.1.152-179.1992.

Yan, Y., Tan, K.S., Li, C., Tran, T., Chao, S.S., Sugrue, R.J., et al., 2016. Human nasal epithelial cells derived from multiple subjects exhibit differential responses to H3N2 influenza virus infection in vitro. J. Allergy Clin. Immunol. 138, 276–281.e15. https://doi.org/10.1016/j.jaci.2015.11.016.

Yoon, S.-W., Webby, R.J., Webster, R.G., (2014). Evolution and Ecology of Influenza A Viruses. In: Current Topics in Microbiology and Immunology. pp. 359–375. doi: 10.1007/82_2014_396.

Zhang, L., Button, B., Gabriel, S.E., Burkett, S., Yan, Y.u., Skiadopoulos, M.H., Dang, Y.L., Vogel, L.N., McKay, T., Mengos, A., Boucher, R.C., Collins, P.L., Pickles, R.J., Philipson, L., 2009. CFTR delivery to 25% of surface epithelial cells restores normal rates of mucus transport to human cystic fibrosis airway epithelium. PLoS Biol. 7 (7), e1000155. https://doi.org/10.1371/journal.pbio.1000155.

Supplementary table S1 Gene names, qPCR primer sequences, and amplicon lengths used to characterize the gene expression in porcine mucosal explants.

Gene name	Gene symbol	Forward Sequence (5' to 3')	Reverse Sequence (5' to 3')	Amplicon length
ACTB (1109)	Actin, Beta	F: GGATGCAGAAGGAGATCACG	R: ACACGGAGTACTTGCGCTCT	84
ADAR (1135)	Adenosine deaminase, RNA-specific	F: GAATTGTCCCGAGTCTCCAA	R: CTGAGTAGGTCCCTGCGGTA	83
AOAH (93)	Acyloxyacyl hydrolase	F: TTCGGCTTACCAGATGGA	R: CTTGTTTAGCTGGCCGAG	95
ARG1 (203)	Arginase	F: TCCAAGGTCTGTGGGAAAAG	R: ATCGCCATACTGTGGTCTCC	108
B2M (7)	Beta-2-Microglobulin	F: TGAAGCACGTGACTCTCGAT	R: CTCTGTGATGCCGGTTAGTG	70
CASP1 (184)	Caspase 1	F:GAAGGACAAACCCAAGGTGA	R: TGGGCTTTCTTAATGGCATC	147
CASP3 (383)	Caspase 3	F: CTGGCAAACCCAAACTTTTC	R: GTCCCACTGTCCGTCTCAAT	79
CASP9 (513)	Caspase 9	F: CTGTGAGGACCTGCTGACC	R: CGGAGGAAATTAAAACAGCCAGG	96
CCL2 (293)	C-C Motif Chemokine Ligand 2	F:CTTCTGCACCCAGGTCCTT	R: CGCTGCATCGAGATCTTCTT	93
CCL20 (995)	C-C Motif Chemokine Ligand 20	F: CTGCAGCAAGTCAGAAGCAG	R: GCTGTGTGAAGCCCATGATA	95
CCL3 (236)	C-C Motif Chemokine Ligand 3	F: CTCTGCAGCCAGGTCTTCTC	R: CTACGAATTTGCGAGGAAGC	97
CCL5 (121)	C-C Motif Chemokine Ligand 5	F:CTCCATGGCAGCAGTCGT	R: AAGGCTTCCTCCATCCTAGC	121
CCL8 (1066)	Chemokine ligand 8	F: GCCAGATTCAGTCTCCATCC	R: AGGGGATCTTTCCATTGACC	62
CCR7 (607)	Chemokine (C-C Motif) Receptor 7	F: TCCACGTCTGCAAACTCATC	R: GTCGATGCTGATGCAGAGAA	83
CD163 (150)	CD163	F:CACATGTGCCAACAAAATAAGAC	R: CACCACCTGAGCATCTTCAA	130

Gene name	Gene symbol	Forward Sequence (5' to 3')	Reverse Sequence (5' to 3')	Amplicon length
CD209 (586)	CD209	F: CGGAGCAGAAATTCCTGAAG	R: CATTGCCAGGAACCTTCATT	94
CD86 (560)	CD86	F: CATCGTCTGTGTCCTGCAAC	R: CACAGGTGGCTTTGCATCTA	82
CHL1 (1140)	Cell Adhesion Molecule L1 Like	F: TTCAAAGGGCTGTGGAAAAC	R: AAACCAGCCTTGAGTGGAG A	100
CSF2 (251)	Colony stimulating factor 2	F: CCGAGGAAACTTCCTGTGAA	R: GCAGTCAAAGGGGATGGTA A	92
CXCL10 (111)	Chemokine (C-X-C Motif) Ligand 10	F:CCCACATGTTGAGATCATTGC	R: GCTTCTCTCTGTGTTCGAGG A	141
CXCL10 (994)	Chemokine (C-X-C Motif) Ligand 10	F: TTCGCTGTACCTGCATCAAG	R: CAACATGTGGGCAAGATTG A	99
CXCL11 (795)	C-X-C Motif Chemokine Ligand 11	F: TATTCAAGGCTTCCCCATGT	R: TCTGCCACTTTCACTGCTTTT	78
CXCL2 (146)	Chemokine (C-X-C Motif) Ligand 2	F: GAAGATGCTAAACAAGAGCAG TG	R: AGCCAAATGCATGAAACACA	147
CXCL9 (793)	C-X-C Motif Chemokine Ligand 9	F: AGCAGTGTTGCCTTGCTTTT	R: ATGCAGGAACAACGTCCATT	92
DDX58(RIG-I) (357)	DExD/H-Box Helicase 58 or RIG-I	F: TTGCTCAGTGCAATCTGGTC	R: CTTCCTCTGCCTCTGGTTTG	79
EIF2AK2 (492)	Eukaryotic Translation Initiation Factor 2 Alpha Kinase 2	F: AGGCTGGCGTCTTAGATGTATT	R: AGGTCGTTTCTTGGGGTCAT T	83
FAS (510)	Fas Cell Surface Death Receptor	F: CACTGTAACCCTTGCACCAC	R: TGGAACACTTCTCTGCATTT GG	86

Gene name	Gene symbol	Forward Sequence (5' to 3')	Reverse Sequence (5' to 3')	Amplicon length
FCGR1A (255)	Fc Fragment Of IgG, High Affinity Ia, Receptor (CD64)	F: GGCAGTGATCACCTTGCAG	R: ATGGGGTCCCTCACATTGTA	79
FLT3 (581)	CD135 / Fms-Related Tyrosine Kinase 3	F: GCTGGAGGAGGAAGAGGACT	R: TCCCTTTGGCCACTTGATAG	77
FOS (470)	FBJ Murine Osteosarcoma Viral Oncogene Homolog	F:GGAACAGTTGTCCCCAGAAG	R: TGTCAGTCAGCTCCCTCCTC	104
FOXO3A (642)	Forkhead Box O3	F: CGGCTGGAAGAACTCTATCCG	R: TCAGGGTTGATGATCCACCAA	105
GZMB (208)	Granzyme B	F: CCAGGACCAGGATAATCGAA	R: GGGTGACGTTGATTGAGCTT	101
GZMK (1148)	Granzyme K	F: AAGTTTGCAACAGCCGAAGT	R: CTTCTGGCCTCTGGTGTCTC	86
HERC5 (1150)	HECT And RLD Domain Containing E3 Ubiquitin Protein Ligase 5	F: TGAAGACGACGACTTTGGAA	R: TGACGTCACTTCCATGAGGA	95
HPRTI (25)	Hypoxanthine phosphoribosyl-transferase I	F: ACACTGGCAAAACAATGCAA	R: TGCAACCTTGACCATCTTTG	71
IDO1 (309)	Indoleamine 2,3-dioxygenase 1	F: GGACCCAAAGCTCTTTTTCA	R: GTCCCAAACGCCTTCATAGA	100
IFI44 (1154)	Interferon Induced Protein 44	F: ATTGCTCACTCACGTGGACA	R: GCTTGAGTTTCACAGGCACA	86
IFI6 (1158)	Interferon alpha inducible protein 6	F: AAGGCGGTATCGCTCTTCTT	R: GAGCTGCTGTTGTCCTCAGA	95
IFIH1/MDA5 (1160)	Interferon induced with helicase C domain 1	F: TCGGATTTTGGAACTCAACC	R: TCTTTGCGATTTCCGTCTCT	80
IFIH1/MDA5 (172)	Interferon induced with helicase C domain 1	F: CAGTGTGCTAGCCTGCTCTG	R: GCAGTGCCTTGTTTCCTCTC	113
IFIT1 (1163)	Interferon-induced protein with tetratricopeptide repeats 1	F: GGCCATTTTGTCTGAATGCT	R: TCAGGGCAAAGAGAGCCTTA	81

Gene name	Gene symbol	Forward Sequence (5' to 3')	Reverse Sequence (5' to 3')	Amplicon length
IFIT3 (1051)	Interferon Induced protein with tetratricopeptide repeats 3	F: ACTGCAGCCCAACAGTCTTT	R: TGATTTGCAGCTCCATTCTG	98
IFITM1 (516)	Interferon Induced Transmembrane Protein 1	F: CACCACGGTGATCACCATCC	R: GCACCAGTTCAGGAAGAGGG	88
IFITM3 (1164)	Interferon induced transmembrane protein 3	F: ATGGTGGGAGACATCATTGG	R: ACCAGAGCCCAGATGTTCAG	71
IFNA1 (200)	Interferon alpha 1	F: TTCCAGCTCTTCAGCACAGA	R: AGCTGCTGATCCAGTCCAGT	86
IFNB1 (222)	Interferon beta 1	F: TGGAGGAAATCATGGAGGAG	R: ACTGTCCAGGCACAGCTTCT	127
IFNB1 (223)	Interferon beta 1	F: AGCACTGGCTGGAATGAAAC	R: TCCAGGATTGTCTCCAGGTC	83
IL28B (IFNL3) (298)	Interleukin 28 (interferon, lambda 3)	F: CCTGGAAGCCTCTGTCATGT	R: TCTCCACTGGCGACACATT	72
IL12B (45)	Interleukin 12 p40	F: GACCAGAAAGAGCCCAAAAAC	R: AGGTGAAACGTCCGGAGTAA	70
IL18 (234)	Interleukin 18	F: CAATTGCATCAGCTTTGTGG	R: TCCAGGTCCTCATCGTTTTC	78
IL18BP (1168)	Interleukin 18 binding protein	F: ACCTGGCCAGAAGAGGAAGT	R: CAGCCAGTAGAGGATGCTGA	96
IL1A (159)	Interleukin 1 alpha	F: GACGAACCCGTGTTGCTG	R: CCATATTGCCATGCTTTTCC	97
IL1B (233)	Interleukin 1, Beta	F:TCTCTCACCCCTTCTCCTCA	R: GACCCTAGTGTGCCATGGTT	60
IL1RAP (275)	Interleukin 1 receptor accessory protein	F: TGCATCTTTGACCGAGACAG	R: GGGCTCAGGACAACAATCAT	98
IL1RN (142)	Interleukin 1 Receptor Antagonist	F:TGCCTGTCCTGTGTCAAGTC	R: GTCCTGCTCGCTGTTCTTTC	90
IL6 (232)	Interleukin 6	F:CCTCTCCGGACAAAACTGAA	R: TCTGCCAGTACCTCCTTGCT	118

Gene name	Gene symbol	Forward Sequence (5' to 3')	Reverse Sequence (5' to 3')	Amplicon length
IL6 (35)	Interleukin 6	F: TGGGTTCAATCAGGAGACCT	R: CAGCCTCGACATTTCCCTTA	116
IRF7 (149)	Interferon Regulatory Factor 7	F: GTGTGCTCCTGTACGGGTCT	R: CTGCAGCAGCTTCTCTGTGT	125
IRF8 (568)	Interferon Regulatory Factor 8	F: TGGGAGAACGACCAGAAGAG	R: CCAGGCCTTGAAGATGGAG	99
IRF9 (290)	Interferon Regulatory Factor 9	F: CATTCAGACTTGGGGAGCAG	R: AAAGGGGCCTCAGTGGTAAC	77
ISG15 (499)	ISG15 Ubiquitin-Like Modifier	F: AGTTCTGGCTGACTTTCGAGG	R: GGTGCACATAGGCTTGAGGT	80
ISG20 (998)	Interferon Stimulated Exonuclease Gene 20	F: AGATCCTGCAGCTCCTGAAA	R: TGCTCATGTTCTCCTTCAGC	84
JAK1 (505)	Janus Kinase 1	F: TGGGCATGGCTGTGTTGG	R: CTTGTAGCTGATGTCCTTGGGA	86
JUN (542)	Jun Proto-Oncogene, AP-1 Transcription Factor Subunit	F: AGTGAAAACCTTGAAAGCGCAG	R: TGGCACCCACTGTTAACGTG	114
MASP2 (229)	Mannan Binding Lectin Serine Peptidase 2	F: GGCAAGGACAGCTGTAAAGG	R: TTCCTCCCACAAACCACTTC	82
MUC1 (118)	Mucin 1	F: GGATTTCTGAATTGTTTTTGCAG	R: ACTGTCTTGGAAGGCCAGAA	116
MUC5AC (919)	Mucin 5AC, Oligomeric Mucus/Gel-Forming	F: GTGGTCTCCTCGACCCTGT	R: CTGCAGATCTGGGTCTCACA	98
MX1 (501)	MX Dynamin Like GTPase 1	F: GCCGAGATCTTTCAGCACCT	R: CGGAGGATGAAGAACTGGATGA	95
MX1 (119)	MX Dynamin Like GTPase 1	F: CCTCCACAGAACTGCCAAG	R: GCAGTACACGATCTGCTCCA	109
NFKB1 (612)	Nuclear Factor Kappa B Subunit 1	F: CCCTGTGAAGACCACCTCTC	R: ATCCCGGAGCTCGTCTATTT	82

Gene name	Gene symbol	Forward Sequence (5' to 3')	Reverse Sequence (5' to 3')	Amplicon length
NOD1 (366)	Nucleotide Binding Oligomerization Domain Containing 1	F: CAGTGGGGTGAAGGTGCTAT	R: TACCTGGCTCCGACATCAGT	99
OAS1 (503)	2'-5'-Oligoadenylate Synthetase 1	F: AAGAAACCCAGGCCTGTGATTC	R: TAGTGCCCCTTCTACCAGCT	99
OAS1 (504)	2'-5'-Oligoadenylate Synthetase 1	F: TGGTACCAGACGTGTAAGAAGAC	R: CTGTTTTCCCGCTTCCTTGC	103
OASL (120)	2'-5'-Oligoadenylate Synthetase Like	F: TGGTACCTGAAGTACGTGAAAGC	R: TACCCACTTCCCAGGCATAG	97
PPIA (154)	peptidylprolyl isomerase A (cyclophilin A)	F: CAAGACTGAGTGGTTGGATGG	R: TGTCCACAGTCAGCAATGGT	138
PTGS2/COX2 (144)	Prostaglandin-Endoperoxide Synthase 2	F: GAACTTACAGGAGAGAAGGAAATGG	R: TTTCTACCAGAAGGGCAGGA	94
RIPK2 (649)	Receptor Interacting Serine/Threonine Kinase 2	F: AACCTCAAAGTCCCTGTCAGC	R: TGTTACTGTCCCAACTGCGA	110
RNASEL (487)	Ribonuclease L	F: GGAGAGCCGTTACAGGACC	R: TCAGATGTTCCAGGTTGCAGT	105
RPL13A (58)	Ribosomal protein L13a	F: ATTGTGGCCAAGCAGGTACT	R: AATTGCCAGAAATGTTGATGC	76
RSAD2 (1178)	Radical S-Adenosyl Methionine Domain Containing 2 (Viperin)	F: AAAGACGTGTCCTGCTTGGT	R: GCCCGTTTCTACAGTTCAGG	100
SERPING1 (1183)	Serpin family G member 1	F: CCCATTTCACAGACCCAACT	R: ACCAGGATCACCAAGCTCAG	79
STAT1 (122)	Signal Transducer And Activator Of Transcription 1	F: CCTTGCAGAATAGAGAACATGATAC	R: CCTTTCTCTTGTTGTCAAGCATT	108
STAT2 (1186)	Signal Transducer And Activator Of Transcription 2	F: GCTGGTGAGACTCCAGGAAG	R: TTGAACTTCCGGAAACCTTG	93

Gene name	Gene symbol	Forward Sequence (5' to 3')	Reverse Sequence (5' to 3')	Amplicon length
SAA (243)	Serum Amyloid A	F: CAGAGATGGGCATCATTCCT	R: TGGCATCGCTGATCACTTTA	184
TBP (155)	TATA box binding protein	F: ACGTTCGGTTTAGGTTGCAG	R: CAGGAACGCTCTGGAGTTCT	96
TIMP1 (1194)	Tissue inhibitor of metalloproteinase 1	F: CTGCGGATACTTCCACAGGT	R: CAAAACTGCAGGTGGTGATG	98
TLR1 (188)	Toll like receptor 1	F: CCTTCAAGACCTTAACACACAGAG	R: CAGATTTACTGCGGTGCTGA	100
TLR3 (123)	Toll like receptor 3	F: ATTGTGCAAAAGATTCAAGGTG	R: TCTTCGCAAACAGAGTGCAT	130
TLR8 (127)	Toll like receptor 8	F: GCAAAGACCACCACCAACTT	R: ATCCGTCAGTCTGGGAATTG	129
TRAF2 (1000)	TNF Receptor Associated Factor 2	F: ACCAGAAGGTGACCCTGATG	R: GGAAGGAGGACGAGCTCAC	90
YWHAE (156)	Tyrosine 3-monooxygenase/tryptophan 5-monooxygenase	F: GCTGCTGGTGATGATAAGAAGG	R: AGTTAAGGGCCAGACCCAAT	124

Supplementary table S2 Relative gene expression levels (RE) of 82 genes in porcine mock NEs as a result of *ex vivo* culturing. Changes still significant after correction for multiple testing (Benjamini–Hochberg false discovery rate) is shown in green under P-value. Fold changes in red are more than 4 fold upregulated, fold changes in green are more than 4 times downregulated. SEM = Standard error of mean.

	-20 hours		**0 hour**		**24 hours**		**48 hours**			
	RE	SEM	RE	SEM	RE	SEM	RE	SEM	**P-Value**	Gene Ontology (GO) - Biological Process
IL6(232)	1.0	0.9	55.73	4.2	16.42	2.1	17.38	8.6	**3.75E-05**	positive regulation of acute inflammatory response
IL6(35)	1.0	0.9	43.53	2.2	9.83	1.1	10.90	4.5	**4.64E-05**	positive regulation of acute inflammatory response
ARG1(203)	1.0	0.4	27.83	8.3	29.65	6.6	39.09	9.6	**9.80E-07**	immune system process
COX2/PTGS2(144)	1.0	0.6	18.62	2.6	16.00	1.8	12.17	3.5	**1.89E-06**	lipid metabolic process
CSF2(251)	1.0	0.5	17.76	3.2	66.67	12.3	113.51	14.8	**8.00E-08**	immune response
CXCL2(146)	1.0	0.7	13.36	1.7	10.20	1.3	4.81	0.8	**0.000543**	inflammatory response
IL1A(159)	1.0	0.1	9.55	1.9	8.80	1.0	7.10	1.0	**6.30E-07**	inflammatory response
CCL5(121)	1.0	0.2	1.22	0.0	0.42	0.1	0.12	0.0	**1.13E-05**	regulation of chronic inflammatory response
FLT3(581)	1.0	0.3	1.19	0.4	0.16	0.0	0.14	0.1	**9.19E-05**	leukocyte homeostasis
OAS1(504)	1.0	0.3	0.97	0.4	0.16	0.1	0.08	0.0	**0.000577**	response to virus
B2M(7)	1.0	0.1	0.96	0.0	0.37	0.0	0.30	0.0	**8.00E-08**	
AOAH(93)	1.0	0.2	0.81	0.2	0.15	0.0	0.11	0.0	**1.05E-05**	inflammatory response
IFIT1(1163)	1.0	0.4	0.68	0.3	0.07	0.0	0.04	0.0	**2.95E-05**	response to virus
SERPING1(1183)	1.0	0.3	0.64	0.2	0.08	0.0	0.11	0.1	**9.51E-05**	negative regulation of complement activation, lectin pathway
TLR1(188)	1.0	0.3	0.63	0.1	0.26	0.1	0.14	0.0	**0.000101**	toll-like receptor signalling pathway
MX1(119)	1.0	0.4	0.62	0.1	0.21	0.1	0.16	0.1	**0.0005**	response to virus
STAT1(122)	1.0	0.2	0.52	0.0	0.26	0.0	0.26	0.1	**0.000281**	positive regulation of defense response to virus by host
IFI44(1154)	1.0	0.3	0.50	0.1	0.13	0.0	0.07	0.0	**0.000161**	response to virus
CD163(150)	1.0	0.5	0.35	0.3	0.03	0.0	0.02	0.0	**6.07E-05**	inflammatory response
GZMK(1148)	1.0	0.4	0.35	0.1	0.06	0.0	0.06	0.0	**5.21E-05**	positive regulation of apoptotic process
IFI6(1158)	1.0	0.2	0.34	0.1	0.12	0.0	0.05	0.0	**0.000128**	negative regulation of cysteine-type endopeptidase activity involved in apoptotic process
CXCL10(994)	1.0	0.3	0.27	0.1	0.04	0.0	0.02	0.0	**2.04E-06**	inflammatory response
TLR8(127)	1.0	0.4	0.26	0.1	0.05	0.0	0.06	0.0	**0.000231**	toll-like receptor signalling pathway, viral RNA
CXCL11(795)	1.0	0.5	0.26	0.2	0.04	0.0	0.01	0.0	**1.14E-06**	inflammatory response
CXCL10(111)	1.0	0.4	0.19	0.1	0.03	0.0	0.02	0.0	**1.05E-06**	inflammatory response
CXCL9(793)	1.0	0.5	0.16	0.1	0.01	0.0	0.00	0.0	**1.30E-07**	inflammatory response
IFNB(222)	1.0	0.5	11.32	9.2	1.52	0.4	0.77	0.3	0.021031	

	-20 hours		0 hour		24 hours		48 hours			
	RE	SEM	RE	SEM	RE	SEM	RE	SEM	**P-Value**	Gene Ontology (GO) - Biological Process
CCL2(293)	1.0	0.4	9.72	1.7	4.62	0.7	3.10	0.8	0.000778	
CCL20(995)	1.0	0.2	8.67	1.4	10.22	2.2	12.53	7.3	0.011756	
TIMP1(1194)	1.0	0.4	7.42	2.2	1.28	0.4	0.77	0.2	0.00202	
FAS(510)	1.0	0.2	4.75	1.1	2.00	0.1	1.87	0.6	0.001644	
CCR7(A)(607)	1.0	0.4	4.48	1.7	0.78	0.1	0.37	0.1	0.001149	
SAA(243)	1.0	0.5	4.10	1.1	4.59	0.8	5.50	1.7	0.011844	
IL18BP(1168)	1.0	0.2	3.83	0.1	1.30	0.1	1.18	0.6	0.006755	
C-JUN(542)	1.0	0.2	3.52	1.3	3.29	0.6	2.85	0.8	0.032959	
CASP3(383)	1.0	0.1	3.52	0.3	2.96	0.3	4.28	2.0	0.045248	
NFKB1(612)	1.0	0.1	3.02	1.3	2.14	0.4	1.21	0.2	0.025893	
ISG15(499)	1.0	0.4	2.40	0.7	1.11	0.1	0.62	0.1	0.00156	
FOS(470)	1.0	0.4	2.15	0.8	1.49	0.3	0.56	0.2	0.038123	
IL1B(233)	1.0	0.3	1.51	0.2	1.49	0.5	0.48	0.2	0.020271	
IFITM1(516)	1.0	0.2	1.32	0.2	0.34	0.1	0.27	0.1	0.001226	
IDO1(309)	1.0	0.5	1.21	0.0	0.31	0.1	0.24	0.1	0.004721	
IFITM3(1164)	1.0	0.2	1.20	0.0	0.44	0.1	0.38	0.1	0.016851	
IFIH1/MDA5(172)	1.0	0.2	1.05	0.1	0.65	0.1	0.52	0.1	0.011516	
HERC5(1150)	1.0	0.3	0.95	0.1	0.55	0.1	0.45	0.0	0.006231	
GZMB(208)	1.0	0.2	0.91	0.6	0.13	0.1	0.03	0.0	0.002398	
OASL(120)	1.0	0.4	0.91	0.4	0.16	0.1	0.07	0.1	0.001962	
OAS(503)	1.0	0.4	0.84	0.3	0.12	0.0	0.22	0.2	0.009772	
RNASEL(487)	1.0	0.4	0.76	0.2	0.33	0.1	0.36	0.2	0.034628	
ISG20(998)	1.0	0.4	0.75	0.2	0.32	0.1	0.36	0.1	0.021204	
RSAD2(1178)	1.0	0.3	0.73	0.2	0.24	0.1	0.29	0.2	0.005296	
EIF2AK2(492)	1.0	0.2	0.73	0.1	0.27	0.1	0.31	0.1	0.002343	
IFIT3(1051)	1.0	0.5	0.72	0.2	0.12	0.0	0.10	0.0	0.000985	
MX1(501)	1.0	0.5	0.71	0.2	0.26	0.1	0.16	0.0	0.000855	
MX2(1001)	1.0	0.6	0.70	0.2	0.15	0.1	0.12	0.1	0.001753	
STAT2(1186)	1.0	0.2	0.63	0.1	0.29	0.0	0.57	0.3	0.018192	
IRF8(568)	1.0	0.3	0.61	0.1	0.20	0.0	0.22	0.1	0.00124	
CD86(560)	1.0	0.3	0.61	0.2	0.18	0.0	0.14	0.0	0.004518	
CASP1(184)	1.0	0.3	0.60	0.2	0.13	0.1	0.13	0.1	0.007672	

	-20 hours		0 hour		24 hours		48 hours			
	RE	SEM	RE	SEM	RE	SEM	RE	SEM	**P-Value**	Gene Ontology (GO) - Biological Process
IRF7(149)	1.0	0.5	0.45	0.2	0.22	0.1	0.15	0.0	0.009384	
IFNA(200)	1.0	0.2	0.44	0.1	0.18	0.0	0.25	0.1	0.002376	
TLR3(123)	1.0	0.1	0.43	0.1	0.40	0.0	0.43	0.1	0.008238	
CCL8(1066)	1.0	0.6	0.12	0.1	0.07	0.0	0.18	0.1	0.037798	
IFNB1(223)	1.0	0.4	11.88	10.0	1.60	0.5	1.16	0.5	0.060054	
RPL13A(58)	1.0	0.0	0.85	0.1	0.69	0.0	0.72	0.1	0.065649	
DDX58/RIG-I(357)	1.0	0.3	0.71	0.1	0.49	0.1	0.42	0.1	0.089794	
FCGR1A(255)	1.0	0.2	0.33	0.1	0.58	0.1	0.54	0.3	0.120309	
IFIH1(1160)	1.0	0.2	0.84	0.1	0.39	0.1	0.37	0.1	0.18367	
IL1RAP(275)	1.0	0.4	1.35	0.4	2.35	0.5	4.72	2.8	0.201608	
IL1RN(142)	1.0	0.2	0.95	0.2	0.44	0.1	1.13	0.7	0.232532	
IL28B (*IFNL3*)(298)	1.0	0.8	1.31	0.5	0.48	0.2	0.36	0.1	0.258508	
YWHAZ(156)	1.0	0.1	1.19	0.1	1.28	0.1	1.17	0.1	0.272724	
RIPK2(649)	1.0	0.1	2.72	1.4	1.90	0.2	1.62	0.2	0.316888	
MASP-2(229)	1.0	0.1	0.63	0.1	1.24	0.2	0.91	0.1	0.344067	
PPIA(154)	1.0	0.1	1.17	0.1	1.16	0.1	1.29	0.1	0.370298	
JAK1(505)	1.0	0.1	1.57	0.1	1.25	0.1	1.47	0.6	0.650935	
TBP(155)	1.0	0.0	0.84	0.1	0.98	0.0	1.02	0.1	0.667707	
IL18(234)	1.0	0.4	1.47	0.4	1.75	0.3	2.22	0.7	0.697425	
MUC1(118)	1.0	0.4	0.93	0.3	0.83	0.1	1.16	0.2	0.697452	
FOXO3A(642)	1.0	0.1	1.58	0.5	0.98	0.2	1.70	1.0	0.748014	
IL12P40(45)	1.0	0.2	2.36	1.1	1.73	0.6	4.23	2.2	0.8672	
NOD1(366)	1.0	0.2	0.82	0.2	0.77	0.1	1.30	0.6	0.918318	

5 Discussion and Conclusions

As outlined in **Paper 1**, there is an increasing threat of spillover of zoonotic viruses from animals into a susceptible human population. Pigs might act as primary reservoirs or intermediary hosts of zoonotic viruses, emphasising the importance of monitoring and controlling potential zoonotic viruses in swine herds worldwide. Especially, spillover events between pigs and humans are likely to occur, with up to 1 billion production pigs each year globally. Farmers and animal caretakers are in close contact with the pigs, and humans and pigs exchange one of the highest estimated number of viruses compared to other mammals, which creates multiple possibilities for zoonotic events. Thus, investigation of shared viruses is of high interest to avoid future spillover events, which potentially could lead to new pandemics. Indeed, the latest IAV pandemic in 2009 was an IAV originating from swine [12], while evidence also points in the direction of a spillover event from bats with the latest Covid-19 (SARS-CoV-2) pandemic [112, 113]. The immune system plays a central role in protecting the host against invading viruses, such as IAV and SARS-CoV-2. However, the immune cells must balance the response between an effective antiviral immune response while avoiding immunopathology. Concurrently, IAV has several ways to alter and evade the host immune response as described in subsection 2.2.2, making host-pathogen interactions highly complex and relevant to study. To study antiviral immune responses and host-pathogen interactions during IAV infection, innate antiviral immunity was investigated after challenge experiments in pigs using multiple IAV strains with different host adaptation levels, including IAV well-adapted to swine and humans (natural isolates adapted to swine/human after around ten years of circulation in the host) and a less host-adapted ”pre-pandemic” strain (isolated from swine only three years after first detection in humans).

The infecting type of IAV strain highly influences antiviral innate immune responses. We demonstrate that well-adapted IAV induces a fast and strong antiviral innate immune response in the proper host, while IAV adapted to another host, in this case humans, induces a more dampened response. The faster and stronger antiviral immune response observed after infection with a swine-adapted IAV could be linked to activation of more pattern recognition

receptors (PRRs) and their subsequent innate pathways. Besides the RIG-I pathway, which was activated after infection with both swine- and human-adapted IAV, *ZBP1* and *NLRP3* pathways were activated after infection with swine-adapted IAV. Induction of a strong expression of immune factors after infection with the swine-adapted IAV might also be connected to the fact that pigs infected with swine-adapted IAV had the highest viral load in the upper respiratory tract. The less host-adapted ”pre-pandemic” strain induced a prolonged response compared to the swine- and human-adapted strains. A prolonged host immune response has been described during severe IAV infection [114] and a less efficient immune evasion strategy could be involved in this antiviral immune signature as described by us (**Paper 3**). The prolonged host immune response can be connected to an intermediate viral load and to more severe pathological changes (atelectasis (collapse of lung lobe) and the number of affected lung lobes) and clinical signs (Figure 5.1). Based on the viral distribution in upper and lower respiratory tissues, the ”pre-pandemic” strain penetrated deepest into the airways as the highest viral load was found in the lungs, whereas viral load was found to be highest in the upper trachea of the swine- and human-adapted strains (**Paper 2**).

The swine-adapted IAV was able to circumvent a central defence barrier upon infection as secreted mucins, *MUC5AC* and *MUC5B*, were downregulated in the early period of infection together with the transmembrane mucin *MUC12* at several time points both at the beginning of infection and later as well (**Paper 3**). Mucins are heavily glycosylated, and their glycosylation pattern is determined by cell and tissue type and putatively by species-specific expression patterns of glycosyltransferases [56–58]. Thus, mucins act as a barrier for infection and zoonotic transfer, and species- and tissue-specific glycosylation patterns of mucins likely affects the ability of IAV to penetrate the mucus layers and infect the underlying host cells. For optimal infection, receptor binding and release must be balanced with the host receptor glycan repertoire. Over-expression of mucins can form a dysfunctional mucus barrier and induce pathological changes as seen during severe SARS-CoV-2 infection [115, 116]. However, the protective role of mucins (*MUC1, MUC4, MUC13*, and *MUC21*) after SARS-CoV-2 infection of human lung epithelial cells (Calu-3) and in human lung tissue has also been revealed. However, *MUC5AC* upregulation increased susceptibility to most

SARS-CoV-2 isolates *in vitro* [117]. In agreement, upregulation of MUC5AC was reported in critically ill patients with SARS-CoV-2 [115, 118]. Thus, the observed downregulation of *MUC5AC* and reduced pathogenicity after infection with swine-adapted IAV could be linked to host adaptation. Adaptation of IAV in a host after zoonotic transfer is associated with multiple mutations across the entire genome for many years after the zoonotic event to optimise viral fitness and transmission in the new host [119, 120]. Equine H3N8 IAV, which has been circulating in horses since 1963, has evolved to induce higher viral replication and a more efficient cell-to-cell spread in equine cell culture and tracheal explants. The enhanced fitness might be connected to host adaptation as a later IAV strain (isolated from a horse in 2003) was less susceptible to type I interferons (IFNs). Concurrently, the later IAV induced reduced tissue pathogenicity [121]. These findings are in agreement with ours as higher viral replication and reduced pathogenicity and clinical impact together with the ability to evade mucosal host immune responses was found after infection of pigs with the swine-adapted strain compared to the less host-adapted ”pre-pandemic” IAV (Figure 5.1).

Regulation of host metabolism might also be a central factor during adaptation to the host as described in **Paper 4**. Many more mechanisms, such as temperature, pH, the viral polymerase complex, and viral immune escape, might be important in host adaptation and the zoonotic potential of the virus. Alignment of NS sequences from swine-adapted IAV, human-adapted IAV, and the “pre-pandemic” IAV revealed genetic variation between the strains (**Paper 3**), which could contribute to differences in NS1 mediated immune evasion between the IAV strains. Indeed, amino acid substitutions in NS1 have been described in relation to altered immune evasion strategies during evolution from a general inhibition of gene expression (CPSF30 binding) to a more specific blocking of ISGs by interfering with the JAK/STAT pathway. This change in immune evasion could be linked to just two mutations in NS1 [122].

Respiratory explant and air-liquid interface (ALI) cultures infected with IAV induced antiviral host immune responses comparable to responses after *in vivo* infection of pigs (swab samples and respiratory tissue) and are promising 3R compliant tools to study host-pathogen interactions. Indeed, in the investigation of host adaptation of equine H3N8 (described

above), respiratory explants were used to evaluate viral replication and tissue damage, while cell lines were included to investigate viral replication kinetics and host immune responses. The pathological changes observed in the equine explants were consistent with findings in experimentally infected horses [121]. In **Paper 5**, we described that explants cultured *ex vivo* could be used to study antiviral immune responses after infection. The challenges of using explant cultures were described in section 3.2, making the establishment of ALI cultures highly relevant. Additional efforts should be made to characterise and establish ALI cultures to study host-pathogen interactions after IAV infection. The establishment of ALI cultures using human primary or immortalised respiratory cells is highly relevant to model host-pathogen interactions in humans exposed to different IAV strains. The hypotheses emerged in **Paper 3** and **Paper 4**, concerning the involvement of host adaptation in kinetics and magnitude of antiviral responses and in host-pathogen interactions, could be investigated further using ALI cultures of both swine and human cells under very controlled conditions. ALI cultures reflect the environment found *in vivo* and make it possible to collect samples at several time points. The possibility to co-culture cells together with immune cells can make the model more complex and complete. However, investigation of differences in immune cell infiltration and tissue pathology between IAV strains can not be studied in this model. The *in vitro* models can undoubtedly be used for hypothesis testing, but the findings should be validated in a complex *in vivo* model.

In general, the results from this PhD project have increased our knowledge of kinetics and dynamics of the antiviral innate immune response after experimental infection of pigs using IAV with different host adaptation levels. Based on transcriptional analyses, IAV host adaptation and the ability to evade the host immune response are demonstrated to impact the antiviral gene expression signatures. Well-adapted IAV induce a strong and fast host immune response where multiple innate pathways are activated compared to IAV adapted to humans and the less host-adapted ”pre-pandemic” strain. Well-adapted IAV might have evolved an ability to undermine or impair mucins to reach and infect the underlying host cells more efficiently. Furthermore, host adaptation might also be connected to the ability to regulate host nucleotide metabolism to improve viral replication. Host adaptation seems to be linked to

reduced pathogenicity as more severe pathology and viral spread deeper into the respiratory tract and a prolonged host immune response were seen after infection with the less host-adapted ”pre-pandemic” IAV compared to the well-adapted swine strain. Thus, differences in the antiviral innate immune response, viral load and distribution and severity of infection were found between IAV strains with different host adaptation levels (Figure 5.1). Whether the antiviral signatures after infection depend on viral load/distribution, viral adaptation or most likely both remain to be investigated, highlighting the importance of elucidating the host-pathogen response in a holistic manner.

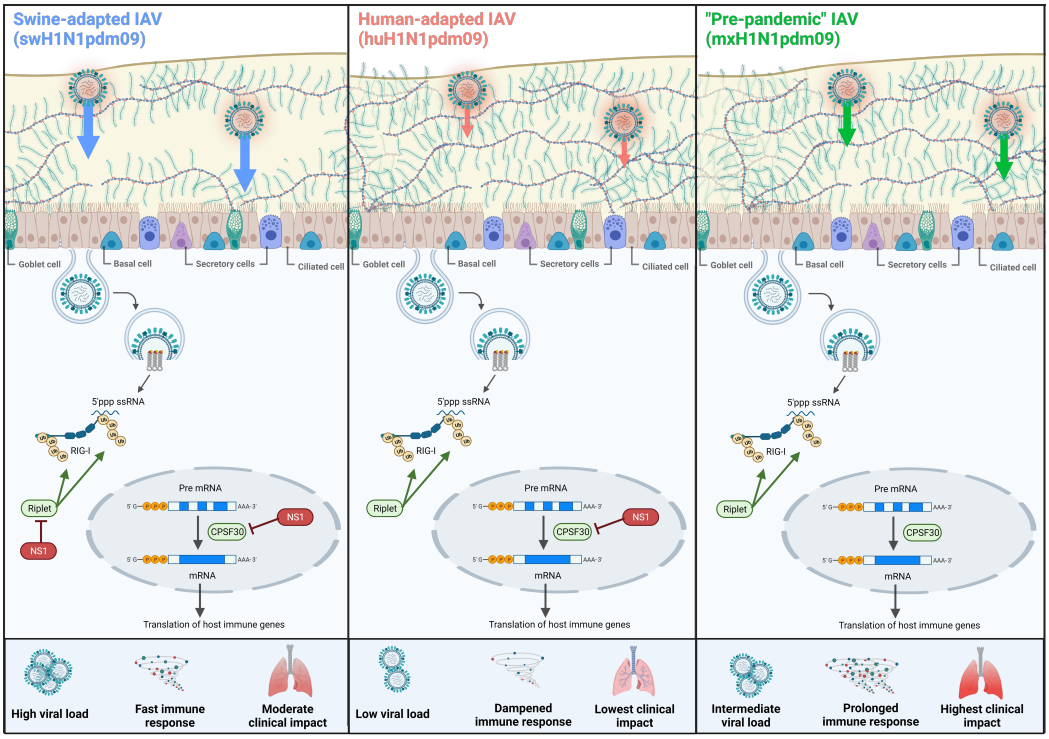

Figure 5.1: Graphical summary of the main findings in the PhD project. The swine-adapted influenza A virus (IAV) interferes with mucus production and has several immune evasion strategies, resulting in high viral load, induction of a fast immune response and moderate clinical impact. The human-adapted IAV has less immune evasion strategies and results in low viral load, a dampened immune response and low clinical impact. The ”pre-pandemic” IAV has less immune evasion strategies and results in intermediate viral load, a prolonged immune response and the highest clinical impact. Created with BioRender.com.

References

[1] WHO. *Fact Sheet Influenza (Seasonal)*. 2018. URL: https://www.who.int/news-room/fact-sheets/detail/influenza-(seasonal).

[2] ECDC. *Factsheet about seasonal influenza*. 2022. URL: https://www.ecdc.europa.eu/en/seasonal-influenza/facts/factsheet.

[3] Dennis J. Alexander. "A review of avian influenza in different bird species". In: *Veterinary Microbiology* 74 (2000), pp. 3–13. DOI: 10.1016/S0378-1135(00)00160-7.

[4] Ramona Trebbien, Lars E. Larsen, and Birgitte M. Viuff. "Distribution of sialic acid receptors and influenza A virus of avian and swine origin in experimentally infected pigs". In: *Virology Journal* 8.434 (2011), pp. 1–14. DOI: 10.1186/1743-422X-8-434.

[5] Robert G. Webster et al. "Evolution and ecology of influenza A viruses". In: *Microbiological Reviews* 56.1 (Aug. 1992), pp. 152–179. DOI: 10.1128/mr.56.1.152-179.1992. URL: https://doc.oie.int/dyn/portal/index.xhtml?page=alo&aloId=29678.

[6] Qi Xu et al. "Influenza H1N1 A/Solomon Island/3/06 Virus Receptor Binding Specificity Correlates with Virus Pathogenicity, Antigenicity, and Immunogenicity in Ferrets". In: *Journal of Virology* 84.10 (2010), pp. 4936–4945. DOI: 10.1128/jvi.02489-09.

[7] Ahmed Mostafa et al. "Zoonotic Potential of Influenza A Viruses: A Comprehensive Overview". In: *Viruses* 10.497 (2018), pp. 1–38. DOI: 10.3390/v10090497.

[8] Lone Simonsen et al. "Global Mortality Estimates for the 2009 Influenza Pandemic from the GLaMOR Project: A Modeling Study". In: *PLoS Medicine* 10.11 (2013), e1001558. DOI: 10.1371/journal.pmed.1001558.

[9] Cécile Viboud et al. "Global Mortality Impact of the 1957-1959 Influenza Pandemic". In: *Journal of Infectious Diseases* 213 (2015), pp. 738–745. DOI: 10.1093/infdis/jiv534.

[10] Cécile Viboud et al. “Multinational Impact of the 1968 Hong Kong Influenza Pandemic: Evidence for a Smoldering Pandemic”. In: *Journal of Infectious Diseases* 192 (2005), pp. 233–248. DOI: 10.1086/431150.

[11] Ann H. Reid et al. “Origin and evolution of the 1918 ”Spanish” influenza virus hemagglutinin gene”. In: *PNAS* 96 (1999), pp. 1651–1656. DOI: 10.1073/pnas.96.4.1651.

[12] Ignacio Mena et al. “Origins of the 2009 H1N1 influenza pandemic in swine in Mexico”. In: *eLife* 5 (2016), pp. 1–21. DOI: 10.7554/eLife.16777.

[13] Kristien Van Reeth. “Avian and swine influenza viruses: our current understanding of the zoonotic risk”. In: *Veterinary Research* 38 (2007), pp. 243–260. DOI: 10.1051/vetres:2006062.

[14] Sofie M.R. Starbæk et al. “Animal Models for Influenza A Virus Infection Incorporating the Involvement of Innate Host Defenses: Enhanced Translational Value of the Porcine Model”. In: *ILAR Journal* 59.3 (2018), pp. 323–337. DOI: 10.1093/ilar/ily009.

[15] Nicholas Hernandez et al. “Life-threatening influenza pneumonitis in a child with inherited IRF9 deficiency”. In: *Journal of Experimental Medicine* 215.10 (2018), pp. 2567–2585. DOI: 10.1084/JEM.20180628.

[16] Aaron R Everitt et al. “IFITM3 restricts the morbidity and mortality associated with influenza”. In: *Nature* 484 (2012), pp. 519–525. DOI: 10.1038/nature10921.

[17] Eric P Griggs et al. “Role of Age in the Spread of Influenza, 2011 – 2019: Data From the US Influenza Vaccine Effectiveness Network”. In: *American Journal of Epidemiology* 191.3 (2022), pp. 465–471. DOI: 10.1093/aje/kwab205.

[18] Rosemary Morgan and Sabra L. Klein. “The intersection of sex and gender in the treatment of influenza”. In: *Current Opinion in Virology* 35.35-41 (2019). DOI: 10.1016/j.coviro.2019.02.009.

[19] Esteban A Hernandez-vargas et al. “Effects of Aging on Influenza Virus Infection Dynamics”. In: *Journal of V* 88.8 (2014), pp. 4123–4131. DOI: 10.1128/JVI.03644-13.

[20] Rebekah Honce and Stacey Schultz-cherry. “Impact of Obesity on Influenza A Virus Pathogenesis, Immune Response, and Evolution”. In: *Frontiers in Immunology* 10 (2019), p. 1071. DOI: 10.3389/fimmu.2019.01071.

[21] Pia Ryt-Hansen et al. “Overvågning af influenza A virus i svin Slutrapport 2021”. In: *Dansk veterinær Konsortium* (2022), pp. 1–31.

[22] N. James MacLachlan and Edward J. Dubovi. “Chapter 21 - Orthomyxoviridae”. In: *Fenner’s Veterinary Virology (Fifth Edition)*. 2017, pp. 389–410. DOI: 10.1016/B978-0-12-800946-8.00021-0.

[23] Ben M Hause et al. “Characterisation of Novel Influenza Virus in Cattle and Swine: Proposal for a New Genus in the Orthomyxoviridae Family”. In: *mBio* 5.2 (2014), pp. 00031–14. DOI: 10.1128/mBio.00031-14.Editor.

[24] Dan Dou et al. “Influenza A Virus Cell Entry, Replication, Virion Assembly and Movement”. In: *Frontiers in Immunology* 9.1581 (2018), pp. 1–17. DOI: 10.3389/fimmu.2018.01581.

[25] Helen M. Wise et al. “A Complicated Message: Identification of a Novel PB1-Related Protein Translated from Influenza A Virus Segment 2 mRNA”. In: *Journal of Virology* 83.16 (2009), pp. 8021–8031. DOI: 10.1128/jvi.00826-09.

[26] Weisan Chen et al. “A novel influenza A virus mitochondrial protein that induces cell death”. In: *Nature Medicine* 7.12 (2001), pp. 1306–1312. DOI: 10.1038/nm1201-1306.

[27] Yukiko Muramoto et al. “Identification of Novel Influenza A Virus Proteins Translated from PA mRNA”. In: *Journal of Virology* 87.5 (2013), pp. 2455–2462. DOI: 10.1128/jvi.02656-12.

[28] B. W. Jagger et al. “An Overlapping Protein-Coding Region in Influenza A Virus Segment 3 Modulates the Host Response”. In: *Science* 337.6091 (2012), pp. 199–204. DOI: 10.1126/science.1222213.

[29] Robert A Lamb and Ching Juh Lai. “Sequence of Interrupted and Uninterrupted mRNAs and Cloned DNA Coding for the Two Overlapping Nonstructural Proteins

of Influenza Virus". In: *Cell* 21 (1980), pp. 475–485. DOI: 10.1016/0092-8674(80)90484-5.

[30] Robert A. Lamb, Ching-Juh Lai, and Purnell W. Choppin. "Sequences of mRNAs derived from genome RNA segment 7 of influenza virus: Colinear and interrupted mRNAs code for overlapping proteins". In: *Proceedings of the National Academy of Sciences of the United States of America* 78.7 (1981), pp. 4170–4174. DOI: 10.1073/pnas.78.7.4170.

[31] Ruikun Du et al. "Revisiting influenza A virus life cycle from a perspective of genome balance". In: *Virologica Sinica* 38.1 (2023), pp. 1–8. DOI: 10.1016/j.virs.2022.10.005. URL: https://doi.org/10.1016/j.virs.2022.10.005.

[32] Gaurav Malik and Yan Zhou. "Innate Immune Sensing of Influenza A Virus". In: *Viruses* 12.755 (2020), pp. 1–26. DOI: 10.3390/v12070755.

[33] Aartjan J.W. te Velthuis and Ervin Fodor. "Influenza virus RNA polymerase: insights into the mechanisms of viral RNA synthesis". In: *Nature Reviews Microbiology* 14 (2016), pp. 479–493. DOI: 10.1038/nrmicro.2016.87.

[34] Leo L. M. Poon et al. "Direct Evidence that the Poly(A) Tail of Influenza A Virus mRNA Is Synthesized by Reiterative Copying of a U Track in the Virion RNA Template". In: *Journal of Virology* 73.4 (1999), pp. 3473–3476. DOI: 10.1128/jvi.73.4.3473-3476.1999.

[35] Leo L. M. Poon, Ervin Fodor, and George G. Brownlee. "Polyuridylated mRNA Synthesized by a Recombinant Influenza Virus Is Defective in Nuclear Export". In: *Journal of Virology* 74.1 (2000), pp. 418–427. DOI: 10.1128/jvi.74.1.418-427.2000.

[36] Eliot K.C. Read and Paul Digard. "Individual influenza A virus mRNAs show differential dependence on cellular NXF1/TAP for their nuclear export". In: *Journal of General Virology* 91 (2010), pp. 1290–1301. DOI: 10.1099/vir.0.018564-0.

[37] Wei Wang et al. "Imaging and characterizing influenza A virus mRNA transport in living cells". In: *Nucleic Acids Research* 36.15 (2008), pp. 4913–4928. DOI: 10.1093/nar/gkn475.

[38] Amie J. Eisfeld, Gabriele Neumann, and Yoshihiro Kawaoka. “At the centre: Influenza A virus ribonucleoproteins”. In: *Nature Reviews Microbiology* 13.1 (2015), pp. 28–41. DOI: 10.1038/nrmicro3367.

[39] Hatice Akarsu et al. “Crystal structure of the M1 protein-binding domain of the influenza A virus nuclear export protein (NEP/NS2)”. In: *EMBO Journal* 22.18 (2003), pp. 4646–4655. DOI: 10.1093/emboj/cdg449.

[40] Edward C. Hutchinson and Ervin Fodor. “Transport of the Influenza Virus Genome from Nucleus to Nucleus”. In: *Viruses* 5 (2013), pp. 2424–2446. DOI: 10.3390/v5102424.

[41] Hyunsuh Kim, Robert G. Webster, and Richard J. Webby. “Influenza Virus: Dealing with a Drifting and Shifting Pathogen”. In: *Viral Immunology* 31.2 (2018), pp. 174–183. DOI: 10.1089/vim.2017.0141.

[42] Wenhan Shao et al. “Evolution of Influenza A Virus by Mutation and Re-Assortment”. In: *International Journal of Molecular Sciences* 18 (2017), p. 1650. DOI: 10.3390/ijms18081650.

[43] José Carlos Mancera Gracia et al. “Influenza A Virus in Swine: Epidemiology, Challenges and Vaccination Strategies”. In: *Frontiers in Veterinary Science* 7 (2020), p. 647. DOI: 10.3389/fvets.2020.00647.

[44] Yoshihiro Kawaoka, Scott Krauss, and Robert G Webster. “Avian-to-Human Transmission of the PB1 Gene of Influenza A Viruses in the 1957 and 1968 Pandemics”. In: *Journal of Virology* 63.11 (1989), pp. 4603–4608. DOI: 10.1128/JVI.63.11.4603-4608.1989.

[45] Rebecca J Garten et al. “Antigenic and Genetic Characteristics of Swine-Origin 2009 A(H1N1) Influenza Viruses Circulating in Humans”. In: *Science* 325 (2009), pp. 197–202. DOI: 10.1126/science.1176225.

[46] Udayan Joseph et al. “The ecology and adaptive evolution of influenza A interspecies transmission”. In: *Influenza and other Respiratory Viruses* 11.1 (2017), pp. 74–84. DOI: 10.1111/irv.12412.

[47] Suxiang Tong et al. “A distinct lineage of influenza A virus from bats”. In: *PNAS* 109.11 (2012), pp. 4269–4274. DOI: 10.1073/pnas.1116200109.

[48] Suxiang Tong et al. “New World Bats Harbor Diverse Influenza A Viruses”. In: *PLoS Pathogens* 9.10 (2013), e1003657. DOI: 10.1371/journal.ppat.1003657.

[49] Miranda De Graaf and Ron A.M. Fouchier. “Role of receptor binding specificity in influenza A virus transmission and pathogenesis”. In: *The EMBO Journal* 33.8 (2014), pp. 823–841. DOI: 10.1002/embj.201387442.

[50] John M. Nicholls et al. “Sialic acid receptor detection in the human respiratory tract: Evidence for widespread distribution of potential binding sites for human and avian influenza viruses”. In: *Respiratory Research* 8.73 (2007), pp. 1–10. DOI: 10.1186/1465-9921-8-73.

[51] Taiana Costa et al. “Distribution patterns of influenza virus receptors and viral attachment patterns in the respiratory and intestinal tracts of seven avian species.” In: *Veterinary research* 43.28 (2012), pp. 1–13. DOI: 10.1186/1297-9716-43-28.

[52] Robert J. Connor et al. *Receptor Specificity in Human, Avian, and Equine H2 and H3 Influenza Virus Isolates*. 1994. DOI: 10.1006/viro.1994.1615.

[53] Gary N. Rogers and Bruce L. D’Souza. “Receptor Binding Properties of Human and Animal H1 Influenza Virus Isolates”. In: *Virology* 173 (1989), pp. 317–322.

[54] Gary N. Rogers and James C. Paulson. “Receptor Determinants of Human and Animal Influenza Virus Isolates: Differences in Receptor Specificity of the H3 Hemagglutinin Based on Species of Origin”. In: *Virology* 127 (1983), pp. 361–373. DOI: 10.1016/0042-6822(83)90150-2.

[55] Daniela S. Rajao, Amy L. Vincent, and Daniel R. Perez. “Adaptation of human influenza viruses to swine”. In: *Frontiers in Veterinary Science* 5.JAN (2019), pp. 1–12. DOI: 10.3389/fvets.2018.00347.

[56] Maitrayee Chatterjee, Jos P.M. van Putten, and Karin Strijbis. “Defensive Properties of Mucin Glycoproteins during Respiratory Infections—Relevance for SARS-CoV-2”. In: *mBio* 11.6 (2020), pp. 02374–20. DOI: 10.1128/mBio.02374-20.

[57] Louisa E. Wallace et al. “Respiratory mucus as a virus-host range determinant”. In: *Trends in Microbiology* 29.11 (2021), pp. 983–992. DOI: 10.1016/j.tim.2021.03.014.

[58] Mark Zanin et al. “The Interaction between Respiratory Pathogens and Mucus”. In: *Cell Host and Microbe* 19 (2016), pp. 159–168. DOI: 10.1016/j.chom.2016.01.001.

[59] Zhuang Gui Chen et al. “Upregulation of cell-surface mucin MUC15 in human nasal epithelial cells upon influenza A virus infection”. In: *BMC Infectious Diseases* 19.622 (2019), pp. 1–11. DOI: 10.1186/s12879-019-4213-y.

[60] Akiko Iwasaki and Padmini S. Pillai. “Innate immunity to influenza virus infection”. In: *Nature Reviews Immunology* 14 (2014), pp. 315–328. DOI: 10.1038/nri3665.

[61] Edin J. Mifsud, Miku Kuba, and Ian G Barr. “Innate Immune Responses to Influenza Virus Infections in the Upper Respiratory Tract”. In: *Viruses* 13.2090 (2021), pp. 1–13. DOI: 10.3390/v13102090.

[62] Stephanie Reikine, Jennifer B Nguyen, and Yorgo Modis. “Pattern recognition and signaling mechanisms of RIG-I and MDA5”. In: *Frontiers in Immunology* 5 (2014), p. 342. DOI: 10.3389/fimmu.2014.00342.

[63] Andreas Pichlmair et al. “RIG-I-Mediated Antiviral Responses to Single- Stranded RNA Bearing 5’-Phosphates”. In: *Science* 314 (2006), pp. 997–1001. DOI: 10.1126/science.1132998.

[64] Loïc Guillot et al. “Involvement of Toll-like Receptor 3 in the Immune Response of Lung Epithelial Cells to Double-stranded RNA and Influenza A Virus”. In: *Journal of Biological Chemistry* 280.7 (2005), pp. 5571–5580. DOI: 10.1074/jbc.M410592200.

[65] Florian Heil et al. “Species-Specific Recognition of Single-Stranded RNA via Toll-like Receptor 7 and 8”. In: *Science* 303.5663 (2004), pp. 1526–1529. DOI: 10.1126/science.1093620.

[66] Sandra S Diebold et al. “Innate Antiviral Responses by Means of TLR7-Mediated Recognition of Single-Stranded RNA”. In: *Science* 303 (2004), pp. 1529–1531. DOI: 10.1126/science.1093616.

[67] Taro Kawai et al. “Interferon-α induction through Toll-like receptors involves a direct interaction of IRF7 with MyD88 and TRAF6”. In: *Nature Immunology* 5.10 (2004), pp. 1061–1068. DOI: 10.1038/ni1118.

[68] Yujuan Chen et al. “Toll-like receptor 3 (TLR3) regulation mechanisms and roles in antiviral innate immune responses”. In: *Journal of Zhejiang University Science B - Biomedicine & Biotechnology* 22.8 (2021), pp. 609–632. DOI: 10.1631/jzus.B2000808.

[69] Chen Wang et al. “TAK1 is a ubiquitin-dependent kinase of MKK and IKK”. In: *Nature* 412 (2001), pp. 346–351. DOI: 10.1038/35085597.

[70] Kenya Honda et al. “Role of a transductional-transcriptional processor complex involving MyD88 and IRF-7 in Toll-like receptor signaling”. In: *Proceedings of the National Academy of Sciences of the United States of America* 101.43 (2004), pp. 15416–15421. DOI: 10.1073/pnas.0406933101.

[71] Satoshi Uematsu et al. “Interleukin-1 receptor-associated kinase-1 plays an essential role for Toll-like receptor (TLR)7- and TLR9-mediated interferon-α induction”. In: *Journal of Experimental Medicine* 201.6 (2005), pp. 915–923. DOI: 10.1084/jem.20042372.

[72] Katherine A. Fitzgerald et al. “IKKϵ and TBKI are essential components of the IRF3 signaling pathway”. In: *Nature Immunology* 4.5 (2003), pp. 491–496. DOI: 10.1038/ni921.

[73] Sonia Sharma et al. “Triggering the Interferon Antiviral Response Through an IKK-Related Pathway”. In: *Science* 300 (2003), pp. 1148–1151. DOI: 10.1126/science.1081315.

[74] S. Paz et al. “Induction of IRF-3 and IRF-7 phosphorylation following activation of the RIG-I pathway”. In: *Cellular and Molecular Biology* 52.1 (2006), pp. 17–28. DOI: 10.1170/T694.

[75] Zhengfan Jiang et al. “Toll-like receptor 3-mediated activation of NF-κB and IRF3 diverges at Toll-IL-1 receptor domain-containing adapter inducing IFN-β”. In: *Pro-*

ceedings of the National Academy of Sciences of the United States of America 101.10 (2004), pp. 3533–3538. DOI: 10.1073/pnas.0308496101.

[76] Megan L. Stanifer, Kalliopi Pervolaraki, and Steeve Boulant. "Differential Regulation of Type I and type III Interferon Signaling". In: *International Journal of Molecular Sciences* 20.1445 (2019), pp. 1–22. DOI: 10.3390/ijms20061445.

[77] Roshan J. Thapa et al. "DAI Senses Influenza A Virus Genomic RNA and Activates RIPK3-Dependent Cell Death". In: *Cell Host and Microbe* 20 (2016), pp. 674–681. DOI: 10.1016/j.chom.2016.09.014. URL: http://dx.doi.org/10.1016/j.chom.2016.09.014.

[78] Teneema Kuriakose et al. "ZBP1/DAI is an innate sensor of influenza virus triggering the NLRP3 inflammasome and programmed cell death pathways". In: *Science Immunology* 1.2 (2016), pp. 1–23. DOI: 10.1126/sciimmunol.aag2045.ZBP1/DAI.

[79] Masaki Mibayashi et al. "Inhibition of Retinoic Acid-Inducible Gene I-Mediated Induction of Beta Interferon by the NS1 Protein of Influenza A Virus". In: *Journal of Virology* 81.2 (2007), pp. 514–524. DOI: 10.1128/JVI.01265-06.

[80] Yuan Lu et al. "Binding of the Influenza Virus NS1 Protein to Double-Stranded RNA Inhibits the Activation of the Protein Kinase That Phosphorylates the eIF-2 Translation Initiation Factor". In: *Virology* 214 (1995), pp. 222–228. DOI: 10.1006/viro.1995.9937.

[81] Xiuyan Wang et al. "Influenza A Virus NS1 Protein Prevents Activation of NF-κB and Induction of Alpha/Beta Interferon". In: *Journal of Virology* 74.24 (2000), pp. 11566–11573. DOI: 10.1128/jvi.74.24.11566-11573.2000.

[82] Michaela Ulrike Gack et al. "Influenza A Virus NS1 Targets the Ubiquitin Ligase TRIM25 to Evade Recognition by the Host Viral RNA Sensor RIG-I". In: *Cell Host and Microbe* 5 (2009), pp. 439–449. DOI: 10.1016/j.chom.2009.04.006.

[83] Ricardo Rajsbaum et al. "Species-Specific Inhibition of RIG-I Ubiquitination and IFN Induction by the Influenza A Virus NS1 Protein". In: *PLoS Pathogens* 8.11 (2012), e1003059. DOI: 10.1371/journal.ppat.1003059.

[84] Aitor Nogales et al. “NS1 Protein Amino Acid Changes D189N and V194I Affect Interferon Responses, Thermosensitivity, and Virulence of Circulating H3N2 Human Influenza A Viruses”. In: *Journal of Virology* 91.5 (2017), pp. 01930–16. DOI: https://doi.org/10.1128/JVI.01930-16.

[85] Benjamin G. Hale et al. “Inefficient Control of Host Gene Expression by the 2009 Pandemic H1N1 Influenza A Virus NS1 Protein”. In: *Journal of Virology* 84.14 (2010), pp. 6909–6922. DOI: 10.1128/jvi.00081-10.

[86] Kalyan Das et al. “Structural basis for suppression of a host antiviral response by influenza A virus”. In: *Proceedings of the National Academy of Sciences of the United States of America* 105.35 (2008), pp. 13093–13098. DOI: 10.1073/pnas.0805213105.

[87] Zhongying Chen, Yongzhong Li, and Robert M. Krug. “Influenza A virus NS1 protein targets poly(A)-binding protein II of the cellular 3’-end processing machinery”. In: *EMBO Journal* 18.8 (1999), pp. 2273–2283. DOI: 10.1093/emboj/18.8.2273.

[88] Shijuan Gao et al. “Influenza A virus-encoded NS1 virulence factor protein inhibits innate immune response by targeting IKK”. In: *Cellular Microbiology* 14.12 (2012), pp. 1849–1866. DOI: 10.1111/cmi.12005.

[89] Benjamin G Hale et al. “The multifunctional NS1 protein of influenza A viruses”. In: *Journal of General Virology* 89 (2008), pp. 2359–2376. DOI: 10.1099/vir.0.2008/004606-0.

[90] Denys A. Khaperskyy et al. “Selective Degradation of Host RNA Polymerase II Transcripts by Influenza A Virus PA-X Host Shutoff Protein”. In: *PLoS Pathogens* 12.2 (2016), e1005427. DOI: 10.1371/journal.ppat.1005427.

[91] A. Rodriguez, A. Pérez-González, and A. Nieto. “Influenza Virus Infection Causes Specific Degradation of the Largest Subunit of Cellular RNA Polymerase II”. In: *Journal of Virology* 81.10 (2007), pp. 5315–5324. DOI: 10.1128/jvi.02129-06.

[92] Zsuzsanna T. Varga et al. “The Influenza Virus Protein PB1-F2 Inhibits the Induction of Type I Interferon at the Level of the MAVS Adaptor Protein”. In: *PLoS Pathogens* 7.6 (2011), e1002067. DOI: 10.1371/journal.ppat.1002067.

[93] Zsuzsanna T. Varga et al. “Influenza Virus Protein PB1-F2 Inhibits the Induction of Type I Interferon by Binding to MAVS and Decreasing Mitochondrial Membrane Potential”. In: *Journal of Virology* 86.16 (2012), pp. 8359–8366. DOI: 10.1128/jvi.01122-12.

[94] Shivani K. Thaker, James Ch’ng, and Heather R. Christofk. “Viral hijacking of cellular metabolism”. In: *BMC biology* 17.59 (2019), pp. 1–15. DOI: 10.1186/s12915-019-0678-9.

[95] Erica L. Sanchez and Michael Lagunoff. “Viral activation of cellular metabolism”. In: *Virology* 479-480 (2015), pp. 609–618. DOI: 10.1016/j.virol.2015.02.038. URL: http://dx.doi.org/10.1016/j.virol.2015.02.038.

[96] Joachim B. Ritter et al. “Metabolic effects of influenza virus infection in cultured animal cells: Intra- and extracellular metabolite profiling”. In: *BMC Systems Biology* 4.61 (2010), pp. 1–22. DOI: 10.1186/1752-0509-4-61.

[97] Heather S. Smallwood et al. “Targeting Metabolic Reprogramming by Influenza Infection for Therapeutic Intervention”. In: *Cell Reports* 19 (2017), pp. 1640–1653. DOI: 10.1016/j.celrep.2017.04.039. URL: http://dx.doi.org/10.1016/j.celrep.2017.04.039.

[98] Lukas Bahati Tanner et al. “Lipidomics identifies a requirement for peroxisomal function during influenza virus replication”. In: *Journal of Lipid Research* 55 (2014), pp. 1357–1365. DOI: 10.1194/jlr.M049148.

[99] Shipra Sharma et al. “Influenza A viral nucleoprotein interacts with cytoskeleton scaffolding protein α-actinin-4 for viral replication”. In: *FEBS Journal* 281.13 (2014), pp. 2899–2914. DOI: 10.1111/febs.12828.

[100] Roy T. Avalos, Zhong Yu, and Debi P. Nayak. “Association of Influenza Virus NP and M1 Proteins with Cellular Cytoskeletal Elements in Influenza Virus-Infected Cells”. In: *Journal of Virology* 71.4 (1997), pp. 2947–2958. DOI: 10.1128/jvi.71.4.2947-2958.1997.

[101] Marja J.A.H. van Zeijl and Karl S. Matlin. “Microtubule perturbation inhibits intracellular transport of an apical membrane glycoprotein in a canine kidney epithelial cells.” In: *Cell regulation* 1 (1990), pp. 921–936. DOI: 10.1091/mbc.1.12.921.

[102] Martha Simpson-Holley et al. “A Functional Link between the Actin Cytoskeleton and Lipid Rafts during Budding of Filamentous Influenza Virions”. In: *Virology* 301 (2002), pp. 212–225. DOI: 10.1006/viro.2002.1595.

[103] Sukhmani Bedi and Akira Ono. “Friend or Foe: The Role of the Cytoskeleton in Influenza A Virus Assembly”. In: *Viruses* 11.46 (2019), pp. 1–21. DOI: 10.3390/v11010046.

[104] Tania Nolan, Rebecca E. Hands, and Stephen A. Bustin. “Quantification of mRNA using real-time RT-PCR”. In: *Nature Protocols* 1.3 (2006), pp. 1559–1582. DOI: 10.1038/nprot.2006.236.

[105] Stephen A. Bustin et al. “The MIQE guidelines: Minimum Information for Publication of Quantitative Real-Time PCR Experiments”. In: *Clinical Chemistry* 55.4 (2009), pp. 611–622. DOI: 10.1373/clinchem.2008.112797.

[106] Radoje Drmanac et al. “Human Genome Sequencing Using Unchained Base Reads on Self-Assembling DNA nanoarrays”. In: *Science* 327.5961 (2010), pp. 78–81. DOI: 10.1126/science.1181498.

[107] Sara Goodwin, John D. McPherson, and W. Richard McCombie. “Coming of age: Ten years of next-generation sequencing technologies”. In: *Nature Reviews Genetics* 17 (2016), pp. 333–351. DOI: 10.1038/nrg.2016.49.

[108] Complete Genomics. *DNBSEQ Technology*. URL: https://completegenomics.mgiamericas.com/en/technology.

[109] Jerrold Tannenbaum and B. Taylor Bennett. “Russell and Burch’s 3Rs then and now: The need for clarity in definition and purpose”. In: *Journal of the American Association for Laboratory Animal Science* 54.2 (2015), pp. 120–132.

[110] Sylvia S. Reemers et al. “Cellular host transcriptional responses to influenza A virus in chicken tracheal organ cultures differ from responses in in vivo infected trachea”.

In: *Veterinary Immunology and Immunopathology* 132 (2009), pp. 91–100. DOI: 10.1016/j.vetimm.2009.04.021.

[111] Victoria Meliopoulos et al. “Primary Swine Respiratory Epithelial Cell Lines for the Efficient Isolation and Propagation of Influenza A Viruses”. In: *Journal of Virology* 94.24 (2020), pp. 01091–20. DOI: 10.1128/jvi.01091-20.

[112] Peng Zhou et al. “A pneumonia outbreak associated with a new coronavirus of probable bat origin”. In: *Nature* 579 (2020), pp. 270–273. DOI: 10.1038/s41586-020-2012-7. URL: http://dx.doi.org/10.1038/s41586-020-2012-7.

[113] Susanna K.P. Lau et al. “Possible Bat Origin of Severe Acute Respiratory Syndrome Coronavirus 2”. In: *Emerging Infectious Diseases* 26.7 (2020), pp. 1542–1547. DOI: 10.3201/eid2607.200092.

[114] Sook San Wong et al. “Severe Influenza Is Characterized by Prolonged Immune Activation: Results from the SHIVERS Cohort Study”. In: *Journal of Infectious Diseases* 217 (2018), pp. 245–256. DOI: 10.1093/infdis/jix571.

[115] Wenju Lu et al. “Elevated MUC1 and MUC5AC mucin protein levels in airway mucus of critical ill COVID-19 patients”. In: *Journal of Medical Virology* 93 (2021), pp. 582–584. DOI: 10.1002/jmv.26406.

[116] Yuying Liu et al. “Mucus production stimulated by IFN-AhR signaling triggers hypoxia of COVID-19”. In: *Cell Research* 30.12 (2020), pp. 1078–1087. DOI: 10.1038/s41422-020-00435-z.

[117] Scott B. Biering et al. “Genome-wide bidirectional CRISPR screens identify mucins as host factors modulating SARS-CoV-2 infection”. In: *Nature Genetics* 54.8 (2022), pp. 1078–1089. DOI: 10.1038/s41588-022-01131-x.

[118] Jiangping He et al. “Single-cell analysis reveals bronchoalveolar epithelial dysfunction in COVID-19 patients”. In: *Protein and Cell* 11.9 (2020), pp. 680–687. DOI: 10.1007/s13238-020-00752-4.

[119] S. Bhatt et al. “The evolutionary dynamics of influenza A virus adaptation to mammalian hosts”. In: *Philosophical Transactions of the Royal Society B: Biological Sciences* 368.1614 (2013). DOI: 10.1098/rstb.2012.0382.

[120] Pablo R. Murcia, James L. N. Wood, and Edward C. Holmes. “Genome-Scale Evolution and Phylodynamics of Equine H3N8 Influenza A Virus”. In: *Journal of Virology* 85.11 (2011), pp. 5312–5322. DOI: 10.1128/jvi.02619-10.

[121] Julien A.R. Amat et al. “Long-term adaptation following influenza A virus host shifts results in increased within-host viral fitness due to higher replication rates, broader dissemination within the respiratory epithelium and reduced tissue damage”. In: *PLoS Pathogens* 17.12 (2021), e1010174. DOI: 10.1371/journal.ppat.1010174.

[122] C. Chauché et al. “Mammalian Adaptation of an Avian Influenza A Virus Involves Stepwise Changes in NS1”. In: *Journal of Virology* 92.5 (2018), pp. 01875–17. DOI: 10.1128/jvi.01875-17.

DTU Bioengineering
Technical University of Denmark
Søltofts Plads, Building 224
DK-2800 Kgs. Lyngby

www.bioengineering.dtu.dk